

University of Reading



Improving natural crop resistance to fungal pathogens: Biophysical characterisation of plant defence protein interactions with biomembranes

by

Olga Barbara Florek

A thesis submitted for the degree of Doctor of Philosophy

School of Chemistry, Food and Pharmacy

Department of Food and Nutritional Sciences

September 2016

Declaration

I confirm that this is my own work and the use of all material from other sources has been properly and fully acknowledged.

Signed:

Olga B. Florek

CONTENTS

ABSTRACT	I
LIST OF ABBREVIATIONS	II
LIST OF FIGURES	IV
LIST OF TABLES	XV
Chapter 1. INTRODUCTION AND THE AIM OF THE PROJECT	1
1.1 Plant defence proteins	2
1.1.1 Thionins	3
1.1.2 Puroindolines	5
1.1.3 Defensins	7
1.2 Possible modes of antimicrobial action	8
1.3 Fungal membrane models	10
1.4 Structures and features of the proteins used in the experiments	15
1.5 Aim of the project	18
1.5.1. Objectives of the project	19
Chapter 2. METHODOLOGY	21
2.1 Introduction	21
2.2 Monolayer experiments	22
2.2.1 Langmuir Trough and Surface Pressure Measurements	22
2.2.1.1 <i>Monolayer Behaviour Upon Compression</i>	24
2.2.2 X-Ray Reflectometry	26
2.3 Bilayer experiments	27
2.3.1 Lipid Vesicles (Liposomes)	28
2.3.2 Differential Scanning Calorimetry (DSC)	29
2.3.3 Lipid Bilayers Deposited on the Solid Support	30
2.3.3.1 <i>Vesicles Spreading</i>	30
2.3.3.2 <i>Langmuir-Blodgett dipping and Langmuir-Schaeffer dipping</i>	31
2.3.4 Attenuated Total Reflectance-Fourier Transform Infrared Spectroscopy (ATR-FTIR)	32
2.3.5 Design of a Dipping Trough for the ATR-FTIR Experiments	33

2.3.6 Neutron Reflectometry (NR)	34
2.4 Conclusions	37
Chapter 3. ISOLATION AND PURIFICATION OF THE DEFENCE PROTEINS FROM WHEAT FLOUR	38
3.1 Introduction	38
3.1.1 Purification of Puroindolines and Purothionins	38
3.1.2 Purification of γ -Purothionins	38
3.2 Materials and Methods	39
3.2.1 Chemicals	39
3.2.2 Extraction of Pin-a, β -Pth and α_2 -Pth	39
3.2.2.1 <i>Protein Extraction from Wheat Endosperm using Triton X-114</i>	39
3.2.2.2 <i>Extraction of the Pin-a Containing Protein Fraction from the non-CMC-Bound Proteins</i>	40
3.2.2.3 <i>Extraction of the Purothionin Rich Protein Fraction from the CMC-Bound Proteins</i>	40
3.2.2.4 <i>RP-HPLC Purification of the Crude Purothionin Extracts</i>	41
3.2.2.5 <i>Cation Exchange Purification of the Crude Pin-a Extracts</i>	41
3.2.3 Extraction of γ -Purothionins	43
3.2.3.1 <i>Removal of Lipids and Volatiles</i>	43
3.2.3.2 <i>Extraction of the NaCl-soluble Proteins</i>	43
3.2.3.3 <i>Fractionation of the NaCl-soluble protein extract</i>	43
3.2.3.4 <i>RP-HPLC Purification of the Ammonium Bicarbonate-insoluble Extracts</i>	44
3.2.4 Sodium Dodecyl Sulphate Polyacrylamide Gel Electrophoresis	45
3.3 Results	46
3.3.1 Pin-a Purification	46
3.3.2 β -Pth and α_2 -Pth Purification	48
3.3.3 γ -Purothionins Purification	49
3.4 Conclusions	51
Chapter 4. LIPID MONOLAYER STUDIES	53
4.1 Introduction	53
4.2 Materials	54

4.3 Surface Pressure Measurements	55
4.3.1 Method Development: Lysozyme vs. DPPG	56
4.3.2 β -Pth vs. Saturated Phospholipid Systems	59
4.3.3 β -Pth vs. Saturated and Unsaturated Lipid Systems	65
4.3.4 Pin-a, α_2 -Pth and β -Pth vs. DPPS	67
4.4 X-Ray Reflectometry (XRR)	70
4.4.1 Discussion of the XRR Results	72
4.5 Conclusions	81
Chapter 5. LIPID BILAYER STUDIES - PART I – NR SYSTEM DEVELOPMENT AND ATR-FTIR STUDIES	82
5.1 Introduction	82
5.2 Materials	83
5.3 Neutron Reflectometry (NR) Experiments	84
5.3.1 Lipid Bilayer Preparation on the Solid Support by Langmuir-Blodgett and Langmuir-Schaeffer Dipping	85
5.3.2 System Development: the Effect of the Inner Leaflet Lipid on the Multilayer Structure	88
5.4 Development and Lipid Characterisation for the Attenuated Total Reflectance-Fourier Transform Infrared Spectroscopy (ATR-FTIR) Spectroscopy	91
5.4.1 Bilayer Deposition: Vesicles Solution Spreading	92
5.4.2 Bilayer Deposition Method Development: the Langmuir-Blodgett and Langmuir-Schaeffer Dipping	93
5.4.3 ATR-FTIR Analysis of the Protein Adsorption to the Phospholipid Bilayers Formed by Different Methods	97
5.4.4 ATR-FTIR Study of the Wheat Defence Proteins Adsorption to the Fungal Bilayer	99
5.5 Conclusions	103

Chapter 6. LIPID BILAYER STUDIES - PART II – NEUTRON REFLECTOMETRY EXPERIMENTS	104
6.1 Introduction	104
6.2 Materials	106
6.3 Bilayer Preparation: Surface Pressure Changes	107
6.4 Neutron Reflectometry Data Fitting	110
6.5 Results	115
6.5.1 β -Pth vs. Net Charge-Varying Saturated Lipid Systems	115
6.5.2 β -Pth vs. Fatty Acid Chain Saturation-Varying Lipid Systems	125
6.5.3 β -Pth vs. Steroid-Containing Lipid Systems	136
6.5.4 Pin-a vs. Saturated Phospholipid Bilayers	140
6.5.5 β -Pth and Pin-a 1:1 mol/mol Mixture vs. Saturated Phospholipid Bilayers	144
6.6 Conclusions	148
Chapter 7. STUDIES ON LIPID VESICLES	151
7.1 Introduction	151
7.2 Materials and Vesicles Preparation	152
7.3 Dynamic Light Scattering (DLS) Measurements	152
7.4 Differential Scanning Calorimetry (DSC) Experiments	153
7.5 Results	154
7.5.1 Vesicles Size Determination by Dynamic Light Scattering (DLS)	154
7.5.2 Differential Scanning Calorimetry (DSC) Sample Preparation Development: Effect of the Sample Vortexing on the DSC Results	155
7.5.3 Repeatability of the Measurements	156
7.5.4 β -Pth vs. DPPC and the Effect of the Lipid Batch on the DSC Profile	158
7.5.5 β -Pth vs. Vesicle Systems with Varying Net Charge	160
7.5.6 Various Wheat Defence Proteins vs. DPPS MLVs	162
7.5.7 Experiments on Small Unilamellar Vesicles (SUVs)	162
7.6 Conclusions	165
Chapter 8. CONCLUDING REMARKS AND FUTURE WORK	167
ACKNOWLEDGEMENTS	171
APPENDIX	172

ABSTRACT

The mechanism of action of the wheat defence proteins (puroindolines and purothionins) as antifungal agents was investigated by monitoring their interactions with the lipid systems mimicking the structures of the yeast cell membrane. The membrane models used were: monolayers at the air/liquid interface, flat bilayers at the solid/liquid interface and the folded bilayers in aqueous solutions (lipid vesicles).

Each lipid model was interacted with defence proteins as single protein or mixed protein systems. The consequent changes in the structures of lipid membranes were then monitored by means of various biophysical techniques selected to probe different aspects of interfacial system.

Surface pressure measurements on a Langmuir trough revealed the preference of wheat defence proteins towards membranes dominated by anionic, saturated phospholipids and, together with X-Ray Reflectometry (XRR) studies, revealed different interaction kinetics dependent on the phospholipid chain saturation. The monolayer studies also suggested that there existed antifungal synergy between the two groups of proteins: puroindolines and purothionins.

Protein penetration to the flat lipid bilayers was analysed by Attenuated Total Reflectance-Fourier-Transform Infrared Spectroscopy (ATR-FTIR) and Neutron Reflectometry (NR). The bilayer studies enabled to assess the lipid flipping between the leaflets and confirmed the protein's strong adsorptive properties towards the anionic, saturated phospholipids. Protein interactions with the lipid vesicles were assessed by means of Differential Scanning Calorimetry (DSC) and revealed the dependence of the protein's membrane-solubilising properties on the lipid net charge.

The project also involved the development of the technique for the controlled flat lipid bilayer deposition on the ATR-FTIR solid support. For this purpose, a new Langmuir trough was designed and equipped with a dipping arm, allowing the covering of the support with the two-lipid-molecule-thick bilayers.

The findings from the research provided an insight into the antifungal mode of action of wheat defence protein.

LIST OF ABBREVIATIONS

2D-NMR	Two-dimensional Nuclear Magnetic Resonance
AFM	Atomic force microscopy
Ala / A	Alanine
APS	Ammonium persulphate
Arg / R	Arginine
Asn / N	Asparagine
Asp / D	Aspartic acid
ATR-FTIR	Attenuated Total Reflectance Fourier-Transform Infrared spectroscopy
BAM	Brewster Angle Microscopy
BSA	Bovine serum albumin
CL	Cardiolipin
CMC	Carboxymethyl cellulose
Cys / C	Cysteine
DLS	Dynamic Light Scattering
DOPC	1,2-dioleoyl- <i>sn</i> -glycero-3-phosphocholine
DOPE	1,2-dioleoyl- <i>sn</i> -glycero-3-phosphoethanolamine
DPPC	1,2-dipalmitoyl- <i>sn</i> -glycero-3-phosphocholine
DPPG	1,2-dipalmitoyl- <i>sn</i> -glycero-3-phospho-(1'- <i>rac</i> -glycerol)
DPPS	1,2-dipalmitoyl- <i>sn</i> -glycero-3-phospho-L-serine
DSC	Differential Scanning Calorimetry
DSPC	1,2-distearoyl- <i>sn</i> -glycero-3-phosphocholine
DTGS	Deuterated triglycine sulphate
EDTA	Ethylenediamine tetraacetic acid
ER-FTIR	External-Reflectance Fourier-Transform Infrared spectroscopy
FPLC	Fast Performance Liquid Chromatography
Gln / Q	Glutamine
Glu / E	Glutamic acid
Gly / G	Glycine
HEPES	4-(2-hydroxyethyl)-1-piperazineethanesulfonic acid
His / H	Histidine
Ile / I	Isoleucine
ITC	Isothermal Titration Calorimetry
LB	Langmuir-Blodgett
LC-MS	Liquid Chromatography-Mass Spectrometry
Leu / L	Leucine
LS	Langmuir-Schaeffer
LTP	Lipid-transfer protein
LUV	Large unilamellar vesicle
Lys / K	Lysine
Met / M	Methionine
MLV	Multilamellar vesicle
MW	Molecular weight
NMR	Nuclear Magnetic Resonance
NR	Neutron Reflectometry
PA	Phosphatidic acid
PC	Phosphatidylcholine

PE	Phosphatidylethanolamine
Phe / F	Phenylalanine
PI	Phosphatidylinositol
Pin	Puroindoline
POPS	1-palmitoyl-2-oleoyl- <i>sn</i> -glycero-3-phospho-L-serine
Pro / P	Proline
PS	Phosphatidylserine
PTFE	Polytetrafluoroethylene
Pth	Purothionin
ROI	Regions of interest
RP-HPLC	Reversed-Phase High Performance Liquid Chromatography
SDS	Sodium Dodecyl Sulphate
SDS-PAGE	Sodium Dodecyl Sulphate - Polyacrylamide Gel Electrophoresis
Ser / S	Serine
SLD	Scattering Length Density
SMW	Silicon-scattering-length-density-matched water
SP	Surface pressure
SUV	Small unilamellar vesicle
TCA	Trichloroacetic acid
TEMED	N,N,N',N'-Tetramethylethylenediamine
TFA	Trifluoroacetic acid
Thr / T	Threonine
Trp / W	Tryptophan
TX-114	Triton-X114 (<i>tert</i> -octylphenoxypolyethoxyethanol)
Tyr / Y	Tyrosine
UHQ	Ultra high quality
UV	Ultraviolet
Val / V	Valine
XRR	X-Ray Reflectometry

LIST OF FIGURES

Figure 1.1 A scheme of the wheat grain showing aleurone and endosperm: the structures from which the wheat defence proteins were isolated [reproduced by kind permission of Springer Science and Bus Media B V via RightsLink, 17.03.2017]. ⁸	2
Figure 1.2 The predicting results of disulfide bonding state of Pin-b. AA, amino acid sequence; DB_state, predicted disulfide bonding state (1 = disulfide bonded, 0 = not disulfide bonded); DB_conf, confidence of disulfide bonding state prediction (0 = low to 9 = high). ³⁷	5
Figure 1.3 Sequences of the Trp-rich loops of the wild-type Pin-b and the mutants Pin-bH and Pin-bS. ⁴⁹	6
Figure 1.4 Evolutionary phylogenetic tree of the plant thionins and defensins [reproduced by kind permission of Elsevier via Rightslink, 15.03.2017]. ⁵⁹	8
Figure 1.5 Cartoon representation of the three modes of altering membrane permeability by antimicrobial proteins illustrating a barrel-stave mechanism, toroid pore mechanism and carpet mechanism. ⁶³	9
Figure 1.6 Structural formulas of the lipids used in the monolayer experiments. Hydrophobic parts of the molecules are marked yellow, hydrophilic parts of the molecules are marked blue.	13
Figure 1.7 (a) Membrane lipid properties and (b) the structure of a eukaryotic cell (not containing a cell wall) with the detailed depiction of endoplasmic reticulum (ER) membrane and plasma membrane (PM) showing the asymmetric phospholipid distribution between the membrane leaflets. Abbreviations used: PtdCho – phosphatidylcholine, PtdEtn – phosphatidylethanolamine, SM – sphingomyelin [reproduced by kind permission of Nature Publishing Group via RightsLink, 15.03.2017]. ⁸⁶	15
Figure 1.8 (a) Stick diagrams of the 20 final structures of Pin-a bound to sodium dodecyl sulphate (SDS) obtained by the 2D-Nuclear Magnetic Resonance (2D-	17

NMR) analysis; (b) Ribbon diagram of the averaged structure of Pin-a with the side chains of all Trp residues (blue) and positively charged residues (pink) are visible. (c) Charge distribution on the surface of Pin-a: positive and neutral potentials are blue and white, respectively [reproduced by kind permission of American Society for Microbiology via RightsLink, 15.03.2017].⁹³

Figure 1.9 Three-dimensional structure of β -Pth, showing the α -helices (marked blue), β -sheets (marked pink) and the four disulphide bridges (marked yellow) stabilising the protein's structure.⁹⁵ 18

Figure 2.1 Scheme of the Langmuir trough apparatus used for preparation and monitoring of monolayers at the air/liquid interface. 22

Figure 2.2 Diagram of a Wilhelmy plate partially immersed in water. 23

Figure 2.3 Schematic representation of a surface pressure – mean molecular area isotherm [reproduced by kind permission of John Wiley and Sons Limited via PLSClear, 8.03.2017] .¹⁰⁵ 24

Figure 2.4 Schemes of a small unilamellar vesicle (A), a large unilamellar vesicle (B) and a multilamellar vesicle (MLV) formed of phospholipids. Red spheres represent the polar phospholipid headgroups and the blue springs represent the hydrophobic chains of fatty acid residues. 28

Figure 2.5 Scheme of a differential scanning calorimeter suitable for liquid analysis. 29

Figure 2.6 Scheme of the phospholipid bilayer formation on the germanium crystal placed in an ATR-FTIR cell by means of the vesicles spreading technique. 30

Figure 2.7 Diagrams of the Langmuir-Blodgett (1) and the Langmuir-Schaeffer (2) dipping of a silicon block used for preparation of the phospholipid bilayers. The red arrows indicate the direction of the block's motion. Langmuir-Blodgett dipping image is a simplified scheme as it does not account for covering of all the block's walls. 31

Figure 2.8 Cross-section of an ATR-FTIR cell with a Ge crystal and the protein solution adapters.	32
Figure 2.9 Simple scheme of the dipping trough containing a deep well enabling to immerse the solid supports.	33
Figure 2.10 Length cross section of a dipping trough containing the ATR-FTIR cell with the attached tubing.	34
Figure 2.11 The scheme of an NR experiment carried out at the solid/liquid interface containing a silicone block as a solid substrate.	37
Figure 3.1 Diagram of the Pin-a and β -Pth and α_2 -Pth extraction and purification.	42
Figure 3.2 Diagram of the γ -Purothionins extraction and purification.	44
Figure 3.3 FPLC chromatogram (A) and SDS-PAGE (B) analysis of the fractions collected during Resource S cation exchange purification of the Pin-a rich crude protein extract.	47
Figure 3.4 RP-HPLC chromatogram obtained from purothionin rich fraction of the Triton X-114 wheat protein extract.	48
Figure 3.5 SDS-PAGE analysis of the pellets (1p and 2p) and supernatants (1s and 2s) after final ammonium bicarbonate wash of the NaCl-soluble protein extract.	49
Figure 3.6 RP-HPLC chromatogram (A) and SDS-PAGE (B) analysis of the fractions collected during Cosmosil C4 RP-HPLC purification of the ammonium bicarbonate-insoluble crude protein extract.	50
Figure 4.1 An 80 mL Langmuir trough used for monitoring the surface pressure changes caused by the adsorption of the tested protein / protein mixture to the lipid monolayer.	55
Figure 4.2 A 10 mL trough used for carrying out the monolayer experiments basing on the monitoring of the changes in the surface pressure.	56

Figure 4.3 Surface pressure – Area isotherm of DPPG showing the surface pressure point at which a sample of lysozyme was injected (*).	57
Figure 4.4 Surface pressure <i>vs.</i> time measurements showing the change in surface pressure during the adsorption of lysozyme to the condensed phase DPPG monolayers on 10 mL trough (left) and 80 mL trough (right).	58
Figure 4.5 Surface pressure – Area isotherm of the saturated phospholipid systems showing the surface pressure point at which a sample of β -Pth was injected (*).	59
Figure 4.6 Surface pressure – Area isotherms of the DPPC:DPPS 1:1 mol:mol monolayer presenting the multiple compressions of the film.	61
Figure 4.7 An example of the blank monolayer experiment showing the changes in surface pressure after the injection of the phosphate buffer pH 7.0 sample to the condensed phase DPPC monolayer.	62
Figure 4.8 Surface pressure <i>vs.</i> time isotherms showing the change in surface pressure after the injection of the β -Pth to the condensed phase saturated phospholipid monolayers with varying net charge values.	63
Figure 4.9 Surface pressure – Area isotherm of the saturated DPPS and unsaturated POPS phospholipid systems showing the surface pressure point at which a sample of β -Pth was injected (*).	65
Figure 4.10 Surface pressure <i>vs.</i> time isotherms showing the change in surface pressure after the injection of the β -Pth to the condensed phase of saturated DPPS monolayers (blue) and unsaturated POPS monolayers (red).	66
Figure 4.11 Experiment room at I07 XRR reflectometer in which the monolayer studies were carried out. The Langmuir trough used for creating the lipid monolayers was enclosed in the chamber, into which helium was pumped to minimise the destructive effects of X-rays on the monolayer.	71
Figure 4.12 XRR reflectivity profiles with the model data fits (left) plotted against the momentum transfer Q and the scattering length density profiles these fits describe (right), plotted against the distance Z , for the DPPS condensed	74

phase monolayer held at 22 mN/m (1), β -Pth-adsorbed DPPS monolayer after 60 min (2), 90 min (3), 120 min (4) and 150 min (5).

Figure 4.13 Overlapped XRR scattering length density profiles plotted vs. distance Z, obtained from the reflectivity data fitting of the experiment on β -Pth interacting with condensed phase DPPS monolayers. 75

Figure 4.14 Surface pressure measurements of the β -Pth-adsorbed DPPS condensed phase monolayer. The numbers on the plot correspond to the reflectivity profiles in Figure 4.12. 75

Figure 4.15 XRR reflectivity profiles with the model data fits (left) plotted against the momentum transfer Q and the scattering length density profiles these fits describe (right), plotted against the distance Z, for the POPS condensed phase monolayer held at 22 mN/m (1), β -Pth-adsorbed POPS monolayer after 20 min (2), 80 min (3), 140 min (4) and 200 min (5). 78

Figure 4.16 Overlapped XRR scattering length density profiles plotted vs. distance Z, obtained from the reflectivity data fitting of the experiment on β -Pth interacting with condensed phase POPS monolayers. The film components listed in black font relate to the protein-adsorbed monolayer, whereas the red font components correspond to the POPS only monolayer. 79

Figure 4.17 Surface pressure measurements of the β -Pth-adsorbed POPS condensed phase monolayer. The numbers on the plot correspond to the reflectivity profiles in Figure 4.15. 79

Figure 5.1 Langmuir-Blodgett dip of the silicon block using purpose-built Langmuir trough. The block is moved upwards through the lipid monolayer deposited on the water surface and its vertical surfaces become covered with the monolayer. 85

Figure 5.2 Calibration of the dipping arm position before the Langmuir-Schaeffer dip of the silicon block. The process sets the dipping arm in the horizontal position in respect to the water surface, allowing the controlled coverage of the silicon block's surface with the lipids present on the water surface. 86

Figure 5.3 A sample cell used for the Neutron Reflectometry solid-support experiments with the lipid bilayer-covered solid substrate enclosed. The buffer and protein solutions were delivered to the cell through the attached tubing.	87
Figure 5.4 Interior of the NR instrument Inter showing three NR cells containing the lipid-bilayer covered silicon blocks.	88
Figure 5.5 Reflectivity data (left) and the fits describing these data (right) of the double symmetric POPS bilayer. The isotopic contrasts applied were: D ₂ O (red line), SMW (green line), H ₂ O (blue line).	89
Figure 5.6 An ATR-FTIR cell with the attached adapters through which the protein solution was injected during the experiments.	92
Figure 5.7 Langmuir-Blodgett dip of the germanium ATR-FTIR crystal using the purpose-built Langmuir trough showing the fully immersed crystal right before being dragged up through the condensed phase lipid monolayer kept at the constant surface pressure.	94
Figure 5.8 Scheme of the dipping trough preparation for the LS-dip showing the insert and the ATR-FTIR cell to be placed at the bottom of the trough's dipping well.	95
Figure 5.9 Langmuir-Schaeffer dip of the germanium ATR-FTIR crystal using purpose-built Langmuir trough. The lipid-monolayer-covered Ge crystal will pierce the lipid monolayer spread on the water surface and will be inserted to the ATR-FTIR cell placed at the bottom of the trough's well.	96
Figure 5.10 ATR-FTIR results on the lysozyme adsorption to the symmetric dipped DPPC bilayer (left) showing spectra of: 1) the lipid bilayer before injection, 2) right after injection, 3) 1 h after injection, 4) 24 h after injection, and the DPPC bilayer formed by spreading vesicles (right) showing spectra of: 1) the lipid bilayer before injection, 2) right after injection, 3) 1 h after injection, 4) 2 h after injection and 5) 24 h after injection. The two peaks of interest shown are the carbonyl stretch at $\sim 1750\text{ cm}^{-1}$ indicating the presence of the phospholipid and the Amide I band at $\sim 1650\text{ cm}^{-1}$ indicating the presence of the protein.	97

Figure 5.11 ATR-FTIR results on the lysozyme adsorption to the bare Ge interface, symmetric dipped DPPC bilayer and the DPPC bilayer formed by vesicles spreading.	99
Figure 5.12 ATR-FTIR results on the β -Pth adsorption to the symmetric dipped DPPC bilayer (left) showing spectra of: 1) the lipid bilayer before injection, 2) right after injection, 3) 1 h after injection, 4) 2 h after injection, 5) 24 h after injection and to the asymmetric dipped DPPC:DPSP bilayer (right) showing spectra of: 1) the lipid bilayer before injection, 2) right after injection, 3) 1 h after injection, 4) 2 h after injection and 5) 24 h after injection. The two peaks of interest shown are the carbonyl stretch at $\sim 1750\text{ cm}^{-1}$ indicating the presence of the phospholipid and the Amide I band at $\sim 1650\text{ cm}^{-1}$ indicating the presence of the protein and the PS headgroup.	100
Figure 5.13 ATR-FTIR spectra showing the α_2 -Pth (left) and Pin-a (right) adsorption to the symmetric dipped DPPC:DPSP bilayer: 1) the lipid bilayer before injection, 2) right after injection, 3) 1 h after injection, 4) 2 h after injection, 5) 24 h after injection. The two peaks of interest shown are the carbonyl stretch at $\sim 1750\text{ cm}^{-1}$ indicating the presence of the phospholipid and the Amide I band at $\sim 1650\text{ cm}^{-1}$ indicating the presence of the protein and the PS headgroup.	100
Figure 5.14 ATR-FTIR results on the wheat defence proteins adsorption to the dipped DPPC:DPSP bilayer.	101
Figure 6.1 Compression isotherms of the d-DPPC monolayer showing good repeatability of the compression and expansion processes, indicating high purity of the lipid film.	107
Figure 6.2 Pressure-Area isotherm showing the Langmuir-Blodgett dip of the silicon block being covered with a d-DPPC monolayer.	108
Figure 6.3 Compression isotherms of the h-DPSP monolayer, showing the overall good repeatability of the compression and expansion processes, indicating the high quality of the lipid film.	109

Figure 6.4 Isotherm showing the Langmuir-Schaeffer dip of the silicon block being covered with the outer leaflet lipid mixture h-DPPS:ergosterol 1:1 mol:mol. The marked point indicates the moment of the direct contact of the silicon block's covered surface with the lipid monolayer.	109
Figure 6.5 Neutron reflectivity profiles (left) and the fits describing these profiles (right) of the asymmetrically deposited d-DPPC: h-DPPS bilayer obtained in the three isotopic contrasts: 100% D ₂ O (blue line), silicon-SLD-matched water containing 38% D ₂ O (green line) and 100% H ₂ O (red line).	116
Figure 6.6 NR reflectivity profiles (1 – 6) and the fits describing these profiles (7 – 8) for the asymmetrically deposited h-DPPC:h-DPPS bilayer on its own (1,3,5,7) and interacting with 0.01 mg/mL β-Pth solution (2,4,6,8) obtained in the three isotopic contrasts: 100% D ₂ O (blue line), silicon-SLD-matched water containing 38% D ₂ O (green line) and 100% H ₂ O (red line).	118
Figure 6.7 Neutron reflectivity profiles (left) and the fits describing these profiles (right) of the asymmetrically deposited d-DPPC:(h-DPPS:d-DPPC 1:1 mol/mol) bilayer obtained in the three isotopic contrasts: 100% D ₂ O (blue line), silicon-SLD-matched water containing 38% D ₂ O (green line) and 100% H ₂ O (red line).	121
Figure 6.8 NR reflectivity profiles (1 – 6) and the fits describing these profiles (7 – 8) for the asymmetrically deposited h-DPPC:h-DPPS bilayer on its own (1,3,5,7) and interacting with 0.01 mg/mL β-Pth solution (2,4,6,8) obtained in the three isotopic contrasts: 100% D ₂ O (blue line), silicon-SLD-matched water containing 38% D ₂ O (green line) and 100% H ₂ O (red line).	122
Figure 6.9 Neutron reflectivity profiles (left) and the fits describing these profiles (right) of the asymmetrically deposited d-DPPC:h-POPS bilayer obtained in the three isotopic contrasts: 100% D ₂ O (blue line), silicon-SLD-matched water containing 38% D ₂ O (green line) and 100% H ₂ O (red line).	126
Figure 6.10 NR profiles of the d-DPPC:h-POPS bilayer recorded immediately after the protein injection (left) and the summary of the changes in the profile (right) showing the kinetics of the protein's interaction with the bilayer.	127

- Figure 6.11 NR profiles of the h-DPPC:h-POPS bilayer recorded immediately after the protein injection (left) and the summary of the changes in the profile (right) showing the kinetics of the protein's interaction with the bilayer. 127
- Figure 6.12 NR reflectivity profiles (1 – 6) and the fits describing these profiles (7 – 8) for the asymmetrically deposited h-DPPC:h-POPS bilayer on its own (1,3,5,7) and interacting with 0.01 mg/mL β -Pth solution (2,4,6,8) obtained in the three isotopic contrasts: 100% D₂O (blue line), silicon-SLD-matched water containing 38% D₂O (green line) and 100% H₂O (red line). 128
- Figure 6.13 Neutron reflectivity profiles (left) and the fits describing these profiles (right) of the asymmetrically deposited d-DPPC:(h-DPPC:h-POPS 1:1 mol/mol) bilayer obtained in the three isotopic contrasts: 100% D₂O (blue line), silicon-SLD-matched water containing 38% D₂O (green line) and 100% H₂O (red line). 132
- Figure 6.14 NR reflectivity profiles (1 – 6) and the fits describing these profiles (7 – 8) for the asymmetrically deposited h-DPPC:(h-DPPC:h-POPS 1:1 mol/mol) bilayer on its own (1,3,5,7) and interacting with 0.02 mg/mL β -Pth solution (2,4,6,8) obtained in the three isotopic contrasts: 100% D₂O (blue line), silicon-SLD-matched water containing 38% D₂O (green line) and 100% H₂O (red line). 133
- Figure 6.15 NR reflectivity profiles (1 – 6) and the fits describing these profiles (7 – 8) for the asymmetrically deposited d-DPPC:(h-DPPS:ergosterol 1:1 mol/mol) bilayer on its own (1,3,5,7) and interacting with 0.02 mg/mL β -Pth solution (2,4,6,8) obtained in the three isotopic contrasts: 100% D₂O (blue line), silicon-SLD-matched water containing 38% D₂O (green line) and 100% H₂O (red line). 137
- Figure 6.16 Neutron reflectivity profiles (left) and the fits describing these profiles (right) of the asymmetrically deposited d-DPPC:h-DPPS bilayer obtained in the three isotopic contrasts: 100% D₂O (blue line), silicon-SLD-matched water containing 38% D₂O (green line) and 100% H₂O (red line). 140
- Figure 6.17 NR reflectivity profiles (1 – 6) and the fits describing these profiles (7 – 8) for the asymmetrically deposited h-DPPC:h-DPPS bilayer on its own 142

(1,3,5,7) and interacting with 0.025 mg/mL Pin-a solution (2,4,6,8) obtained in the three isotopic contrasts: 100% D₂O (blue line), silicon-SLD-matched water containing 38% D₂O (green line) and 100% H₂O (red line).

Figure 6.18 Neutron reflectivity profiles (left) and the fits describing these profiles (right) of the asymmetrically deposited d-DPPC:h-DPPS bilayer obtained in the three isotopic contrasts: 100% D₂O (blue line), silicon-SLD-matched water containing 38% D₂O (green line) and 100% H₂O (red line). 144

Figure 6.19 NR reflectivity profiles (1 – 6) and the fits describing these profiles (7 – 8) for the asymmetrically deposited h-DPPC:h-DPPS bilayer on its own (1,3,5,7) and interacting with (Pin-a:β-Pth 1:1 mol:mol 0.0125:0.005 mg/mL) solution (2,4,6,8) obtained in the three isotopic contrasts: 100% D₂O (blue line), silicon-SLD-matched water containing 38% D₂O (green line) and 100% H₂O (red line). 146

Figure 7.1 Size distribution by number of the DPPC vesicles: MLVs (green) obtained after five freeze-thawing cycles and SUVs (red) obtained after 2 hours of sonication at 45°C. 154

Figure 7.2 DSC measurements of β-Pth added to the DPPS MLVs in 1:10 protein:lipid molar ratio (red line) and of the DPPS MLVs on their own (blue line) without vortexing (left plot) and with vortexing (right plot). 155

Figure 7.3 DSC measurements of the DPPC:DPPS 1:1 mol:mol MLVs. Dates and repeats of the experiments are shown in the legend. 157

Figure 7.4 DSC measurements of β-Pth added to the DPPC:DPPS 1:1 mol:mol MLVs in 1:100 protein:lipid molar ratio. The numbers of repeats are shown in the legend. 157

Figure 7.5 DSC measurements of β-Pth added to the DPPC MLVs (batch 1) in various molar ratios. 158

Figure 7.6 DSC measurements of β-Pth added to the DPPC MLVs (batch 2) in 1:10 protein:lipid molar ratio. 159

Figure 7.7 DSC measurements of β -Pth added to the DPPS MLVs in various protein:lipid molar ratios.	160
Figure 7.8 DSC measurements of β -Pth added to the DPPC:DPPS 1:1 mol:mol MLVs in various protein:lipid molar ratios.	161
Figure 7.9 DSC measurements of various wheat defence proteins added to the DPPS MLVs in 1:10 protein:lipid molar ratios.	162
Figure 7.10 DSC thermograms of the DPPC SUVs (blue line) and DPPC SUVs interacting with β -Pth in 1:10 protein:lipid molar ratio. ¹⁸⁰	163
Figure 7.11 DSC thermograms of the DPPS SUVs (blue line) and DPPS SUVs interacting with β -Pth in 1:10 protein:lipid molar ratio. ¹⁸⁰	164
Figure 7.12 DSC thermograms of the DPPS:DPPC 1:1 mol:mol SUVs (blue line) and DPPS:DPPC 1:1 mol:mol SUVs interacting with β -Pth in 1:10 protein:lipid molar ratio (green line). ¹⁸⁰	164
Figure 1. FPLC elution profiles showing the purification of Pin-a from the crude wheat flour extracts, carried out by Luke Clifton (A), ⁸⁰ Michael Sanders (B) ¹³³ and Olga Florek (C). Pin-a peaks marked with red circle.	173
Figure 2. SDS-PAGE results of the Pin-a purification peaks corresponding to the chromatograms in Figure 1, obtained by Luke Clifton (A), ⁸⁰ Michael Sanders (B) ¹³³ and Olga Florek (C). Pin-a bands marked with red circle.	174
Figure 3. RP-HPLC chromatograms showing the purothionin purification by Michael Sanders (A) ¹³³ and Olga Florek (B).	175
Figure 4. Deconvoluted mass spectrum from raw data for β -Pth indicating the purity of the mass fragments. ¹³³	175
Figure 5. Deconvoluted mass spectrum of Pin-a corresponding to peak 1 in Figure 1 C and indicating the purity of the mass fragments.	176

LIST OF TABLES

Table 1.1 Primary structures of the defence proteins isolated from wheat – underlined: amino acids conserved in all proteins, red: conserved amino acids of the three thionins, green: conserved amino acids of the two defensins.	7
Table 1.2 Phospholipid composition of the yeast cell membrane – study by Zinser <i>et al.</i> ⁷¹	11
Table 1.3 Summary of the data on the proteins used in the experiments. Hydrophobic amino acids are marked bold and basic amino acids are marked red. The 3-D models were generated at www.proteinmodelportal.org using the protein sequences, therefore there is no tryptophan-rich loop (underlined in the sequence) shown in the Pin-a three-dimensional structure.	16
Table 2.1 Techniques used to study the protein-lipid interactions and the information provided by each technique.	21
Table 2.2 Summary of the XRR data used for the analysis.	27
Table 2.3 Summary of the NR data used for the analysis.	35
Table 4.1 Experimental conditions of the surface pressure measurements: lysozyme <i>vs.</i> condensed phase DPPG monolayer.	57
Table 4.2 Summary of the experiment results of the lysozyme interacting with condensed phase DPPG monolayers using two different trough volumes. The P value corresponds to the result of an independent 2-tailed t-test.	58
Table 4.3 Experimental conditions of the surface pressure measurements: β -Pth <i>vs.</i> condensed phase saturated phospholipid monolayers.	62
Table 4.4 Summary of the monolayer experiments of β -Pth (final concentration in the subphase 0.48 μ M) interacting with saturated phospholipid systems. An independent 2-tailed t-test showed significant differences at $P \leq 0.05$.	64

Table 4.5 Summary of the monolayer experiments of β -Pth (final concentration in the subphase 0.48 μ M) interacting with the saturated and unsaturated lipid systems. An independent 2-tailed t-test showed significant differences at $P \leq 0.05$.	67
Table 4.6 Summary of the monolayer experiments of β -Pth, Pin-a and their 1:1 mol:mol mixture interacting with condensed DPPS monolayers. An independent 2-tailed t-test was used for indicating the significant differences (marked bold) at $P \leq 0.05$.	68
Table 4.7 Summary of the monolayer experiments of β -Pth, α_2 -Pth and their 1:1 mol:mol mixture interacting with condensed DPPS monolayers. An independent 2-tailed t-test was used for indicating the significant differences at $P \leq 0.05$.	69
Table 4.8 Fitting parameters obtained for the XRR experiment on β -Pth adsorption to the condensed phase DPPS monolayers.	76
Table 4.9 Fitting parameters obtained for the XRR experiment on β -Pth adsorption to the condensed phase POPS monolayers.	80
Table 5.1 Summary of the fitting parameters obtained for the double POPS bilayer experiment. The SLD values were kept constant and only the hydration parameter varied. The SLD values with no uncertainties were kept constant throughout the process of data fitting.	90
Table 5.2 Summary of the ATR-FTIR experiments on the lysozyme adsorption.	98
Table 5.3 Summary of the ATR-FTIR results on the wheat defence proteins adsorption to the dipped DPPC:DPPS bilayer. An independent 2-tailed t-test was used for indicating the significant differences (marked bold) at $P \leq 0.05$.	102
Table 6.1 Composition of the d-DPPC: h-DPPS bilayer showing the mixing of the lipids between the two leaflets. The water content values do not take into account the hydration levels of the phospholipid headgroups.	116
Table 6.2 Results of the NR experiment on 0.01 mg/mL β -Pth interacting with the h-DPPC:h-DPPS lipid bilayer. The SLD values with no uncertainties were kept constant throughout the process of data fitting.	119

Table 6.3 Summary of the NR experiment on 0.01 mg/mL β -Pth interacting with the h-DPPC:h-DPPS lipid bilayer.	120
Table 6.4 Composition of the d-DPPC:(h-DPPS:d-DPPC 1:1 mol/mol) bilayer showing the mixing of the lipids between the two leaflets. The water content values do not take into account the hydration levels of the phospholipid headgroups.	121
Table 6.5 Results of the NR experiment on 0.01 mg/mL β -Pth interacting with the h-DPPC:(h-DPPS:h-DPPC 1:1 mol/mol) lipid bilayer. The SLD values with no uncertainties were kept constant throughout the process of data fitting.	124
Table 6.6 Summary of the NR experiment on 0.01 mg/mL β -Pth interacting with the h-DPPC:(h-DPPS:h-DPPC 1:1 mol/mol) lipid bilayer.	125
Table 6.7 Composition of the d-DPPC:h-POPS bilayer showing the mixing of the lipids between the two leaflets. The water content values do not take into account the hydration levels of the phospholipid headgroups.	126
Table 6.8 Results of the NR experiment on 0.01 mg/mL β -Pth interacting with the h-DPPC:h-POPS lipid bilayer. The SLD values with no uncertainties were kept constant throughout the process of data fitting.	130
Table 6.9 Summary of the NR experiment on 0.01 mg/mL β -Pth interacting with the h-DPPC:h-POPS lipid bilayer.	131
Table 6.10 Composition of the d-DPPC:(h-DPPC:h-POPS 1:1 mol/mol) bilayer showing the mixing of the lipids between the two leaflets. The water content values do not take into account the hydration levels of the phospholipid headgroups.	132
Table 6.11 Results of the NR experiment on 0.02 mg/mL β -Pth interacting with the h-DPPC:(h-DPPC:h-POPS 1:1 mol/mol) lipid bilayer. The SLD values with no uncertainties were kept constant throughout the process of data fitting.	135
Table 6.12 Summary of the NR experiment on 0.02 mg/mL β -Pth interacting with the h-DPPC:h-POPS lipid bilayer.	136

Table 6.13 Composition of the d-DPPC:(h-DPPS:ergosterol 1:1 mol/mol) bilayer showing the mixing of the lipids between the two leaflets. The water content values do not take into account the hydration levels of the phospholipid headgroups.	136
Table 6.14 Summary of the NR experiment on 0.02 mg/mL β -Pth interacting with the d-DPPC:(h-DPPS: ergosterol 1:1 mol/mol) lipid bilayer.	138
Table 6.15 Results of the NR experiment on 0.02 mg/mL β -Pth interacting with the d-DPPC:(h-DPPS: ergosterol 1:1 mol/mol) lipid bilayer. The SLD values with no uncertainties were kept constant throughout the process of data fitting.	139
Table 6.16 Composition of the d-DPPC:h-DPPS bilayer showing the mixing of the lipids between the two leaflets. The water content values do not take into account the hydration levels of the phospholipid headgroups.	141
Table 6.17 Summary of the NR experiment on 0.025 mg/mL Pin-a interacting with the h-DPPC:h-DPPS lipid bilayer.	141
Table 6.18 Results of the NR experiment on 0.025 mg/mL Pin-a interacting with the h-DPPC:h-DPPS lipid bilayer. The SLD values with no uncertainties were kept constant throughout the process of data fitting.	143
Table 6.19 Composition of the d-DPPC:h-DPPS bilayer showing the mixing of the lipids between the two leaflets. The water content values do not take into account the hydration levels of the phospholipid headgroups.	145
Table 6.20 Summary of the NR experiment on (Pin-a: β -Pth 1:1 mol:mol 0.0125:0.005 mg/mL) solution interacting with the h-DPPC:h-DPPS lipid bilayer.	145
Table 6.21 Results of the NR experiment on (Pin-a: β -Pth 1:1 mol:mol 0.0125:0.005 mg/mL) solution interacting with the h-DPPC:h-DPPS lipid bilayer. The SLD values with no uncertainties were kept constant throughout the process of data fitting.	147
Table 6.22 Summary of the NR bilayer experiments showing the properties of the analysed lipid systems and the protein effect on their structure.	149
Table 8.1 Summary of the information gathered from all experiments in the study.	168

Table 1. Neutron scattering length values of the elements appearing in this study.	172
Table 2. Volumes of the bonds and functional groups used for calculating the scattering length densities of the molecules.	172

Chapter 1

INTRODUCTION AND THE AIM OF THE PROJECT

The increased crop productivity is one of the aims of the agricultural development. New strategies are applied to produce food of the improved quality. Among the measures taken are: the use of artificially selected plant varieties that are more resistant to diseases, efficient agricultural practice such as crop rotation or the use of fertilizers and pesticides. However, many of these actions have shown undesirable side effects such as environmental pollution. These inconveniences gave rise to the development in studies oriented at finding natural ways of boosting plant immunity to infections.

Plants, as most living organisms, are constantly exposed to microbial attack or injury, to which they have developed efficient physical barriers such as a surface layer of wax or a thick cell wall. Moreover, plants are able to respond chemically to these adverse conditions by synthesising antimicrobial compounds, among which are saponins (glycosylated steroids), cyanogenic glycosides, phenolic compounds and defence proteins / peptides.^{1,2} The latter ones are of a growing interest due to their potential use as natural biocidal agents.

In general, the antimicrobial peptides share the following features:³

- (1) Relatively small size – they have low molecular weight (less than 7 kDa).
- (2) Positive charge at neutral pH – characterised by the presence of basic amino acids in their structures.
- (3) Amphipathicity - value of the polar/non-polar amino acid usually from 0.5 to 1.2.
- (4) They adopt a secondary structure stabilized by disulphide bridges.
- (5) They are believed to act at the membrane level of the invaded cells and their biological activity appears to have its origin in their sequence and structural characteristics.

The antimicrobial activity of the peptides was examined in many studies. For example, cecropin A, a peptide isolated from the Cecropia moth (*Hyalophora cecropia*), was shown to be lethal to the selected pathogenic fungal species from the genera *Aspergillus* and *Fusarium*, when introduced to the solution containing the conidia of the aforementioned fungi.⁴

Moreover, the expression of the gene coding the insect-derived antimicrobial peptide thanatin(S) in the *Arabidopsis thaliana* plants supported the host's resistance to pathogenic fungi *Botrytis cinerea*, powdery mildew, and pathogenic bacteria *Pseudomonas syringae*.⁵

Therefore, the defence proteins and peptides could serve not only as the environmentally friendly enhancers of the plants' immunity against the phytopathogens but they could also find their application *in vitro*: as preservatives or pharmaceutical antimicrobial agents.

1.1 Plant defence proteins

There are many types of the plant defence proteins and they can be isolated from various parts of the plant.⁶ Most of these proteins, however, were found to be located in the seeds.⁷ This project focused on the defence proteins isolated from the grains of the common wheat, *Triticum aestivum* (see the grain structure in Figure 1.1). The wheat defence proteins can be classified into the following groups: thionins, indolines, defensins and lipid-transfer proteins.²

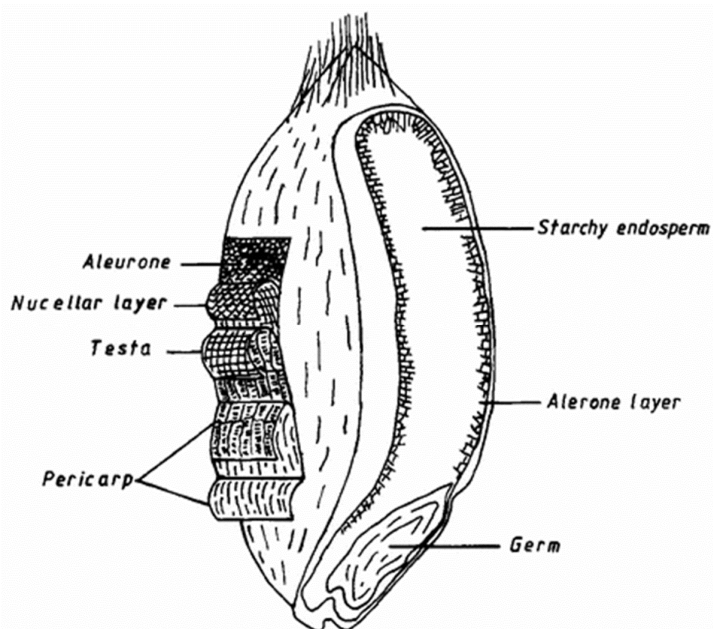


Figure 1.1 A scheme of the wheat grain showing aleurone and endosperm: the structures from which the wheat defence proteins were isolated [reproduced by kind permission of Springer Science and Bus Media B V via RightsLink, 17.03.2017].⁸

The first three protein families, all isolated from wheat endosperm,² will be the subject of this study. To simplify further discussion, the low-molecular-weight peptides, such as thionins and defensins, will be referred to as proteins throughout this work.

1.1.1 Thionins

Thionins are a family of basic ($pI > 8$), cysteine-rich and low-molecular-weight (~ 5 kDa) proteins sharing high sequential and structural similarities.⁹ They are divided into 5 groups.

Type I are 45 amino acids long, basic and contain eight cysteine residues, and were first reported in the wheat grain endosperm.¹⁰ Three different type I purothionins from wheat have been isolated: α_1 , α_2 , and β .^{11,12} Type II thionins were first extracted from barley leaves (α -hordothionin and β -hordothionin) and are slightly less basic than type I, typically 46-47 amino acids long with four disulphide bonds.¹³ Type III are 45-46 amino acids and were found in stems and leaves of mistletoe species.¹⁴ Crambin, isolated from seeds of *Crambe abyssinica*, is a representative of the type IV thionins – it is neutral, 46 amino acids long and has three disulphide bonds.¹⁵ Type V thionin has been isolated from wheat endosperm and shares some structural similarities with type I.¹⁶

Thionins were shown to act against wide range of pathogenic organisms.² For example, purothionins were shown to be inhibiting the growth of the phytopathogenic bacteria from the genera *Pseudomonas*, *Xanthomonas*, *Erwinia*, and *Corynebacterium*.¹⁰ Another group of organisms susceptible to the biocidal action of purothionins were the yeast of the *Saccharomyces* genera cultivated in various media.¹⁷ Moreover, purothionins caused membrane leakages in the mammalian cell cultures, *i.e.* baby hamster kidney cells.¹⁸ The biocidal properties of purothionins were further stressed in the study by Kramer *et al.*,¹⁹ who found that the proteins caused high mortality of the tobacco hornworm's (*Manduca sexta*) larvae. Furthermore, expressing the gene coding for the barley thionin α -hordothionin in the transgenic tobacco plant resulted in the increased plant's immunity against the bacterial plant pathogen *Pseudomonas syringae*.²⁰ This study confirmed the protective role of thionins *in vivo*.

The structure of purothionins resembles the letter L (see Table 1.3) – a molecule consists of two antiparallel α -helices (forming a helix-turn-helix motif), a C-terminal coil and two short antiparallel β strands (which form one antiparallel β -sheet) - their tertiary structure is

stabilised by four disulphide bonds, salt bridges and intramolecular hydrogen bonds.²¹ The groove between the α -helices and β -sheets contains a Tyr13 residue which is believed to play an important role in cell leakage.¹⁸ Wada *et al.*²² have suggested the involvement of positive charge in thionins' mode of action; it has been noted that a decrease of the positive charge leads to a reduction of the toxicity, in proportion to the number of modified groups.

A few hypotheses have been proposed regarding the mechanisms of thionins' toxicity, *e.g.* formation of ion channels,²³ lipid rafts²⁴ and solubilisation of membrane phospholipids.²⁵ Moreover, there are studies with model membranes,²⁶ proposing solubilisation to be the cause of membrane leakage.

Furthermore, studies on the interaction of β -Pth with bacterial lipid membranes models have shown that it is able to penetrate deeply into the lipid acyl chain regions of condensed phase anionic lipid monolayers.²⁷ This finding could support the formation of ion channels by the thionins (proposed above),²³ by considering the protein penetration as the initial stage of the pore formation. This work also stressed the importance of the role of the wheat defence protein's structure in the adsorptive properties towards the anionic phospholipids by revealing the differences in the penetrative abilities of β -Pth, Pin-a and Pin-b (see section 1.1.2 for more information on the latter two proteins).²⁷

The study by Richard *et al.*²⁸ confirmed the importance of the initial electrostatic attraction of β -Pth towards the anionic saturated phospholipids in the protein-lipid interactions and revealed that the protein decreases the lipid's lateral diffusion in the anionic phospholipid bilayer.

The molecular structure of purothionins and, in particular, their hydrophobicity, has been shown to play an important role in the proteins' ability to interact with the anionic phospholipids, *i.e.* the more hydrophobic α_2 -Pth removed more phospholipid from interfacial monolayers than α_1 -Pth, as revealed by the Neutron Reflectometry (NR) and Brewster Angle Microscopy (BAM) monolayer studies carried out by Clifton *et al.*²⁹

The thionins from barley were shown to cooperate with the barley lipid-transfer-proteins in their antifungal activity towards *Fusarium solani* cultures.³⁰ For the findings on the synergy between the thionins and indolines, please refer to section 1.1.2.

1.1.2 Puroindolines

Puroindolines (Pins) are basic, cysteine-rich, lipid-binding family of the wheat defence proteins having molecular weight of ~ 13 kDa.³¹ Two puroindoline isoforms are known, Pin-a and Pin-b, both containing a Trp-rich domain which is believed to be the site of interaction with lipid membranes (see Figure 1.3).³² Pin-a domain consists of five Trp residues (WRWKKWK), whereas Pin-b has a truncated domain containing three Trp residues (WPTKWK).^{33,34} The infrared studies revealed that Pin-a and Pin-b have similar secondary structure: at pH 7 they consist of approximately 30% α -helices, 30% β -sheets and 40% unordered structures.³⁵ For the more detailed structure of Pin-a, please refer to Figure 1.8.

The proteins' structure is stabilised by the presence of disulphide bridges created by the covalent bonds between the cysteine residues.³⁶ Figure 1.2 shows the putative positions of the disulphide bridges.

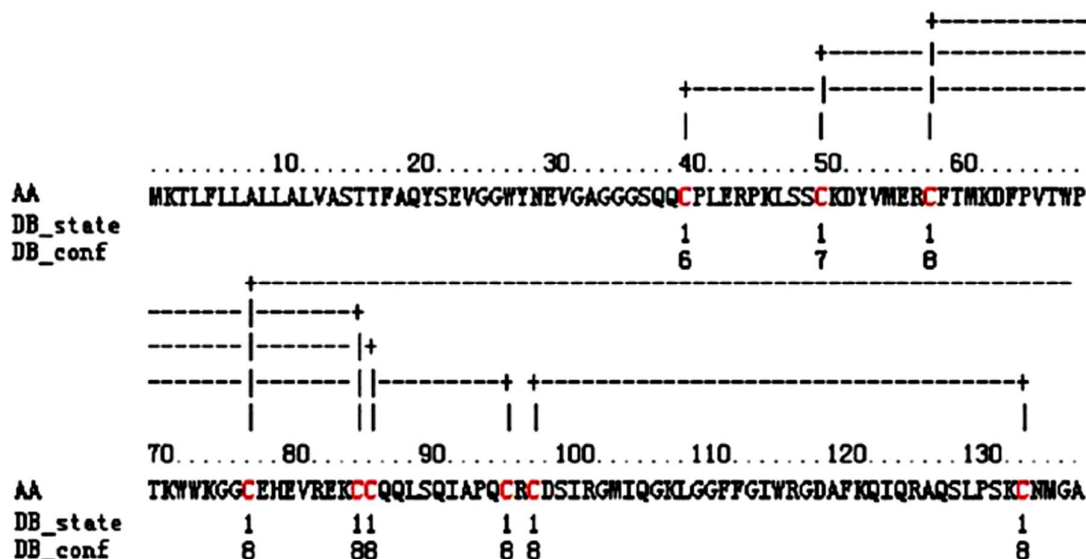


Figure 1.2 The predicting results of disulfide bonding state of Pin-b. AA, amino acid sequence; DB_state, predicted disulfide bonding state (1 = disulfide bonded, 0 = not disulfide bonded); DB_conf, confidence of disulfide bonding state prediction (0 = low to 9 = high).³⁷

Puroindolines have been reported to act against fungi as well as Gram-positive and Gram-negative bacteria.³⁸ For instance, Capparelli *et al.*³⁹ revealed the antimicrobial activity of the recombinant puroindolines against *Escherichia coli* and *Staphylococcus aureus* strains. The findings by Jing *et al.*⁴⁰ stressed the importance of the Trp-rich domain in the antimicrobial activity of Pins against the aforementioned bacterial strains.

These proteins have also been shown to bind preferentially to anionic phospholipids⁴¹ and are known to contribute to the wheat texture, which is an important flour quality determinant.^{42,43} Puroindolines were discovered as part of friabilin, a protein complex believed to mediate the grain hardness by controlling adhesion of the starch-gluten interface.⁴⁴ Pin-a and Pin-b proteins were later distinguished from the friabilin complex as the compounds directly contributing to the grain hardness.⁴⁵

An allelic variation in Pin-b gene (*Pinb-D1b*) leads to the formation of Pin-b mutant forms such as Pin-bH, found in Hereward wheat variety (containing Gly-46 to Ser-46 substitution) or the Soissons-wheat-variety-derived Pin-bS (Trp-44 to Arg-44 mutation), which apparently influence grain hardness, although the precise mechanism for this remains unsolved.^{46,47,48}

Differences in the primary structure of Trp-rich loops between the three forms of Pin-b are illustrated below.

	29		48
Pin-b	C	F T M K D F P V T W P T K W W K G G C	
Pin-bH	C	F T M K D F P V T W P T K W W K <u>S</u> G C	
Pin-bS	C	F T M K D F P V T W P T K W <u>R</u> K G G C	

Figure 1.3 Sequences of the Trp-rich loops of the wild-type Pin-b and the mutants Pin-bH and Pin-bS.⁴⁹

Such point mutations also affect the level of interactions with lipid membranes, which has been demonstrated by surface pressure measurements carried out by Clifton *et al.*⁵⁰ Pin-bS mutant appeared to penetrate the lipid membranes to a lesser extent than the wild-type Pin-b.⁵⁰ Similar conclusion was drawn from the Neutron Reflectometry study by Sanders *et al.* (2016).⁵¹

The point mutation has been also shown to have a significant effect on synergistic interaction between Pin-a and Pin-b during the lipid membrane penetration.⁵² Further investigation of the puroindoline-lipid interactions revealed that Pins form a protein layer below the lipid surface of approximately 35 Å thickness.^{27,49,50}

Sanders *et al.* (2013)⁵³ have examined the possibility of the synergistic lipid binding properties between Pins and β-Pth: the obtained results have not shown evidence of strong synergy. Instead, the proteins' behaviour resembled a competitive mechanism depicting

differences in lipid binding modes between Pin and Pth families.⁵³ This inconsistency with the findings by Dubreil *et al.*,³⁸ who observed the synergy between the puroindolines and purothionins could be explained by the fact that Sanders *et al.* used the simple models of bacterial membranes, whereas Dubreil *et al.* focused their research on the antifungal action of the proteins by directly exposing the fungal strains to the protein solutions. Moreover, Dubreil *et al.* used α -purothionin as a representative thionin, whereas the reports by Sanders *et al.* base on the synergy between β -Pth and Pin-a.

These differences stress the complexity of the possible cooperative mechanisms between the puroindolines and purothionins and will be further examined in this project.

1.1.3 Defensins

Initially classified as members of the thionins family, γ -purothionins are a group of wheat defence proteins that, due to the low degree of similarity to α_1 -, α_2 - and β -Pths (see Figure 1.4), have been assigned to a separate class - defensins.⁷ Two forms of γ -Pths have been reported and their structures revealed.⁵⁴

Table 1.1 Primary structures of the defence proteins isolated from wheat – underlined: amino acids conserved in all proteins, red: conserved amino acids of the three thionins, green: conserved amino acids of the two defensins.

α_1 -purothionin ⁵⁵	<u>K</u> <u>S</u> <u>C</u> <u>C</u> <u>R</u> <u>S</u> <u>T</u> <u>L</u> <u>G</u> <u>R</u> <u>N</u> <u>C</u> <u>Y</u> <u>N</u> <u>L</u> <u>C</u> <u>R</u> <u>A</u> <u>R</u> <u>G</u> <u>A</u> <u>Q</u> <u>K</u> <u>L</u> <u>C</u> <u>A</u> <u>G</u> <u>V</u> <u>C</u> <u>R</u> <u>C</u> <u>K</u> <u>I</u> <u>S</u> <u>S</u> <u>G</u> <u>L</u> <u>S</u> <u>C</u> <u>P</u> <u>K</u> <u>G</u> <u>F</u> <u>P</u> <u>K</u>
α_2 -purothionin ⁵⁵	<u>K</u> <u>S</u> <u>C</u> <u>C</u> <u>R</u> <u>T</u> <u>T</u> <u>L</u> <u>G</u> <u>R</u> <u>N</u> <u>C</u> <u>Y</u> <u>N</u> <u>L</u> <u>C</u> <u>R</u> <u>S</u> <u>R</u> <u>G</u> <u>A</u> <u>Q</u> <u>K</u> <u>L</u> <u>C</u> <u>S</u> <u>T</u> <u>V</u> <u>C</u> <u>R</u> <u>C</u> <u>K</u> <u>L</u> <u>T</u> <u>S</u> <u>G</u> <u>L</u> <u>S</u> <u>C</u> <u>P</u> <u>K</u> <u>G</u> <u>F</u> <u>P</u> <u>K</u>
β -purothionin ⁵⁶	<u>K</u> <u>S</u> <u>C</u> <u>C</u> <u>K</u> <u>S</u> <u>T</u> <u>L</u> <u>G</u> <u>R</u> <u>N</u> <u>C</u> <u>Y</u> <u>N</u> <u>L</u> <u>C</u> <u>R</u> <u>A</u> <u>R</u> <u>G</u> <u>A</u> <u>Q</u> <u>K</u> <u>L</u> <u>C</u> <u>A</u> <u>N</u> <u>V</u> <u>C</u> <u>R</u> <u>C</u> <u>K</u> <u>L</u> <u>T</u> <u>S</u> <u>G</u> <u>L</u> <u>S</u> <u>C</u> <u>P</u> <u>K</u> <u>D</u> <u>F</u> <u>P</u> <u>K</u>
γ_1 -purothionin ⁵⁴	<u>K</u> <u>I</u> <u>C</u> <u>R</u> <u>R</u> <u>R</u> <u>S</u> <u>A</u> <u>G</u> <u>F</u> <u>K</u> <u>G</u> <u>P</u> <u>C</u> <u>W</u> <u>S</u> <u>W</u> <u>K</u> <u>N</u> <u>C</u> <u>A</u> <u>Q</u> <u>V</u> <u>C</u> <u>Q</u> <u>Q</u> <u>E</u> <u>G</u> <u>W</u> <u>G</u> <u>G</u> <u>G</u> <u>N</u> <u>C</u> <u>D</u> <u>G</u> <u>P</u> <u>F</u> <u>R</u> <u>R</u> <u>C</u> <u>K</u> <u>C</u> <u>I</u> <u>R</u> <u>Q</u> <u>C</u>
γ_2 -purothionin ⁵⁴	<u>K</u> <u>V</u> <u>C</u> <u>R</u> <u>Q</u> <u>R</u> <u>S</u> <u>A</u> <u>G</u> <u>F</u> <u>K</u> <u>G</u> <u>P</u> <u>C</u> <u>V</u> <u>S</u> <u>D</u> <u>K</u> <u>N</u> <u>C</u> <u>A</u> <u>Q</u> <u>V</u> <u>C</u> <u>L</u> <u>Q</u> <u>Q</u> <u>E</u> <u>G</u> <u>W</u> <u>G</u> <u>G</u> <u>G</u> <u>N</u> <u>C</u> <u>D</u> <u>G</u> <u>P</u> <u>F</u> <u>R</u> <u>R</u> <u>C</u> <u>K</u> <u>C</u> <u>I</u> <u>R</u> <u>Q</u> <u>C</u>

Many defensins exhibit powerful antifungal properties,^{57,58} which makes them another point of interest of this project.

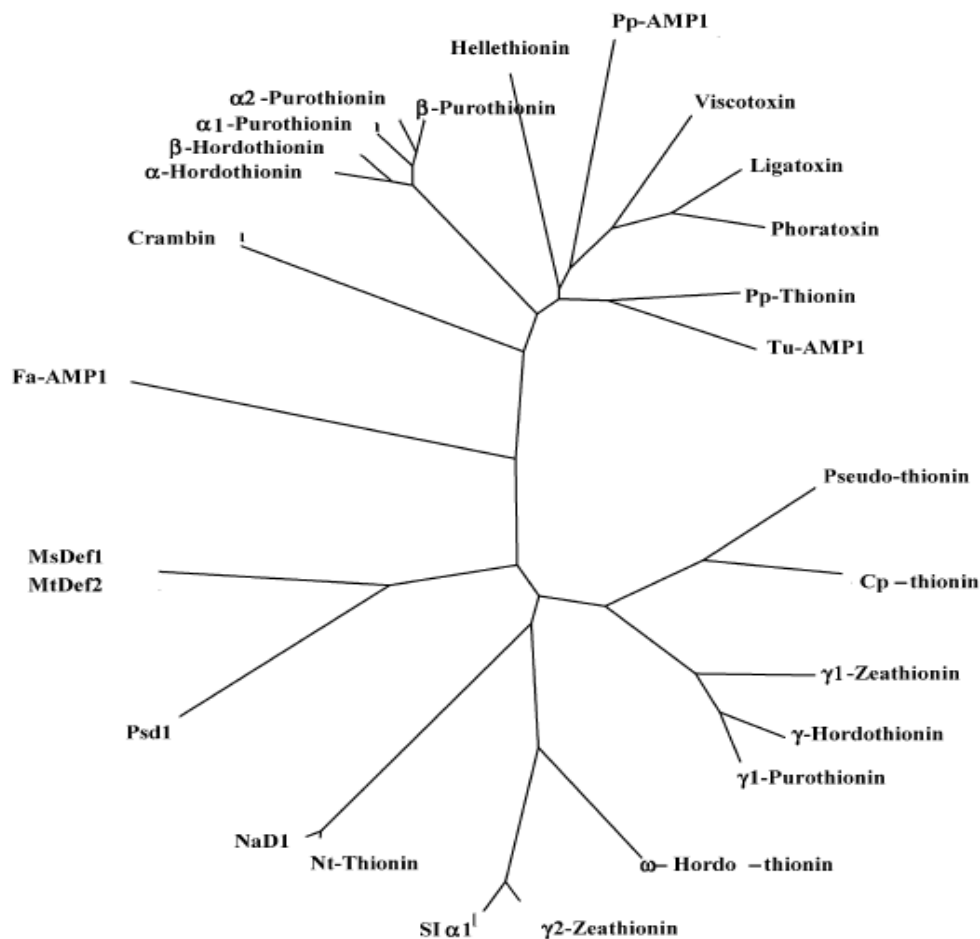


Figure 1.4 Evolutionary phylogenetic tree of the plant thionins and defensins [reproduced by kind permission of Elsevier via Rightslink, 15.03.2017].⁵⁹

1.2 Possible modes of antimicrobial action

A common idea of the antimicrobial activity of the defence proteins is their initial binding to lipid membranes which is believed to occur *via* electrostatic interactions.⁶⁰ Further events depend on the protein-lipid system and are the subject of many studies.⁶⁰ Several concepts have been proposed to describe the mode of the biocidal activity of various proteins and among them are barrel-stave, toroid pore (also referred to as toroidal or wormhole mechanism⁶¹) and carpet mechanisms,⁶⁰ as illustrated in Figure 1.5.

The barrel-stave concept, first described by Ehrenstein and Lecar,⁶² assumes that after binding to a lipid, the protein undergoes transition forcing lipids aside leading to local membrane thinning. Afterwards, the hydrophobic part of the protein inserts itself into the

membrane. More protein molecules aggregate and form a pore thanks to which more protein can enter the cell.

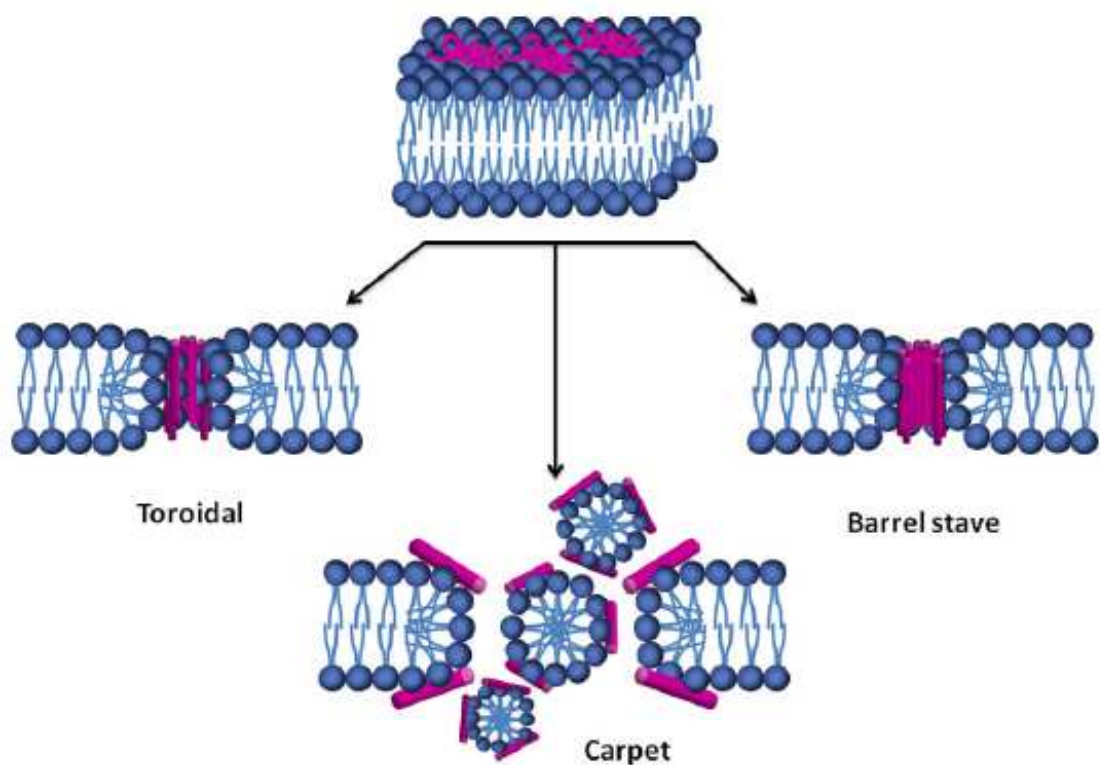


Figure 1.5 Cartoon representation of the three modes of altering membrane permeability by antimicrobial proteins illustrating a barrel-stave mechanism, toroid pore mechanism and carpet mechanism.⁶³

In the toroid pore mechanism, used by Matsuzaki *et al.*⁶⁴ to describe the action of magainin, the protein orientates itself parallel to the lipid membrane causing a strain and disruption of an outer leaflet. When the threshold concentration is reached, protein changes its position to perpendicular to the membrane and becomes finally intercalated between the lipids, which gives rise to a transmembrane channel formation.

The carpet mechanism, introduced to describe the action of dermaseptin,⁶⁵ assumes initial accumulation of the protein at the membrane. After the threshold concentration of the protein is reached, the unfavourable energetics leads to loss of membrane integrity which finally results in dissolution of the membrane.

However, as the above models were proposed by observing a few groups of antimicrobial proteins, the behaviour of the proteins analysed in this project can be described by alternative concepts.

1.3 Fungal membrane models

To examine the protein-lipid interactions, one needed to develop model membrane systems which would represent a cellular envelope of a fungus. Sanders *et al.* (2016)⁵¹ revealed the dependence of the wheat defence proteins' adsorptive properties on the lipid composition of the bacterial membrane models. This topic will be expanded in this project using the fungal membrane models. This subsection presents the reasoning behind the choice of the analysed lipid membrane systems.

A representative organism of the fungal plasma membrane structure was baker's yeast *Saccharomyces cerevisiae* – a species frequently selected as a research tool due to the relative simplicity of its lipidome and uncomplicated growth requirements.⁶⁶ This organism has been shown to be affected by the growth-inhibiting action of purothionins, which further justifies its use as a model for the experiments in this study.¹⁷

Yeast plasma membrane is approximately 9 nm thick and separates the other cell compartments from the external medium.⁶⁷ It is formed of a lipid bilayer with membrane proteins 'immersed' in it.⁶⁸ The lipid composition of the cell membrane is prone to change under different growth conditions.^{69,70} As a result, many studies present varying lipid compositions of the yeast plasma membrane.⁷¹⁻⁷⁴

The study by Zinser *et al.*⁷¹ was chosen to create the simple membrane models for the experiments as it provided one of the first lipid profiles of the baker's yeast membranes (see Table 1.2). The study by Martin *et al.*⁷⁵ enabled to further expand the lipid composition as it revealed the fatty acid composition of the yeast cell membrane.

The starting model for the experiments will be a simple, zwitterionic DPPC (dipalmitoylphosphatidylcholine, PC 16:0) monolayer which will create the neutral charge at the interface and the lipid's saturation will enable the dense packing of the molecules (see

Figure 1.6). In the study by Zinser *et al.*,⁷¹ the phosphatidylcholines were shown to be the second most abundant zwitterionic phospholipid group in the yeast plasma membrane and the most common in the other cellular components. The dipalmitoyl chains formed the biggest proportion of the saturated lipid fatty acids in yeast, as revealed by Martin *et al.*⁷⁵ The monolayers composed of DPPC have been widely used for the studies on the protein-lipid interactions, *e.g.* by Miano *et al.*⁷⁶

Table 1.2 Phospholipid composition of the yeast cell membrane – study by Zinser *et al.*⁷¹

Phospholipid's name	% of total phospholipid
Phosphatidylcholine – PC	16.8
Phosphatidylethanolamine - PE	20.3
Phosphatidylinositol - PI	17.7
Phosphatidylserine - PS	33.6
Cardiolipin – CL	0.2
Phosphatidic acid - PA	3.9
Others	6.9

The analogous membrane, possessing the negative charge, will be composed of the anionic DPPS (dipalmitoylphosphatidylserine, PS 16:0) molecule, as shown in the study by Zinser *et al.*⁷¹ to belong to the most abundant anionic phospholipid group in the yeast's cell membrane (see the structure of the molecule in Figure 1.6). To further examine the influence of the lipid's net charge on the interactions with the proteins, a membrane system consisting of equimolar ratios of DPPC and DPPS will be included in the experiments.

Moreover, phosphatidylcholines and phosphatidylserines are the components found in high proportions of the cell membranes of other fungi, *e.g.* selected strains of human pathogen *Candida albicans*⁷⁷ and plant pathogen ergot - *Claviceps purpurea*.⁷⁸ Therefore, the findings from the experiments on these phospholipids could contribute to the development of the natural pharmaceuticals and natural pesticides.

Another feature of the yeast cell membrane to be analysed will be its fluidity. As shown by Palma-Guerrero *et al.*,⁷⁹ this property of the fungal membrane was shown to determine the organism's sensitivity towards antimicrobial agent chitosan. Fluidity will be examined by building the membrane models containing a degree of unsaturation of the phospholipid chains. For this purpose, a partially unsaturated phospholipid POPS (1-palmitoyl-2-oleoylphosphatidylserine, PS 16:0 18:1) will be chosen to increase the chance for the interaction's visibility due to the presence of the anionic PS headgroup.⁸⁰ Moreover, POPS contains the two fatty acid chains C 16:0 and C18:1 shown to be the most common in the yeast's natural membrane.⁷⁵

The results from the experiments on the POPS system will be compared with the ones obtained for the saturated anionic analogue DPPS assuming that the introduction of two more carbon atoms in the oleoyl chains will not contribute to the difference between the results obtained for the two lipid systems (see the molecular structures in Figure 1.6).

The phospholipids containing two unsaturated fatty acid chains in their structure, *e.g.* dioleoylphosphatidylcholine (DOPC), produced very unstable monolayers (data not shown), possibly because of their adhesion to the hydrophobic polytetrafluoroethylene (PTFE) barriers and walls of the Langmuir trough (see Chapter 2, page 22) and subsequent removal of them from the air/liquid interface. Similar behaviour of such phospholipids was observed by other researchers (Luke Clifton, personal communication, October 2013). Therefore, the partially unsaturated POPS system was used for the experiments.

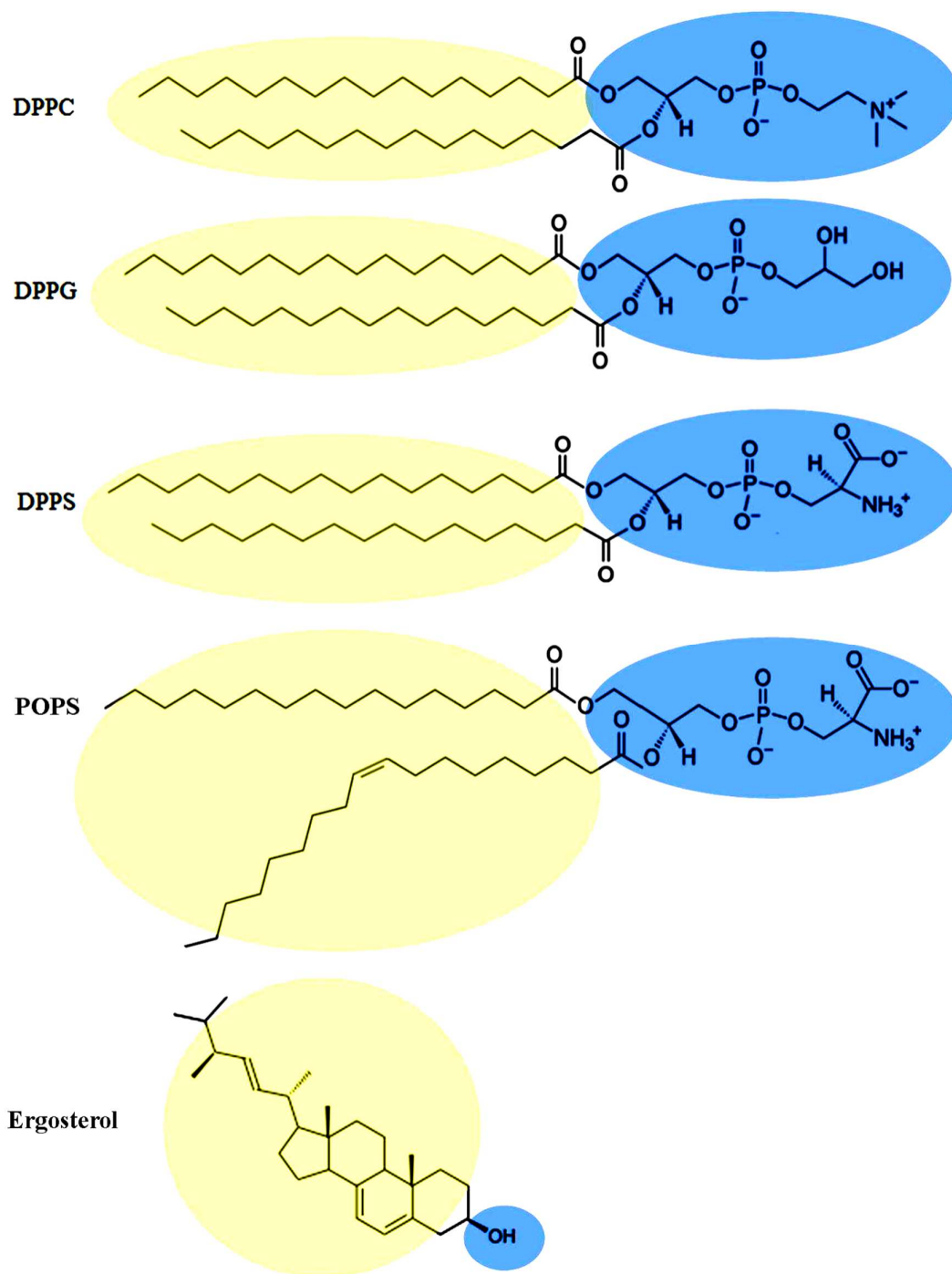


Figure 1.6 Structural formulas of the lipids used in the monolayer experiments. Hydrophobic parts of the molecules are marked yellow, hydrophilic parts of the molecules are marked blue.

The steroids in the natural membranes are believed to act as membrane stabilisers, providing rigidity for the regions containing more fluidic lipids and more space for the regions with the tightly packed saturated lipids.⁸¹ To examine the steroid's effect on the protein-lipid

interactions, an equimolar mixture of DPPS and ergosterol, the most common steroid in the fungal membrane⁷¹ will be another lipid system used for the experiments.

For training and method development purposes, dipalmitoylphosphatidylglycerol (DPPG), a saturated anionic phospholipid found in bacterial cell membranes,⁸² was used in the monolayer experiments. This lipid was shown to form stable monolayers at the air/liquid interface and served as a model of the bacterial cell membrane in the previous studies on the antibacterial behaviour of the wheat defence proteins.^{29,52}

The abovementioned fungal lipid models will be recreated as flat bilayers deposited on the solid support and as lipid vesicles (liposomes) to better mimic the natural structure of the membrane and, in case of liposomes, include the membrane's curvature. Use of the lipid bilayers is also a chance to introduce membrane's phospholipid composition asymmetry between the inner and the outer leaflet.⁸³ In case of the artificial membranes, the phospholipid flipping between the layers occurs spontaneously,⁸⁴ whereas the natural membranes' asymmetry is supported by the enzymes called flippases, floppases and scramblases.⁸⁵

As a result of the mentioned enzymes' action, the yeast's cell membrane is highly asymmetrical, *i.e.* sphingolipids and phosphatidylcholine are located mainly in the exoplasmic leaflet whereas phosphatidylserine (PS), phosphatidylethanolamine (PE), phosphatidylinositol (PI) and phosphatidic acid (PA) are confined to the cytosolic part of membrane.⁸³ The lipid systems proposed for the experiments will not reflect the full complexity of the natural membrane, nonetheless they will enable to examine the role played by the specific feature of the lipid system in the protein-lipid interactions.

The above mentioned properties of the membrane lipids building the eukaryotic cell membrane are summarised in Figure 1.7.

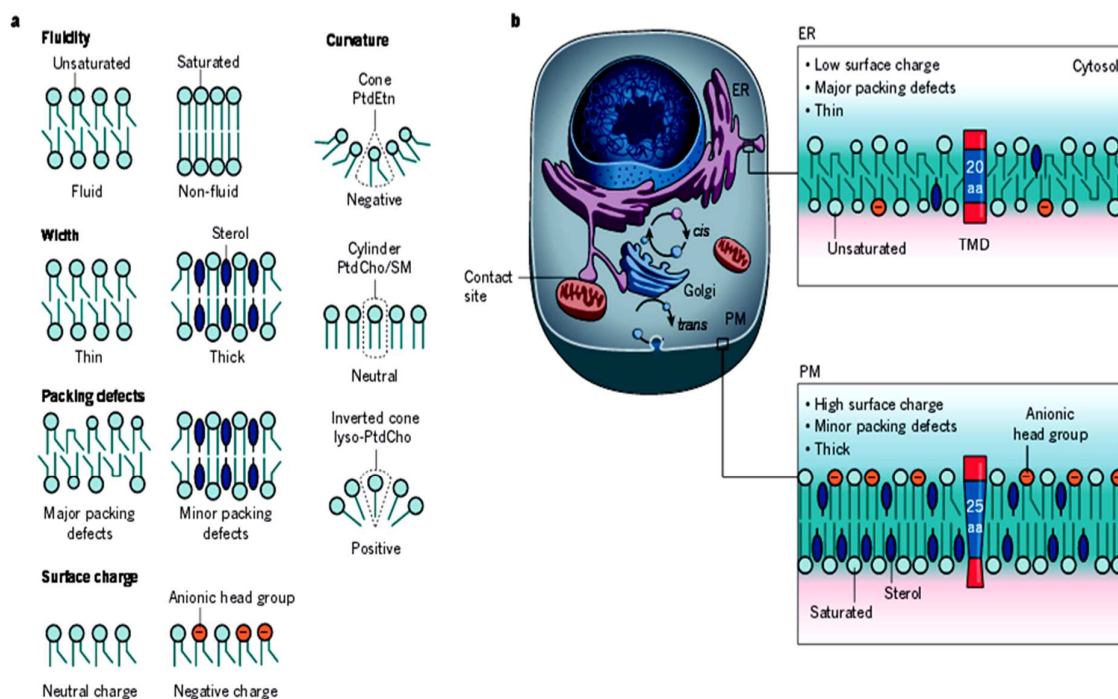



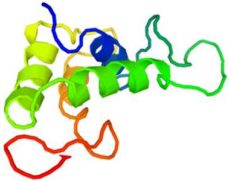
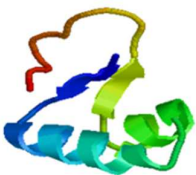
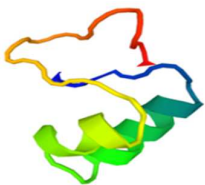
Figure 1.7 (a) Membrane lipid properties and (b) the structure of a eukaryotic cell (not containing a cell wall) with the detailed depiction of endoplasmic reticulum (ER) membrane and plasma membrane (PM) showing the asymmetric phospholipid distribution between the membrane leaflets. Abbreviations used: PtdCho – phosphatidylcholine, PtdEtn – phosphatidylethanolamine, SM – sphingomyelin [reproduced by kind permission of Nature Publishing Group via RightsLink, 15.03.2017].⁸⁶

1.4 Structures and features of the proteins used in the experiments

The proteins mentioned in this section will be introduced to the prepared lipid membrane models (see page 10) and the changes in the lipid system's structures will be monitored by means of the analytical methods described in Chapter 2.

For training and method development purposes, chicken egg white lysozyme was chosen as an easily obtainable protein with isoelectric point:⁸⁷ 11.35 – a value close to the ones of the defence proteins pI:⁸⁸ 10.50-11.00, which in turn justified the use of lysozyme for the study on its interaction with anionic phospholipid membrane. The high values of the abovementioned isoelectric points arise from the relatively high content of the basic amino acids in the proteins' sequences (see Table 1.3). Furthermore, lysozyme has been shown to interact with the anionic phospholipids in the study by Lad⁸⁹ and would, therefore, serve as a good model to estimate the repeatability of the experiments.

Table 1.3 Summary of the data on the proteins used in the experiments. Hydrophobic amino acids are marked bold and basic amino acids are marked red. The 3-D models were generated at www.proteinmodelportal.org using the protein sequences, therefore there is no tryptophan-rich loop (underlined in the sequence) shown in the Pin-a three-dimensional structure.

Protein's name	3-D model	Sequence (Reference)
Lysozyme		KVFG R CELAAAM KRH GLDNY R GYSLG NWVCAAKFESNFNTQATN R NTDGDST YGILQINS R WWCNDG R TPGSRNLCNIP CSALLSSDITASVNCA KK IVSDGNMGMN AWVAW R R CKGTDVQAW R GCRL (90)
Pin-a		DVAGGGGAQQCPVETKLNSC R NYLLD R CSTM K DFPVT WR <u>WWK</u> WWK GGCQE LLGECCS R LGQMPPQ R CNIQGSIQG DLGGIFGFQ R R ASK V IQEAK N LPP R C NQGPPCNIPGTIG (91)
β -Pth		K SC C STLGRNCYNLC R ARGAQ K LCAN V C R C KLTSGLSCP K DF P K (56)
α_2 -Pth		K SC R TTLGRNCYNLC R SRGAQ K LCST V C R C KLTSGLSCP K GF P K (55)

Pin-a has been widely studied by Clifton *et al.*^{27,80,92} in the context of its physical and lipid-binding properties and was used in this project to assess its antifungal action.

Pin-a's three-dimensional structure obtained from the two-dimensional nuclear magnetic resonance (2D-NMR) studies is shown in Figure 1.8(a). The structure of the tryptophan-rich domain, believed to take part in the protein's antimicrobial action,⁶³ is illustrated in Figure 1.8(b) and the protein's charge distribution, believed to initiate its interactions with microbial

membranes,⁶³ is presented in Figure 1.8(c). For more details on Pin-a's properties, see section 1.1.2.

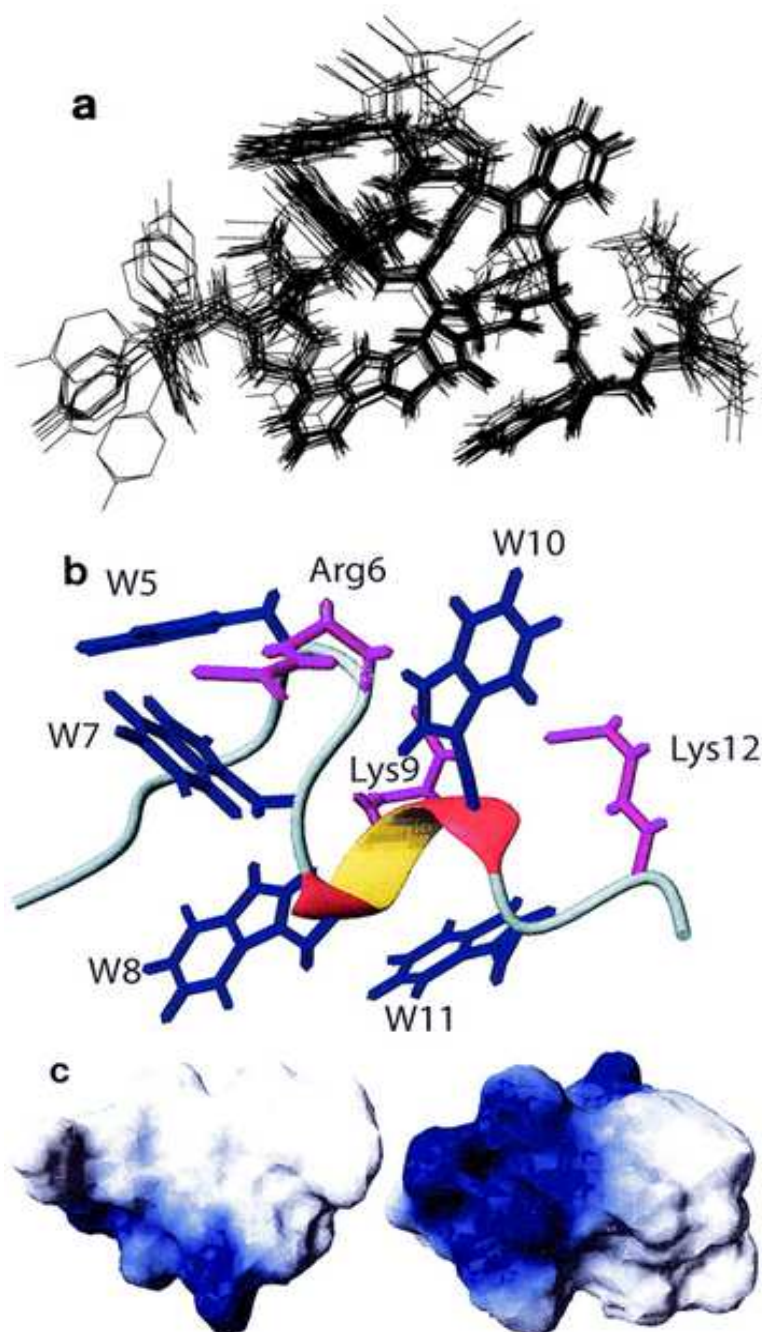


Figure 1.8 (a) Stick diagrams of the 20 final structures of Pin-a bound to sodium dodecyl sulphate (SDS) obtained by the 2D-Nuclear Magnetic Resonance (2D-NMR) analysis; (b) Ribbon diagram of the averaged structure of Pin-a with the side chains of all Trp residues (blue) and positively charged residues (pink) are visible. (c) Charge distribution on the surface of Pin-a: positive and neutral potentials are blue and white, respectively [reproduced by kind permission of American Society for Microbiology via RightsLink, 15.03.2017].⁹³

Pin-a's potential cooperative / competitive behaviour with purothionins was assessed by introducing an equimolar mixture of Pin-a and β -Pth as the tested protein solution.

The cooperative properties of β -Pth will be also assessed with another purothionin, α_2 -Pth. The findings will be compared with the ones obtained by Sanders *et al.* (2013).⁵³ β -Pth was also used to assess the lipid's net charge effect on the strength of the interactions due to its antifungal properties.⁹⁴ See protein's detailed structure in Figure 1.9.

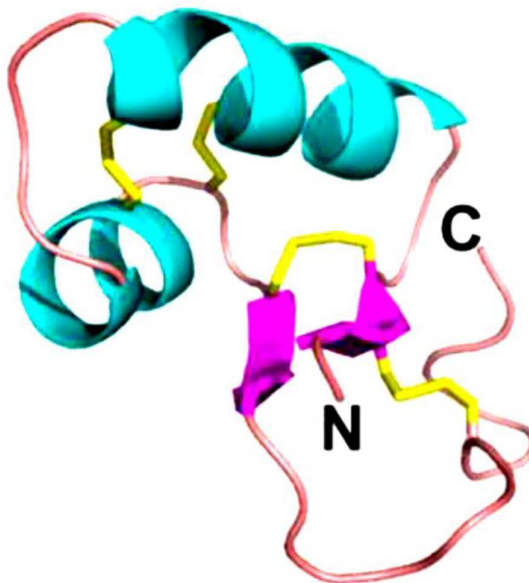


Figure 1.9 Three-dimensional structure of β -Pth, showing the α -helices (marked blue), β -sheets (marked pink) and the four disulphide bridges (marked yellow) stabilising the protein's structure.⁹⁵

For more details on the protein's properties, please refer to section 1.1.1.

1.5 Aim of the project

The aim of the project is to investigate the individual and synergistic activity of the plant defence proteins against various fungal cell membrane models. Recent studies focused on the characterisation of the lipid membrane interactions of the puroindoline and purothionin proteins (both isolated from common wheat – *Triticum aestivum*) using air/liquid monolayer and solid/liquid bilayer membrane models.^{27,29}

Moreover, preliminary experiments shown that there is a synergistic activity between some members of the puuroindoline family.⁹⁶ These results, together with the fact that plant defence proteins are often found co-located in the host, led to the hypothesis that synergistic or cooperative activity between Pins, Pths and defensins, such as γ -Pth, can act to increase microbial membrane disruption and, therefore, their antipathogenic activity.

Understanding of the toxicity mechanisms may provide new models and strategies for developing the novel antimicrobial agents, which could not only augment plant immunity but also enhance the efficiency of conventional antibiotics. The other expectations of these new compounds are the minimal chances of the pathogenic species developing resistance to these agents and that these will also be more environmentally friendly compared to commonly used chemical agents.

1.5.1. Objectives of the project

The following objectives needed to be completed to test the hypothesis of the study and complete the aim of the project.

- To obtain the sufficient amount of high purity wheat defence proteins to be tested: the previously verified protocols described in Chapter 3 will be used for isolating and purifying Pin-a, β -Pth and α_2 -Pth. Moreover, a new isolation and purification method will be tested for obtaining two defensins: γ_1 -Pth and γ_2 -Pth. The purity and the identity of the proteins will be confirmed by means of SDS-PAGE and mass spectrometry techniques (see Chapter 3 for more details).
- To examine the protein-lipid interactions in the lipid monolayer systems: the purified proteins' effect on the lipid monolayers will be analysed by means of surface pressure measurements and X-Ray Reflectometry (XRR), which will provide the preliminary information on the strength of the proteins' antifungal action and will allow to choose the protein-lipid combinations to be further analysed.
- To study the protein-lipid interactions in the flat lipid bilayer systems: the flat lipid bilayers will be created on the solid supports and the changes in their structure upon the protein adsorption will be analysed by means of Attenuated Total Reflectance-Fourier Transform Infrared Spectroscopy (ATR-FTIR) and Neutron Reflectometry (NR). To cover the ATR-FTIR solid supports with lipids, the Langmuir trough equipped with the

dipping well and the dipping arm will be designed and purchased and the dipping protocol developed.

- To describe the protein-lipid interactions in the folded lipid bilayer systems, also known as lipid vesicles or liposomes: the multilamellar vesicles and the small unilamellar vesicles will be created, their sizes assessed by means of Dynamic Light Scattering (DLS) and the membrane solubilisation caused by the protein will be determined by Differential Scanning Calorimetry (DSC).

The obtained results will contribute to better understanding of the wheat defence proteins' antipathogenic mode of action and will reveal the potential synergistic / competitive behaviour between the puroindolines and purothionins.

Chapter 2

METHODOLOGY

2.1 Introduction

Protein interactions with lipids can be studied in a variety of systems, *e.g.* in the solution (using vesicles), at the solid/liquid interface (by means of supported mono- and multilayers) or at the air/liquid interface (involving lipid monolayers). Table 2.1 lists some of the techniques employed to examine these phenomena.

Table 2.1 Techniques used to study the protein-lipid interactions and the information provided by each technique.

Technique	Examined property of the system	Reference
Attenuated Total Reflectance-Fourier Transform Infrared Spectroscopy (ATR-FTIR)	Structural changes of the protein upon adsorption and penetration into supported lipid layers at the solid/liquid interface	97
Brewster Angle Microscopy (BAM)	Visual change in lipid monolayer structure during protein adsorption, thickness of a monolayer	98
Differential Scanning Calorimetry (DSC)	Effect of the protein addition on the stability of the lipid vesicles	99
External Reflectance-FTIR (ER-FTIR)	Structural changes of the protein upon adsorption and penetration into lipid monolayers at the air/liquid interface	100
Isothermal Titration Calorimetry (ITC)	Kinetics, binding ratios and thermodynamics of protein lipid interaction	101
Neutron Reflectometry (NR)	Quantitative analysis of the protein adsorbed lipid layers, layer thickness	102
Nuclear Magnetic Resonance (NMR)	Secondary structure, orientation and penetration of membrane surface of lipid vesicles	28
Surface Pressure (SP) Measurements	Penetration/perturbation of lipid monolayers by a protein at the air/liquid interface	103

2.2 Monolayer experiments

2.2.1 Langmuir Trough and Surface Pressure Measurements

The Langmuir technique is frequently used for monitoring phase transitions of a monolayer through surface pressure measurements.³ It exploits proteins' amphipathicity as the biological activity of these surface-active compounds occurs at lipid membrane interfaces, which makes the Langmuir technique suitable for studying peptides interactions with lipid monolayers. The advantage of this technique is that it allows for *in situ* study of interactions occurring at the air/liquid interface without causing disruption to the monolayer system. The troughs used for the experiments were equipped with movable barriers and surface pressure sensor, as illustrated in Figure 2.1.

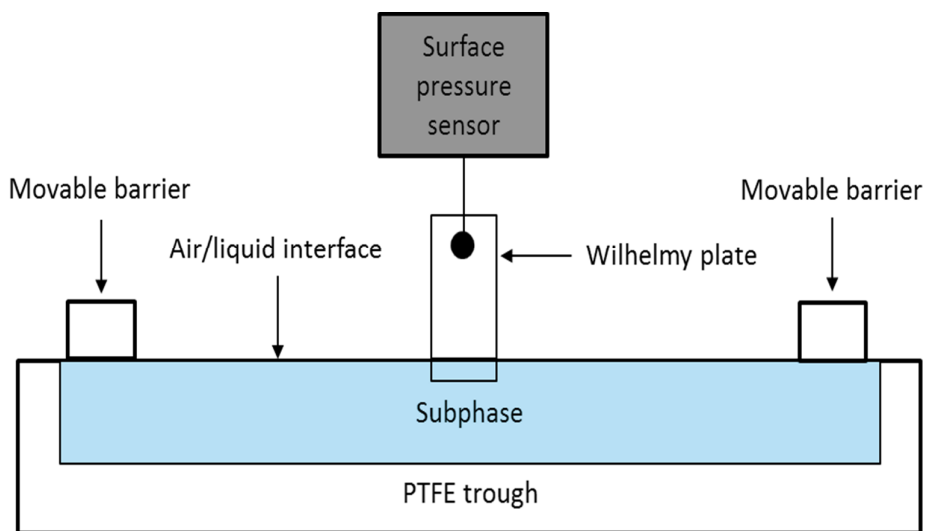


Figure 2.1 Scheme of the Langmuir trough apparatus used for preparation and monitoring of monolayers at the air/liquid interface.

Surface pressure measurements were taken by means of a Wilhelmy plate method (see: Figure 2.2).

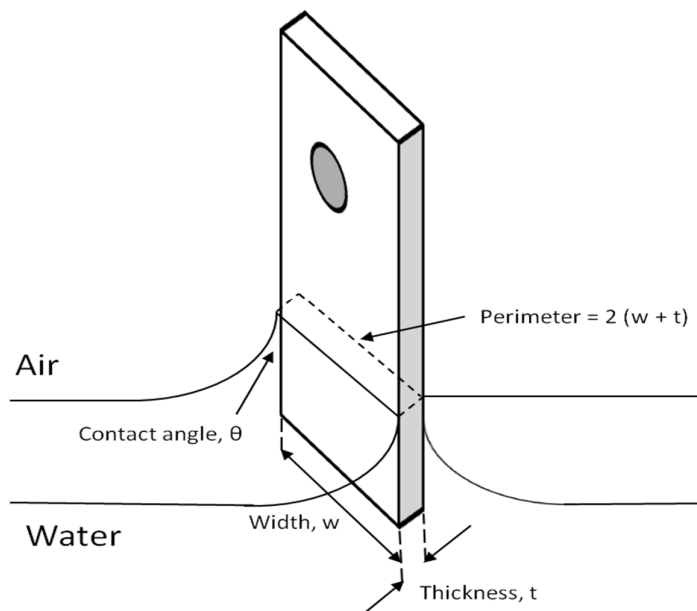


Figure 2.2 Diagram of a Wilhelmy plate partially immersed in water.

The filter paper plate, attached to the surface pressure sensor, is partially immersed in the liquid allowing measurement of the surface tension (γ) from the following formula:

$$\gamma = \frac{F}{2(w+t)} \quad (1)$$

where F is the net force acting down on the plate, w is the width of the plate and t is its thickness.

Surface pressure (π) is then calculated by subtracting the measured surface tension (γ) from the surface tension of a clean water surface (γ_0 - equal to 72.8 mN/m under ambient conditions):

$$\pi = \gamma_0 - \gamma \quad (2)$$

Material adsorbed at the surface will contribute to the change of the interface properties thus altering surface tension and surface pressure. Hence, monitoring of the surface pressure is used to detect interfacial changes upon the film compression or adsorption of material from the bulk of the solution to its surface.¹⁰⁴

2.2.1.1 Monolayer Behaviour Upon Compression

Substances capable of forming monolayers are amphipathic (or amphiphilic), *i.e.* they possess both hydrophilic and hydrophobic parts in their molecules. Another requirement for a monolayer to occur is the amphipathic balance within a molecule - if a substance is too hydrophilic, it will be dragged into the bulk of the subphase and dissolved. On the other hand, too much hydrophobicity could force molecules to form thicker multilayer films on surface or to evaporate. The molecules at the interface are anchored, strongly oriented and with no tendency to form a layer more than one molecule thick.

Phospholipids are an example of monolayer-forming amphiphiles and are therefore convenient tools to mimic the biological membranes at the air/liquid interface. The behaviour of a phospholipid monolayer upon compression is described by a surface pressure-mean molecular area isotherm – or a π -A curve (see: Figure 2.3).

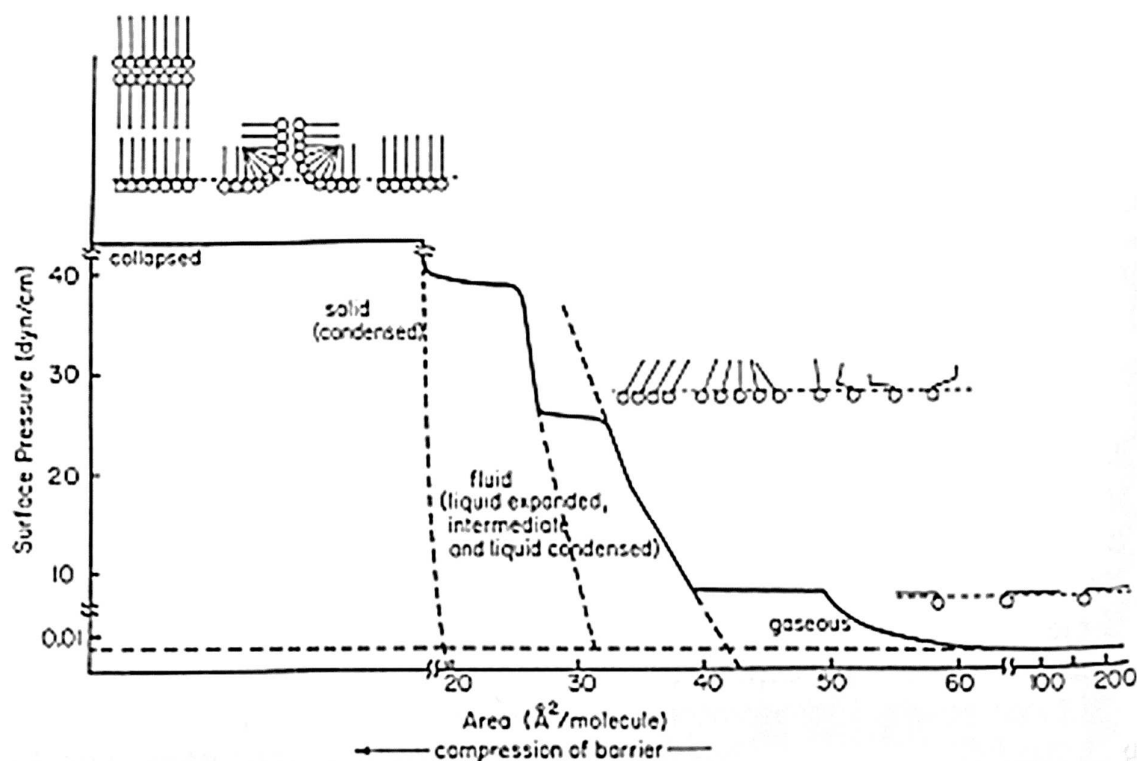


Figure 2.3 Schematic representation of a surface pressure – mean molecular area isotherm [reproduced by kind permission of John Wiley and Sons Limited via PLSClear, 8.03.2017].¹⁰⁵

Typically, one can distinguish 4 stages of compression:

1. Gaseous phase – in which a relatively big area is available for the molecules, allowing them to float freely, mostly lying flat on surface without exerting much force on each other; this phase is characterized by a constant dipole moment and exponential decrease of surface pressure with increasing surface area.
2. Liquid-expanded phase – surface pressure increases much more steeply with decreasing area; intermolecular distances are much greater than in bulk liquids.
3. Liquid-condensed phase - molecules become relatively close to each other, tilted with respect to the surface.
4. Solid (condensed) phase – molecules are packed as closely as possible, vertical isotherm indicates low compressibility.

At very low compression areas the isotherm becomes broken and the monolayer is said to have collapsed. At collapse pressure film loses its monomolecular form and multilayers are formed - the molecules are ejected out of monolayer plane into either subphase (more hydrophilic molecules) or superphase (less hydrophilic molecules).

However, many amphiphiles do not express exactly this kind of behaviour upon compression and form different types of films:

- Condensed films – *e.g.* stearic and higher fatty acid chains acids; at high areas molecules are not completely separated from each other, *i.e.* cohesion between molecules is strong enough to maintain molecules in small clusters on surface. Due to this strong coherence surface pressure remains very low as the film is compressed and then rises rapidly when molecules become tightly packed together.
- Expanded films – *e.g.* oleic acid – give much more expanded films than corresponding saturated acids – *i.e.* the value of surface pressure is greater for any value of mean molecular area. The presence of a double bond lessens the intermolecular cohesion.
- Gaseous films – formed by molecules of negligible size with no lateral adhesion between them – ideally, their π -A curve would resemble a rectangular hyperbola.

Many factors contribute to the lipid behaviour upon compression. Among them are size and number of the polar head groups as well as number, length, saturation and branching of the hydrocarbon chains.

2.2.2 X-Ray Reflectometry

X-rays have been widely employed to investigate the structure of chemical compounds, *e.g.* by Shankland *et al.*¹⁰⁶ X-Ray Reflectometry (XRR) is a technique used for studying the details of the surface structure.¹⁰⁷ In this technique X-rays are used to scan the electron density perpendicular to the surface, which allows to obtain the information on the surface roughness, thin film thickness and density.¹⁰⁸ XRR involves measurement of the X-ray reflectivity, R , defined as:

$$R = \frac{I}{I_0} \quad (3)$$

where: I is the reflected intensity and I_0 is the intensity of the incident beam.

Reflectivity is measured over a range of angles close to the critical angle of reflection, *i.e.* an angle at which all incoming wave intensity is reflected. Reflectivity varies not only with the structure of the interface but also with the beam wavelength and the angle of incidence. To account for these differences, one can plot the reflectivity as a function of momentum transfer, Q , defined as:

$$Q = \frac{4\pi \sin\phi}{\lambda} \quad (4)$$

where: ϕ is the angle of incidence of a beam and λ is the beam's wavelength.

The obtained reflectivity profiles are then fitted into structural models by the modelling software, as described in Chapter 4 (page 71). The changes in the obtained reflectivity profiles correspond to the differences in the monolayer structure upon the adsorption of the protein.²⁹

As X-rays interact mainly with the electron clouds of the atoms, the heavier the element (characterised by the high atomic mass and atomic number) they encounter, the stronger they are scattered. Scattering length density (SLD, ρ) is a quantity which characterises the scattering properties of a molecule and which is used for the qualitative and quantitative characterisation of the analysed film.

The X-ray scattering length density (xrSLDs) of a molecule (or its part) was calculated from the following formula:

$$\text{xrSLD} = \frac{r_e}{V} \sum_i Z_i \quad (5)$$

where: r_e is the Bohr electron radius (2.818×10^{-15} m), V is the volume of a molecule or its part (see Appendix, Table 2, page 172) and Z_i is the atomic number of the component i .

The values of the calculated xrSLDs can be found in the table below (see Appendix, page 172 for an example of the calculation).

Table 2.2 Summary of the XRR data used for the analysis.

Compound	Molecular Formula	Molecular Weight [g/mol]	Molecular Volume* [Å ³]	$r_e \times \Sigma Z$ [Å × 10 ⁻⁵]	xrSLD [Å ⁻² × 10 ⁻⁶]
PS headgroup	C ₈ H ₁₁ NO ₁₀ P	312.00	275.40	453.70	16.47
DPDS	C ₃₈ H ₇₃ NO ₁₀ P	735.00	1088.00	1135.65	10.44
DP tails	C ₃₀ H ₆₂	423.00	812.60	681.96	8.39
PO tails	C ₃₂ H ₆₄	448.85	773.20	721.41	9.33
POPS	C ₄₀ H ₇₅ NO ₁₀ P	761.00	1048.60	1175.11	11.21
β-Pth	C ₂₀₃ H ₃₅₆ N ₆₇ O ₅₆ S ₈	4946.00	5921.70	7380.34	12.46

*calculated as described in the Appendix, page 172.

XRR experiments were carried out at the I07 beamline at the Diamond Light Source (Harwell, Oxfordshire, UK). The I07 instrument uses a double-crystal deflection system, which allows the angle of incidence to be varied without moving the sample.¹⁰⁹ More details on the experimental procedure can be found in Chapter 4, page 70.

2.3 Bilayer experiments

Lipid bilayers are a more realistic representation of the cell membrane structure than the lipid monolayers. Experiments involving the lipid bilayer systems were therefore believed to better reflect the antimicrobial activity of the wheat defence proteins. Two lipid bilayer systems were used: bilayers deposited on a solid support and the spherical bilayers enclosed in the form of lipid vesicles (liposomes) in the aqueous medium.

2.3.1 Lipid Vesicles (Liposomes)

Lipid vesicles (liposomes) are spherical structures formed of at least one lipid bilayer. They are a versatile research tool^{110,111,112} and have also found application as drug carriers.¹¹³ They are obtained by hydration of a dried lipid precipitate: this causes spontaneous formation of spherical structures in the aqueous medium with hydrophilic headgroups pointing outwards and inwards of the vesicle and hydrophobic tails isolated from the aqueous medium – contributing to the backbone of the spherical shape.¹¹⁴

Liposomes can be divided into 3 groups according to their size:¹¹⁴

- Small unilamellar vesicles (SUVs) – of a size 25-100 nm in diameter.
- Large unilamellar vesicles (LUVs) ranging from 100 to 500 nm in diameter.
- Multilamellar vesicles (MLVs) of a diameter above 500 nm – the multiple lipid bilayers forming concentric spherical shells.

The structures of the 3 liposome types are presented in Figure 2.4.

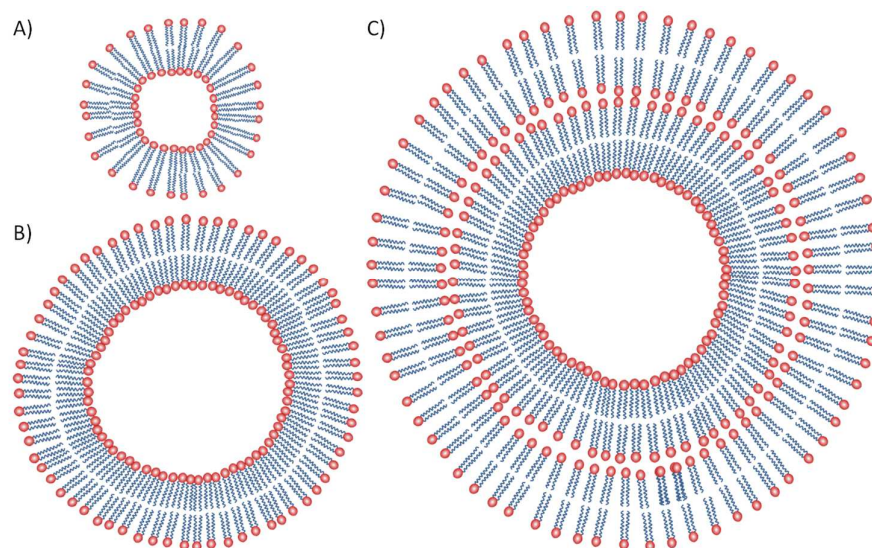


Figure 2.4 Schemes of a small unilamellar vesicle (A), a large unilamellar vesicle (B) and a multilamellar vesicle (MLV) formed of phospholipids. Red spheres represent the polar phospholipid headgroups and the blue springs represent the hydrophobic chains of fatty acid residues.

One of the advantages of using the vesicles in membrane research is their similarity to the natural cell membrane: vesicles provide not only the bilayer structure but also sphericity of a

natural membrane, which enables to examine the impact of the cell's curvature on studying the interactions of compounds with membranes.

2.3.2 Differential Scanning Calorimetry (DSC)

Differential Scanning Calorimetry (DSC) is a thermoanalytical technique allowing for monitoring the energy changes in the system upon heating. It is applied for stability testing¹¹⁵ and monitoring the interactions between the molecules.¹¹⁶

In this technique a sample is placed in the sample heating chamber and a reference containing *e.g.* a sample solvent is poured into the reference chamber (see Figure 2.5). In a typical experiment both chambers are heated at equal rates and the energy changes caused by the thermal transitions of the sample are visualised as peaks.

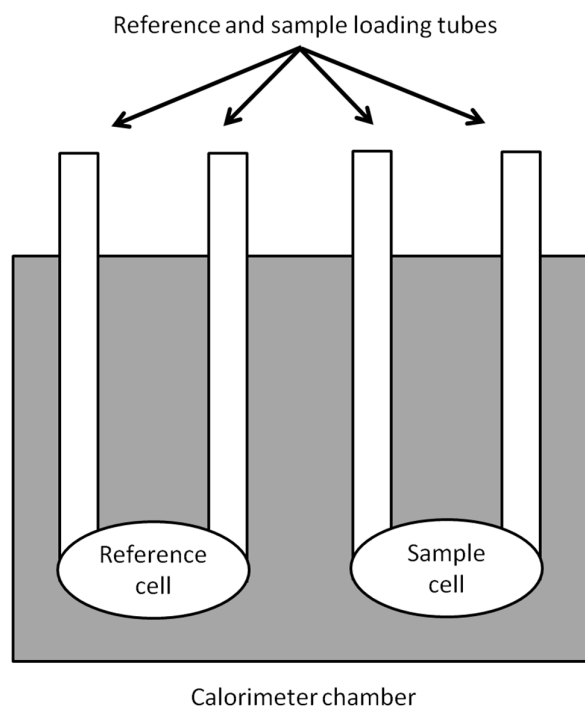


Figure 2.5 Scheme of a differential scanning calorimeter suitable for liquid analysis.

Changes in the values of the lipid vesicle sample's thermal transition maxima, peak shapes and intensities arise from the interactions with other compounds present in the sample and reflect how strong was the impact of the compounds on the structure of the lipid vesicles.¹¹⁷

2.3.3 Lipid Bilayers Deposited on the Solid Support

Lipid deposition on a solid support (sometimes referred to as a solid substrate) employs many methods, among which are: Langmuir-Blodgett/Schaeffer dipping and vesicles spreading.¹¹⁸

2.3.3.1 Vesicles Spreading

Vesicles spreading is one of the simplest methods used for formation of the supported lipid bilayers.¹¹⁹ In this method, a dispersion of the small unilamellar vesicles is brought into contact with the hydrophilic surface of the solid support.¹²⁰

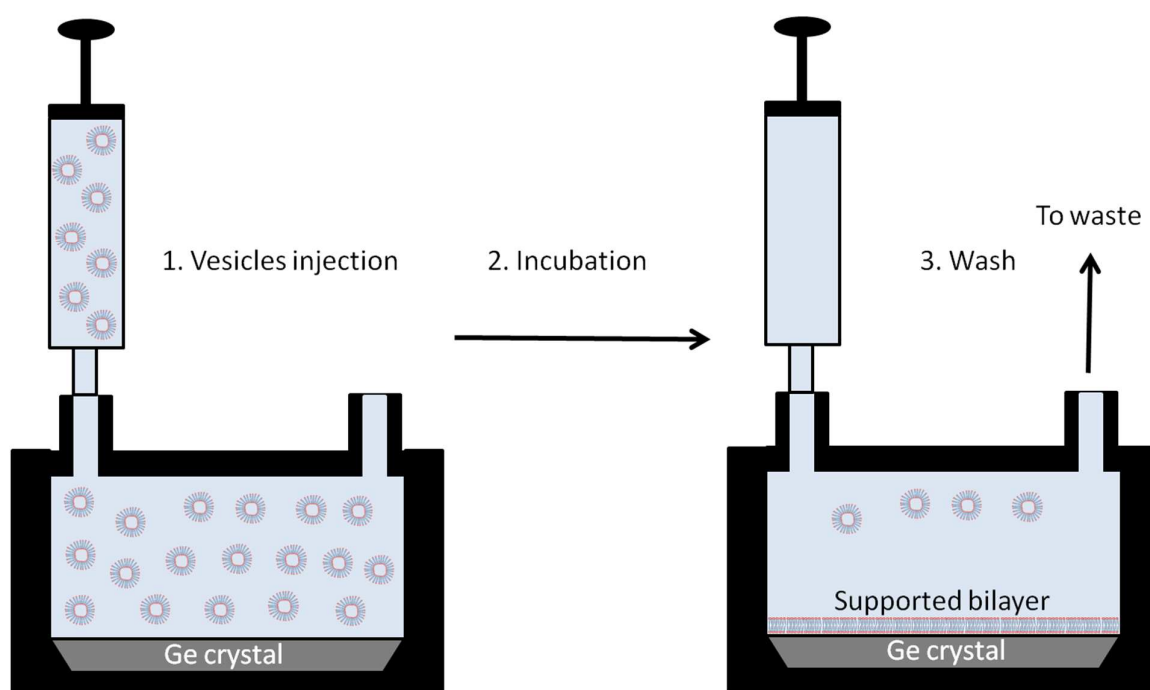


Figure 2.6 Scheme of the phospholipid bilayer formation on the germanium crystal placed in an ATR-FTIR cell by means of the vesicles spreading technique.

When the vesicles are in contact with the hydrophilic solid support, they spontaneously unfold and form a bilayer in about an hour at room temperature.^{121,122} The excess of vesicles is flushed out and the bilayer is not exposed to air during the spreading process – see Figure 2.6. The formed bilayers can be then analysed by means of *e.g.* ATR-FTIR.

2.3.3.2 Langmuir-Blodgett dipping and Langmuir-Schaeffer dipping

The Langmuir-Blodgett and Langmuir-Schaeffer dipping methods involve the covering of the solid support with a single one-molecule-thick layer of an amphiphile, *e.g.* a phospholipid monolayer.¹²³

Langmuir-Blodgett dip bases on immersing a solid support into the monolayer with the covered surface being perpendicular to the air/water interface (see Fig. 2.7).¹²⁴ Langmuir-Schaeffer dip involves lowering the solid support surface directly onto the monolayer by maintaining the surface to be covered in parallel to the air-liquid interface (see Fig. 2.7).¹²⁴

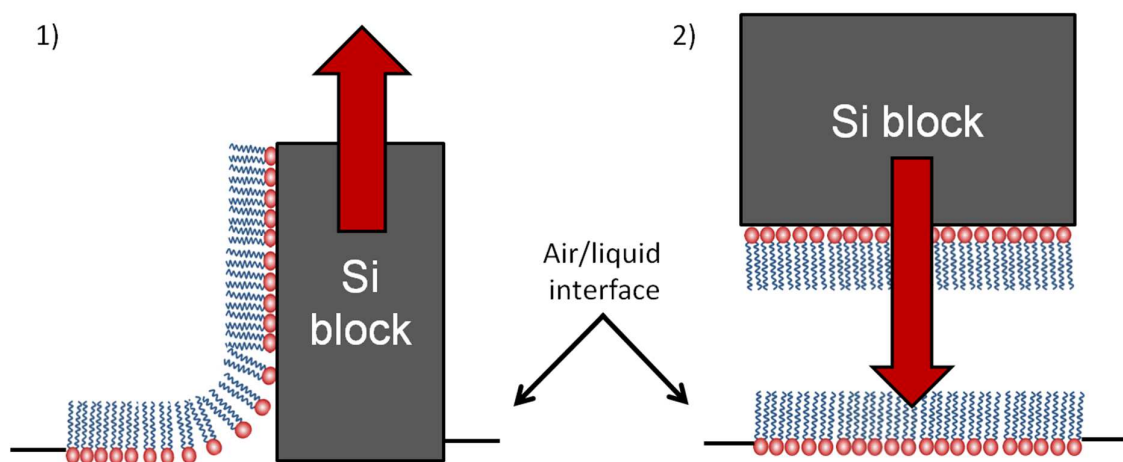


Figure 2.7 Diagrams of the Langmuir-Blodgett (1) and the Langmuir-Schaeffer (2) dipping of a silicon block used for preparation of the phospholipid bilayers. The red arrows indicate the direction of the block's motion. Langmuir-Blodgett dipping image is a simplified scheme as it does not account for covering of all the block's walls.

Covering the solid substrates using Langmuir-Blodgett method followed by the Langmuir-Schaeffer dip results in the high quality bilayers suitable for research purposes.⁸⁴ These techniques provide the better control of the deposition process compared to the vesicles spreading: the deposition surface pressures range from 32 to 40 mN/m.^{124,123} The obtained bilayer samples can be further analysed by means of ATR-FTIR or NR techniques. More details on the dipping process can be found in Chapter 5, page 85.

2.3.4 Attenuated Total Reflectance-Fourier Transform Infrared Spectroscopy (ATR-FTIR)

Infrared spectroscopy monitors the absorption of infrared radiation (10^{-4} to 10^{-2} cm^{-1} wavenumbers) by the sample. The absorbed energy is assigned to discrete quantized frequency of vibrations occurring between atoms forming a bond in a molecule. Therefore, if a wide range of beam wavelengths is passed through a sample, the exiting beams will include a ‘fingerprint’ of a sample, which is then analysed by a detector. Finally, the resultant signal is transformed to give the infrared spectra of the sample.¹²⁵

Attenuated Total Reflectance-FTIR bases on the phenomenon of the total internal reflection of infrared beam passing through a crystal made of a material with high refractive index.¹¹⁸ Infrared beam ‘scratches’ the surface of a sample enabling investigation of the film composition, as illustrated in Figure 2.8.

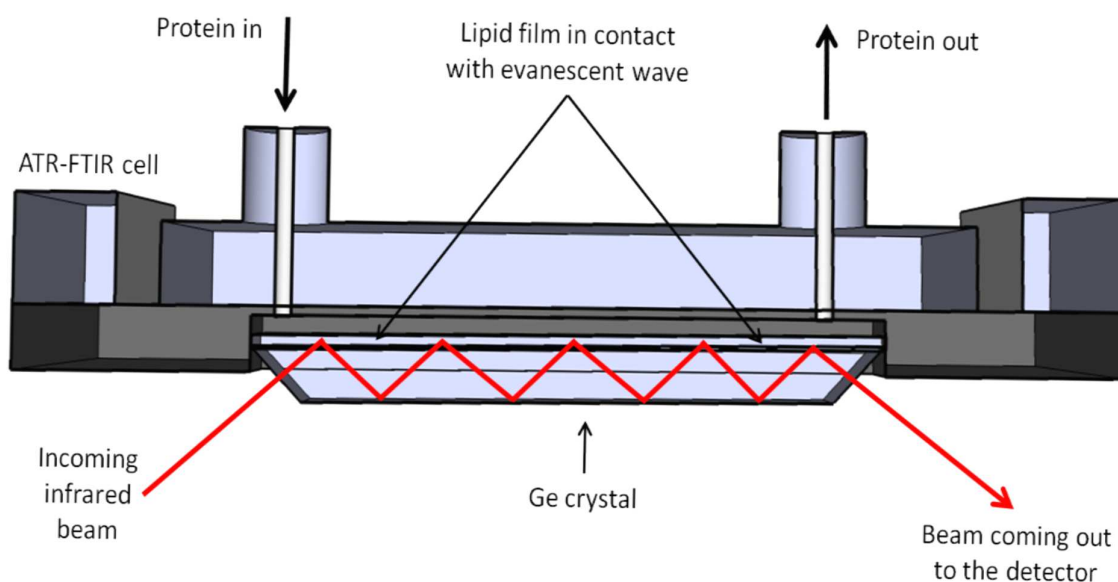


Figure 2.8 Cross-section of an ATR-FTIR cell with a Ge crystal and the protein solution adapters.

In this technique, a germanium crystal is covered with a phospholipid bilayer and put into an ATR cell which is then placed in the FTIR instrument. The protein solution is then flushed through the cell and the protein adsorption is monitored by observing the size of the peak in the Amide I region (~ 1650 cm^{-1}).¹²⁵

2.3.5 Design of a Dipping Trough for the ATR-FTIR Experiments

To allow the controlled deposition of the lipid bilayers on the ATR-FTIR crystals, one needed to design the Langmuir trough fitted with a well and a dipping arm.

The designed trough consists of a flat top wide enough for preparation of the condensed lipid monolayers and the dipping well which contains an insert for the ATR-FTIR cell at its bottom – as illustrated in Figures 2.9 and 2.10.

The trough's well has been designed to accommodate the crystal in the Langmuir-Blodgett and Langmuir-Schaeffer dipping positions, ATR-FTIR cell, insert to support the cell with the attached adapters through which the protein solution is passed during the analysis.

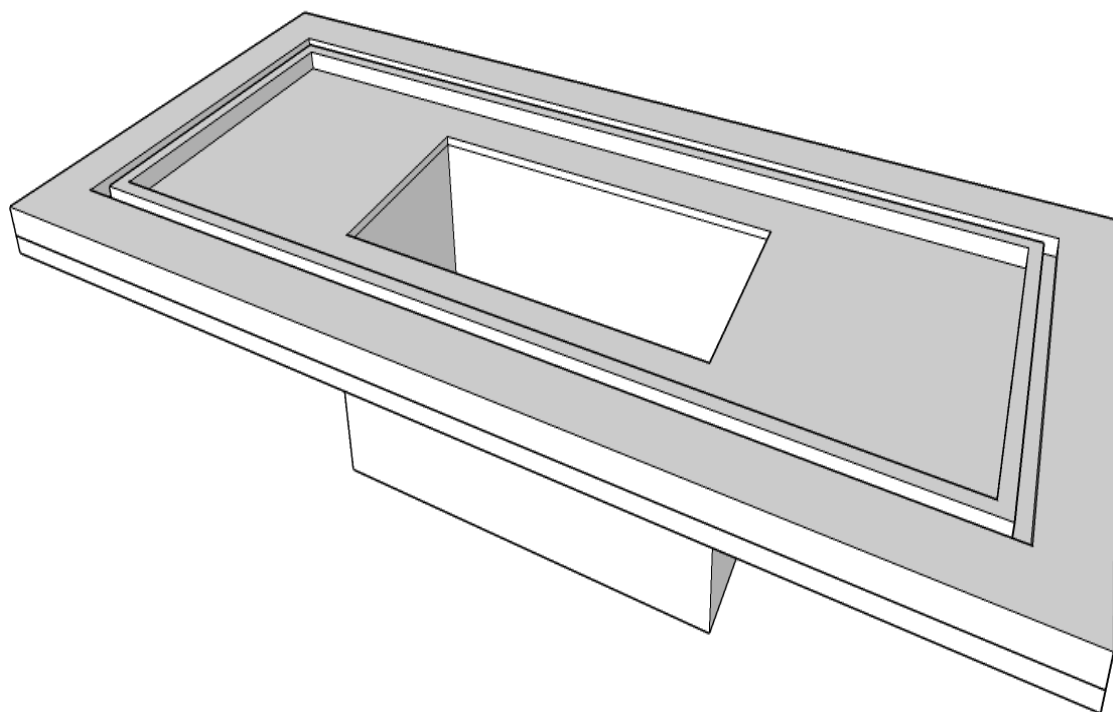


Figure 2.9 Simple scheme of the dipping trough containing a deep well enabling to immerse the solid supports.

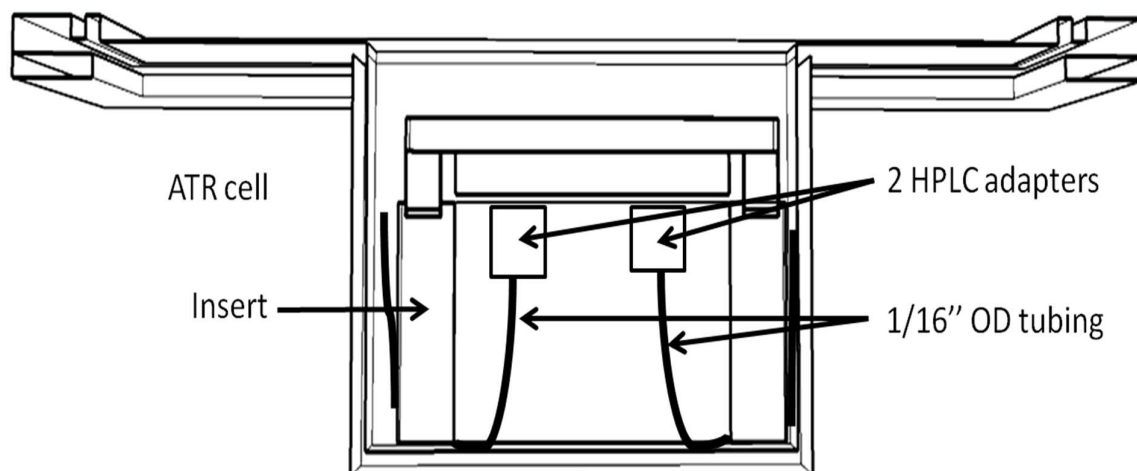


Figure 2.10 Length cross section of a dipping trough containing the ATR-FTIR cell with the attached tubing.

A photograph presenting the assembled trough and the detailed description of the dipping process can be found in Chapter 5 (pages 92 and 93).

2.3.6 Neutron Reflectometry (NR)

Neutron Reflectometry (NR) is a technique used widely for studying the structure of thin films, such as protein-adsorbed lipid monolayers in the studies by Lu *et al.*¹²⁶, Zhao *et al.*¹²⁷ and Clifton *et al.*²⁹

Similarly as in XRR technique, the reflected beams are detected and the reflectivity profiles are plotted against the momentum transfer. However, the fundamental difference between the neutrons and X-rays is that the first ones interact with atomic nuclei and not the electron clouds.¹⁰⁸ Therefore, the scattering lengths, and thus the probability of scattering the neutrons, are not increasing with the atomic number but are more variable among the atoms.¹²⁸

The fact that neutrons interact with nuclei allows to distinguish between the layer's components by applying the isotopic contrast.¹²⁹ This means carrying out the experiment in which one component or a few components are substituted with their isotopic equivalents,

e.g. replacing H₂O subphase with D₂O subphase in monolayer experiments or analysing the monolayer composed of partially- or fully-deuterated lipids. These equivalents have different neutron scattering properties, resulting from the relatively big difference between the scattering length of hydrogen and deuterium atoms¹²⁸ and allow the emphasis of the components of interest.

Table 1 in the Appendix (see page 172) contains the scattering length values of the elements occurring in this study. Neutron scattering length densities (SLDs) of the molecules (or their parts) were calculated from the formula below:

$$\text{SLD} = \frac{\sum b}{V} \quad (6)$$

Where: *b* is the scattering length of the atom in the molecule and *V* is the volume of the molecule or its part (see Appendix, Table 2, page 172). Protein SLDs have been obtained from the Biomolecular Scattering Length Density Calculator created by Luke Clifton and Daniel Myatt and available at <http://psldc.isis.rl.ac.uk/Psldc/> - assuming the level of replacement of the exchangeable hydrogen atoms equal to 95%.

Table 2.3 Summary of the NR data used for the analysis.

Compound	Molecular Formula	Molecular Weight [g/mol]	Molecular Volume* [Å ³]	Scattering Length $\sum b$ [Å × 10 ⁻³]	SLD [Å ⁻² × 10 ⁻⁶]
PS headgroup	C ₈ H ₁₁ NO ₁₀ P	312	275	0.84	3.06
DP h-tails**	C ₃₀ H ₆₂	423	813	-0.32	-0.39
PO h-tails**	C ₃₂ H ₆₄	449	773	-0.27	-0.34
PC headgroup	C ₁₀ H ₁₈ NO ₈ P	311	342	0.60	1.98
DP d-tails***	C ₃₀ D ₆₂	485	813	6.13	7.45
Ergosterol	C ₂₈ H ₄₄ O	397	634	0.27	0.43
Pin-a in D ₂ O	C ₅₅₉ H ₆₅₀ N ₁₆₈ O ₁₄₆ S ₁₂ D ₂₂₅	13151	15553	51.71	3.33
Pin-a in SMW	C ₅₅₉ H ₇₉₀ N ₁₆₈ O ₁₄₆ S ₁₂ D ₈₅	13038	15553	38.06	2.45
Pin-a in H ₂ O	C ₅₅₉ H ₈₇₅ N ₁₆₈ O ₁₄₆ S ₁₂	12968	15553	29.69	1.91
β-Pth in D ₂ O	C ₂₀₃ H ₂₅₅ N ₆₇ O ₅₆ S ₈ D ₁₀₁	5029	5921	20.42	3.45
β-Pth in SMW	C ₂₀₃ H ₃₁₈ N ₆₇ O ₅₆ S ₈ D ₃₈	4958	5921	11.63	1.96
β-Pth in H ₂ O	C ₂₀₃ H ₃₅₆ N ₆₇ O ₅₆ S ₈	4946	5921	10.15	1.71

*calculated as described in the Appendix, page 172.

**h-tails refers to the fatty acid chains whose hydrogen atoms have not been replaced with the deuterium isotope.

***d-tails refers to the fatty acid chains whose all hydrogen atoms have been replaced with the deuterium isotope.

Protein SLDs have been calculated for 3 isotopic contrasts: D₂O, silicon-scattering-length-density-matched-water (SMW, containing 38% D₂O) and water. The values of the calculated SLDs used in the study can be found in Table 2.3. See Appendix, page 173 for an example of the calculated SLD.

The reflectivity profiles obtained from different isotopic compositions are fitted to the pre-defined structural models basing on the layer's composition, thickness and roughness (more details can be found in Chapter 6, page 110). The fitted scattering length density for each layer, denoted further as ρ , corresponds to the volume fraction of each component in the system by:

$$\rho_{\text{contrast1}} = \varphi_{\text{lipid}} \times \text{SLD}_{\text{lipid}} + \varphi_{\text{protein}} \times \text{SLD}_{\text{protein}} + \varphi_{\text{water}} \times \text{SLD}_{\text{water}} \quad (7)$$

where φ is the volume fraction of the layer's component and SLD is the component's calculated scattering length density (see Table 2.3).

Volume fractions of the components can be calculated by solving a system of equations obtained from fitting the data from the experiments with varied isotopic contrasts.

Knowing the volume fractions of the components, it is possible to calculate the area A (in Å²) occupied by the component's molecule:

$$A = \frac{\sum b}{\tau \varphi \text{SLD}_{\text{component}}} \quad (8)$$

where τ is the layer thickness obtained from data fitting.

Once the area is obtained, one can derive the surface excess Γ (mg/m²) for each component from the equation below:

$$\Gamma = \frac{MW}{6.02 A} \quad (9)$$

where: MW is the molecular weight of the component.

The sum of the surface excesses in each layer gives the total surface excess of the peptide or lipid at the interface. The quantity can be used to describe the 'degree' of the component's adsorption to the interface.

In a typical NR experiment carried out at the solid/liquid interface, the solid substrate is covered with a lipid mono- or multilayer and the substrate is enclosed in the solid/liquid cell

which allows the lipid layer to come in contact with the protein solution. The cell is then placed in the neutron reflectometer room and the neutron beams are passed through the sample at varying angles and wavelengths (see Figure 2.11).

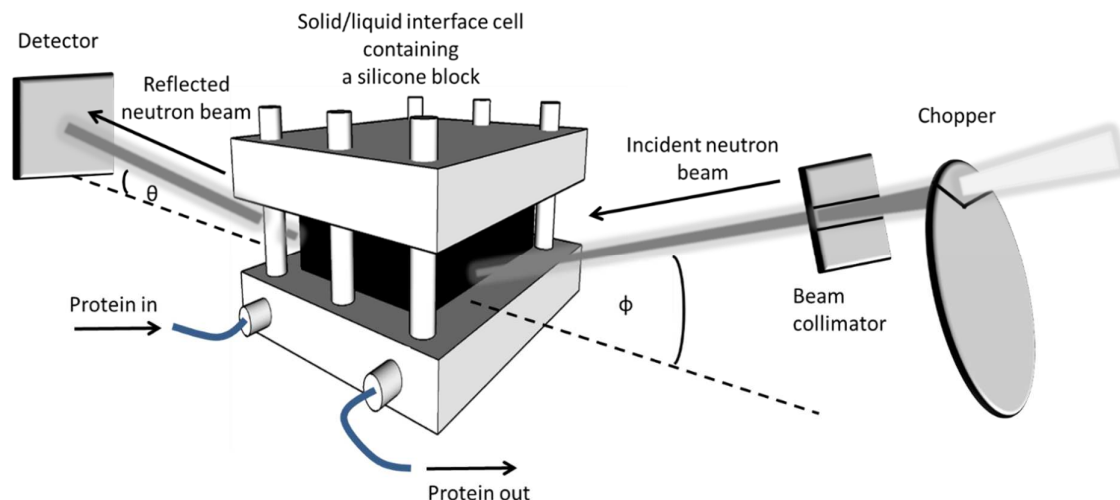


Figure 2.11 The scheme of an NR experiment carried out at the solid/liquid interface containing a silicone block as a solid substrate.

The beam is passed through a series of rotating devices called choppers, which allow to select the specified neutron wavelength range from the incoming neutron beam.¹²⁹ The post-chopper beam is then targeted at the sample by the collimator which aligns it in the proper direction.¹²⁹ The intensities of the reflected beams are collected by the detector and the obtained reflectivity profiles are then fitted and analysed.

2.4 Conclusions

The analysis of protein-lipid interactions can be carried out by many techniques. The techniques can be applied to lipid mono- and bilayer systems. Each system provides different information on the interaction and can be used for various stages of research.

For example, surface pressure measurements carried out on lipid monolayers serve as the simplest tool for detection of the interaction and the systems showing the most noticeable changes upon the protein adsorption are further investigated by means of more advanced analytical techniques, *e.g.* NR and ATR-FTIR on the lipid bilayer systems.

Chapter 3

ISOLATION AND PURIFICATION OF THE DEFENCE PROTEINS FROM WHEAT FLOUR

3.1 Introduction

3.1.1 Purification of Puroindolines and Purothionins

The purification protocol is based on a method developed by Day *et al.*¹³⁰ The procedure involves extraction of lipid binding and membrane proteins with Triton X-114 (TX-114) – a non-ionic surfactant frequently used for this purpose.¹³¹ The obtained extract contains both puroindoline isoforms, Pin-a and Pin-b, as well as purothionins and other membrane proteins. Pin-b and purothionins are separated from Pin-a by adsorption onto carboxymethyl cellulose (CMC). The Pin-a rich fraction is then precipitated and washed twice with cold 1:3 (v/v) diethyl ether:ethanol mixture. Further separation of the CMC-bound (Pin-b rich) fraction is achieved by means of ‘salting out’ of purothionins fraction with 3 M NaCl. Finally, purothionins are purified by means of Reversed-Phase High Performance Liquid Chromatography (RP-HPLC) as described by Jones *et al.*⁵⁵ and puroindolines by means of Cation Exchange Chromatography as described by Day *et al.*¹³⁰

3.1.2 Purification of γ -Purothionins

The protocol is based on a method described by Colilla *et al.*⁵⁴ It involves removal of lipids from wheat flour followed by the extraction of NaCl-soluble proteins. The salt-soluble protein extracts are then fractionated with ammonium bicarbonate to remove anionic proteins and the ammonium bicarbonate-insoluble crude extracts are purified by means of RP-HPLC as carried out by Colilla *et al.*⁵⁴

3.2 Materials and Methods

3.2.1 Chemicals

Acrylamide/bis-acrylamide 30% solution, TEMED (N,N,N',N'-Tetramethylethylenediamine), wide range molecular weight markers (6.5 kDa – 200 kDa) (aprotinin [6.5 kDa], α -lactalbumin [14.2 kDa], trypsin inhibitor [20 kDa], trypsinogen [24 kDa], carbonic anhydrase [29 kDa], glyceraldehyde-3-phosphate dehydrogenase [36 kDa], ovalbumin [45 kDa], glutamic dehydrogenase [55 kDa], albumin [66 kDa], phosphorylase B [97 kDa], β -galactosidase [116 kDa], myosin [200 kDa]), SDS-PAGE (Sodium Dodecyl Sulphate – Polyacrylamide Gel Electrophoresis) sample buffer (4% sodium dodecyl sulphate (SDS), 20% glycerol, 10% 2-mercaptoethanol, 0.004% bromophenol blue, 0.125 M Tris HCl; pH \approx 6.8), diethyl ether, ethanol, acetone, chloroform (HPLC grade), methanol, acetonitrile (HPLC grade) and ammonium persulphate (APS) were obtained from Sigma-Aldrich (Dorset, UK). Carboxymethyl cellulose (CMC) pre-swollen micro granular CM52 was purchased from Whatman (Maidstone, UK). Triton X-114 (*tert*-octylphenoxypolyethoxyethanol), SimplyBlue SafeStain Coomassie G-250 stain, sodium dodecyl sulphate, potassium chloride, sodium chloride, EDTA (ethylenediamine tetraacetic acid di-sodium salt dihydrate), phosphate buffer salts, ammonium bicarbonate, Tris base [Tris(hydroxymethyl)aminomethane], glycine, hydrochloric acid (HCl), petroleum ether (b.p. 40 - 60°C), ammonium acetate, trichloroacetic acid (TCA) and trifluoroacetic acid (TFA) were purchased from Fisher Scientific (Loughborough, UK). Water used was Ultra High Quality (UHQ) water obtained from ELGA Purelab Ultra purification system (ELGA Lab Water, High Wycombe, UK). Claire wheat variety flour was kindly donated by Hovis Ltd (Watnall, UK).

3.2.2 Extraction of Pin-a, β -Pth and α_2 -Pth

3.2.2.1 Protein Extraction from Wheat Endosperm using Triton X-114

Wheat flour (500 g) was mixed with 2.5 L of PEK buffer (0.05 M sodium phosphate, pH 7.6, 0.05 M KCl, 5 mM EDTA) at 4°C for 1 hour to wash out starch and cellular components. The solution was centrifuged at $3,500 \times g$ for 10 minutes and the resulting pellet was stirred with 2.5 L of 4% TX-114 in PEK buffer at 4°C for 1 hour to extract membrane bound proteins. The extract was then centrifuged at $13,000 \times g$ for 10 minutes and the pellet containing cell debris discarded. The pH of the supernatant was adjusted to 4.5 with glacial acetic acid.

Twenty-four grams of CMC was added to the extract and the resulting mixture was stirred overnight at 4°C. The mixture was centrifuged at $13,000 \times g$ for 10 minutes.

3.2.2.2 *Extraction of the Pin-a Containing Protein Fraction from the non-CMC-Bound Proteins*

The TX-114 rich supernatant was incubated at 30°C for one hour and centrifuged at $13,000 \times g$ for 10 minutes. The TX-114-poor upper phase was discarded and the lower detergent rich phase (approx. 600 mL) was stirred with 1.2 L of a 1:3 (v/v) mixture of diethyl ether and ethanol at -20°C. The solution was stored overnight at -20°C to precipitate the non-CMC-bound proteins and centrifuged ($13,000 \times g$, 10 minutes). The supernatant was removed and the pellet was washed twice with 800 mL of the 1:3 (v/v) mixture of diethyl ether and ethanol at -20°C. The pellet was dried under vacuum and dissolved in 80 mL of 0.05 M acetic acid. The solution was dialysed against 0.05 M acetic acid (2×5 L, at 4°C for 48 h) and freeze-dried. The lyophilized protein extract was stored at -20°C prior to further purification.

3.2.2.3 *Extraction of the Purothionin Rich Protein Fraction from the CMC-Bound Proteins*

The CMC pellet was washed twice with 0.05 M acetic acid (400 mL) to remove the traces of TX-114 and the non-CMC-bound proteins, and centrifuged at $13,000 \times g$ for 10 minutes. After discarding the supernatant, the CMC-bound proteins were eluted by mixing the pellet with 160 ml of 1 M NaCl in 0.05 M acetic acid and stirring at 4°C for 1 hour. The solution was then filtered through a 0.2 μ m filter and the CMC pellet was discarded. Twenty-eight grams of solid NaCl was added to the filtrate to give a final concentration of 4 M. The mixture was stirred at 4°C for 1 hour, then centrifuged at $13,000 \times g$ for 10 minutes and the supernatant (purothionin rich fraction) was separated from the pellet – the Pin-b rich fraction. The supernatant was dialysed against 0.05 M acetic acid (2×5 L, at 4°C for 48 h) and freeze-dried. The lyophilized protein extract was stored at -20°C prior to HPLC purification.

3.2.2.4 RP-HPLC Purification of the Crude Purothionin Extracts

The method was based on the protocol developed by Jones *et al.*⁵⁵ RP-HPLC technique involves using the non-polar stationary phases (*e.g.* silica beads with covalently attached hydrocarbon chains) and the mobile phases with the gradually increasing hydrophobicity. The hydrophobicity gradient is achieved by raising the amount of the organic solvent present in the running buffer. The compounds bound to the stationary phase are sequentially eluted basing on the difference in their hydrophobicity.

The apparatus used was ÄKTA Fast Protein Purification System (FPLC) purchased from GE Healthcare (Little Chalfont, UK) and run by the UNICORN software. The device was used for all protein purification protocols.

Crude purothionin rich samples (0.7 mL each) containing about 7 mg/mL of protein in 15% acetonitrile (CH₃CN) / 0.1% trifluoroacetic acid (TFA) were incubated at 35 °C for 15 min and centrifuged at 13,000 × *g* for 3 minutes. The obtained aggregate-free samples were applied to a Supelco (250 × 10 mm; 5 µm bead size) C18 reversed phase HPLC column (Supelco Analytical, USA). Acetonitrile gradients were obtained by mixing a solution containing 80% CH₃CN in 0.1% TFA with 15% CH₃CN in 0.1% TFA. Purification was carried out at 4°C and the absorbance at 280 nm was monitored. Fractions were manually collected, dialysed against UHQ water (2 × 5 L, at 4°C for 48 h) and freeze-dried. The fractions were stored at -20°C.

3.2.2.5 Cation Exchange Purification of the Crude Pin-a Extracts

The protocol based on the one described by Day *et al.*¹³⁰ Cation Exchange Chromatography uses anionic resins as the stationary phases (*e.g.* sulphonates or carboxylic acid derivatives) and the mobile phase buffers with gradually increasing salt content. The compounds are separated on the bases of their affinity for the anionic resin. The electrostatically bound proteins are eluted by increasing the number of ions that compete with the proteins for the access to the anionic resin.

Crude Pin-a rich samples (4 mL each) containing about 6 mg/mL of protein in 0.05 M ammonium acetate in 25% acetonitrile pH 5.5 were incubated at 35 °C for 30 min and

centrifuged at $13,000 \times g$ for 3 minutes. The resulting aggregate-free samples were injected to a Resource S (6 mL) Cation Exchanger pre-packed column (GE Healthcare, Little Chalfont, UK). Ammonium acetate gradients were obtained by mixing 0.05 M ammonium acetate in 25% acetonitrile pH 5.5 with 1 M ammonium acetate in 25% acetonitrile pH 5.5. The separation process was carried out at 4°C and the absorbance at 280 nm was monitored. Fractions were manually collected, dialysed against UHQ water (2×5 L, at 4°C for 48 h) and freeze-dried. The fractions were stored at -20°C.

The protocol of the puroindolines and purothionins extraction is summarized in Figure 3.1.

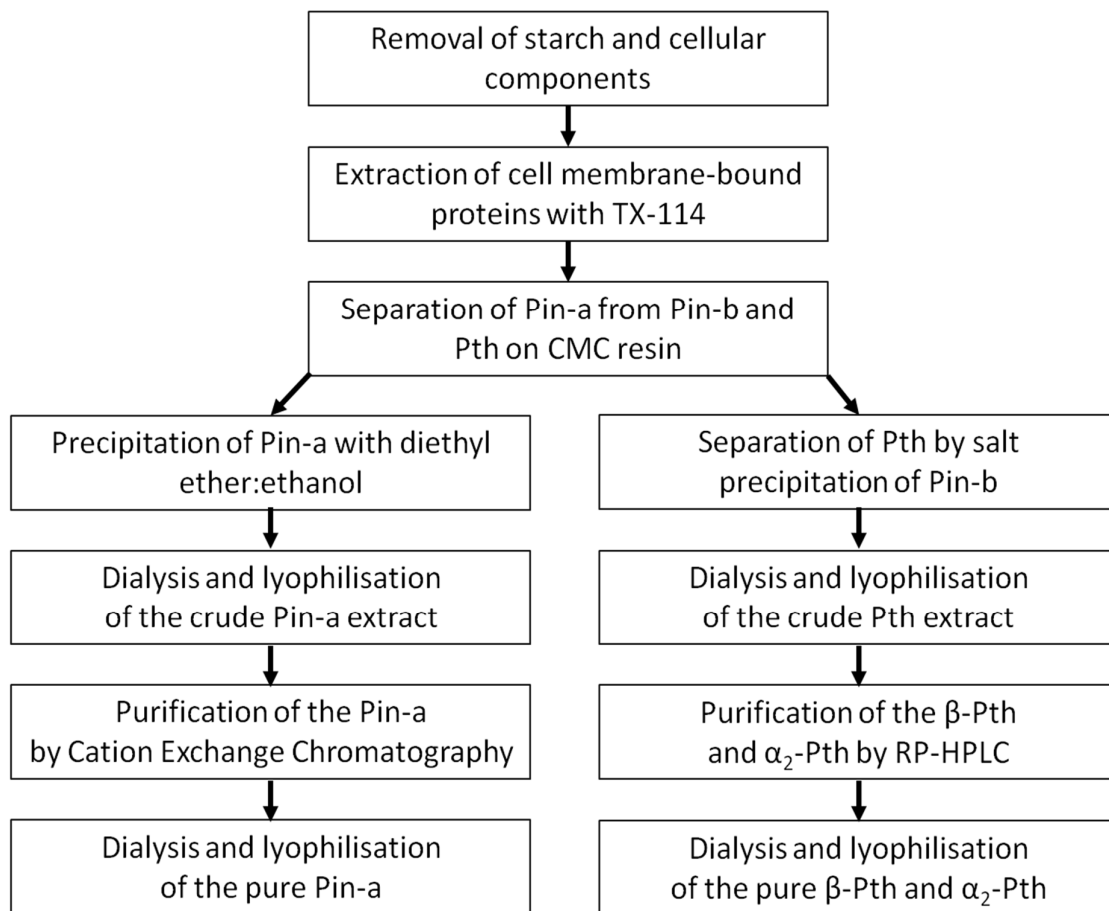


Figure 3.1 Diagram of the Pin-a and β-Pth and α₂-Pth extraction and purification.

3.2.3 Extraction of γ -Purothionins

3.2.3.1 *Removal of Lipids and Volatiles*

Wheat flour (50 g) was stirred with 500 mL of chloroform/methanol (2:1 v/v) mixture for 1 h at room temperature. The solvent was vacuum-evaporated on the rotary evaporator Rotavapor R-215 obtained from BÜCHI (Flavil, Switzerland). The chloroform/methanol (2:1 v/v) extraction was repeated and the solvent vacuum-evaporated. The dried flour cake was dissolved in 500 mL of petroleum ether (b.p. 40 – 60°C) and stirred for 1 h at room temperature. The solvent was vacuum-evaporated as previously.

3.2.3.2 *Extraction of the NaCl-soluble Proteins*

Wheat flour (50 g) was stirred with 500 mL of 0.5 M NaCl for 1 h at 4°C and centrifuged at $13,000 \times g$ for 10 minutes. The supernatant has been collected and the pellet again extracted with 500 mL of 0.5 M NaCl. A 100 % (w/v) trichloroacetic acid (TCA) solution was made by dissolving 250 g of powdered acid in 113.5 mL of UHQ water as described by Sambrook and Russel.¹³² The supernatants were combined (total mass 980.5 g) and to precipitate the proteins 80 mL of 100% (w/v) TCA was added to reach the final concentration of 15%. The mixture was shaken gently, incubated for 1 h at 4°C and centrifuged at $13,000 \times g$ for 10 minutes. The supernatant was removed and the pellet was dissolved in cold acetone (4°C). The salt-soluble protein extract was centrifuged at $10,000 \times g$ for 10 minutes. The supernatant was removed and the acetone wash was repeated to remove the traces of TCA. The residual acetone was vacuum-evaporated in the desiccator. The freeze-dried protein extracts were stored at -20°C prior to HPLC purification.

3.2.3.3 *Fractionation of the NaCl-soluble protein extract*

The dry pellet (~ 200 mg) containing the NaCl-soluble proteins was dissolved in 20 mL of 0.05 M ammonium bicarbonate and stirred overnight at room temperature to extract the anionic proteins and peptides. The solution was centrifuged at $17,000 \times g$ for 10 min. The supernatant was collected and the pellet washed twice with 10 mL of 0.05 M ammonium bicarbonate solution. The supernatants and the pellet were lyophilized.

3.2.3.4 RP-HPLC Purification of the Ammonium Bicarbonate-insoluble Extracts

The method was based on the protocol developed by Colilla *et al.*⁵⁴ The ammonium bicarbonate-insoluble samples (0.7 mL each) containing about 10 mg/mL of protein in 10% acetonitrile / 0.1% TFA were incubated at 35 °C for 15 min and centrifuged at $13,000 \times g$ for 3 minutes. The obtained aggregate-free samples were applied to a Cosmosil (250 × 20 mm; 5 μm bead size) C4 reversed phase HPLC column (Nacalai Tesque, Japan). Acetonitrile gradients were obtained by mixing a solution containing 80% CH₃CN in 0.1% TFA with 10% CH₃CN in 0.1% TFA. The separation process was carried out at 4°C and the absorbance at 220 nm was monitored. Fractions were manually collected, dialysed against UHQ water (2 × 5 L, at 4°C for 48 h) and freeze-dried. The fractions were stored at -20 °C. The ammonium bicarbonate-soluble samples could not have been applied to a column due to their precipitation at 4°C.

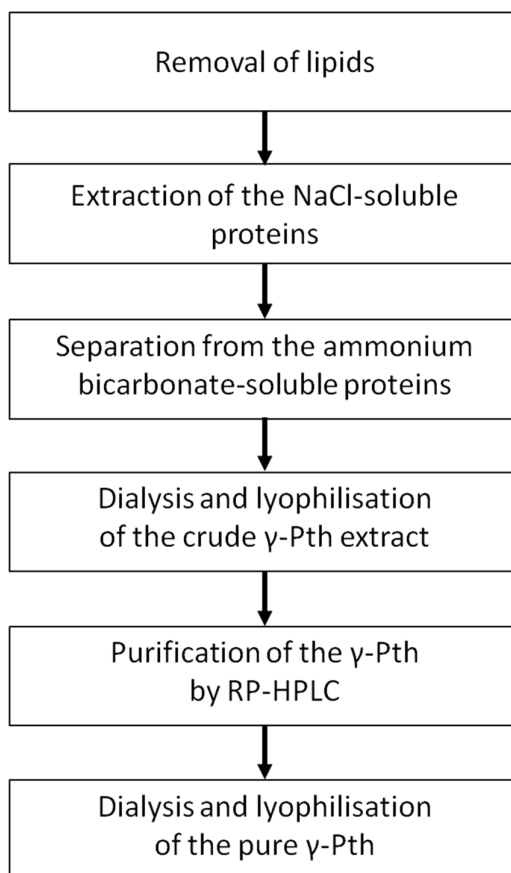


Figure 3.2 Diagram of the γ -Pth extraction and purification.

The summary of the γ -Pths extraction and purification protocol is presented in Figure 3.2.

3.2.4 Sodium Dodecyl Sulphate Polyacrylamide Gel Electrophoresis

The purity of the eluted fractions was assessed with SDS-PAGE (Sodium Dodecyl Sulphate Polyacrylamide Gel Electrophoresis). The technique involves separation of the proteins basing on their mass to charge ratio. SDS binds to a protein molecule (approximately 1.4 g per 1 g protein), linearises it and imparts a negative charge. The denatured and charged protein samples are placed in the polyacrylamide gel lanes and subjected to the external constant electric field. The distance they travel, dependent on the proteins' molecular weights, is compared to the distances travelled by the protein molecular weight markers, thus allowing the preliminary identification of the samples and their purity assessment.

The analysis was carried out using 12% polyacrylamide resolving gels of a 2 mm thickness. Each gel slab consisted of two layers: a stacking layer allowing the proteins to combine into one band and travel at equal rate and the resolving gel where the protein separation took place. For 4 gel slabs, 25 mL of 12% resolving gel was prepared by mixing 8.2 mL of UHQ H₂O, 10 mL of 30% acrylamide/bis-acrylamide mix, 6.3 mL of 1.5 M Tris pH 8.8, 0.25 mL of 10% SDS, 0.25 mL of 10% APS and 0.01 mL of TEMED. The stacking gel (6 mL for 4 gel slabs) was prepared by combining 4.1 mL of UHQ H₂O, 1 mL of 30% acrylamide/bis-acrylamide mix, 0.75 mL of 1 M Tris pH 6.8, 0.06 mL of 10% SDS, 0.06 mL of 10% APS and 0.006 mL of TEMED.

The apparatus used was a BioRad Mini-PROTEAN Tetra Cell SDS-PAGE kit into which 2 gel slabs were placed for each analysis. The gels and the apparatus were filled with approximately 700 mL of the pre-prepared SDS-PAGE running buffer (3.03 g Tris base, 14.4 g glycine, 1 g SDS per litre). Protein samples (20 μ L each) were combined with equal volumes of the SDS-PAGE sample buffer (4% SDS, 20% glycerol, 10% 2-mercaptoethanol, 0.004% bromphenol blue, 0.125 M Tris HCl; pH \approx 6.8) and incubated at 100°C for 10 minutes to denature the proteins, reduce the disulphide bridges and impart a negative charge on the protein molecules.

The denatured protein samples (20 μ L each) were added to the appropriate lanes of the stacking gel. To the outermost lanes 5 μ L of the wide range molecular weight markers solution was added. Gels were run at 150 V for 45 minutes, flushed with UHQ water and

stained in approximately 100 mL of the Coomassie G-250 solution for 1 h. The gels were de-stained by incubating in approximately 100 mL of the UHQ water for 1 hour.

3.3 Results

3.3.1 Pin-a Purification

Figure 2.3 illustrates a typical elution profile of the Pin-a rich sample and the result of the electrophoretic analysis of the marked peaks. The profile corresponds well to the chromatograms obtained by Clifton⁸⁰ and Sanders¹³³ using the Mono S Cation Exchange column (see Figure 1, Appendix, page 173). Both researchers reported a peak of a relatively high intensity eluting at ~ 0.4 M ammonium acetate concentration (see peak 1, Figure 3.3 A); it appeared as a prominent band in the SDS-PAGE analysis of the crude extract confirming the relatively high content of the associated protein.

The peak emerged as a single SDS-PAGE band at approximately 15 kDa suggesting the presence of a puroindoline¹³⁴ and the high purity of the protein. Basic nature of the puroindolines is the most probable explanation of the proteins' SDS-PAGE band appearing at 15 kDa,⁹¹ as opposed to their true molecular weight of 13 kDa.⁹¹ The shift towards a higher molecular weight is believed to be caused by the counter-balancing of the negative charge imparted by SDS with the positive charge present on the basic amino acid residues.

High content of the protein eluting at 0.4 M ammonium acetate concentration and the matching results of the other researchers^{80,133} confirmed that the peak 1 contained the Pin-a protein. Peak's content was analysed by means of Liquid Chromatography-Mass Spectrometry (LC-MS) and confirmed the presence of Pin-a (see Figure 5, Appendix, page 176).

Peak 2 representing protein eluting at around 0.55 M ammonium acetate concentration and appearing on the SDS-PAGE gel at 15kDa is most probably Pin-b.

The SDS-PAGE results are in agreement with the ones obtained by Clifton⁸⁰ and Sanders¹³³ (see Figure 2, Appendix, page 174).

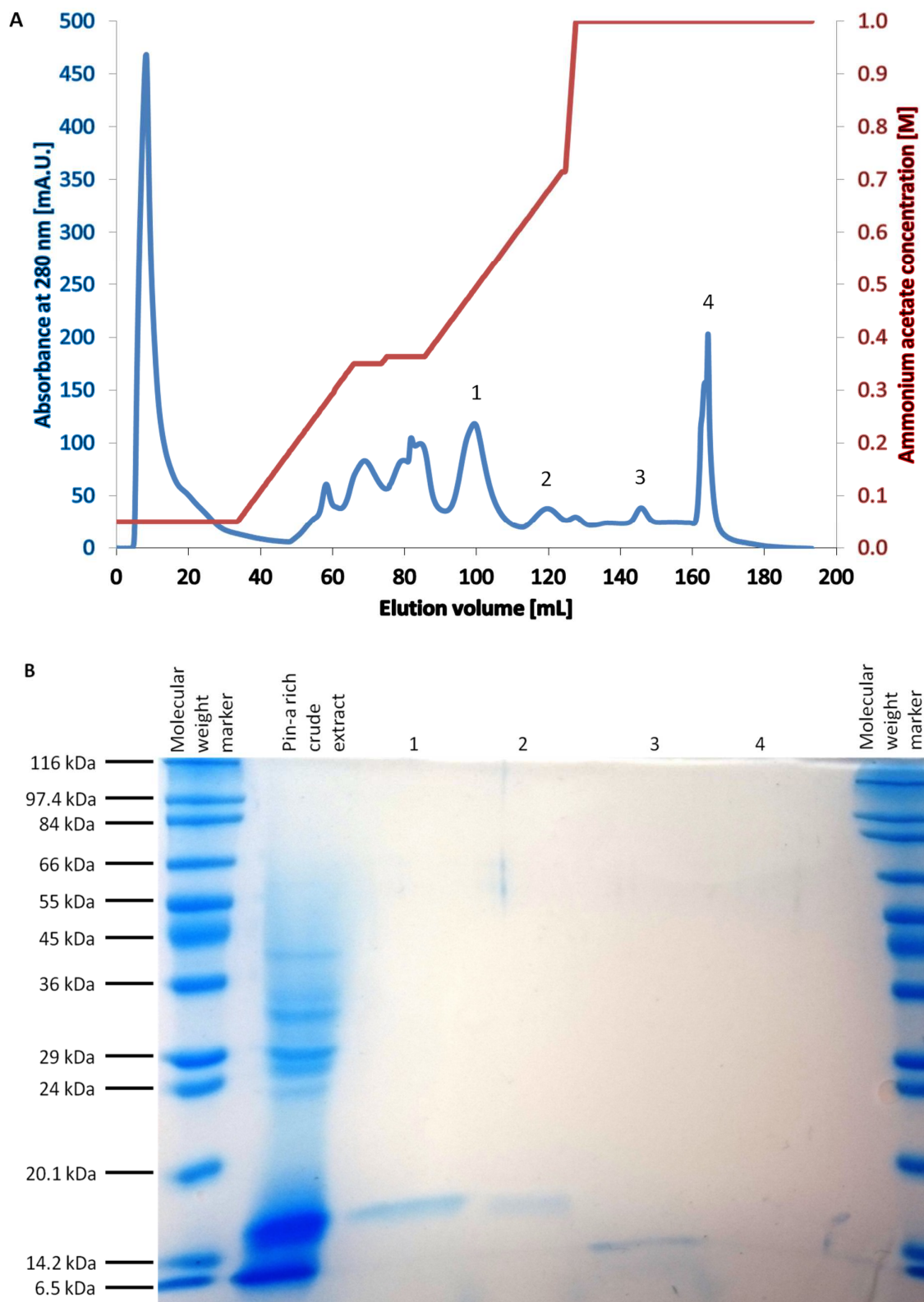


Figure 3.3 FPLC chromatogram (A) and SDS-PAGE (B) analysis of the fractions collected during Resource S cation exchange purification of the Pin-a rich crude protein extract.

3.3.2 β -Pth and α_2 -Pth Purification

Figure 2.4 shows a typical elution profile of a purothionin rich sample. The purification took place in the HPLC mode which increased the resolution of the peaks, as compared to the chromatograms obtained from the Resource S purification of Pin-a.

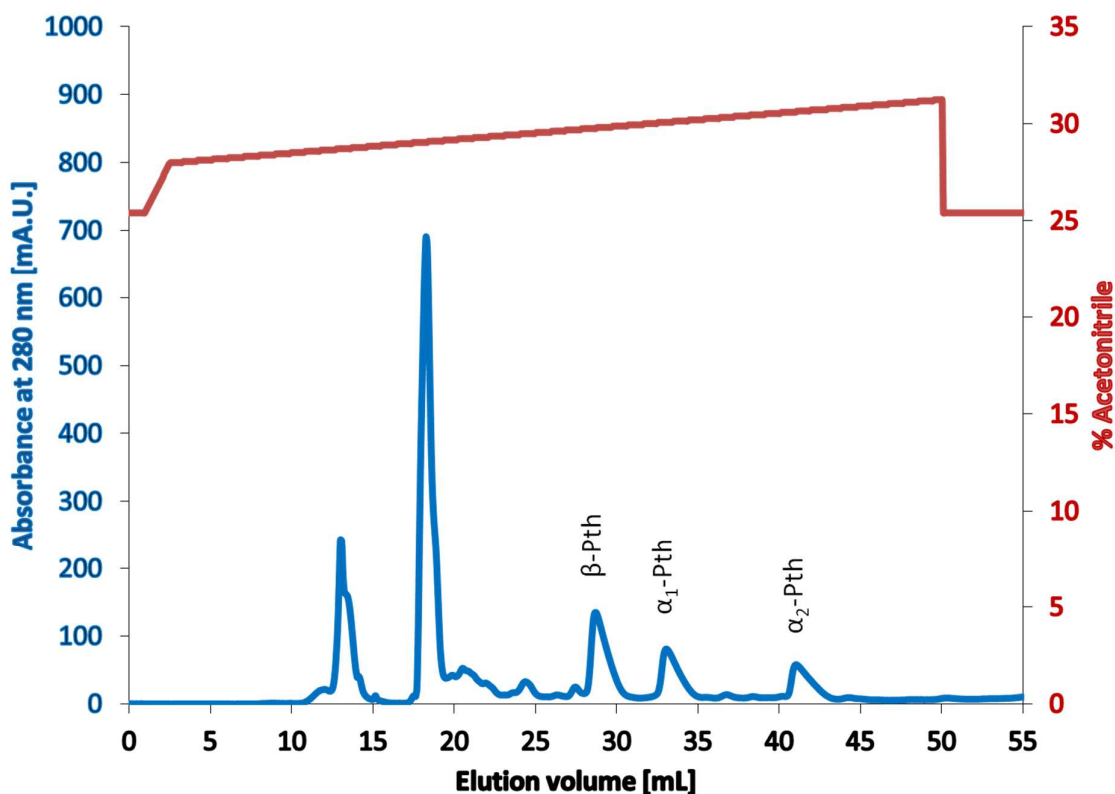


Figure 3.4 RP-HPLC chromatogram obtained from purothionin rich fraction of the Triton X-114 wheat protein extract.

The obtained chromatogram matches the results achieved by Sanders¹³³ (see Figure 3, Appendix, page 175). The fractions eluted at 28, 34 and 42 mL were trypsin-digested, subjected to LC-MS analysis and identified as β -Pth, α_1 -Pth and α_2 -Pth, respectively by others (Luke Clifton, personal communication, 5.07.2013). The mass spectrum of β -Pth, described by Sanders,¹³³ can be found in Figure 4, Appendix, page 175. α_2 -Pth fraction used in the experiments was the one used by Clifton *et al.* in the research characterizing the protein hydrophobicity impact on the interactions with anionic phospholipid monolayers.²⁹

3.3.3 γ -Purothionins Purification

Figure 3.5 shows the SDS-PAGE analysis of the ammonium bicarbonate-soluble and insoluble fractions obtained from ammonium bicarbonate partitioning of the NaCl-soluble extracts as described in section 3.2.3.3.

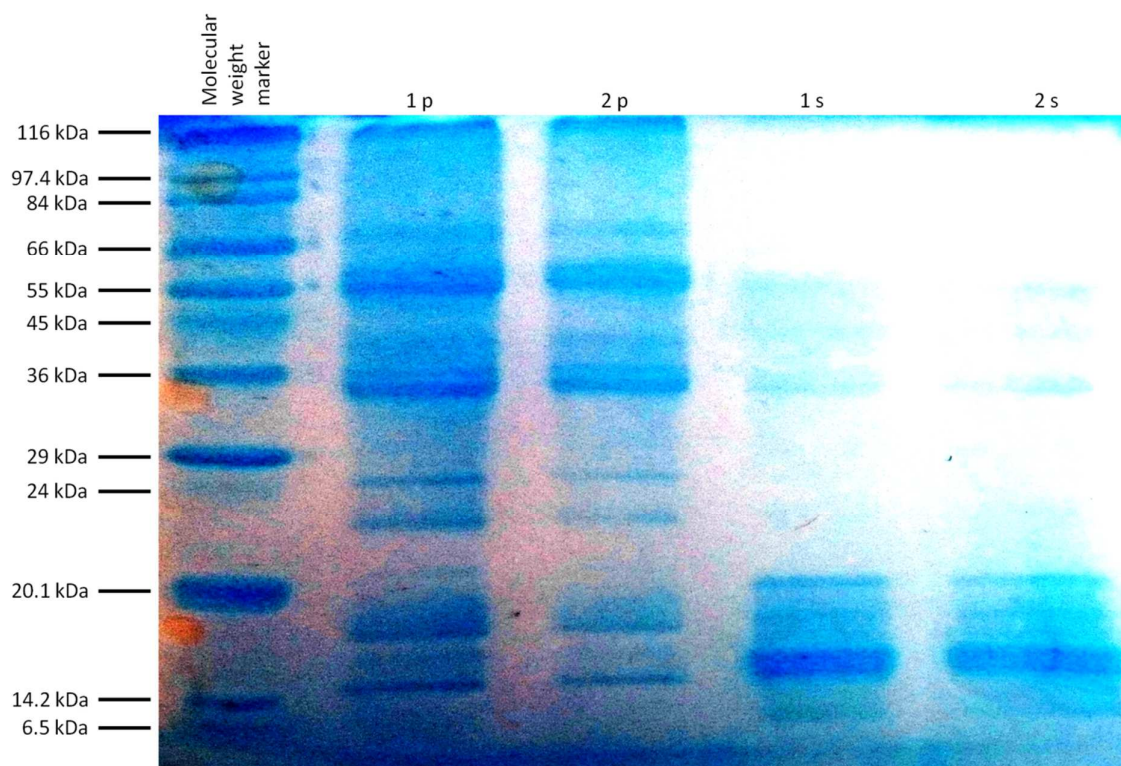


Figure 3.5 SDS-PAGE analysis of the pellets (1p and 2p) and supernatants (1s and 2s) after final ammonium bicarbonate wash of the NaCl-soluble protein extract.

The similarity of the SDS-PAGE profiles between 1p and 2p samples, as well as between 1s and 2s ones suggests good reproducibility of the ammonium bicarbonate washing process. Both pellet and supernatant appeared to contain the abundance of the NaCl-soluble proteins. The dark bands appearing below 6.5 kDa in 1p and 2p samples could be the γ -Pth isoforms.

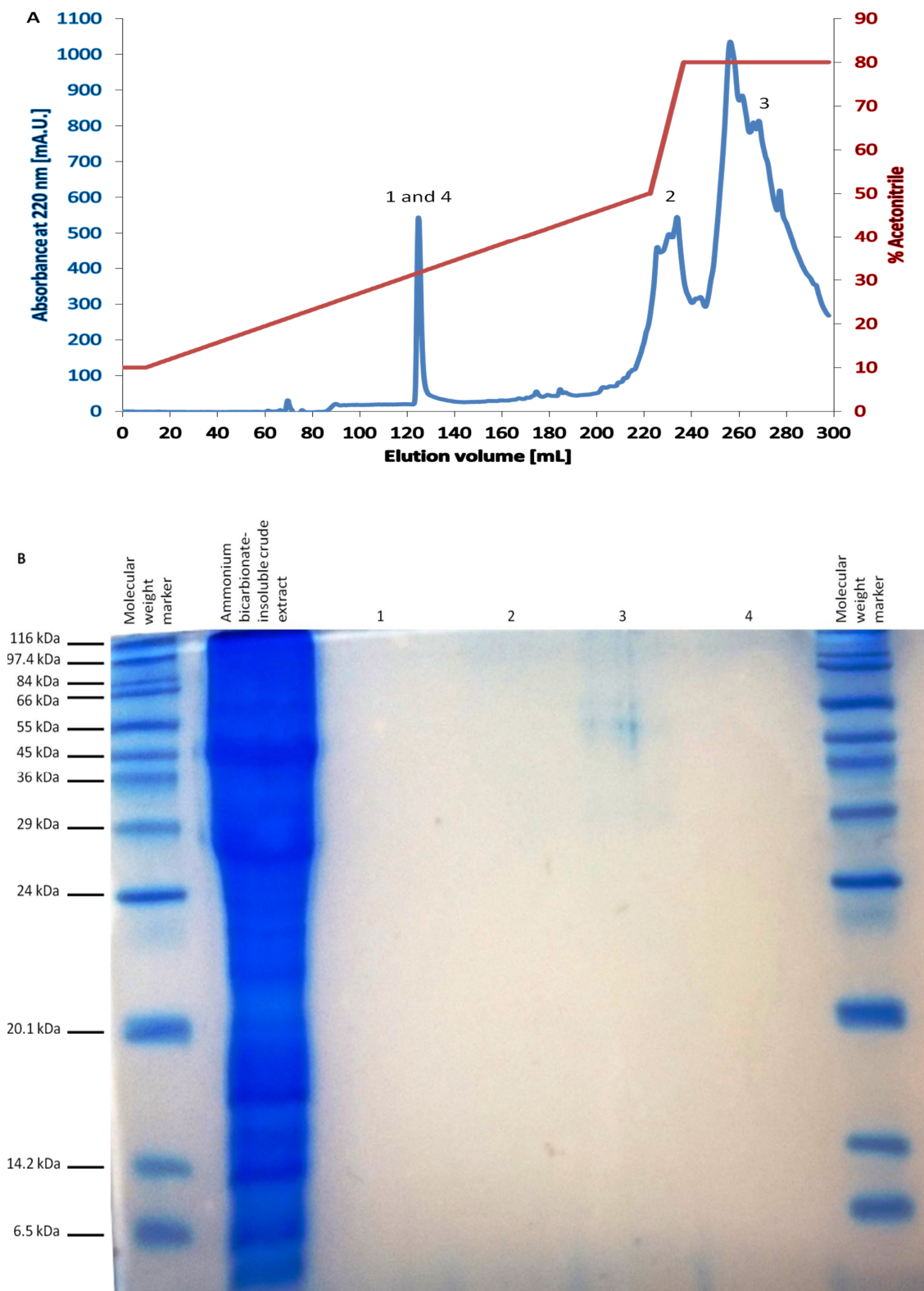


Figure 3.6 RP-HPLC chromatogram (A) and SDS-PAGE (B) analysis of the fractions collected during Cosmosil C4 RP-HPLC purification of the ammonium bicarbonate-insoluble crude protein extract.

The elution profile in Figure 3.6 shows a good separation of the peak eluting at 35% acetonitrile concentration, which corresponds well with the results obtained by Colilla *et al.*⁵⁴ However, the absorbance at 280 nm monitoring revealed no peak, indicating that the compound does not possess any phenol derivatives in its structure (data not shown). This was in contradiction to both γ_1 - and γ_2 -Pths amino acid sequences (see Chapter 1, page 7) containing both tryptophan and phenylalanine.

SDS-PAGE analysis of the peak did not reveal any band, indicating that the sample may contain either a very small peptide (< 5 kDa) or a non-protein compound, *e.g.* a lipid. The mass spectrometry analysis of the peak showed the compound of molecular weight close to 500 g/mol (data not shown), suggesting that it might contain a relatively polar lipid.

The chromatogram also revealed that the sample contained a high proportion of compounds eluting above the 50% acetonitrile concentration, also absorbing at 280 nm. None of the compounds, however, produced a band on the SDS-PAGE gel, which may mean that the peaks consisted either of the very light amino acid chains or their complexes with lipids.

The elution profiles were reproducible but revealed errors made at the extraction stage. The purification process emphasized the importance of the proper lipid removal from the wheat flour and of the protein denaturation avoidance at the crude extraction stage. The future extraction attempts should focus on eliminating the above-mentioned mistakes.

3.4 Conclusions

Purification of the Pin-a and β - and α_2 -Pths was successful and characterized by good reproducibility of the results, well corresponding to the ones obtained by the others.^{80,133} It provided the high purity proteins used in the further described experiments.

The γ -Pth extraction protocol, however, needs to be improved, *e.g.* by introducing the following steps:

- Filtration and/or centrifugation of the organic solvents and flour mixtures between the delipidation stages allowing better separation of the extracted lipids.
- Incubation of the NaCl-soluble protein extracts with 15% TCA for more than 1 h at the temperature lower than 4°C to isolate more proteins and reduce the risk of their denaturation.

- Use of the acetone stored at the temperature below 4°C to minimize the risk of protein denaturation.

Implementation of the abovementioned steps should result in the better protein extraction yield and maintenance of the γ -Pths' native structures.

Chapter 4

LIPID MONOLAYER STUDIES

4.1 Introduction

Once the sufficient amount of protein was obtained as described in Chapter 3, it was possible to carry out the experiments on the protein effect on the various lipid systems. The protein-lipid interactions were preliminarily assessed by means of the Langmuir monolayer technique. It bases on spreading the lipid monolayer on the surface of aqueous solution, compressing it to the surface pressure corresponding to the lipid arrangement in the natural cell membrane, injecting the interacting compound and monitoring the surface pressure changes.³

Using the monolayers allows the precise control of the film thickness and packing density, and can be further developed into forming the multilayers of the accurate thickness. However, the technique requires absolute chemical purity and many artefacts, like dust particles, can disturb the surface pressure readout. Despite the mentioned difficulties, the Langmuir monolayers were successfully employed for studying the interactions of various proteins with artificial cell membranes.

For example, Lad *et al.*¹⁰⁰ in 2005 used the stearic acid and DPPC monolayers to study the interfacial phenomena occurring during the adsorption of lysozyme, bovine serum albumin and human serum albumin. Further investigation of the protein structure on the interactions with the monolayers was carried out by Clifton *et al.*³ who examined the effect of the Pin-b mutations on the protein's adsorption to the DPPG monolayers.

The antimicrobial properties of the cationic peptides were the topic of the study by Lad *et al.*¹³⁵ from 2007, in which the DPPG and DPPC monolayers were subjected to the action of melittin, magainin II and cecropin P1. Sanders *et al.*⁵³ focused their experiments on revealing the synergistic and competitive behaviour of the different groups of wheat defence proteins against the bacterial model membranes: DPPG monolayers. PC and PG monolayers were also used by Chen *et al.*,¹³⁶ who examined the antitumor and antimicrobial properties of the

synthetic peptides and the effect of the steroid presence in the membrane on the strength of the interactions with the peptides.

This chapter describes the monolayer study of the puroindoline and purothionin interactions with phospholipids found in the cell membrane of baker's yeast *Saccharomyces cerevisiae* (see Chapter 1, page 11). The results from these studies will allow to further develop the lipid systems to be analysed, thus providing a primary insight into the antifungal mode of action of the wheat defence proteins.

4.2 Materials

1,2-Dipalmitoyl-*sn*-glycero-3-phosphocholine (DPPC, synthetic, purity > 99%), 1,2-dipalmitoyl-*sn*-glycero-3-phospho-(1'-*rac*-glycerol) (DPPG, synthetic, purity > 99%), 1,2-dipalmitoyl-*sn*-glycero-3-phospho-L-serine (DPPS, synthetic, purity > 99%) and 1-palmitoyl-2-oleoyl-*sn*-glycero-3-phospho-L-serine (POPS, synthetic, purity > 99%) were all purchased from Avanti Polar Lipids (Alabaster, AL, US). All lipids were used without further purification. Lipid solutions of DPPC and POPS (1 g/L) were prepared in HPLC grade chloroform (Sigma Aldrich, Dorset, UK). The solutions containing DPPS and DPPG were prepared in chloroform:methanol mixture 2:1 vol:vol – HPLC grade methanol was purchased from Sigma-Aldrich (Dorset, UK). The solutions were stored at room temperature (saturated lipids) or at -20°C (unsaturated lipids and their mixtures).

Phosphate buffer salts were obtained from Fisher Scientific (Loughborough, UK) and chicken egg white lysozyme (protein \geq 90%) from Sigma Aldrich (Dorset, UK). For surface pressure measurements, protein stock solutions were prepared in 20 mM phosphate buffer solution at pH 7.0 using UHQ grade water (resistivity 18.2 M Ω ·cm obtained from ELGA LabWater purifier – High Wycombe, UK) and the concentrations were checked with UV absorbance at 280 nm.

For the reasons behind the lipids and proteins used in the experiments and their molecular structures, please refer to Chapter 1, pages 10 and 15.

4.3 Surface Pressure Measurements

Surface pressure measurements were carried out using a polytetrafluoroethylene (PTFE) Langmuir trough (model 611, Nima Technology Ltd, Coventry, UK) and the surface tension decrease was monitored *via* a Wilhelmy plate sensor.

The trough was filled with 80 mL of 20 mM phosphate buffer (pH 7). Ten microlitres of the lipid solution (1 g/L) was spread at the air/water interface, the solvent was allowed to evaporate for 10 minutes and the monolayer was compressed to a surface pressure of 22 mN/m at constant barrier speed 10 cm²/min. The monolayer has been compressed and expanded three times to assess the purity of the monolayer and its stability.

Stability of the compressed monolayers was then monitored *via* surface pressure *vs.* time measurements. A sample of an appropriate protein solution was added with a syringe to the subphase, without disturbing the monolayer, as depicted in Figure 4.1.

Changes in surface pressure were then monitored by plotting surface pressure *vs.* time, keeping the interfacial area constant. The experiments on the 80 mL trough were used mainly for assessing the compression behaviour of the lipids and the protein adsorption experiments were carried out on the small PTFE trough (94 × 22 × 5 mm) – see Figure 4.2.

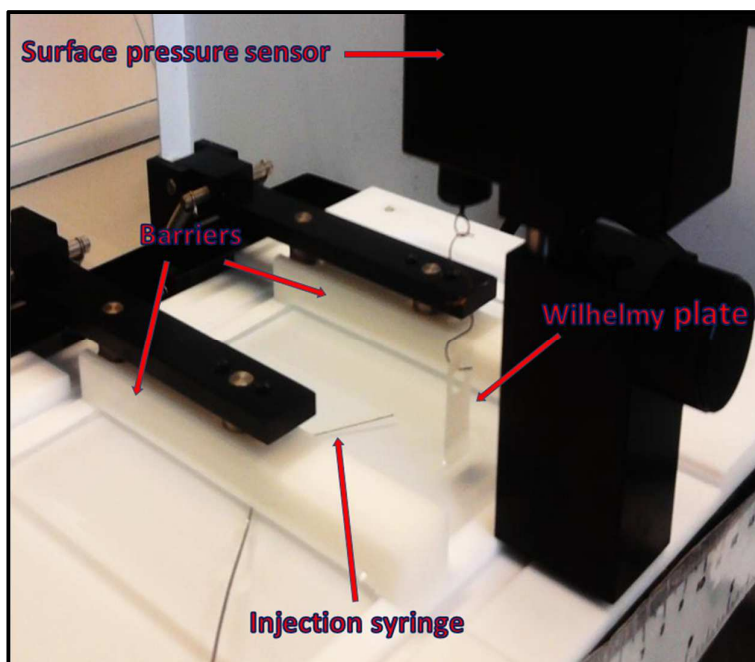


Figure 4.1 An 80 mL Langmuir trough used for monitoring the surface pressure changes caused by the adsorption of the tested protein / protein mixture to the lipid monolayer.

Control experiments were carried out in an analogous manner using a sample of the pure buffer solution instead of the protein solution. The experiments have been done at least in triplicates and reported as the average of three readings corresponding to the total surface pressure change upon the interaction. Standard deviation was used for describing the measurement uncertainty. All experiments were carried out at room temperature: 22-25°C.

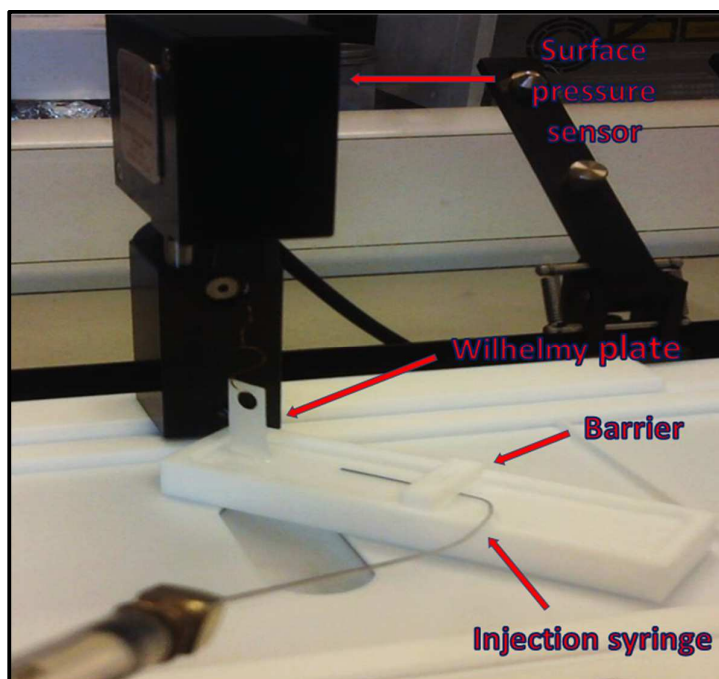


Figure 4.2 A 10 mL trough used for carrying out the monolayer experiments basing on the monitoring of the changes in the surface pressure.

4.3.1 Method Development: Lysozyme vs. DPPG

Lysozyme's effect on the DPPG monolayer was examined at the film surface pressure of 22 mN/m corresponding to the liquid-condensed phase of the lipid compression.¹³⁷ Figure 4.3 shows the surface pressure-area curve of a DPPG monolayer, depicting the conditions the monolayer was held at prior to the protein injection – a constant area per molecule of 56.7 Å². The shape of a DPPG isotherm allows for clear indication of the intermediate compression phases suggesting that at the moment of spreading the molecules are relatively well separated, which was further confirmed by the Brewster Angle Microscopy images obtained by Clifton *et al.*⁵² The isotherm matches the ones obtained by Lad,¹⁰⁰ Sàndez *et al.*⁷ and Liu *et al.*¹³⁸

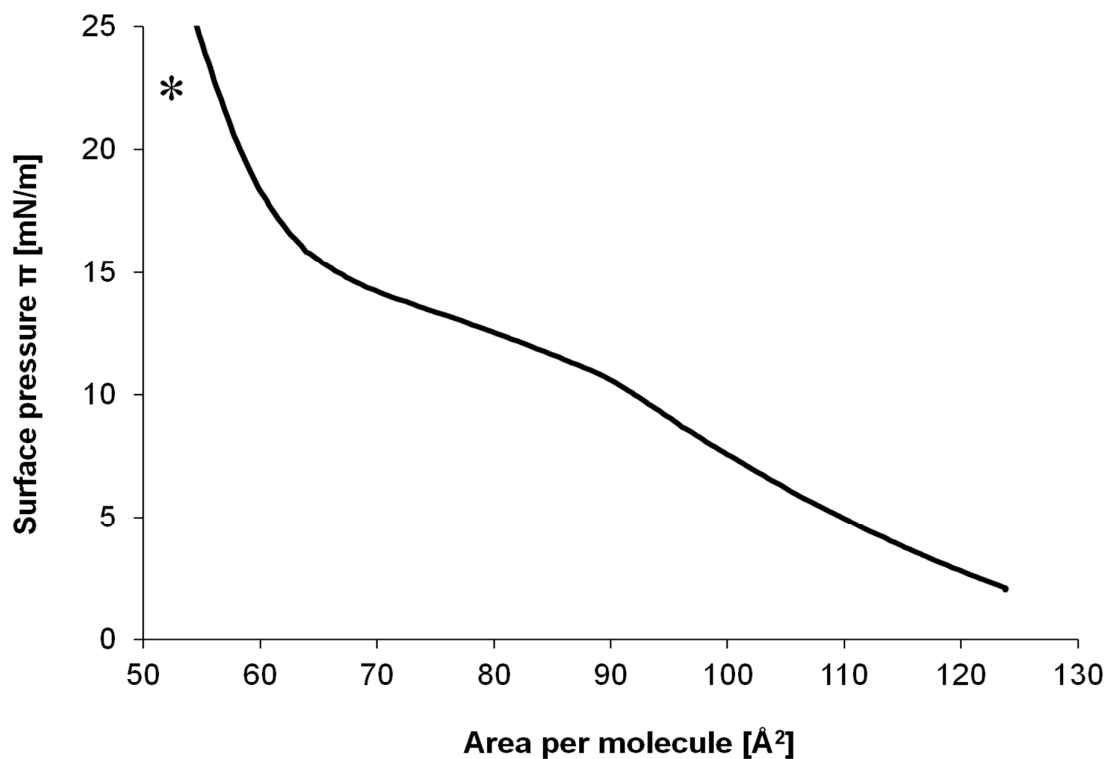


Figure 4.3 Surface pressure – Area isotherm of DPPG showing the surface pressure point at which a sample of lysozyme was injected (*).

The experimental conditions are summarized in the table below.

Table 4.1 Experimental conditions of the surface pressure measurements: lysozyme vs. condensed phase DPPG monolayer.

Components of the analysed system	Amount used per 80 mL subphase (final concentration in the subphase) / per 100 cm ² initial interfacial area	Amount used per 9 mL subphase (final concentration in the subphase) / per 17.16 cm ² initial interfacial area
Protein: Lysozyme	2 mL of 42.64 g/L (72.66 μM)	0.5 mL of 19.76 g/L (72.66 μM)
Lipid: DPPG	10 μL of 1 g/L	2.5 μL of 1 g/L

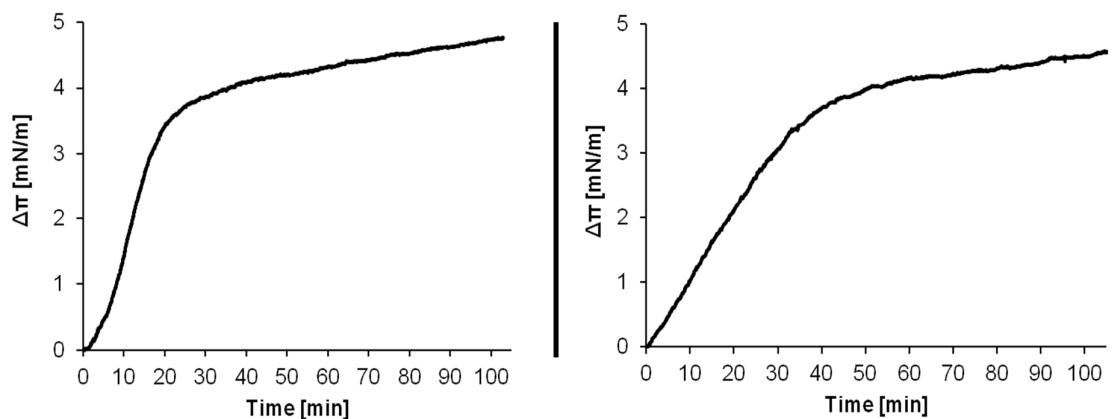


Figure 4.4 Surface pressure vs. time measurements showing the change in surface pressure during the adsorption of lysozyme to the condensed phase DPPG monolayers on 10 mL trough (left) and 80 mL trough (right).

The experiments on both 80 and 10 mL troughs showed a significant rise in surface pressure right after the protein injection. This indicated the strong interaction of lysozyme with the DPPG monolayer. The maximal values reached imply good consistency of the results between the 2 troughs. This is further confirmed by the observed surface pressure changes - in the 80 mL trough they were equal to 4.50 ± 0.23 mN/m whereas in 10 mL trough the surface pressure rose to 4.72 ± 0.73 mN/m. A faster increase of π has been observed in the 10 mL trough due to the faster protein diffusion towards the monolayer caused by the special limitation. The results support the idea of initial electrostatic interactions between a cationic protein and a negatively charged head group of the phospholipid, which ultimately lead to the protein adsorption to a monolayer with the possibility of the monolayer penetration.

Table 4.2 Summary of the experiment results of the lysozyme interacting with condensed phase DPPG monolayers using two different trough volumes. The P value corresponds to the result of an independent 2-tailed t-test.

Trough volume [mL]	Surface pressure rise $\Delta\pi$ [mN/m]	P value
10	4.72 ± 0.73	0.16
80	4.50 ± 0.23	

The independent 2-tailed t-test revealed that there was no significant difference between the results obtained from the 2 trough volumes at the 95% confidence level. The agreement between the experiments carried out on the two different troughs justifies the use of the 10 mL trough for further monolayer experiments with defence proteins. Switching to the lower volume trough enabled to save the amounts of analytes used per experiment and time of the equipment preparation. The 10 mL trough has also been successfully employed by Clifton⁸⁰ and Sanders.¹³³

4.3.2 β -Pth vs. Saturated Phospholipid Systems

The saturated phospholipids DPPC and DPPS, typical of the fungal cell membrane (see: Chapter 1, page 11), were chosen for the preliminary study of the biocidal action of β -Pth. In order to examine the influence of the phospholipid charge, 3 lipid systems were analysed: anionic DPPS, zwitterionic DPPC and the mixture of DPPC and DPPS at the molar ratio 1:1 providing intermediate charge between the anionic and electrostatically neutral systems.

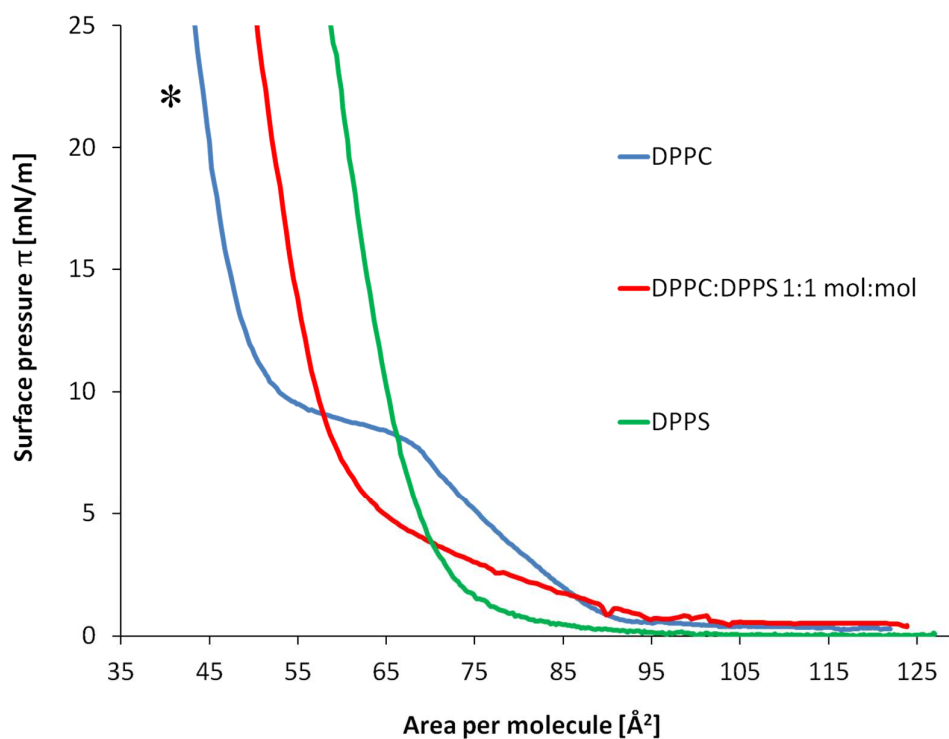


Figure 4.5 Surface pressure – Area isotherm of the saturated phospholipid systems showing the surface pressure point at which a sample of β -Pth was injected (*).

The isotherm of DPPS showed no distinct intermediate phases upon its compression, suggesting that this lipid spontaneously forms condensed domains when spread at the air/water interface (see Figure 4.5 – green line). The isotherm's shape was in good agreement with the one obtained by Ronzon *et al.*¹³⁹ and Rosengarth *et al.*¹⁴⁰ A steep increase of surface pressure at low compression areas is typical of condensed films. Prior to injection, the monolayers were held at 22 mN/m which corresponded to the molecular area of 59.89 Å².

In contrast to DPPS, a DPPC monolayer appears to have better separation of molecules at the moment of spreading. Hence, distinct liquid phases could be observed during the compression, as depicted in Figure 4.5 (blue line), well matching the isotherms from the studies by Lad,¹⁰⁰ Miano *et al.*⁷⁶ and Yun *et al.*¹⁴¹ Before the peptide injection, the monolayers were held in condensed phase at surface pressure of 22 mN/m and the mean molecular area of 44.27 Å².

The 1:1 DPPC:DPPS mixed lipid isotherm resembles a combination of the isotherms of its two components. The liquid phase, approximately at 80 Å², positioned between the DPPC and DPPS curves is likely to represent the intermediate characteristics of the mixed lipid, *i.e.* there is a proportion of the initially separated molecules but not as many as in case of the pure DPPC lipid.

Moreover, the transition to the condensed phase appears to be more gradual than the one of the DPPS lipid, yet quicker than the one of the DPPC monolayer. The protein injection point of the 22 mN/m surface pressure reflected the lipid mean molecular area of 51.34 Å² which is relatively close to the median of the molecular areas between DPPC and DPPS condensed phase monolayers (equal to 52.08 Å²).

Overall, the mixed lipid system seems to represent the middle point between the systems containing only its single components. Similar findings of displaying intermediate features by the mixed lipid systems were reflected in the isotherms obtained by Luna *et al.*,¹⁴² Rosengarth *et al.*,¹⁴⁰ Saleem *et al.*¹⁴³ and Dietrich *et al.*¹⁴⁴

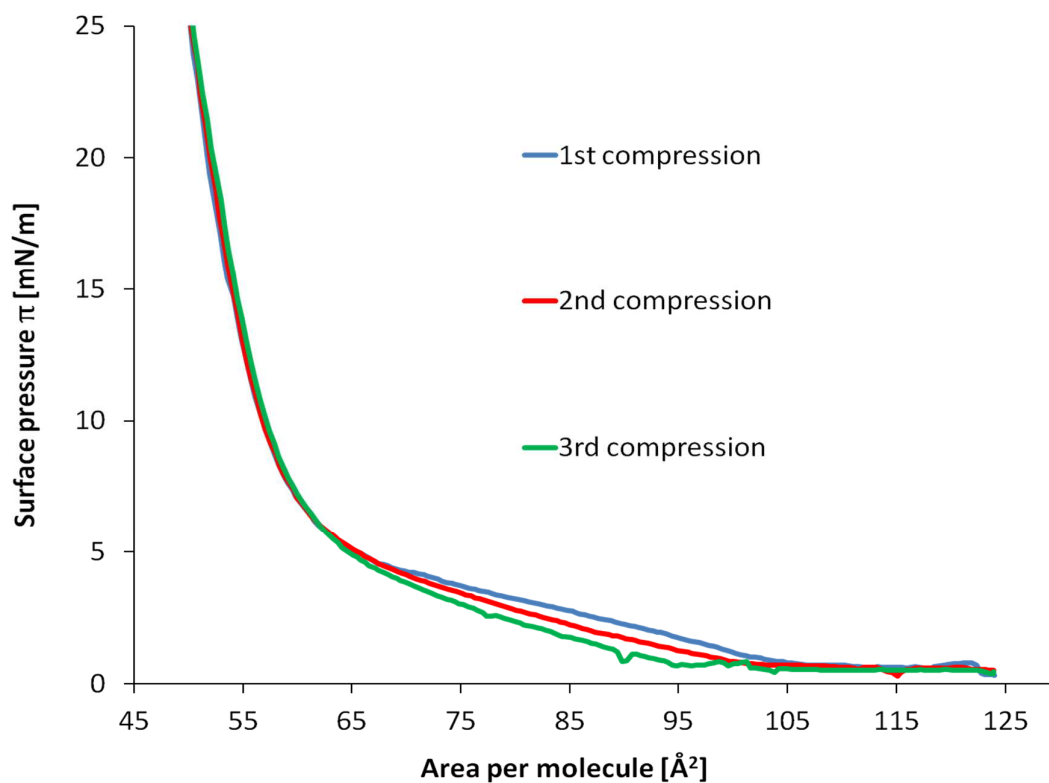


Figure 4.6 Surface pressure – Area isotherms of the DPPC:DPPS 1:1 mol:mol monolayer presenting the multiple compressions of the film.

Mean molecular areas of the condensed phase are also indicative of the accuracy of the lipid samples' concentrations, as the shapes of the isotherms are sensitive to the amount of the amphiphile present at the interface.

Figure 4.6 shows the multiple compressions of the mixed lipid film. The good agreement of the isotherm shapes during each compression is indicative of the high purity of the lipid monolayer and its high quality achieved by the film annealing.¹⁴⁵ Good isotherm repeatability was particularly evident in the condensed phase of the monolayer (18-25 mN/m) which was crucial for the experiments' outcomes.

The blank experiment, illustrated in Figure 4.7 showed a relatively small drop in the surface pressure caused by the moderate relaxation of the monolayer which after 80 minutes still remained in the condensed phase – the overall pressure drop equal to 3.18 mN/m. As there was no clear evidence of any significant change to the monolayer structures for other lipid systems (data not shown), the results of the protein adsorption experiments were reported directly as raw data without the subtraction of the blank experiment values.

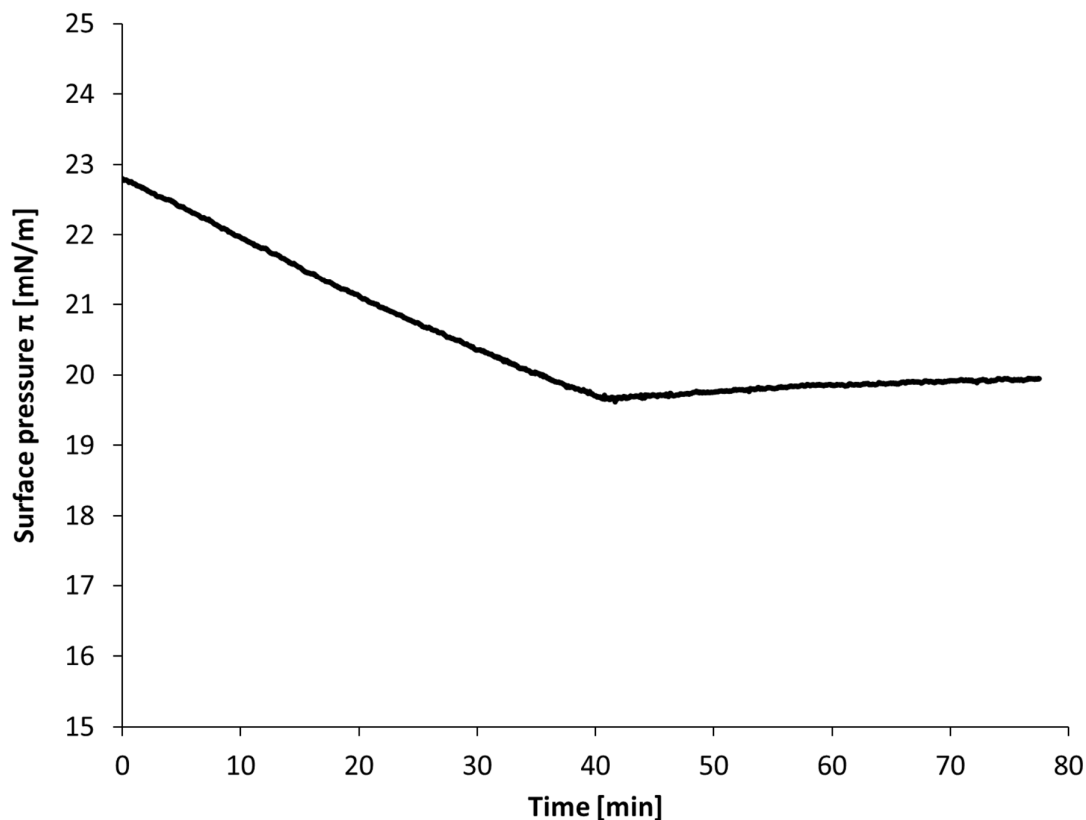


Figure 4.7 An example of the blank monolayer experiment showing the changes in surface pressure after the injection of the phosphate buffer pH 7.0 sample to the condensed phase DPPC monolayer.

Table 4.3 contains the amounts of components used for studying the β -Pth adsorption to the saturated phospholipid monolayers with varying net charge.

Table 4.3 Experimental conditions of the surface pressure measurements: β -Pth vs. condensed phase saturated phospholipid monolayers.

Components of the analysed system	Amount used per 9 mL subphase (final concentration in the subphase) / per 17.16 cm ² initial interfacial area
Protein: β -Pth	0.5 mL of 0.044 g/L (0.48 μ M)
Lipid: DPPC, DPPS, DPPC:DPPS 1:1 mol:mol	2.5 μ L of 1 g/L

Figure 4.8 shows the results of the β -Pth adsorption experiments aiming at studying its interaction with condensed phase saturated phospholipid monolayers differing in the net charge. For the fully zwitterionic DPPC-only monolayer, the overall changes in surface pressure obtained from measurements taken in 10 ml trough were equal to 1.55 ± 0.13 mN/m.

A small increase in π has been observed within the first 5 minutes, indicating the slight rearrangement and/or perturbation of the monolayer.

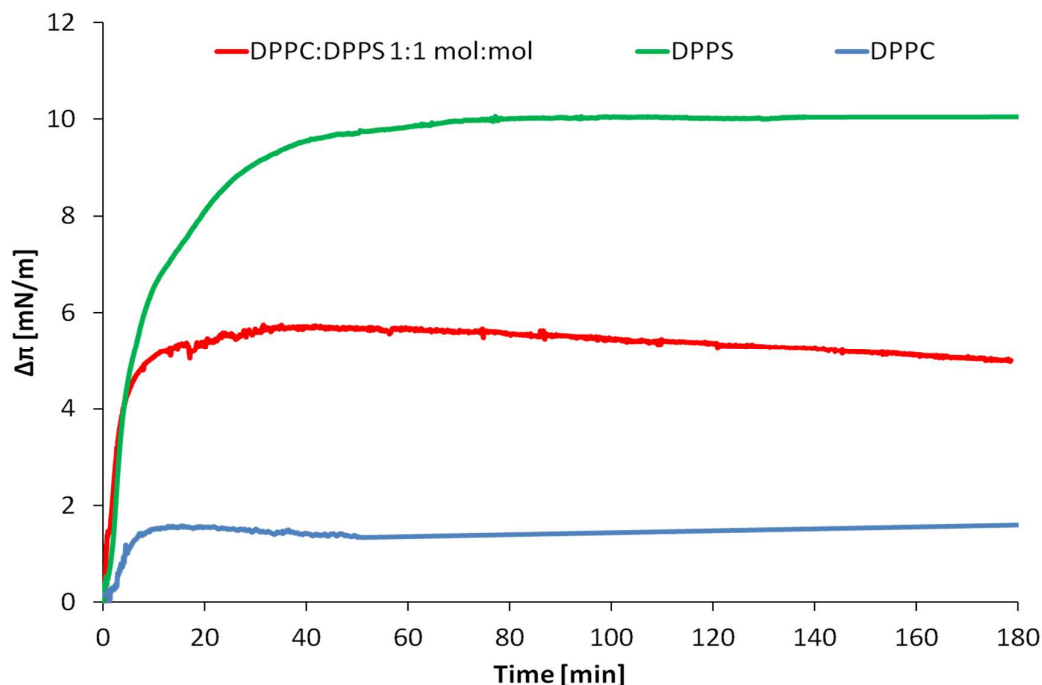


Figure 4.8 Surface pressure vs. time isotherms showing the change in surface pressure after the injection of the β -Pth to the condensed phase saturated phospholipid monolayers with varying net charge values.

Within 50 minutes, the surface pressure values tended to slightly drop which could be assigned to relaxation of the monolayer.¹⁴⁶ From around the 60th minute the surface pressure has been moderately rising, possibly due to the low level of the protein adsorption to the monolayer. The overall rise of the surface pressure, however, was not as pronounced as in the case of the lipid systems containing the negative charge.

Similarly to wild-type Pin-b⁴⁹ and lysozyme (see Figure 4.4), β -Pth appears to be favouring the interactions with anionic phospholipids, which is further confirmed by comparing surface pressure changes caused by this thionin injected below the DPPC monolayer with the results obtained for DPPS monolayer: overall pressure change 1.55 ± 0.13 mN/m and 9.88 ± 0.16 mN/m, respectively (see Table 4.4). The shape of the surface pressure vs. time isotherm for the DPPS-only system resembles the shapes obtained by the experiments on the other strongly interacting protein-lipid systems, *e.g.* β -Pth vs. DPPG²⁷ or melittin vs. DPPG.¹³⁵

Table 4.4 Summary of the monolayer experiments of β -Pth (final concentration in the subphase 0.48 μ M) interacting with saturated phospholipid systems. An independent 2-tailed t-test showed significant differences at $P \leq 0.05$.

Lipid system	Features of the tested system	Surface pressure rise $\Delta\pi$ [mN/m]	Significant difference test	
			P value	Compared system
1. DPPS	Saturated, anionic	9.88 ± 0.16	0.02	2
			< 0.01	3
2. DPPC:DPPS 1:1 mol:mol	Saturated, half-anionic, half-zwitterionic	6.02 ± 0.24	< 0.01	3
3. DPPC	Saturated, zwitterionic	1.55 ± 0.13	See above	

The intermediate lipid system DPPC:DPPS 1:1 mol:mol composed of zwitterionic and anionic phospholipids with the net charge equal to half of the DPPS-only system has been affected by β -Pth to the smaller extent than the fully anionic system but much more than the fully zwitterionic monolayer (see Figure 4.8 and Table 4.4). The surface pressure rise displayed slightly different kinetics than for the DPPS-only system, *i.e.* the saturation was reached around 40th minute and the insignificant drop of the surface pressure was observed thereafter, which could be assigned to the gradual monolayer relaxation.

The overall surface pressure rise value 6.02 ± 0.24 mN/m seems to be relatively close to the arithmetic mean between the values obtained from the experiments on DPPC-only and DPPS-only systems, equal to 5.72 ± 0.15 mN/m. This suggests that there might be a directly proportional relationship between the surface pressure rise and the number of molecules bearing the anionic charge present in the system. However, more studies on the phospholipid systems containing various proportions of zwitterionic and anionic components would need to be carried out to confirm this hypothesis.

What can be stated with certainty is that the monolayer's net charge plays a significant role in the cationic protein interactions with phospholipid membranes. This conclusion is in good agreement with the ones obtained from the studies by Lad,¹⁰⁰ Clifton⁸⁰ and Sanders.¹³³

4.3.3 β -Pth vs. Saturated and Unsaturated Lipid Systems

As mentioned in Chapter 1 (see page 12), fungal membranes contain a significant proportion of unsaturated phospholipids in their cell membranes. It has been shown in the previous section that one could expect much stronger protein-lipid interactions using the anionic phospholipid system than the zwitterionic one. Therefore, to examine the effect of the phospholipid unsaturation on its interaction with the antimicrobial proteins, two anionic phospholipid systems were used for the experiments: the saturated DPPS and unsaturated POPS (see the molecular structures in Chapter 1, Figure 1.6, page 13).

The amounts of components used for the experiments match the ones in Table 4.3. Figure 4.9 shows the compression isotherms of DPPS and POPS phospholipid monolayers. Due to the presence of 2 more carbon atoms and the *cis*-double bond in one of its fatty acid residue chains, the POPS molecule occupies more space than the molecule of a fully saturated DPPS (see Figure 1.6, page 13 for the structure of the molecule). This is confirmed by the obtained value of the POPS mean molecular area at 22 mN/m: 76.44 Å² which is much higher than the one of the DPPS molecule held at the same surface pressure: 44.27 Å².

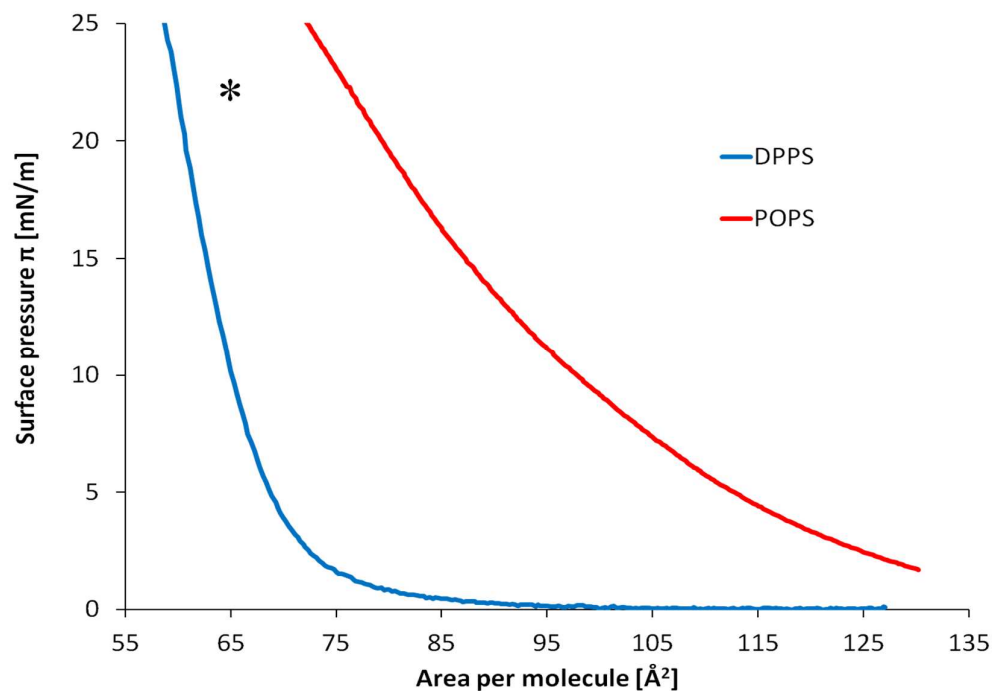


Figure 4.9 Surface pressure – Area isotherm of the saturated DPPS and unsaturated POPS phospholipid systems showing the surface pressure point at which a sample of β -Pth was injected (*).

The shape of the POPS isotherm indicates the smooth transition from the expanded to condensed phase, suggesting no initial spontaneously formed condensed domains as in case of DPPS. The POPS isotherm is well corresponding to the ones obtained by Nerdal *et al.*¹⁴⁷ and Steinkopf *et al.*¹⁴⁸

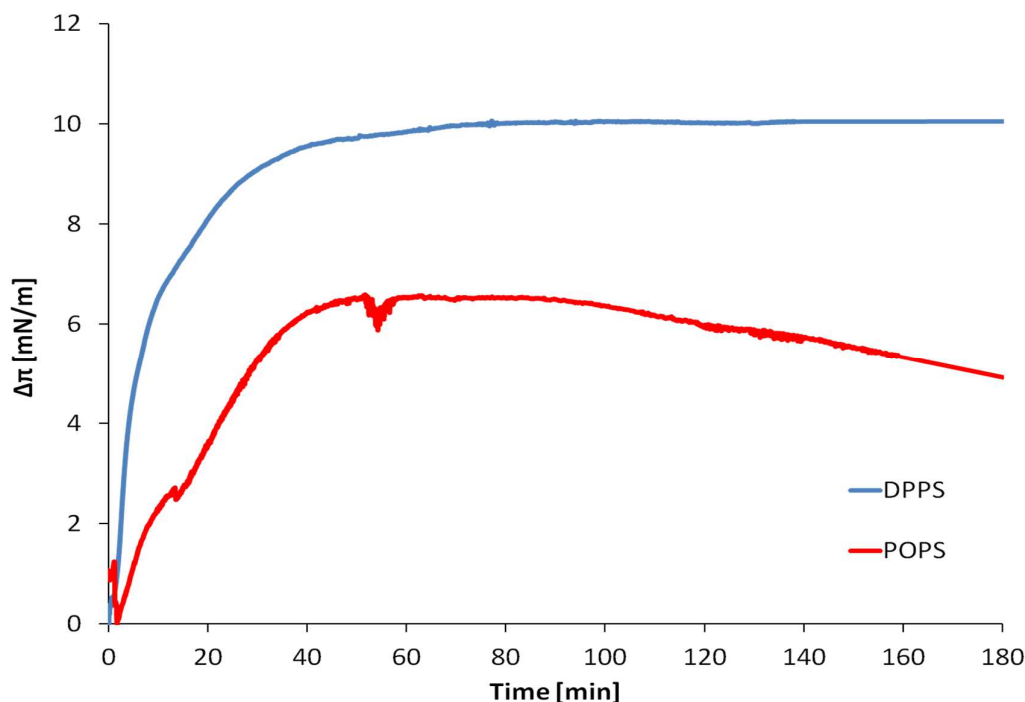


Figure 4.10 Surface pressure vs. time isotherms showing the change in surface pressure after the injection of the β -Pth to the condensed phase of saturated DPPS monolayers (blue) and unsaturated POPS monolayers (red).

Figure 4.10 and Table 4.5 summarise the results of the β -Pth interactions with saturated and unsaturated anionic phospholipid monolayers. Both protein-adsorbed systems showed the notable increase in the surface pressure. However, the POPS system displayed the different interaction kinetics than the DPPS one.

While protein-adsorbed DPPS showed the growth in surface pressure that reached its plateau around 115 min and stayed constant since then, the POPS monolayer appeared to have been saturated by the protein within 50 minutes. Still, after this point, the surface pressure dropped which could be a result of the monolayer loosening and/or slow protein desorption. The results reported in Table 4.5 for POPS monolayer refer to the maximal value of surface pressure reached after 52 minutes.

Table 4.5 Summary of the monolayer experiments of β -Pth (final concentration in the subphase 0.48 μ M) interacting with the saturated and unsaturated lipid systems. An independent 2-tailed t-test showed significant differences at $P \leq 0.05$.

Lipid system	Features of the tested system	Surface pressure rise $\Delta\pi$ [mN/m]	P value
DPPS	Saturated, anionic	9.88 ± 0.16	< 0.01
POPS	Unsaturated, anionic	6.25 ± 0.46	

Similar plot shape including initial overcompression and gradual drop of the surface pressure was observed by Bougis *et al.*¹⁴⁹ who studied the adsorption of cardiotoxin to the negatively charged short-chain phospholipid monolayers.

The maximal change in the surface pressure of the POPS monolayer was significantly lower than the one obtained for the DPPS system (see Table 4.5). This suggests that the saturation of the anionic lipid molecules, and therefore their degree of packing in the monolayer prior to protein injection has a significant impact on their interacting capabilities with the cationic proteins and on the interaction kinetics.

4.3.4 Pin-a, α_2 -Pth and β -Pth vs. DPPS

Some antimicrobial proteins were shown to cooperate with each other to maximise the antimicrobial effect, *e.g.* the thionins' synergistic activity with lipid-transfer-proteins (LTPs) against the fungal pathogens has been described by Molina and Garcia-Olmedo.³⁰ In this section, different wheat defence proteins and their mixtures will be used to examine their impact on the DPPS monolayer. This saturated anionic phospholipid system was chosen as it showed the strongest interactions with β -Pth and therefore the effect of the other proteins could be easily compared.

The compared proteins were Pin-a and α_2 -Pth against β -Pth. To examine the synergy effects between the proteins, a 1:1 mol:mol β -Pth:Pin-a and a 1:1 mol:mol β -Pth: α_2 -Pth solutions

were prepared to study the co-operation or competition between the thionins and indolines and between two different thionins, respectively.

All proteins showed strong interactions with the DPPS monolayer when injected at 0.48 μM final concentration (see Tables 4.6 and 4.7). β -Pth had the strongest effect on the monolayer whereas Pin-a and α_2 -Pth caused only slightly lower surface pressure rises.

The average values of surface pressure rises for β -Pth and Pin-a were found to be smaller when the protein concentration decreased by half (see Table 4.6). However, at the 95% confidence level there were no significant differences shown between the results obtained by injecting the proteins at final concentrations 0.24 μM and 0.48 μM for both proteins, suggesting that the lower concentration could be considered for the future studies on the β -Pth and Pin-a proteins.

Similar conclusion could be drawn for the use of lower concentration of α_2 -Pth as there was no significant difference between the results obtained for the two protein concentrations at the 95% confidence level (see Table 4.7).

Table 4.6 Summary of the monolayer experiments of β -Pth, Pin-a and their 1:1 mol:mol mixture interacting with condensed DPPS monolayers. An independent 2-tailed t-test was used for indicating the significant differences (marked bold) at $P \leq 0.05$.

Tested protein / protein mixture and the final protein concentration in the subphase	Surface pressure rise $\Delta\pi$ [mN/m]	Significant difference test	
		P value	System compared
1. β -Pth 0.48 μM	9.88 \pm 0.16	0.07	2
2. β -Pth 0.24 μM	7.89 \pm 0.97	See above	
3. Pin-a 0.48 μM	8.48 \pm 0.58	0.05	4
4. Pin-a 0.24 μM	7.24 \pm 0.55	See above	
5. (β -Pth:Pin-a 1:1 mol:mol) 0.48 μM	11.59 \pm 0.78	0.02	1
		< 0.01	2
		< 0.01	3
		< 0.01	4

The result for the mixed protein system β -Pth: α_2 -Pth 1:1 mol:mol turned out to be not significantly different from the ones obtained from any other analysed protein system. This suggests that there is no noticeable influence on the interacting capabilities by mixing α_2 -Pth with β -Pth. Taking into account only the average results, one could suspect slight competition between the two thionins, as their mixed system produced an average result 7.34 mN/m, which is lower than the average results obtained by injecting the proteins separately to their final concentration 0.48 μ M. Still, the competitive action between the two thionins cannot be stated as the obtained results were not significantly different.

In contrast to the thionin mixture, the system consisting of Pin-a and β -Pth gave rise to the results that were significantly different from all other compared protein systems (see Table 4.6). Mixing the indoline and the thionin resulted in an increased value of the surface pressure rise: 11.59 ± 0.78 mN/m vs. the 9.88 ± 0.16 mN/m for β -Pth at 0.48 μ M final concentration and 8.48 ± 0.58 mN/m for Pin-a at 0.48 μ M final concentration. This suggests that there is some synergy between the Pin-a and β -Pth proteins and that these proteins used as an equimolar mixture could exhibit stronger antimicrobial properties against the fungi.

Table 4.7 Summary of the monolayer experiments of β -Pth, α_2 -Pth and their 1:1 mol:mol mixture interacting with condensed DPPS monolayers. An independent 2-tailed t-test was used for indicating the significant differences at $P \leq 0.05$.

Tested protein / proteins mixture and the final protein concentration in the subphase	Surface pressure rise $\Delta\pi$ [mN/m]	Significant difference test	
		P value	System compared
1. β -Pth 0.48 μ M	9.88 ± 0.16	0.07	2
2. β -Pth 0.24 μ M	7.89 ± 0.97	See above	
3. α_2 -Pth 0.48 μ M	8.39 ± 0.22	0.07	4
4. α_2 -Pth 0.24 μ M	7.98 ± 0.19	See above	
5. (β -Pth: α_2 -Pth 1:1 mol:mol) 0.48 μ M	7.34 ± 0.61	0.05	1
		0.46	2
		0.08	3
		0.20	4

Similar study has been carried out by Sanders *et al.*⁵³ on the thionin, indoline and mixed protein systems adsorption to the condensed phase DPPG, in which β -Pth and Pin-a were not found to express any synergy. Moreover, the study suggested the competitive behaviour between β -Pth and Pin-b.⁵³

Differences in the mentioned study would imply that there may be different competitive and co-operative behaviours between the different members of the thionin and indoline family and that these properties might be influenced by the concentration in the subphase and the anionic phospholipid used.

4.4 X-Ray Reflectometry (XRR)

Monolayer experiments can be developed by using the Langmuir trough in combination with advanced biophysical techniques, such as Neutron Reflectometry (NR)¹²⁷ or X-Ray Reflectometry (XRR).¹⁰⁷

The XRR experiments were carried out at the I07 beamline at the Diamond Light Source (Harwell Science and Innovation Campus, Chilton, UK) at a wavelength of 0.992 Å (12.5 keV). The beamline uses a double-crystal deflector allowing the angle of incidence at the sample position to be varied without moving the sample.¹⁰⁹

The samples were prepared in an analogous way to the one applied in the surface pressure experiments. The Langmuir trough used was a 380 mL model obtained from Nima Technology (Coventry, UK).

To avoid the sample damage by the high-energy X-ray beam, a fast shutter was employed and the trough was placed in the protective chamber containing a helium atmosphere (see Figure 4.11).

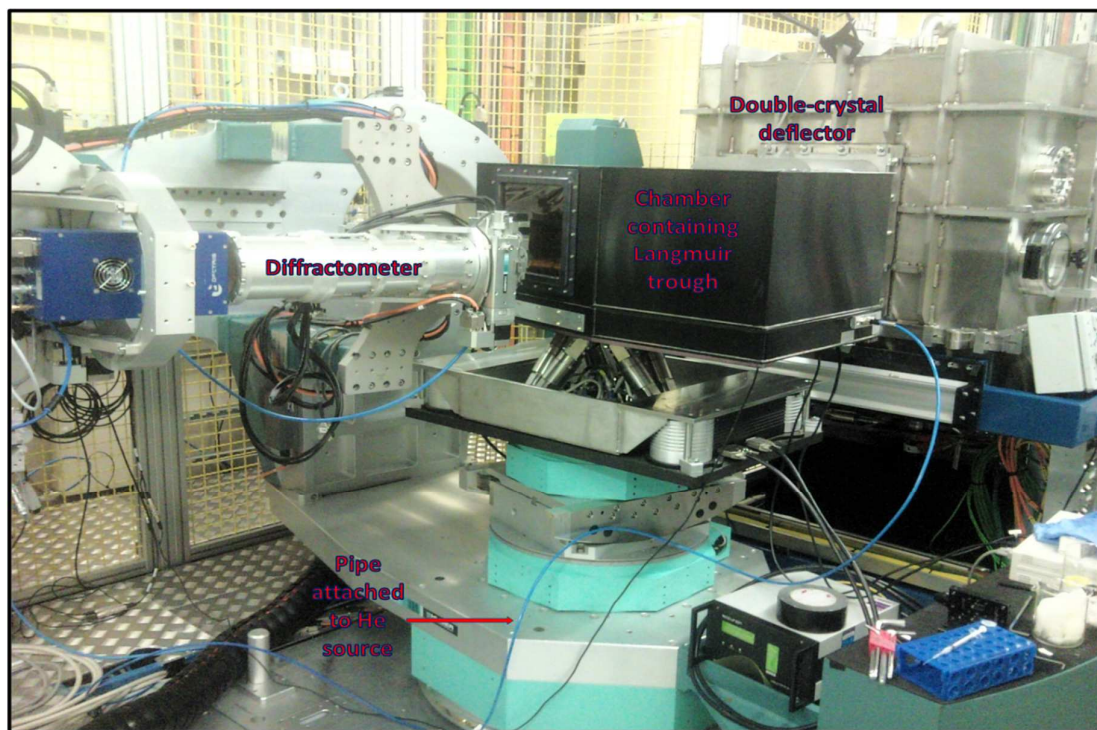


Figure 4.11 Experiment room at I07 XRR reflectometer in which the monolayer studies were carried out. The Langmuir trough used for creating the lipid monolayers was enclosed in the chamber, into which helium was pumped to minimise the destructive effects of X-rays on the monolayer.

The reflectivity was measured in three momentum transfer ranges with decreasing attenuation to include the full dynamic range of measurement. The Dectris Pilatus 100 k detector used two ‘regions of interest’ (ROI) to measure the signal and the background at the same time. The background has been subtracted from all the data.

The XRR profiles were analysed using the data fitting software RasCal (developed by Arwel Hughes, ISIS Spallation and Neutron Source, Harwell, UK), which describes interface as a series of slabs, each of which characterised by its SLD, thickness and roughness. The reflectivity for the modelling starting point is then calculated and compared with experimental data. The xrSLD values used for the data fitting can be found in Chapter 2 (page 27). The three-layer fitting model, consisting of the lipid tails layer, lipid headgroup layer and the protein layer, was applied as it has been proven successful for the previous XRR monolayer studies.

Two phospholipid monolayer systems DPPS and POPS have been analysed and prepared in an analogous manner as in the surface pressure measurements section. The injected protein

samples were 1 mL of 0.89 g/L β -Pth solution to achieve the 0.48 μ M final protein concentration in the subphase.

4.4.1 Discussion of the XRR Results

Figures 4.12 and 4.13 contain the results of the XRR experiments on the DPPS monolayer. The corresponding fitting parameters can be found in Table 4.8 and the surface pressure measurements in Figure 4.14. The experiment was characterised by an overall good match of the reflectivity profiles to the fits (see Figure 4.12, plots on the left).

The surface pressure rise 10.13 mN/m (obtained by subtracting the minimum surface pressure value from its maximum during the experiment) for the β -Pth-adsorbed DPPS monolayer experiment is very close to the value obtained from the experiments on the 10 mL trough equal to 9.88 ± 0.16 mN/m.

The changes in the tails region SLD can be described as gradually increasing within 90 minutes to the approximately stabilised after this time. Tails thickness rose to about 18 Å within the first hour to later fluctuate around the value 17.5 Å. This indicates that there was a slightly denser packing of the molecules in the tails region as compared to their arrangement prior to injection. The degree of the molecules packing seemed to have ultimately stabilised. Similar changes to the dipalmitoyl tails were observed by Majewski and Stec²⁶ studying the purothionins mixture adsorption to the mixed DPPC:DPPS monolayer after 180 min.

Headgroup's thickness decreased upon the protein action by around 2 Å and fluctuated around 8-9 Å for the next 150 minutes. The layer's SLD rose by $2 \times 10^{-6} \text{ \AA}^{-2}$ within 60 min and the value slightly decreased after this time to oscillate around $14.71 \times 10^{-6} \text{ \AA}^{-2}$. This suggests the condensation of matter within 60 minutes and the slight loosening of molecular arrangement after 1 h. Lipid monolayer's roughness has increased by approximately 1 Å upon the adsorption. The slight differences between the headgroup SLD values plotted in Figure 4.13 and the corresponding values gathered in Table 4.8 occurred due to the roughness parameter applied by the fitting software.

Protein layer's thickness kept changing throughout the experiment, which could indicate the significant dynamics of the layer resulting from the continuing adsorption and desorption of the protein to the interface. This can be confirmed by the surface pressure values which

reached plateau around 150 min, indicating dynamics at the interface occurring within this time (see Figure 4.14).

The overall changes for the DPPS experiment have not been as pronounced as the ones obtained by Clifton *et al.*⁵² who analysed the adsorption of α_1 -Pth and α_2 -Pth to the DPPG monolayers. This could be assigned to the nature of the phospholipid headgroup, *i.e.* DPPS was characterised by much higher initial SLD values in this part of a molecule. The matching observation was the increase of the palmitoyl tails' SLD upon the adsorption indicating the tighter packing of these parts of the molecule.

To summarise, there were clear changes in the interfacial structure of the DPPS monolayer upon the protein adsorption and they resulted in the tighter packing of the molecules at the interface.

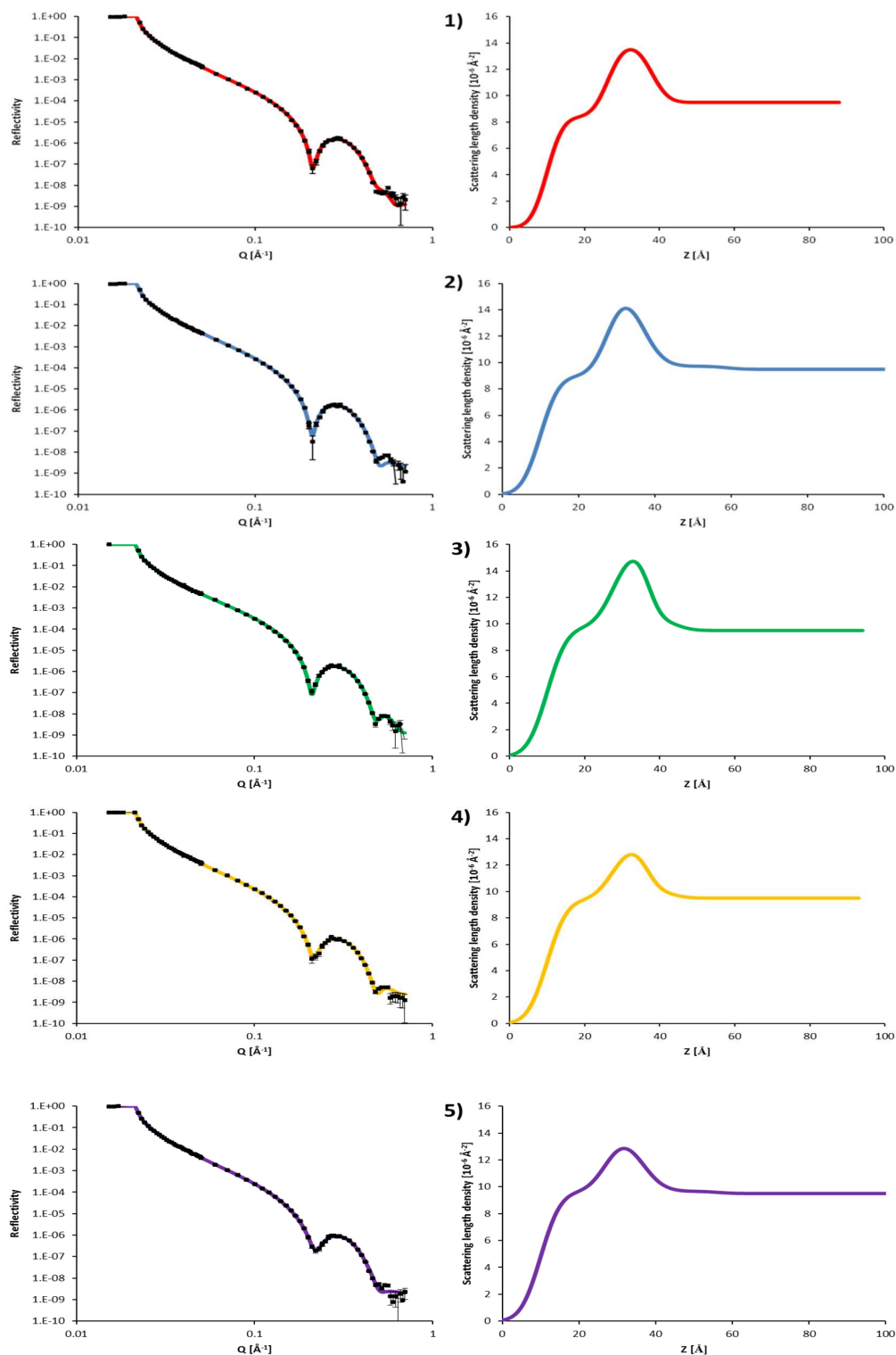


Figure 4.12 XRR reflectivity profiles with the model data fits (left) plotted against the momentum transfer Q and the scattering length density profiles these fits describe (right), plotted against the distance Z , for the DPPS condensed phase monolayer held at 22 mN/m (1), β -Pth-adsorbed DPPS monolayer after 60 min (2), 90 min (3), 120 min (4) and 150 min (5).

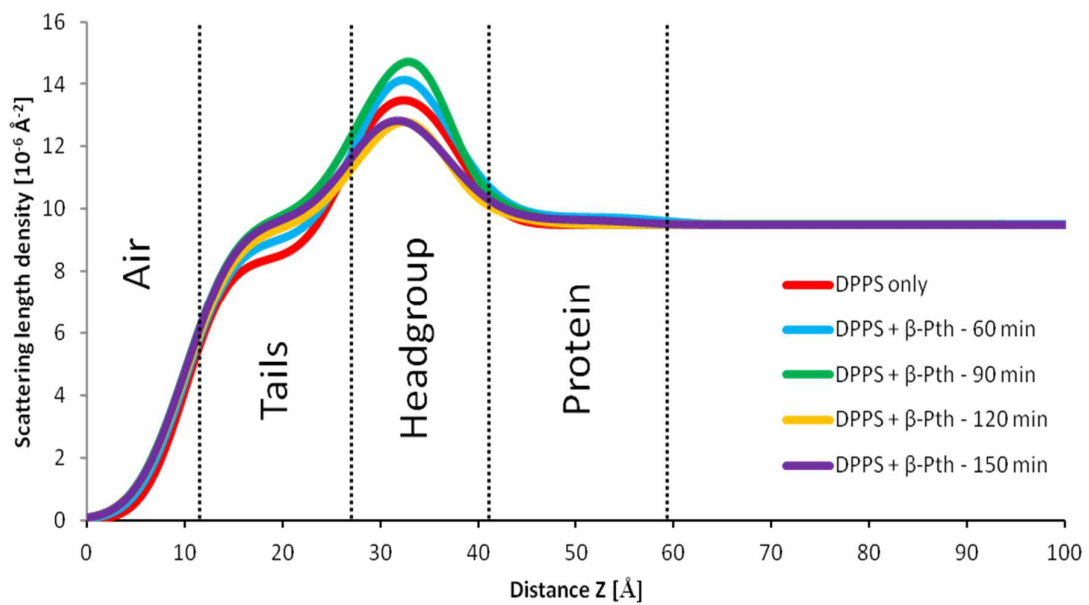


Figure 4.13 Overlaid XRR scattering length density profiles plotted vs. distance Z , obtained from the reflectivity data fitting of the experiment on β -Pth interacting with condensed phase DPPS monolayers.

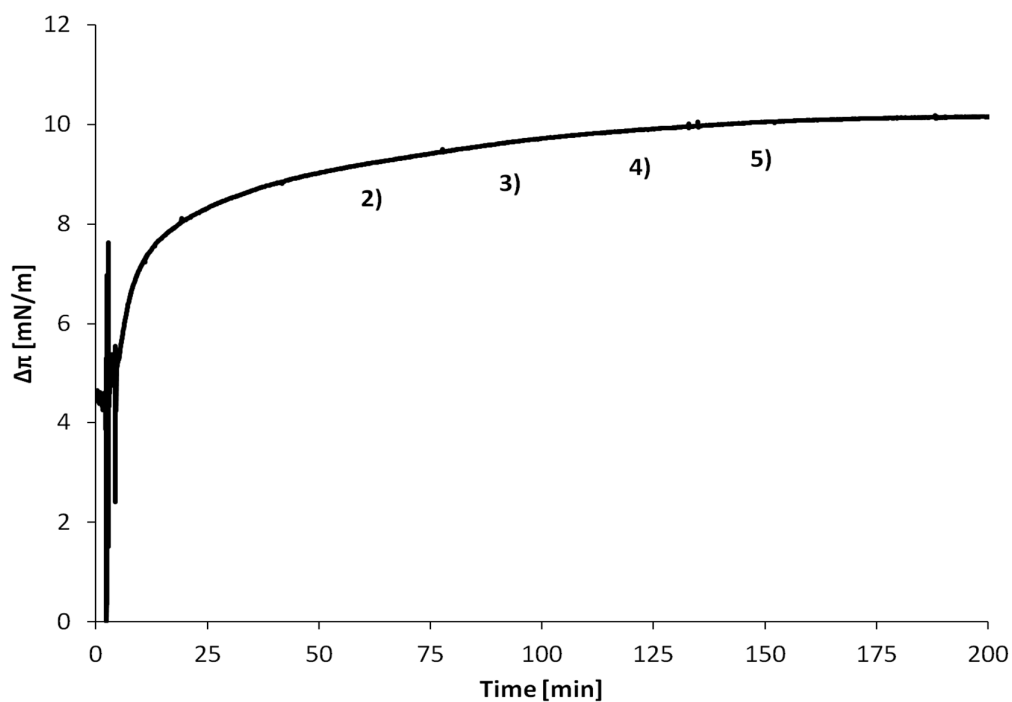


Figure 4.14 Surface pressure measurements of the β -Pth-adsorbed DPPS condensed phase monolayer. The numbers on the plot correspond to the reflectivity profiles in Figure 4.12.

Table 4.8 Fitting parameters obtained for the XRR experiment on β -Pth adsorption to the condensed phase DPPS monolayers.

System	Tails		Headgroup		Lipid monolayer roughness [Å]	Protein		Protein layer roughness [Å]	Surface pressure [mN/m]
	Thickness [Å]	SLD [10^{-6}Å^{-2}]	Thickness [Å]	SLD [10^{-6}Å^{-2}]		Thickness [Å]	SLD [10^{-6}Å^{-2}]		
1. DPPS only	16.26 ± 0.06	8.39 ± 0.05	11.77 ± 0.05	13.93 ± 0.10	3.40 ± 0.02	N/A	N/A	N/A	22.00
2. DPPS + β -Pth – 60 min	18.04 ± 0.04	8.96 ± 0.05	8.19 ± 0.15	16.47 ± 0.05	3.87 ± 0.03	22.66 ± 0.03	9.73 ± 0.15	4.61 ± 0.11	26.58
3. DPPS + β -Pth – 90 min	17.65 ± 0.09	9.69 ± 0.31	9.28 ± 0.23	15.74 ± 0.29	4.15 ± 0.09	7.63 ± 2.60	10.30 ± 0.10	2.77 ± 0.10	27.00
4. DPPS + β -Pth – 120 min	17.44 ± 0.09	9.33 ± 0.10	9.01 ± 0.15	13.60 ± 0.07	4.13 ± 0.04	7.07 ± 1.23	10.02 ± 0.06	2.96 ± 0.09	27.26
5. DPPS + β -Pth – 150 min	17.62 ± 0.05	9.59 ± 0.09	8.00 ± 0.06	14.71 ± 0.14	4.09 ± 0.03	20.64 ± 0.41	9.66 ± 0.10	4.80 ± 0.09	27.43

The experiment on the POPS monolayer revealed a dramatic change in the interface structure upon the protein adsorption. A drop in tails thickness and 5-fold increase in their SLD could be an indication of the molecules rearrangement into much more condensed structures (see Table 4.9). This result is in good agreement with the sudden increase in the surface pressure (see Figure 4.17), the shape of which is well corresponding to the kinetics of the previous surface pressure experiments (see Table 4.6). Similarly to the DPPS monolayer tails, the POPS tails seemed to have achieved the stabilised structure around 90 minutes after protein injection.

Headgroup region experienced a dramatic decrease in thickness while roughly maintaining its SLD value. This could indicate the replacement of some of the water molecules initially hydrating the hydrophilic headgroups by the protein molecules.

The fitting parameters in Table 4.9 also point out that the changes in the protein layer were not as pronounced as in case of the DPPS monolayer, which suggests the relative stabilisation of the analysed system. The protein layer's SLD insignificantly dropped indicating the slight loosening of the molecules and/or desorption of the protein.

Lipid monolayer roughness and the protein layer roughness did not change notably during the experiment, the lipid monolayer seemed to become slightly smoother within the first 20 minutes of the interaction and this level was maintained throughout the experiment.

In general, the lipid monolayer underwent the rapid changes, clearly seen from the dramatic difference in the reflectivity profiles. The structure stabilised within 90 minutes and the overall kinetics profile matched the one obtained in the analogous experiments (see Figure 4.10).

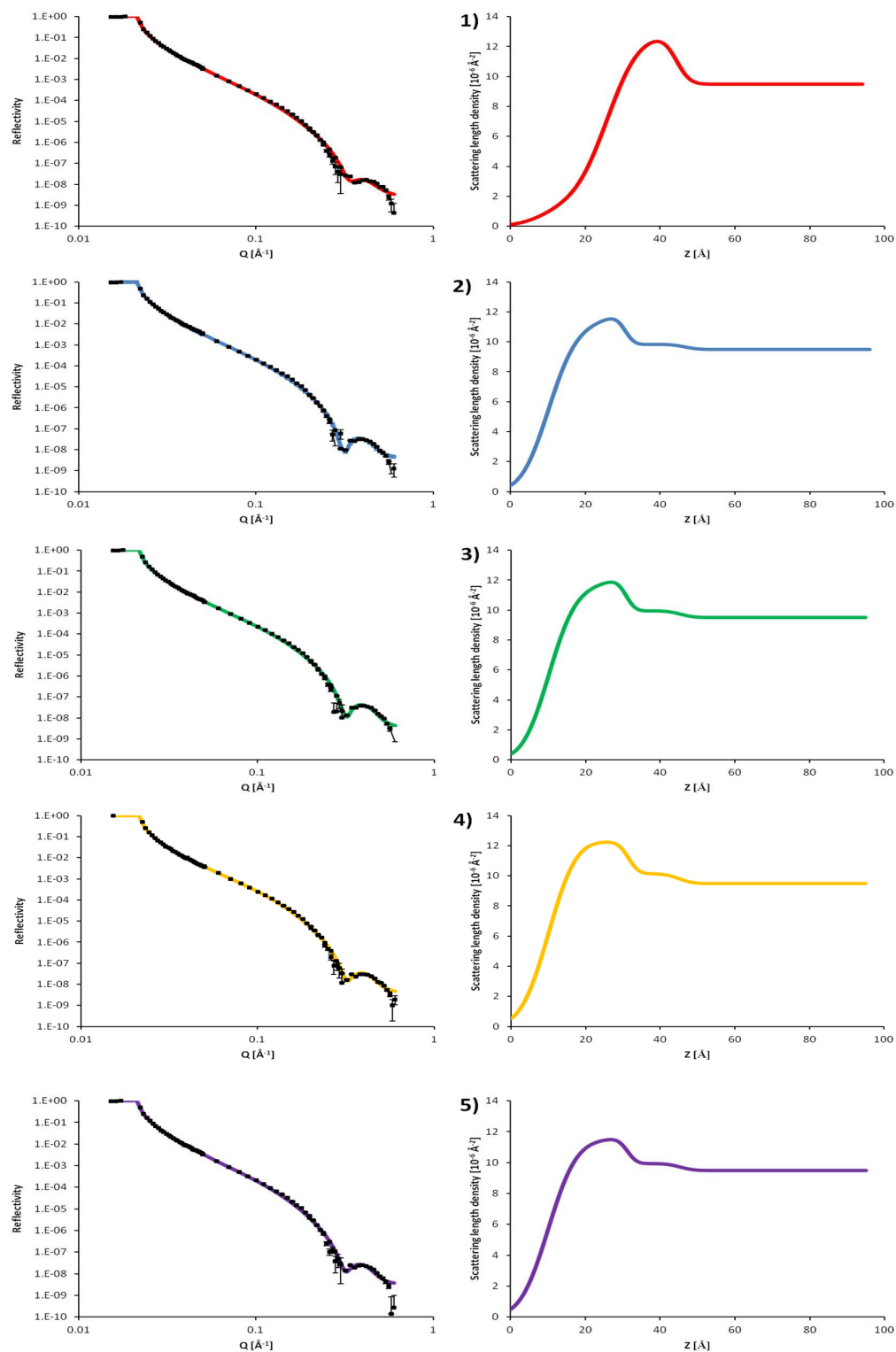


Figure 4.15 XRR reflectivity profiles with the model data fits (left) plotted against the momentum transfer Q and the scattering length density profiles these fits describe (right), plotted against the distance Z , for the POPS condensed phase monolayer held at 22 mN/m (1), β -Pth-adsorbed POPS monolayer after 20 min (2), 80 min (3), 140 min (4) and 200 min (5).

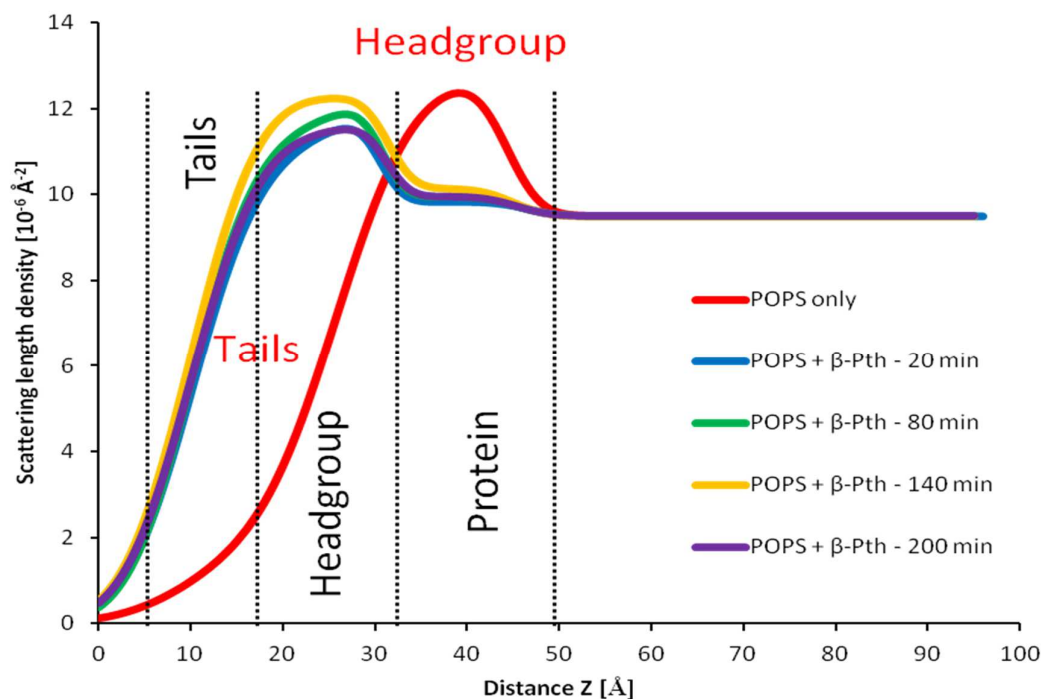


Figure 4.16 Overlaid XRR scattering length density profiles plotted vs. distance Z, obtained from the reflectivity data fitting of the experiment on β -Pth interacting with condensed phase POPS monolayers. The film components listed in black font relate to the protein-adsorbed monolayer, whereas the red font components correspond to the POPS only monolayer.

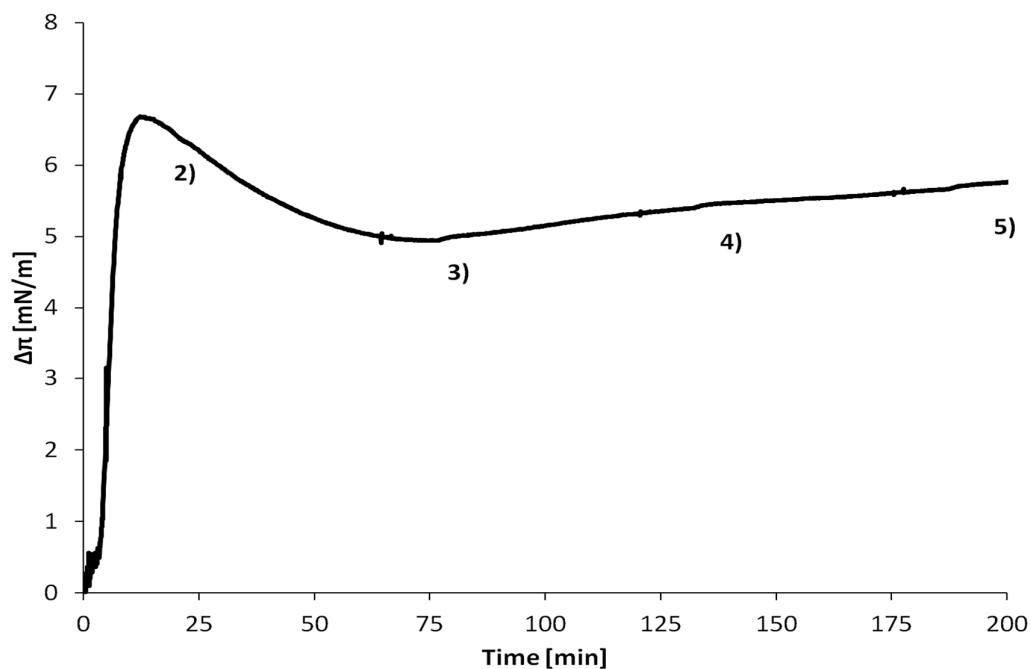


Figure 4.17 Surface pressure measurements of the β -Pth-adsorbed POPS condensed phase monolayer. The numbers on the plot correspond to the reflectivity profiles in Figure 4.15.

Table 4.9 Fitting parameters obtained for the XRR experiment on β -Pth adsorption to the condensed phase POPS monolayers.

System	Tails		Headgroup		Lipid monolayer roughness [Å]	Protein		Protein layer roughness [Å]	Surface pressure [mN/m]
	Thickness [Å]	SLD [10^{-6}Å^{-2}]	Thickness [Å]	SLD [10^{-6}Å^{-2}]		Thickness [Å]	SLD [10^{-6}Å^{-2}]		
1. POPS only	15.93 ± 0.41	1.79 ± 0.28	18.37 ± 0.27	12.71 ± 0.65	6.55 ± 0.09	N/A	N/A	N/A	21.90
2. POPS + β -Pth – 20 min	12.60 ± 0.18	10.75 ± 0.16	8.00 ± 0.12	11.87 ± 0.16	5.66 ± 0.05	15.98 ± 1.26	9.84 ± 0.99	2.00 ± 0.12	28.32
3. POPS + β -Pth – 80 min	12.76 ± 0.19	11.25 ± 0.16	8.00 ± 0.11	12.13 ± 0.13	5.49 ± 0.05	14.64 ± 1.15	9.94 ± 0.08	2.00 ± 0.10	26.90
4. POPS + β -Pth – 140 min	12.84 ± 0.54	12.46 ± 0.17	8.58 ± 0.25	12.22 ± 0.24	5.83 ± 0.04	13.59 ± 1.57	10.14 ± 0.19	2.18 ± 0.19	27.37
5. POPS + β -Pth – 200 min	12.59 ± 0.21	11.33 ± 0.18	8.62 ± 0.17	11.61 ± 0.15	5.83 ± 0.03	14.14 ± 1.12	9.95 ± 0.09	2.00 ± 0.12	27.66

Both experiments provided a more detailed insight into the structural changes of the interface upon the protein adsorption and reflected the dynamic processes at the interface. These XRR experiments could not be used, however, for the qualitative analysis of the interface and thus assessing the level of protein insertion into each layer. This inconvenience can be solved by using the isotopic substitution and the use of neutron reflectometry (see Chapters 5 and 6).

4.5 Conclusions

The monolayer experiments were used to preliminary assess the protein-lipid interactions. The protein adsorption was confirmed to be driven by the electrostatic attraction to the anionic phospholipids. The reduction of charge significantly lowered the extent of the structural changes in the monolayer upon the protein adsorption.

The kinetics of the interactions turned out to be affected by the level of packing of the molecules at the interface. The monolayer was continuously becoming more condensed in the case of the saturated lipids. Unsaturation of the phospholipid tails resulted in a quick rise of the surface pressure that gradually fell indicating the relaxation of the monolayer and/or desorption of the material. The structural changes were examined in more detail by XRR and confirmed the dependence on the process' kinetics on the phospholipid saturation.

Pin-a and β -Pth showed the slight synergy in the form of an equimolar mixture against the DPPS. In contrast, β -Pth in combination with α_2 -Pth did not reveal significant differences in the lipid-adsorbing properties.

Certain differences between the experiments above and the previous studies on the wheat defence proteins could indicate the antimicrobial activity dependence on the anionic headgroup structure (the previously analysed phospholipid was DPPG).

To summarise, all monolayer experiments provided the preliminary knowledge on the protein-lipid interacting systems and enabled to select the protein-lipid combinations to be further examined by means of the advanced biophysical techniques.

Chapter 5

LIPID BILAYER STUDIES

PART I – NEUTRON REFLECTOMETRY SYSTEM DEVELOPMENT AND ATR-FTIR STUDIES

5.1 Introduction

As shown in Chapter 4, phospholipids can be used as the building blocks of the biological membrane models in the form of the monolayers spread at the air/liquid interface. These simple systems, however, do not reflect the true structure of the biological membranes, whose backbone is formed of the phospholipid bilayer.

Artificial lipid bilayers form, therefore, a better model of the natural membranes than the lipid monolayers, as they can deliver the naturally occurring phenomena of the lipid flipping between the leaflets.¹⁵⁰

The bilayers served as a research tool in many studies. For example, the lipid-flipping between the leaflets and thus the true structure of the created lipid bilayers were the subject of the work by Gerelli *et al.*¹⁵¹ Similar study, enabling to characterise the composition of the model outer membrane of the Gram-negative bacteria cell, was carried out by Clifton *et al.*⁸⁴ Bilayers can be also used to study the adsorption of the biocompounds to the interfaces, *e.g.* adsorption of the lipopeptide surfactant bilayers to the solid liquid interface, as analysed by Jia *et al.*¹⁵²

Moreover, artificial lipid bilayers can be subjected to the action of various compounds. For instance, lactoferrin and lysozyme adsorption to the floating lipid bilayer was studied by Clifton *et al.*¹⁵³ The effect of an antifungal agent, amphotericin B, on the model fungal bilayers was investigated by Foglia *et al.*¹⁵⁴

One way to create the lipid multilayers is by spreading the solution of the lipid vesicles in the chamber containing the target solid surface exposed to the coverage. The vesicles spontaneously unfold and create multilayers (see Chapter 2, page 30 for more details).

Langmuir-Blodgett and Langmuir-Schaeffer techniques are the other methods of the bilayer deposition on the solid substrate (sometimes referred to as solid support), allowing to obtain the lipid films of the controlled level of the molecules packing and the controlled number of layers (see Chapter 2, page 31 for more details). The formed multilayers are then placed in the chamber or compartment allowing them to be brought into contact with the injected solution, which in this study contained the wheat defence proteins.

Thus obtained samples were later analysed by means of ATR-FTIR to study the adsorption of the protein to the interface and its penetration of the formed lipid bilayer. The created lipid bilayers were also exposed to the stream of neutrons and the neutron reflectivity profiles were recorded, allowing to assess qualitatively and quantitatively the structure of the phospholipid bilayer.¹⁵³ More details on ATR-FTIR and NR methods can be found in Chapter 2, pages 32 and 34.

5.2 Materials

1,2-Dipalmitoyl-*sn*-glycero-3-phosphocholine (DPPC, synthetic, purity > 99%), 1,2-dipalmitoyl-*sn*-glycero-3-phospho-L-serine (DPPS, synthetic, purity > 99%) and 1-palmitoyl-2-oleoyl-*sn*-glycero-3-phospho-L-serine (POPS, synthetic, purity > 99%) were all purchased from Avanti Polar Lipids (Alabaster, AL, US). Lipid solutions were prepared and stored as for the monolayer experiments (see Chapter 4, page 54). HEPES (4-(2-hydroxyethyl)-1-piperazineethanesulfonic acid) was purchased from Sigma-Aldrich (Dorset, UK).

The protein stock solutions were prepared in the H₂O and D₂O phosphate buffer solution at pH/pD 7.0 using UHQ grade water (resistivity 18.2 MΩ·cm obtained from ELGA LabWater purifier – High Wycombe, UK) and the deuterium oxide (D₂O, 99.9 atom % D, purchased from Sigma Aldrich, Dorset, UK). The protein concentrations were checked with the UV absorbance at 280 nm.

The ATR-FTIR solid supports in the form of germanium (Ge) crystals (74 mm x 10 mm lower base dimensions – the surface exposed to the bilayer coverage and protein adsorption; thickness 6 mm) were obtained from Crystran (Dorset, UK) and the NR solid supports in the form of silicon (Si) crystals, also referred to as silicon blocks (50 mm x 80 mm bilayer

coverable surface polished to the 3 Å roughness, thickness 20 mm), were purchased from PI-KEM (Tamworth, UK).

The saturated phospholipids DPPC and DPPS were chosen to create the phospholipid bilayer systems as they are the most abundant in the natural fungal membrane (see Chapter 1, page 11). The mono-unsaturated anionic phospholipid POPS was used to introduce the fluidity of the phospholipid membrane, the characteristic feature of the fungal membrane (see Chapter 1, page 12).

The bilayer nomenclature applied throughout this chapter was the following:

‘Name_of_the_Lipid_in_the_Inner_Leaflet:

Name_of_the_Lipid_or_Lipid_Mixture_in_the_Outer_Leaflet’,

e.g. DPPC: DPPS bilayer means that the lipid deposited in the inner leaflet was DPPC and that the outer leaflet was composed of DPPS.

5.3 Neutron Reflectometry (NR) Experiments

Neutron Reflectometry has been widely employed to study the structures of the lipid monolayer and bilayer systems.

For instance, Dabkowska *et al.*¹⁵⁵ used NR to investigate the effect of the presence of the membrane protein cytochrome c on the structure of the lipid bilayers. The technique also enables to study the adsorption processes to the interfaces, *e.g.* the assembly of the β -hairpin proteins to the water surface, as analysed by Lu *et al.*¹⁵⁶ The protein-lipid interactions at the air/liquid interfaces were the subject of the NR studies by Clifton *et al.*^{29,153}

In NR experiments, by applying the isotopic substitution of the components, one is able to detect their position and amount in relation to other components. For more details on the principles of the technique, please refer to Chapter 2, page 34.

5.3.1 Lipid Bilayer Preparation on the Solid Support by Langmuir-Blodgett and Langmuir-Schaeffer Dipping

The lipid bilayers have been prepared using the purpose-built Langmuir trough equipped with a dipping arm and the water level calibration device (all obtained from KSV Nima, Biolin Scientific, Finland). The bilayer deposition was carried out at the ISIS Neutron and Muon Spallation Source (Harwell, UK). The artificial membranes were created on the Piranha-cleaned surface (covered with a thin layer of silicon oxide SiO_2 after cleaning) of the silicon crystals.⁸⁴

For the Langmuir-Blodgett dip, the silicon block was vertically attached to the LB-dip sample holder (see Figure 5.1) and fully immersed to the 0.05 M calcium chloride subphase at the room temperature. This solution has been shown to produce better lipid coverage due to the opposite-charge-driven, more ordered arrangement of the lipid molecules.¹⁵⁷

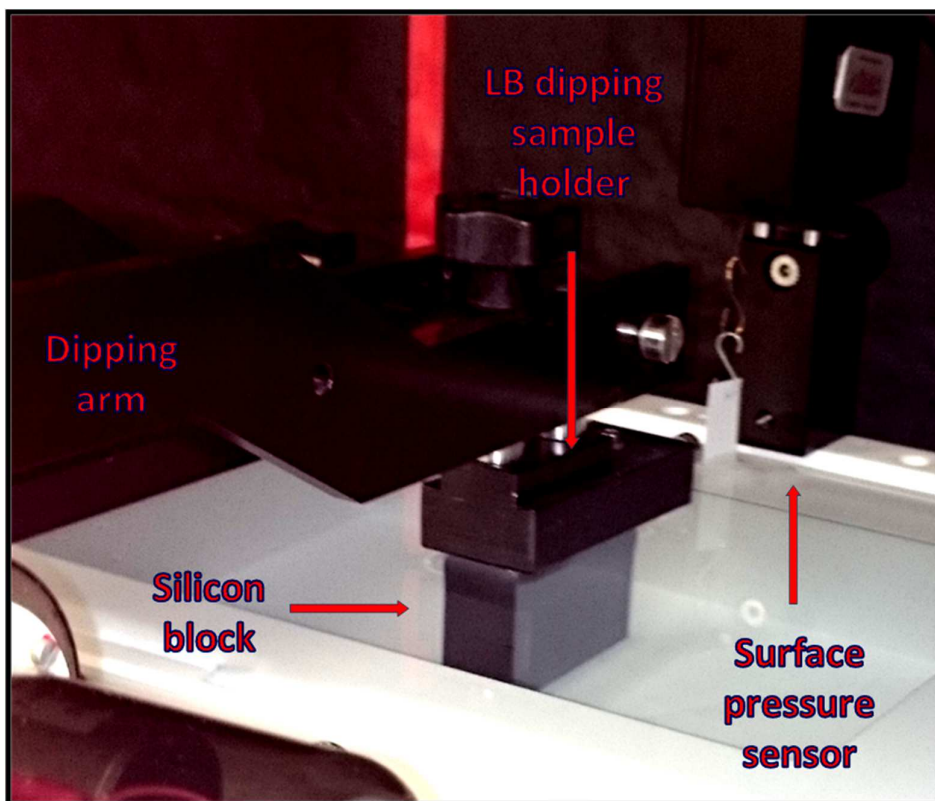


Figure 5.1 Langmuir-Blodgett dip of the silicon block using purpose-built Langmuir trough. The block is moved upwards through the lipid monolayer deposited on the water surface and its vertical surfaces become covered with the monolayer.

The surface cleanliness was checked and the lipid monolayers were prepared as described in Chapter 4 (see page 55). The submerged silicon block was then lifted at the speed of 4 mm/min while the surface pressure was kept constant at 35 mN/m.

When the block detached from the monolayer surface, the monolayer and the subphase were removed and the lower base of the NR cell was placed into an insert at the bottom of the trough's dipping well. The fresh, cold (4°C) calcium chloride solution was poured into the trough and the temperature of the subphase was kept constant at 4°C throughout the LS-dip stage. The lowered temperature kept the anionic lipid molecules closer to each other, thereby lowering the negative-charge-driven repulsion effects between the headgroups, which could lower the final coverage of the bilayer's outer leaflet.

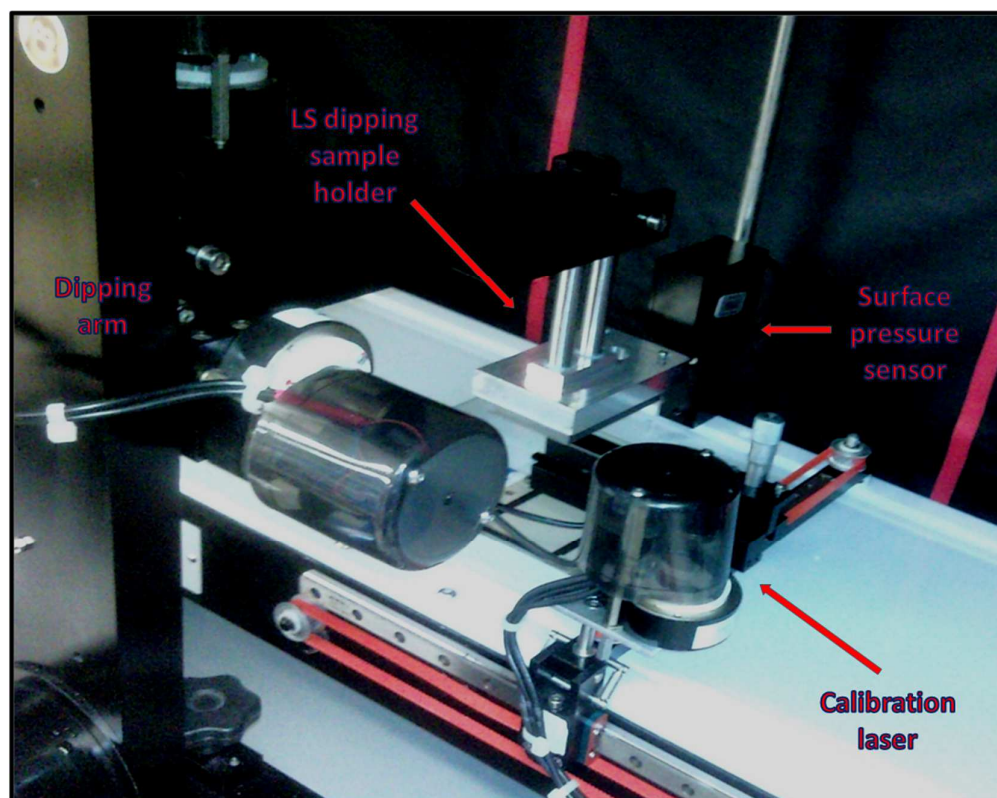


Figure 5.2 Calibration of the dipping arm position before the Langmuir-Schaeffer dip of the silicon block. The process sets the dipping arm in the horizontal position in respect to the water surface, allowing the controlled coverage of the silicon block's surface with the lipids present on the water surface.

The LB-dipped silicon block, covered with one-molecule-thick layer of the lipid (the bilayer's inner leaflet) was then attached horizontally to the LS-dip sample holder (see: Figure 5.2). The liquid surface was then analysed with the calibration laser and the sample

holder's position was adjusted to allow the fully horizontal position of the attached block in relation to the liquid surface below it.

The monolayer formed of the lipid or lipid mixture to be present in the bilayer's outer leaflet was prepared as described previously. The monolayer was compressed to 35 mN/m and the pressure was kept constant throughout the LS-dip. The sample holder was lowered to a few mm above the liquid surface and was then further lowered at the constant speed of 4 mm/min. The fully immersed block was then lowered to the NR cell base at the bottom of the trough, the sample holder was removed and, still under liquid surface, the upper base of the NR cell was attached to keep the silicon block in the cell and prevent the liquid leakage (see: Figure 5.3).

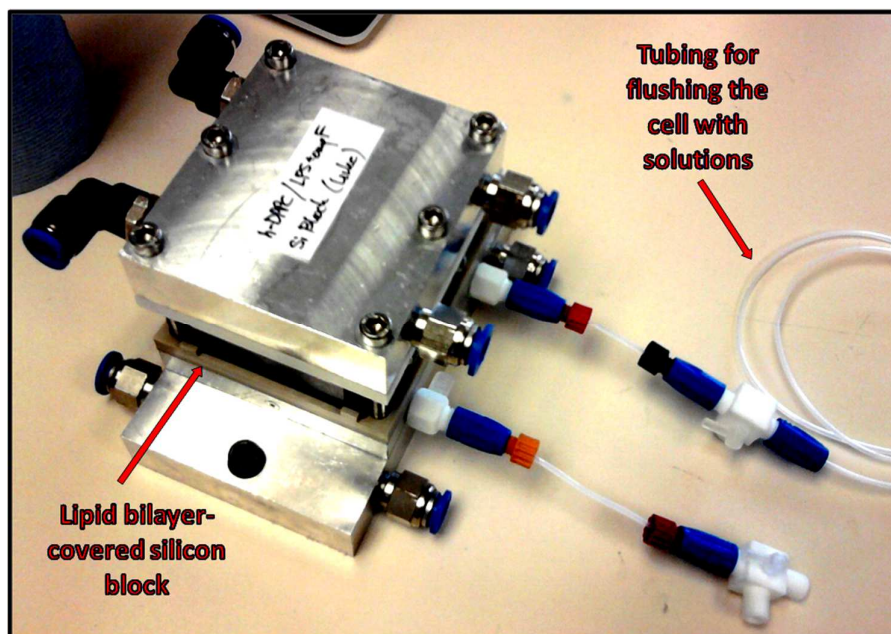


Figure 5.3 A sample cell used for the Neutron Reflectometry solid-support experiments with the lipid bilayer-covered solid substrate enclosed. The buffer and protein solutions were delivered to the cell through the attached tubing.

The NR cells containing the lipid bilayer-covered silicon blocks were then placed in the NR instrument rooms (see Figure 5.4) and flushed with D_2O to remove the traces of calcium ions, which could react with the phosphate buffer salts forming the precipitate. Afterwards, the cells were flushed with three pH 7.0/pD 7.0 buffer solutions providing the three isotopic contrasts: 100 % D_2O , silicon-SLD-matched water (SMW) containing 38% D_2O and 100% H_2O . The NR reflectivity profiles were measured for each of the contrasts. The samples were

then flushed with the appropriate protein solutions prepared in the aforementioned buffers and the reflectivity profiles were taken for each contrast, as previously.

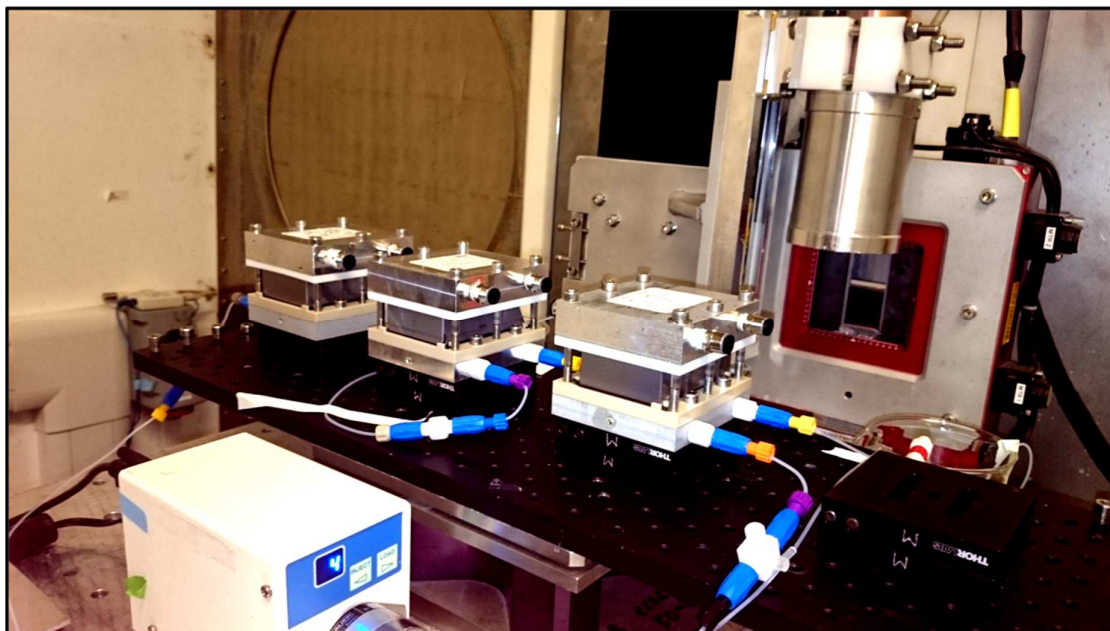


Figure 5.4 Interior of the NR instrument Inter showing three NR cells containing the lipid-bilayer covered silicon blocks.

5.3.2 System Development: the Effect of the Inner Leaflet Lipid on the Multilayer Structure

To examine the effect of the phospholipid chain unsaturation on the antimicrobial action of the wheat defence proteins, a symmetric POPS: POPS bilayer was created as described in section 5.3.1. The anionic phospholipid was chosen for the experiment as it produced the stable monolayers (see Chapter 4, page 65) and was a good representative of the fungal membrane phospholipid (see Introduction, page 11).

The NR instrument used was SURF at the ISIS Neutron and Muon Spallation source (Harwell, UK). The obtained reflectivity profiles were then fitted to the pre-defined models using the reflectivity data fitting software RasCal¹⁵⁸ which takes into account layer's composition, thickness and roughness. Moreover, the programme introduces the hydration parameter, which can be applied to directly determine the water percentage in the fitted layer throughout all 3 contrasts.

The followed protocol described in section 5.3.1 produced a multilayer structure, as shown in Figure 5.5.

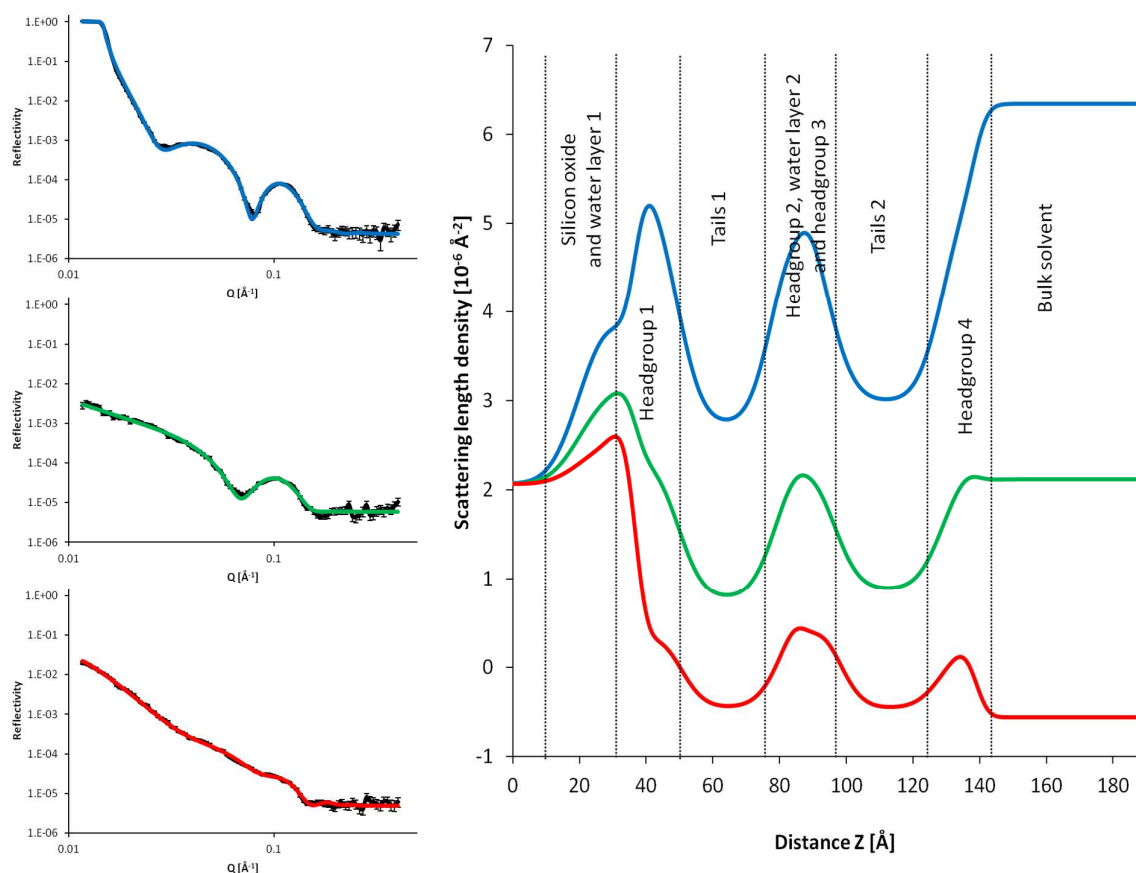


Figure 5.5 Reflectivity data (left) and the fits describing these data (right) of the double symmetric POPS bilayer. The isotopic contrasts applied were: D₂O (red line), SMW (green line), H₂O (blue line).

The reflectivity profiles obtained in 3 different contrasts did not resemble the shapes obtained typically for the fully hydrogenated (not containing any deuterated component) lipid bilayer.⁸⁴ Therefore, the pre-defined fitting model was set to be: two POPS bilayers separated by thin layers of water (see the summary of the fitting parameters in Table 5.1): one layer attached to the silicon surface and the other floating just above the first one. This model turned out to be fitting perfectly to the obtained reflectivity data.

The created double POPS bilayer appeared to be very fragile and was fully removed by another D₂O flush of the NR cell (data not shown). The folding into the double bilayer could be explained by the higher mobility of the molecules due to the presence of the unsaturated phospholipid chain and the fact that the silicon oxide covered block's surface, serving as a source of unpaired electrons producing a slightly negative charge could have a repelling effect on the anionic headgroups of POPS, thereby decreasing the chance of their attachment to the block's surface.

Table 5.1 Summary of the fitting parameters obtained for the double POPS bilayer experiment. The SLD values were kept constant and only the hydration parameter varied. The SLD values with no uncertainties were kept constant throughout the process of data fitting.

Layer	Thickness [Å]	SLD [10^{-6}Å^{-2}]	ϕ_{lipid}	ϕ_{water}	A_{lipid} [Å ²]	Γ_{lipid} [mg m ⁻²]	Roughness [Å]
Layer 1: silicon oxide	16.593 ± 0.754	3.410	N.A.	0.221 ± 0.012	N.A.		7.000 ± 0.638
Layer 2: water layer 1	0.000 ± 0.834	N.A.	N.A.	1.000	N.A.		3.000 ± 0.976
Layer 3: headgroup 1	12.761 ± 0.709	3.060	0.309 ± 0.086	0.691 ± 0.086	69.810 ± 19.764	0.742 ± 0.210	5.861 ± 0.229
Layer 4: tails 1	29.217 ± 1.570	-0.343	0.537 ± 0.017	0.463 ± 0.017	49.274 ± 3.077	1.513 ± 0.094	
Layer 5: headgroup 2	8.000 ± 0.722	3.060	0.205 ± 0.079	0.795 ± 0.079	168.031 ± 66.200	0.308 ± 0.122	
Layer 6: water layer 2	0.783 ± 1.044	N.A.	N.A.	1.000	N.A.		3.000 ± 1.092
Layer 7: headgroup 3	8.000 ± 0.792	3.060	0.500 ± 0.050	0.500 ± 0.050	250.000 ± 35.198	0.207 ± 0.029	6.202 ± 0.402
Layer 8: tails 2	33.696 ± 0.802	-0.343	0.500 ± 0.010	0.500 ± 0.010	45.892 ± 1.456	1.625 ± 0.052	
Layer 9: headgroup 4	9.542 ± 0.555	3.060	0.250 ± 0.026	0.750 ± 0.026	115.446 ± 13.655	0.449 ± 0.053	

Therefore, for the future experiments the zwitterionic phospholipid DPPC was chosen for the component of the inner leaflet as it decreased the risk of the charge-driven repulsion from the silicon oxide surface. Moreover, the chosen phospholipid is abundant in the fungal membrane (see Chapter 1, page 11) and thus the future bilayer models would still well correspond to the natural membrane.

5.4 Development and Lipid Characterisation for the Attenuated Total Reflectance-Fourier Transform Infrared Spectroscopy (ATR-FTIR) Spectroscopy

Infrared experiments on the solid Ge supports were carried out to assess the protein adsorption and its penetration into the artificial lipid bilayers representing the fungal cell membrane.

ATR-FTIR was used for many solid/liquid interface studies, *e.g.* Hübner and Mantsch¹⁵⁹ used the polarised ATR-FTIR to investigate the structures of the lipid multilayers by determining the orientation of the carbonyl groups. Bahng *et al.*¹⁶⁰ investigated the effect of an antimicrobial peptide indolicidin on the phospholipid bilayers. β -lactoglobulin interactions with lipid bilayers were the subject of the work by Verity *et al.*,¹⁶¹ who used ATR-FTIR and atomic force microscopy (AFM) simultaneously.

For the ATR-FTIR experiments in this study, the lipid bilayers were prepared by following the two methods: vesicles spreading and Langmuir-Blodgett and Langmuir-Schaeffer dipping (see the sections 5.4.1 and 5.4.2 for details). The lipid-covered crystals were then placed in the ATR-FTIR cell obtained from Specac (Orpington, UK) with the attached tubing adapters (see Figure 5.6).

The ATR-FTIR cell containing the crystal was put into the ATR-FTIR accessory (purchased from Specac, Orpington, UK) inside the sample chamber of the ThermoNicolet Nexus instrument (Madison, WI, USA) and allowed to dry overnight. Protein solutions (1.2 mL) prepared in the D₂O phosphate buffer were injected to reach the final concentration in the cell of 0.48 μ M (0.01 g/L solutions of α ₂-Pth and β -Pth and 0.025 g/L of Pin-a).

The instrument was fitted with a deuterated triglycine sulphate detector (DTGS) and connected to an air-dryer to purge the instrument of water and carbon dioxide. All FTIR

spectra were collected at a resolution 4 cm^{-1} , where 128 interferograms were collected, co-added, and ratioed against a background spectrum of the D_2O buffer solution.

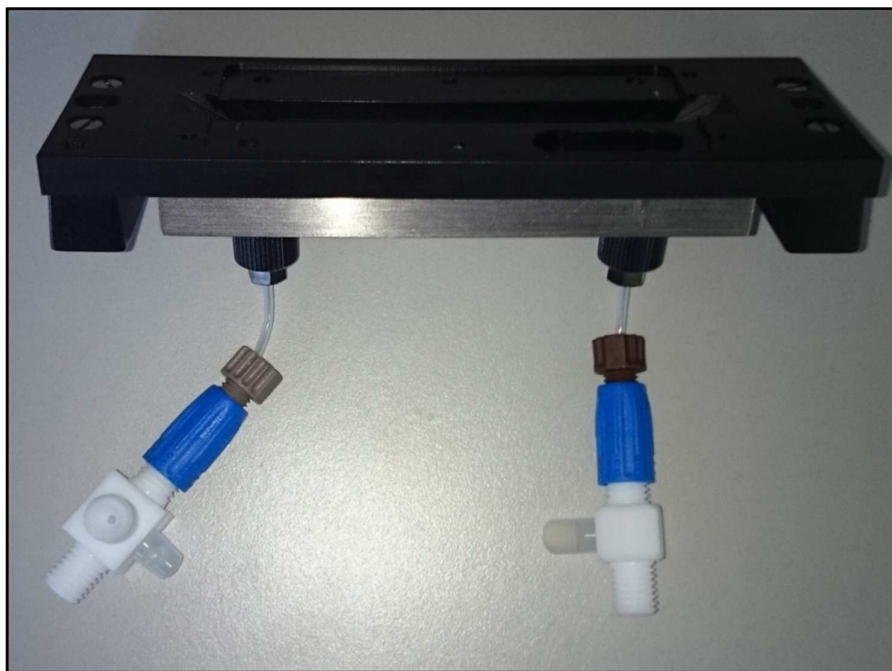


Figure 5.6 An ATR-FTIR cell with the attached adapters through which the protein solution was injected during the experiments.

Interactions of the protein with the lipid bilayer were observed by monitoring the Amide I band at $\sim 1650\text{ cm}^{-1}$.^{125,162} Deuterium oxide has been chosen as the solvent because, as opposed to H_2O , it does not absorb infrared radiation in the Amide I region, thus allowing better analysis of the protein contribution to the spectra.¹⁰⁰

5.4.1 Bilayer Deposition: Vesicles Solution Spreading

Lipid vesicles (liposomes) were prepared according to the protocol found at <http://avantilipids.com/tech-support/liposome-preparation/> (see the details in Chapter 7, page 152).

The DPPC multilamellar vesicles (DPPC MLVs) solution of the 1 g/L concentration was prepared in the D_2O phosphate buffer. The cleaned and dried germanium crystal was placed

in the ATR-FTIR cell and the cell was put into the ATR accessory in the sample chamber of the FTIR instrument.

The D₂O phosphate buffer solution was injected *via* syringe into the cell through the attached adapters (see Figure 5.6) to completely fill the cell. Afterwards, the background scan was taken. The vesicles solution (1.2 mL) was then injected in the same way into the cell to fully replace the buffer, and left to incubate at room temperature overnight.

The solution was flushed out with D₂O phosphate buffer and the lipid-only FTIR sample scan was taken. Lysozyme solution (1.2 mL of 4.26 g/L to reach the final concentration 0.48 μM) in the D₂O phosphate buffer was injected into the cell and the sample scans were taken right after injection, 1 h, 2 h and 24 h after injection.

5.4.2 Bilayer Deposition Method Development: the Langmuir-Blodgett and Langmuir-Schaeffer Dipping

In the further experiments, the covering of the Ge crystal with a lipid bilayer involved a two-stage process: first step was the vertical Langmuir-Blodgett (LB) lipid monolayer deposition (see the details in Chapter 2, page 31). The crystal, already covered with a single lipid layer accounting for the inner leaflet of the bilayer, was then subjected to the Langmuir-Schaeffer (LS) horizontal dip into a fresh lipid monolayer and immediately placed in the ATR-FTIR cell (see the details in Chapter 2, page 32).

The bilayers were created using a purpose-built PTFE dipping Langmuir trough obtained from Brown & Waite Engineering (Daventry, UK). The trough was equipped with the dipping well of approximately 1 L volume and the software-steered dipping arm with the vacuum-driven crystal holder (see Figure 5.7 and 5.9).

Before each use, the trough was wiped twice with ethanol and UHQ water, and filled next with UHQ water to obtain a few mm high meniscus above the trough's rim. The cleanliness of the surface was checked by monitoring the surface pressure while closing the barriers. If the surface pressure increase was observed, the impurities were removed from the surface by vacuum-suction.

The ATR-FTIR crystal was cleaned by gently wiping its surface with isopropyl alcohol and allowing it to air-dry. For the LB-dip the clean, dry crystal was then vertically attached to the sample holder of the dipping arm (with the crystal bases facing the sides) and fully immersed under the surface of the UHQ water (see: Figure 5.7). The surface's cleanliness was checked again as described previously and any impurities were removed. If necessary, more UHQ water was added to equalise the initial level.

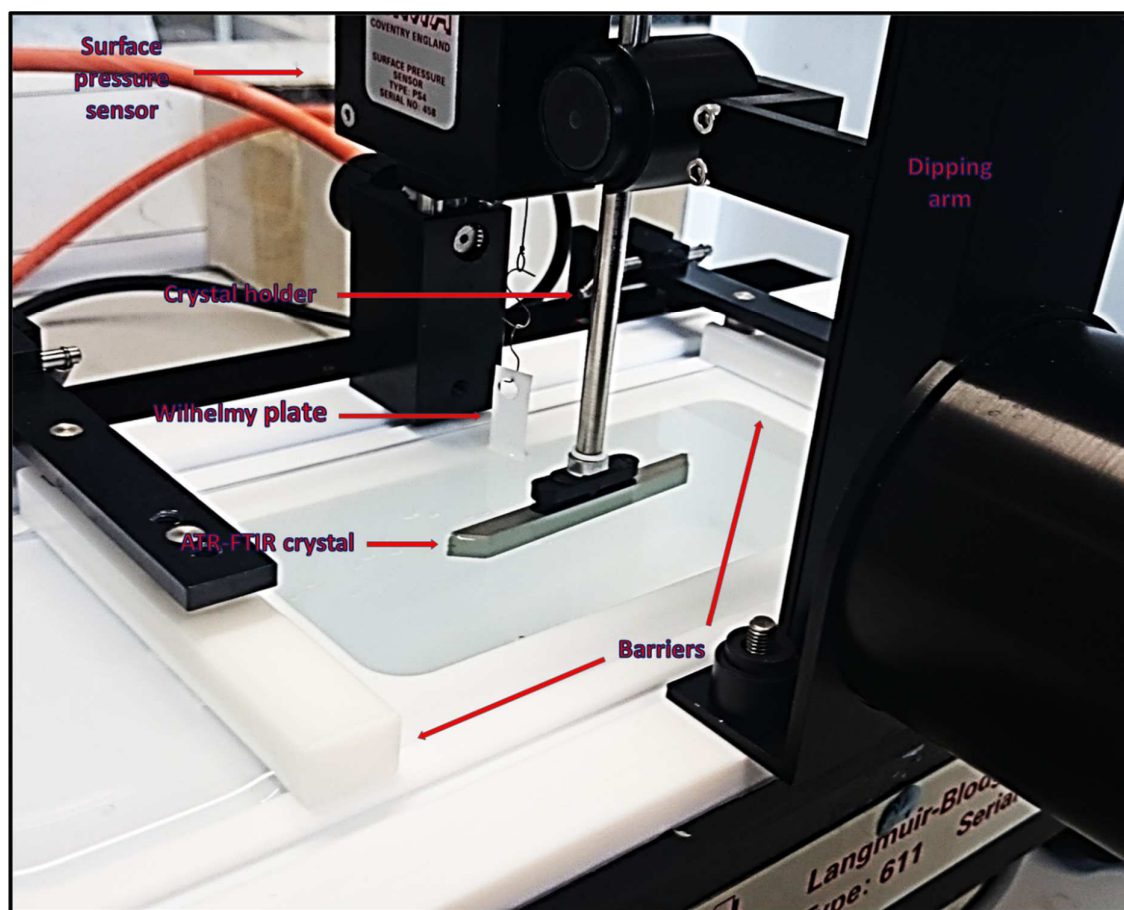


Figure 5.7 Langmuir-Blodgett dip of the germanium ATR-FTIR crystal using the purpose-built Langmuir trough showing the fully immersed crystal right before being dragged up through the condensed phase lipid monolayer kept at the constant surface pressure.

The condensed phase lipid monolayer was then created on the water surface in the way described in Chapter 4, page 55. For the reasons described in section 5.3.2 (see page 88), DPPC was chosen as the lipid used for the first monolayer, which after the dipping process would account for the inner leaflet of the created bilayer.

The lipid molecules were compressed to the surface pressure of 35 mN/m, which represented the upper limit of the liquid-condensed phase or the solid-condensed phase of the monolayer, and at the same time prevented the monolayer collapse. This relatively high surface pressure allowed to reach the high level of coverage of the crystal surface with the lipids.

The monolayer was kept at the constant surface pressure of 35 mN/m by the Nima software's 'Pressure Control' function allowing the barriers to move accordingly. With this software function on, the crystal was dragged up at the constant speed of 3 mm/min by the software-controlled dipping arm.

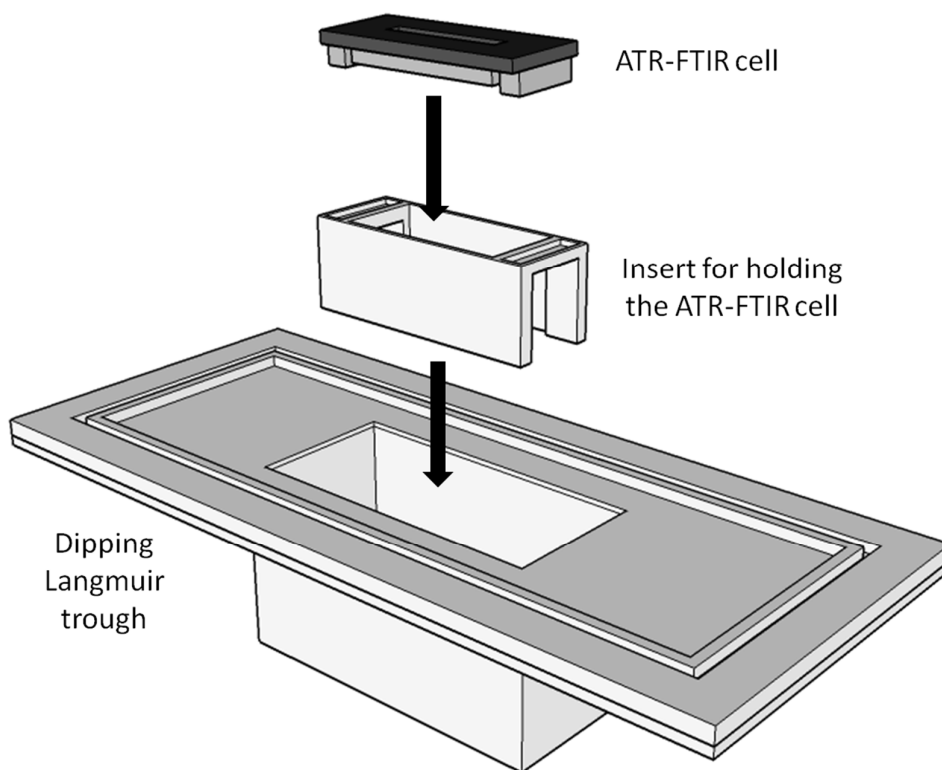


Figure 5.8 Scheme of the dipping trough preparation for the LS-dip showing the insert and the ATR-FTIR cell to be placed at the bottom of the trough's dipping well.

When the crystal was lifted high enough to detach from the water surface, the LB-dip has finished and thus obtained lipid monolayer-covered crystal was put on the tissue with its bigger base (the surface of interest) fronting upwards, and covered to protect from the dust.

The lipid monolayer was removed by vacuum suction and the UHQ water was poured out. For the LS-dip the PTFE insert for holding the ATR-FTIR cell was placed at the bottom of

the trough's dipping well, onto which the ATR-FTIR cell was put (see Figures 5.8 and 2.10 in Chapter 2, page 34). The trough was then filled with the fresh UHQ water and the crystal was attached horizontally (bigger base facing down) to the arm holder just above the water surface (see Figure 5.9).

The surface cleanliness was checked and the monolayer formed of the lipid to be found in the bilayer's outer leaflet was prepared as described previously. The surface pressure was software-controlled to be constant at 35 mN/m and the dipping arm was steered to lower at the constant speed of 3 mm/min.

After piercing the monolayer's surface the crystal was lowered directly to the ATR-FTIR cell, the crystal holder was detached and removed and, still under water surface, the cell's upper base was screwed on top of the crystal thereby holding it firmly and preventing the leakage.

The ATR-FTIR cell was dried with the paper towel, placed in the FTIR instrument's sample chamber and left to dry overnight. A fresh bilayer was created before each experiment.

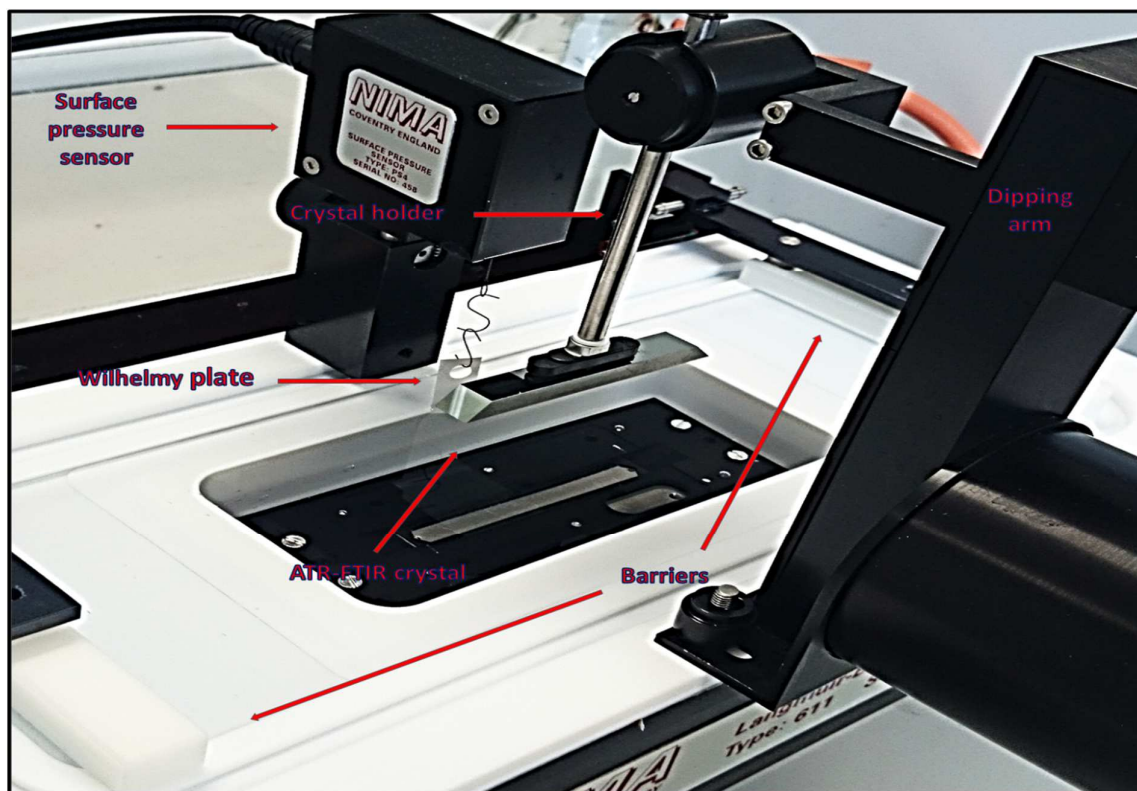


Figure 5.9 Langmuir-Schaeffer dip of the germanium ATR-FTIR crystal using purpose-built Langmuir trough. The lipid-monolayer-covered Ge crystal will pierce the lipid monolayer spread on the water surface and will be inserted to the ATR-FTIR cell placed at the bottom of the trough's well.

5.4.3 ATR-FTIR Analysis of the Protein Adsorption to the Phospholipid Bilayers Formed by Different Methods

Two different bilayer deposition methods were compared to choose the one giving the more reliable results for the future bilayer experiments. Lysozyme has been chosen as the testing compound due to the reasons stated in Chapter 1 (see page 15) and due to the fact that it adsorbs to the bare interfaces.¹⁰² DPPC was chosen as the model phospholipid as it did not interact strongly with the cationic proteins (see Chapter 4, Figure 4.8)

Therefore, the adsorption of lysozyme to the symmetric DPPC bilayer and the protein penetration to the solid interface could be a preliminary indication of the bilayer's coverage directly associated with the bilayer's overall quality. The DPPC bilayer with a high coverage would then form a barrier between the lysozyme and the bare interface.

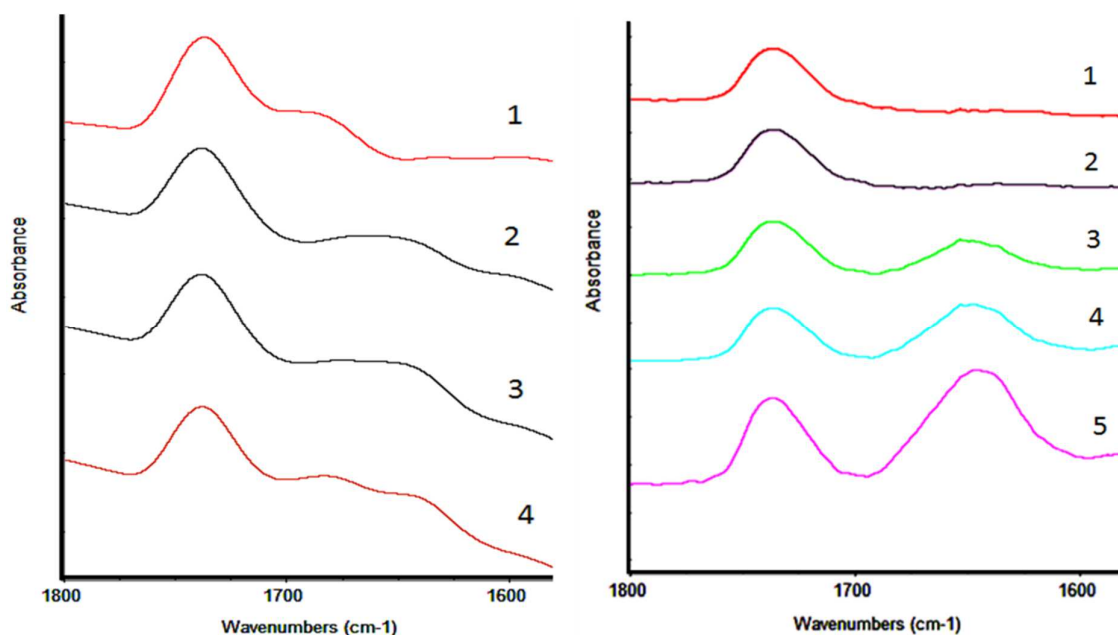


Figure 5.10 ATR-FTIR results on the lysozyme adsorption to the symmetric dipped DPPC bilayer (left) showing spectra of: 1) the lipid bilayer before injection, 2) right after injection, 3) 1 h after injection, 4) 24 h after injection, and the DPPC bilayer formed by spreading vesicles (right) showing spectra of: 1) the lipid bilayer before injection, 2) right after injection, 3) 1 h after injection, 4) 2 h after injection and 5) 24 h after injection. The two peaks of interest shown are the carbonyl stretch at $\sim 1750\text{ cm}^{-1}$ indicating the presence of the phospholipid and the Amide I band at $\sim 1650\text{ cm}^{-1}$ indicating the presence of the protein.

The wheat defence protein interaction with the lipid monolayers the air-liquid interface has been widely studied by FTIR.²⁹ It involved monitoring of the changes in the Amide I band (\sim

1650 cm^{-1}) indicating the protein penetration of the lipid monolayer and the lipid acyl chains vibrations (~ 2920 and 2850 cm^{-1}) informing about the state of the phospholipid tails upon the interaction.

Lysozyme was shown to adsorb strongly to the bare germanium interface, as shown in Figure 5.11. The carbonyl stretch peak ($\sim 1750 \text{ cm}^{-1}$) was observed in both DPPC bilayer experiments, indicating the lipid presence at the solid-liquid interface. There was no significant difference in the acyl chain vibrations region (2920 and 2850 cm^{-1}), suggesting no dramatic changes to the lipid tails arrangement (data not shown).

A slight increase in the Amide I peak was observed for the lysozyme-adsorbed DPPC bilayer formed by the LB-dip and LS-dip (see Figures 5.10, 5.11 and Table 5.2). The initial dipped DPPC bilayer showed a tiny peak fused with the carbonyl stretch peak, indicating possible contamination of the bilayer caused by the initial stages of the dipping method development. However, the Amide I area was not strongly affected by this contamination.

Table 5.2 Summary of the ATR-FTIR experiments on the lysozyme adsorption.

Time	Integrated Amide I peak area		
	Adsorption to the bare Ge crystal surface	Adsorption to the symmetric DPPC dipped bilayer	Adsorption to the symmetric DPPC bilayer formed by vesicles spreading
Right after injection	0.2728	0.0680	0.1870
1 h after injection	0.3406	0.0970	0.3150

In contrast to the first bilayer's spectrum, the FTIR spectrum of the DPPC bilayer formed by the vesicles showed a significant increase in the Amide I region after 24 h incubation with the protein solution, indicating the lysozyme's penetration to the interface. Knowing that this protein does not interact strongly with DPPC,⁸⁹ it can be speculated that the bilayer produced by vesicles spreading must have contained the holes in at least one of the points from which the infrared beam reflected (see Chapter 2, Figure 2.8).

Moreover, it cannot be said with certainty that the structures formed by vesicles spreading were of the exactly two phospholipid molecules thickness. This uncertainty, together with the

risk of the uneven bilayer coverage, were the arguments for using the LB-dip and the LS-dip methods to produce the lipid bilayers in the future experiments.

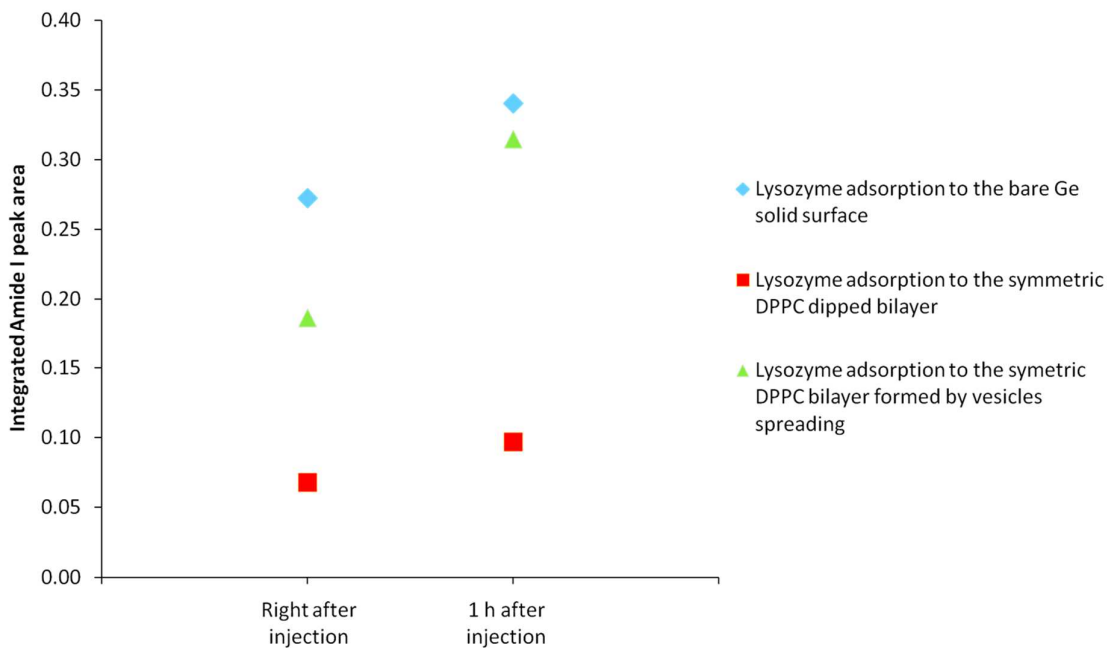


Figure 5.11 ATR-FTIR results on the lysozyme adsorption to the bare Ge interface, symmetric dipped DPPC bilayer and the DPPC bilayer formed by vesicles spreading.

5.4.4 ATR-FTIR Study of the Wheat Defence Proteins Adsorption to the Fungal Bilayer

Artificial phospholipid membranes, representing a fungal cell membrane, were created by depositing the DPPC as the inner leaflet lipid (see section 5.3.2) by the LB-dip and DPPC or DPPS as the outer leaflet lipid by LS-dip on the ATR-FTIR germanium crystal.

The formed bilayers were then allowed to interact with the wheat defence protein solutions in the D₂O phosphate buffer (see Table 5.2 for the experiment details). The experiments were carried out in triplicates. The use of DPPS as the outer leaflet lipid meant the initial presence of the Amide I peak (see molecule's structure in the Chapter 1, page 13).¹²⁵ Therefore, the results were reported as the rise in the Amide I peak area, *i.e.* the difference between the integrated peak area at the specified time-point reduced by the integrated peak area of the unaffected bilayer.

Figure 5.12 illustrates the effect of the outer leaflet lipid's net charge on the bilayer's interaction with β -Pth.

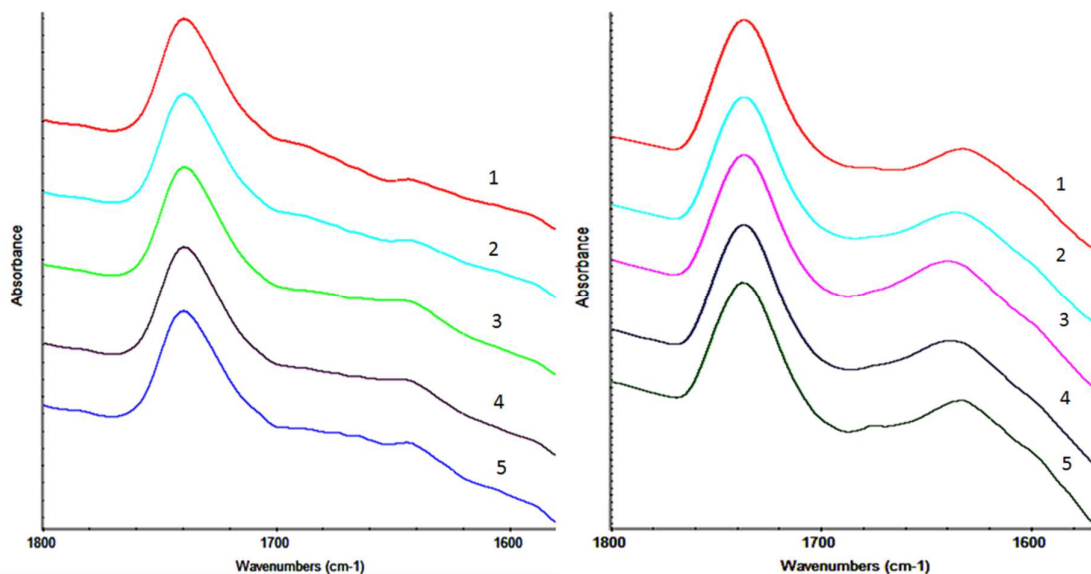


Figure 5.12 ATR-FTIR results on the β -Pth adsorption to the symmetric dipped DPPC bilayer (left) showing spectra of: 1) the lipid bilayer before injection, 2) right after injection, 3) 1 h after injection, 4) 2 h after injection, 5) 24 h after injection and to the asymmetric dipped DPPC:DPPS bilayer (right) showing spectra of: 1) the lipid bilayer before injection, 2) right after injection, 3) 1 h after injection, 4) 2 h after injection and 5) 24 h after injection. The two peaks of interest shown are the carbonyl stretch at $\sim 1750\text{ cm}^{-1}$ indicating the presence of the phospholipid and the Amide I band at $\sim 1650\text{ cm}^{-1}$ indicating the presence of the protein and the PS headgroup.

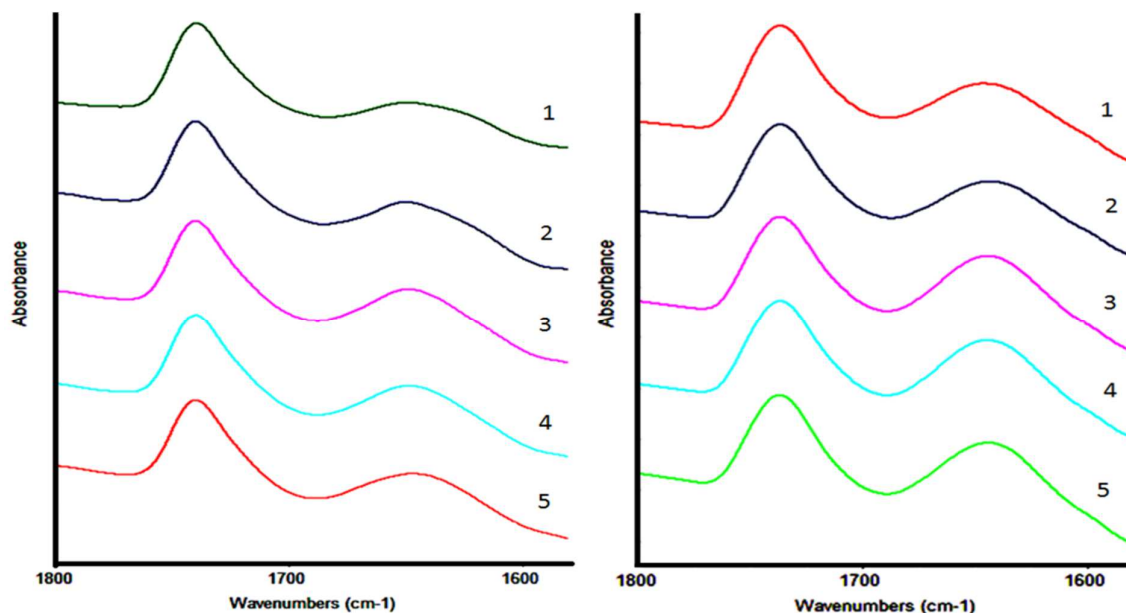


Figure 5.13 ATR-FTIR spectra showing the α_2 -Pth (left) and Pin-a (right) adsorption to the symmetric dipped DPPC:DPPS bilayer: 1) the lipid bilayer before injection, 2) right after injection, 3) 1 h after injection, 4) 2 h after injection, 5) 24 h after injection. The two peaks of interest shown are the carbonyl stretch at $\sim 1750\text{ cm}^{-1}$ indicating the presence of the phospholipid and the Amide I band at $\sim 1650\text{ cm}^{-1}$ indicating the presence of the protein and the PS headgroup.

For the symmetric DPPC:DPPC bilayer, no significant rise in the Amide I area was observed within 24 h, indicating that there was hardly any penetration of the protein to the bilayer and interface.

The Amide I area of the DPPC:DPPS spectrum, on the other hand, showed a noticeable rise (see Table 5.3 for details), pointing out the penetration of the bilayer by β -Pth. This is in agreement with the findings from the monolayer studies, confirming the huge impact the lipid's charge has on the protein adsorption (see Chapter 4, page 63) and its potential antimicrobial action.

Two other wheat defence proteins were tested against the DPPC:DPPS bilayer: Pin-a and α_2 -Pth, both already shown to interact with DPPS monolayers (see Chapter 4, pages 68 and 69). Similarly to β -Pth, both proteins penetrated the DPPC:DPPS bilayer (see Figure 5.14 and Table 5.3) causing an increase in the Amide I peak area.

Pin-a caused the biggest changes to the Amide I area, similarly to α_2 -Pth. However, β -Pth adsorption produced the smallest overall rise in the Amide I area (significantly different from the other proteins' effect, as shown in Table 5.3), which does not correspond to the results obtained for the three proteins interacting with the DPPS monolayer (see Chapter 4, pages 68 and 69).

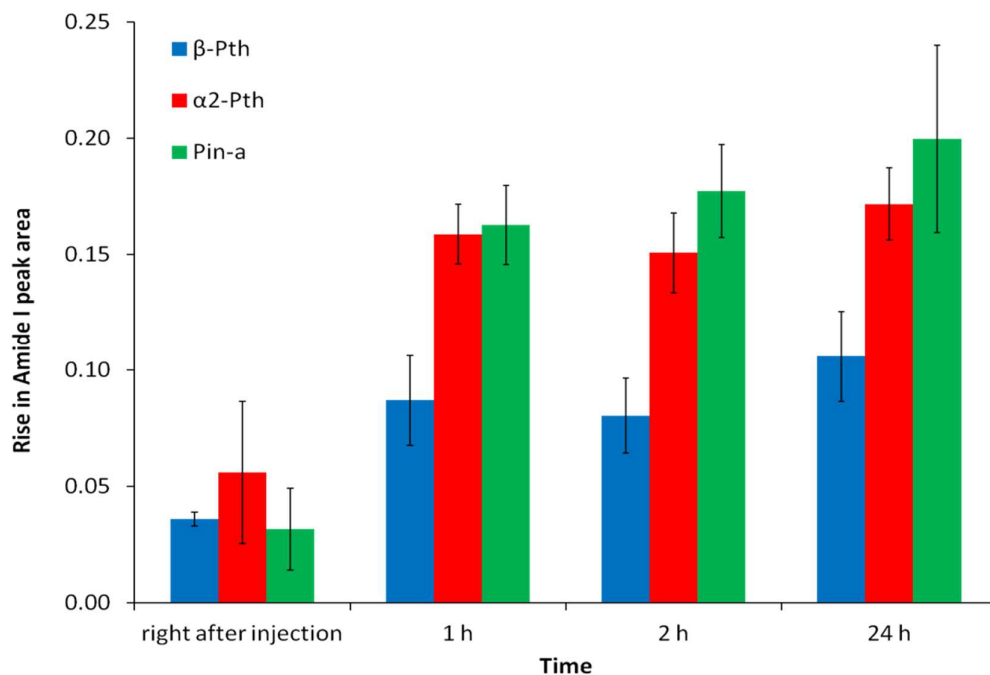


Figure 5.14 ATR-FTIR results on the wheat defence proteins adsorption to the dipped DPPC:DPPS bilayer.

This inconsistency, together with the relatively big deviation between the experiment replicates, can be explained by the fact that the lipid mixing might have occurred spontaneously and randomly between the leaflets of the bilayer.

To assess the lipid mixing in the bilayer, the NR bilayer experiments were carried out (see Chapter 6) by using the tail-deuterated DPPC in the inner leaflet and the hydrogenated DPPS in the outer leaflet.

For all experiments no significant change in the area of acyl chain vibrations peaks was observed (data not shown), suggesting that the phospholipid tails were hardly affected by the action of any protein.

Table 5.3 Summary of the ATR-FTIR results on the wheat defence proteins adsorption to the dipped DPPC:DPPS bilayer. An independent 2-tailed t-test was used for indicating the significant differences (marked bold) at $P \leq 0.05$.

Time	Rise in the integrated Amide I peak area			P value		
	Protein added: β -Pth (0.010 mg/ml)	Protein added: α_2 -Pth (0.010 mg/ml)	Protein added: Pin-a (0.025 mg/ml)	β -Pth result compared with Pin-a	β -Pth result compared with α_2 -Pth	Pin-a result compared with α_2 -Pth
Right after injection	0.0360 \pm 0.0030	0.0560 \pm 0.0306	0.0317 \pm 0.0176	0.71	0.38	0.31
1 h after injection	0.0870 \pm 0.0193	0.1587 \pm 0.0129	0.1627 \pm 0.0171	< 0.01	< 0.01	0.76
2 h after injection	0.0803 \pm 0.0161	0.1507 \pm 0.0172	0.1773 \pm 0.0200	< 0.01	< 0.01	0.16
24 h after injection	0.1060 \pm 0.0195	0.1717 \pm 0.0155	0.1997 \pm 0.0402	0.04	0.01	0.35

ATR-FTIR technique proved to be a useful tool to preliminarily assess the interactions between the wheat defence proteins and the phospholipid bilayers. However, one cannot assess the degree of penetration into each layer using this technique. Therefore, neutron reflectometry data were carried out to provide a more detailed view on the proteins' interaction with fungal membranes.

5.5 Conclusions

The bilayer studies provided a more in-depth and more realistic analysis of the wheat defence proteins' antimicrobial action.

Two techniques were used for studying the structures of the artificial bilayers: ATR-FTIR and Neutron Reflectometry (NR). The preliminary NR studies revealed the importance of the charge influence on the bilayer attachment to the solid surface and allowed to improve the analysed bilayer system by introducing a zwitterionic lipid on the inner leaflet.

For ATR-FTIR studies, the two bilayer deposition methods were tested: vesicles spreading and the Langmuir-Blodgett/Langmuir-Schaeffer dipping. The second method turned out to provide the high quality bilayers with the higher lipid coverage than the first method.

The ATR-FTIR experiments used a newly developed bilayer deposition and interaction analysis protocols. The studies on Pin-a, α_2 -Pth and β -Pth confirmed the proteins' preference for their interaction with the anionic lipids. The slight differences between the levels of interaction between each protein did not match the levels of interactions obtained during the monolayer studies, suggesting that the additional factors like lipid flipping between the leaflets and the bilayer coverage could be the artefacts causing the aforementioned deviations.

The protein-lipid systems in the ATR-FTIR experiments were examined in more detail by NR (see Chapter 6), which enabled to assess the lipid flipping between the leaflets and the degree of the protein penetration to the lipid bilayer.

Chapter 6

LIPID BILAYER STUDIES

PART II – NEUTRON REFLECTOMETRY EXPERIMENTS

6.1 Introduction

As shown in Chapter 5, lipid bilayers deposited on the solid surface can serve as the model membranes in the analysis of the protein-lipid interactions. Langmuir-Blodgett and Langmuir-Schaeffer dipping turned out to be the better bilayer deposition methods when compared to the vesicles spreading and were chosen for the production of the lipid bilayers in the next experiments.

It has also been shown that the choice of the lipid deposited on the inner leaflet of the bilayer plays an important role in the bilayer's stability and coverage (see Chapter 5, page 89). Therefore, the experiments described in this chapter were carried out on the lipid bilayers containing zwitterionic lipid DPPC on their inner leaflets, which increased the bilayer coverage and stability.

The technique used for the experiments in this chapter, Neutron Reflectometry (NR), has been widely used for studying the structure of the thin films adsorbed at the interfaces, *e.g.* the adsorption of bovine serum albumin (BSA) to the silicon surface as in the research by Cowsill *et al.*¹⁶³

The technique proved successful in monitoring the wheat defence protein interactions with model bacterial membranes. For example, Clifton *et al.*²⁷ described in 2011 the different lipid-binding mechanisms between Pin-a and β -Pth by allowing the protein to adsorb to the DPPG monolayers.

Analogous monolayers were also exposed to the action of α_1 -Pth and α_2 -Pth in the work by Clifton *et al.*²⁹ from 2012, which revealed the relationship of the protein's hydrophobicity and its lipid-binding properties: the more hydrophobic α_2 -Pth removed more lipid from the air/liquid interface.

The mode of antimicrobial action of Pin-b and its isoform Pin-bS (see Chapter 1, page 5 for more details) was examined by Sanders *et al.*⁵¹ using NR and stressed the influence of both protein and lipid structures on the strength and mode of the protein-lipid interactions.

Neutron Reflectometry also enabled to determine the structure of the lipid bilayers deposited on the solid support, as shown by Clifton *et al.*⁸⁴ who analysed the lipid flipping between the leaflets of the bacterial outer membrane model, and described the role of the divalent ions on the lipid deposition process and the bilayer's stability.¹⁵⁷

Another subject studied by NR were floating bilayer systems, providing natural membrane fluidity, as summarised by Fragneto *et al.*¹⁶⁴ For example, Hughes *et al.*¹⁶⁵ developed the dipping protocols for the formation of the floating bilayer and analysed the structure of the distearoylphosphatidylcholine (DSPC) floating bilayer using NR.

The lipid bilayers were also subjected to the action of the external compounds and their effect on the bilayer structure was assessed, as in the study by Clifton *et al.*,¹⁵³ who examined the adsorption of lactoferrin and lysozyme to the model membrane of the Gram-negative bacterium *Escherichia coli*.

For more details on the NR technique principles, please refer to Chapter 2, page 34.

This chapter focuses on the NR experiments carried out on the wheat defence protein-adsorbed model fungal bilayers. The obtained information on the changes in the lipid bilayers' structure upon the protein adsorption can be then used for assessing the strength of the protein-lipid interaction and thus the degree and mode of the antifungal action of the tested protein. Therefore, the lipid systems analysed in this chapter reflect the different structural characteristics of the natural lipid membranes and their impact on the strength of the interaction with various wheat defence proteins.

The synergy between the two proteins, Pin-a and β -Pth has been assessed by exposing the model fungal bilayer to the solution composed of the 1:1 molar ratio of the two compounds and analysing the changes in the bilayer structure by means of Neutron Reflectometry.

6.2 Materials

1,2-Dipalmitoyl-*sn*-glycero-3-phosphocholine (DPPC, synthetic, purity > 99%), 1,2-dipalmitoyl(d62)-*sn*-glycero-3-phosphocholine (tail-deuterated d-DPPC, synthetic, purity > 99%), 1,2-dipalmitoyl-*sn*-glycero-3-phospho-L-serine (DPPS, synthetic, purity > 99%) and 1-palmitoyl-2-oleoyl-*sn*-glycero-3-phospho-L-serine (POPS, synthetic, purity > 99%) were all purchased from Avanti Polar Lipids (Alabaster, AL, US). Ergosterol (purity \geq 95%) was obtained from (Sigma Aldrich, Dorset, UK). Lipid solutions were prepared and stored as for the monolayer experiments (see: Chapter 4, page 55).

The protein stock solutions were prepared in the H₂O and D₂O phosphate buffer solution at pH/pD 7.0 using UHQ grade water (resistivity 18.2 M Ω ·cm obtained from ELGA LabWater purifier – High Wycombe, UK) and the deuterium oxide (D₂O, 99.9 atom % D, purchased from Sigma Aldrich, Dorset, UK). The protein concentrations were checked with the UV absorbance at 280 nm.

The saturated phospholipids DPPC and DPPS were chosen to form the phospholipid bilayer systems as they are the most abundant in the natural fungal membrane (see Chapter 1, page 11). To create the isotopic contrast for NR experiments and thus assess the lipid flipping between the bilayer leaflets, a tail-deuterated DPPC (later referred to as d-DPPC) was applied.

The mono-unsaturated anionic phospholipid POPS introduced the fluidity of the phospholipid bilayer, the characteristic feature of the fungal membrane (see Chapter 1, page 12).

Ergosterol, a steroid found in fungal membranes (see Chapter 1, page 13) was used to assess the effect of the steroid presence on the structure of the artificial bilayers and its impact on the interaction with the wheat defence proteins.

The bilayer nomenclature applied throughout this chapter was the following:

‘Name_of_the_Lipid_in_the_Inner_Leaflet:

Name_of_the_Lipid_or_Lipid_Mixture_in_the_Outer_Leaflet’,

e.g. d-DPPC: h-DPPS bilayer means that the lipid deposited in the inner leaflet was tail-deuterated DPPC and that the outer leaflet was composed of the fully hydrogenated DPPS.

The lipid bilayers containing the d-DPPC on the inner leaflet were used for assessing the lipid mixing between the leaflets and the bilayers containing only fully hydrogenated lipids were

used for the quantitative analysis of the layers forming the protein-adsorbed systems and, thus, allowing to determine the strength of the protein interaction with the bilayer.

The latter lipid systems were chosen to determine the amount of protein in each layer because the protein scattering length densities were the highest in such lipid systems, thereby making the fully hydrogenated lipid system more sensitive to the SLD changes occurring upon the adsorption (see Chapter 2, Table 2.3, page 35 for more details).

6.3 Bilayer Preparation: Surface Pressure Changes

This section focuses on the molecular side of the dipping process, illustrating the surface pressure changes occurring at LB-dip and LS-dip stages. Figure 6.1 shows multiple compressions obtained during the d-DPPC film annealing (a cycle of expansions and compressions of the monolayer) and their good repeatability indicating the good quality of the film. Similarly to its hydrogenated component (see Chapter 4, Figure 4.5, page 59), d-DPPC shows the distinct gaseous, liquid-expanded, liquid-condensed and solid phases during its compression.

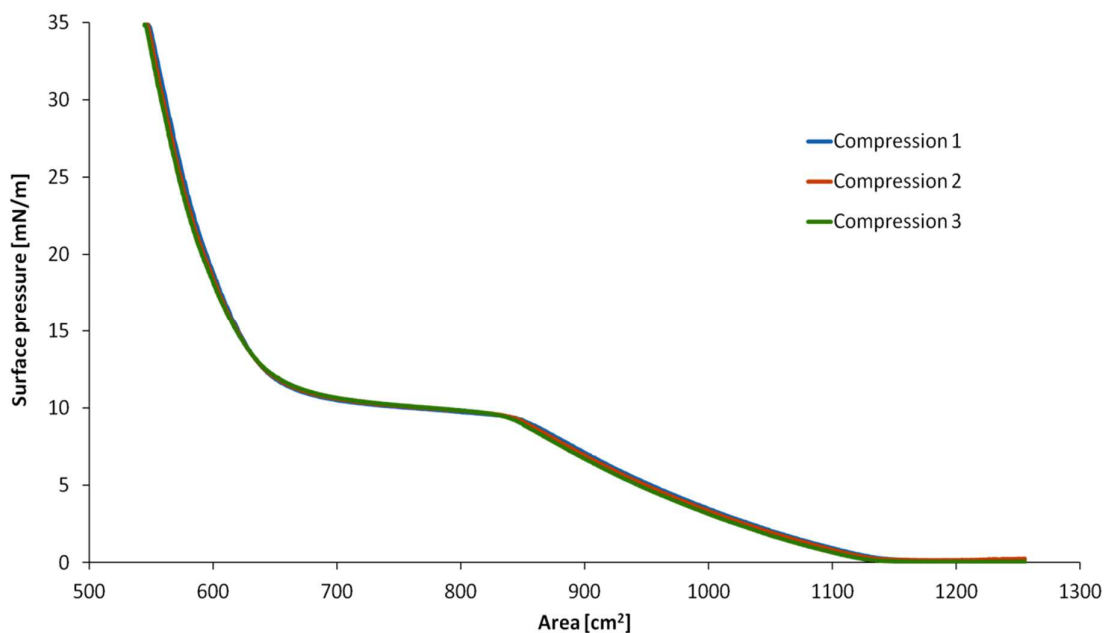


Figure 6.1 Compression isotherms of the d-DPPC monolayer showing good repeatability of the compression and expansion processes, indicating high purity of the lipid film.

Figure 6.2 shows the LB-dip stage of the deposition process held at constant pressure of 35 mN/m. The low deviation around this number during the dipping suggests the good quality of the deposition leading to the high lipid coverage. The moment of the bilayer detaching was characterised by the sudden drop in the surface pressure caused by the elimination of the solid immersed in the subphase. The software-driven barriers moved then to the trough's middle to retain the set value.

The small spikes present around 500 – 520 cm² were a result of the unavoidable vibrations caused by *e.g.* the door being closed nearby. Fortunately, these imperfections happened very rarely and did not affect the quality of the obtained bilayer, as verified by the obtained reflectivity data.

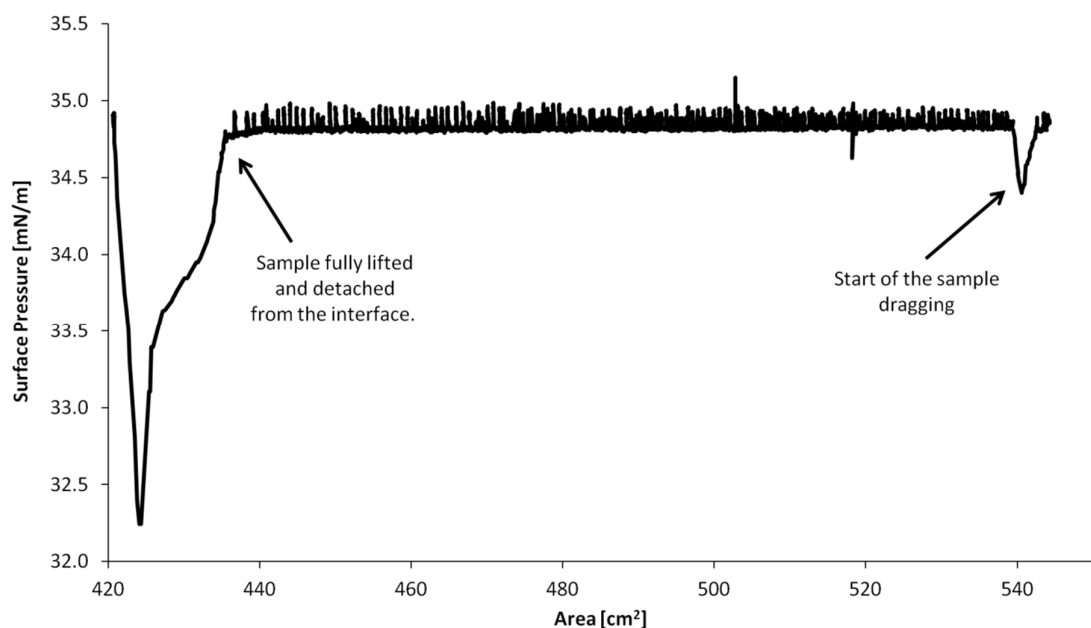


Figure 6.2 Pressure-Area isotherm showing the Langmuir-Blodgett dip of the silicon block being covered with a d-DPPC monolayer.

Figure 6.3 illustrates the repeatability of the film compressions obtained for the h-DPPS monolayer being prepared for the outer leaflet deposition. The shape of the isotherm corresponds well to the one obtained for the monolayer studies (see Chapter 4, Figure 4.5).

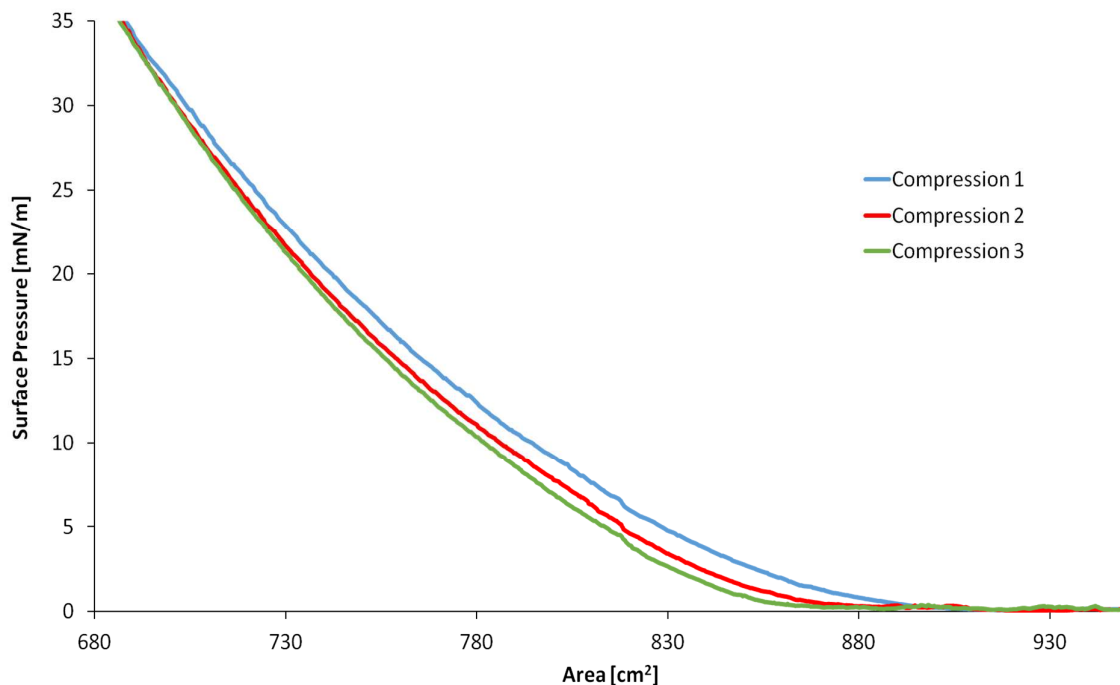


Figure 6.3 Compression isotherms of the h-DPPS monolayer, showing the overall good repeatability of the compression and expansion processes, indicating the high quality of the lipid film.

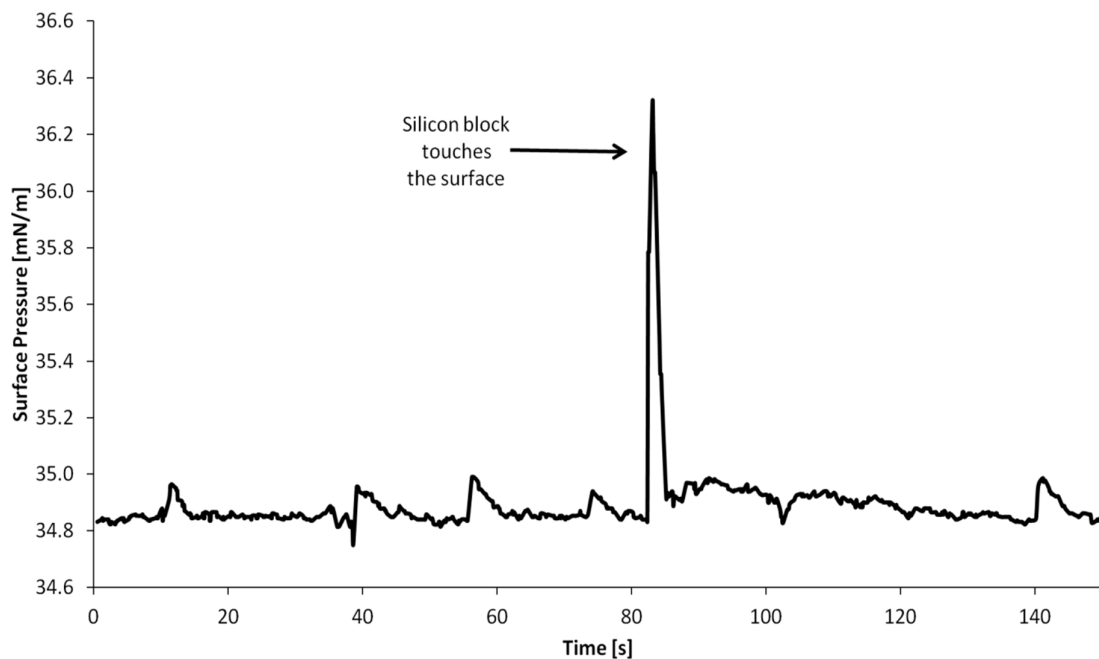


Figure 6.4 Isotherm showing the Langmuir-Schaeffer dip of the silicon block being covered with the outer leaflet lipid mixture h-DPPS:ergosterol 1:1 mol:mol. The marked point indicates the moment of the direct contact of the silicon block's covered surface with the lipid monolayer.

The changes in the surface pressure recorded during the LS-dip are presented in Figure 6.4. Similarly to the LB-dip, one can see the software-driven surface pressure being kept constant at the value of 35 mN/m. A spike in the surface pressure, appearing around 80th second of the recording, is an indication of the surface being pierced by the block, and immediate reaction of the barriers to restore the pre-defined pressure of 35 mN/m.

Software-driven deposition together with the subphase's lowered temperature and the presence of calcium ions provided the high coverage, high quality lipid bilayers for the NR experiments.

6.4 Neutron Reflectometry Data Fitting

The experiments were carried out at the ISIS Neutron and Muon Spallation Source (Harwell, UK). The obtained reflectivity profiles were fitted using RasCal software to the pre-defined lipid bilayer models consisting of five layers: silicon oxide, inner lipid headgroup, inner lipid tails, outer lipid tails and outer lipid headgroup. The protein-adsorbed files had an additional protein layer added between the outer lipid headgroup and the bulk solvent (see Figures 6.5 and 6.6 for the examples). The fitting uncertainties were obtained by the software's bootstrap error analysis.

The following assumptions were made for fitting the lipid bilayer-only reflectivity data:

1. Full bulk solvent exchange for each layer during a contrast change – also applies to the hydration parameter of each layer (see below).
2. Hydration parameter (percentage of water in the layer), allowing to directly determine the water content was applied for all layers. This significantly shortened the time of the data analysis by simplifying the model and guaranteeing the constant water fraction for each contrast.
3. Constant thickness, hydration, SLD and roughness kept for all contrasts – the parameters kept different for each silicon block. This arises from the assumption that the bilayer structure remained intact during the contrast replacement.
4. Theoretical SLDs of the lipids do not change during the contrast variation due to the lack of the exchangeable hydrogen atoms.

The lipid and water volumetric fractions for the lipid-only fits were determined directly from the hydration parameter:

$$\varphi_{\text{lipid}} = 1 - \frac{\text{Lipid hydration parameter}}{100} \quad (10)$$

and:

$$\varphi_{\text{water}} = \frac{\text{Lipid hydration parameter}}{100} \quad (11)$$

To assess the lipid flipping between the leaflets in the lipid-only fits with the deuterated lipid deposited on the inner leaflet, the following approach was employed:

- 1) Water fraction was determined directly from the hydration parameter for the inner tails and outer tails layers as shown in Equation 11 – the results reported in the lipid-mixing tables did not take the headgroups' hydrations into account.
- 2) Inner tails and outer tails regions of the fits were used to determine the lipid mixing owing to the relatively big difference between the tails theoretical SLDs: $7.45 \times 10^{-6} \text{ \AA}^{-2}$ for the deuterated dipalmitoyl tails and $-0.39 \times 10^{-6} \text{ \AA}^{-2}$ for the fully hydrogenated tails. Because of this, the distribution of the lipids between the leaflets can be assessed with a fairly high level of confidence. For more theoretical SLD values, please refer to Chapter 2, Table 2.3, page 35).
- 3) The volumetric fractions of the inner lipid (the lipid deposited during the LB-dip) and the outer lipid (the lipid deposited during the LS-dip) for the inner tails layer and the outer tails layer were calculated using the equations:

$$\text{FIT SLD}_{\text{layer}} = \varphi_{\text{inner lipid}} \times \text{SLD}_{\text{inner lipid}} + \varphi_{\text{outer lipid}} \times \text{SLD}_{\text{outer lipid}} \quad (12)$$

and:

$$\varphi_{\text{inner lipid}} + \varphi_{\text{outer lipid}} = 1 \quad (13)$$

where φ is the volume fraction of the layer component and SLD is the component's calculated scattering length density (see Table 3.3).

Therefore, for the given layer:

$$\varphi_{\text{inner lipid}} = \frac{\text{FIT SLD}_{\text{layer}} - \text{SLD}_{\text{outer lipid}}}{\text{SLD}_{\text{inner lipid}} - \text{SLD}_{\text{outer lipid}}} \quad (14)$$

and:

$$\varphi_{\text{outer lipid}} = 1 - \varphi_{\text{inner lipid}} \quad (15)$$

The lipid volumetric fractions above were describing the layer composed of the lipid only. Therefore, the obtained numbers needed to be corrected to take the fraction of water into account:

$$\varphi_{\text{inner lipid corrected}} = (1 - \varphi_{\text{water}}) \times \varphi_{\text{inner lipid}} \quad (16)$$

and:

$$\varphi_{\text{outer lipid corrected}} = 1 - (\varphi_{\text{inner lipid corrected}} + \varphi_{\text{water}}) \quad (17)$$

The values reported in the tables describing the inner and the outer lipid distribution among the leaflets were the ones obtained from equations 16 and 17. As the differences between the SLDs of the hydrogenated lipid chains were relatively small (see Chapter 2, Table 2.3), it was impossible to determine the level of the lipid mixing between the leaflets in the bilayers formed of the hydrogenated lipids only.

The approach for fitting and analysing the protein-adsorbed reflectivity data was the following:

1. A file containing the fits with the lipid-only reflectivity data was copied and renamed to the protein-adsorbed one, and the reflectivity data files were updated.
2. To keep the analysis relatively simple, no protein penetration and no change in the layer structure were assumed for the inner headgroup and inner tails layers, thus all parameters describing these layers remained unchanged.
3. To simplify the comparison of the components' volumetric fractions before and after the protein adsorption, all lipid components thicknesses were kept constant in both compared files.
4. To allow the better detection of the smallest changes in SLD in the outer headgroup and outer tails layers, the hydration parameter was removed from these layers and the three

separate SLDs (one describing each contrast) were calculated basing on the parameters obtained from the lipid-only fit as below:

$$SLD_{\text{layer,contrast1}} = \phi_{\text{lipid}} \times SLD_{\text{lipid}} + \phi_{\text{water}} \times SLD_{\text{water,contrast1}} \quad (18)$$

The obtained values served as the starting points for the fitting of the layer, thus allowing to better estimate if any SLD changes occurred during the protein adsorption. The removal of the hydration parameter in the lipid-only fits produced the SLD values which gave rise to the unacceptable values of the components' volumetric fractions, *e.g.* numbers greater than 1. Therefore, the hydration parameter was used for all layers in the lipid-only fits.

5. The protein layer has been added in each file, the layer was assigned three protein SLD values, one for each contrast (see Chapter 2, Table 2.3). This took into account the exchangeable hydrogen atoms in the protein molecule. The values were kept constant throughout the fit and one hydration parameter for all contrasts was allowed to fluctuate in order to assess the protein fraction in the layer. The other fitted parameters for this layer were roughness and thickness, the latter one with the starting value 0 Å.
6. The order of unlocking the fitting parameters was as follows:
 - Firstly, only the protein thickness and roughness allowed to be fitted; no protein penetration to the bilayer assumed, only adsorption.
 - Secondly, the outer headgroup SLDs in D₂O, SMW and H₂O contrasts were unlocked, assuming the structural changes in the outer headgroup region only.
 - Finally, the outer tails SLDs in D₂O, SMW and H₂O contrasts were unlocked, assuming the protein presence can affect the structure of the outer headgroup and the outer tails.
7. The adsorbed protein does not remove the lipid molecules, it is assumed that the equilibrium stage was reached by the adsorbed protein and the adsorbed-bilayer structure remained constant throughout the contrast changes. This enabled the thickness and roughness parameters to remain constant for all 3 contrasts.

Monitoring the changes in each layer's SLDs allowed to assess the composition of the layer. The variations in the SLDs of the H₂O contrasts were chosen to assess the protein insertion to the layer as this contrast was the most sensitive to the SLD changes.

The following approach was applied:

- If the fitted SLD value of the outer headgroup decreased, *i.e.* changed in the direction of the SLD of the H₂O value, the change in the water content of the layer (or pore formation) and no protein penetration was assumed.
- If the fitted SLD value of the outer headgroup increased, *i.e.* changed in the direction of the protein's SLD value, the protein was assumed to have reached the layer and its content was calculated as described by Equation (19), assuming no change to the initial proportions between the lipid and water.
- With an increase of the outer headgroup's SLD value, a concomitant increase in the outer tails SLD value was interpreted as the protein insertion to the outer tails layer and the protein amount was calculated analogically as for the outer headgroup layer, following the same assumptions.
- The decrease in the outer headgroup value resulted in all changes in the outer tails SLD values to be interpreted as the changes in the water content, *i.e.* if the protein did not penetrate the headgroup region, it did not penetrate the outer tails region at the same time.

From the assumption that the ratios of lipid to water remain the same when protein penetrates the layer and that the rise in SLD is a consequence of the protein penetration only, one can calculate the protein fraction in the layer:

$$\varphi_{\text{protein}} = \frac{\text{SLD}_{\text{layer from the protein-adsorbed file}} - \text{SLD}_{\text{layer from the lipid-only file}}}{\text{SLD}_{\text{protein in H}_2\text{O}}} \quad (19)$$

When the protein penetrated the layer, the water and lipid volumetric fractions were assumed to stay in the same ratios as they were in case of the lipid-only file, therefore the lipid fraction was:

$$\varphi_{\text{lipid in the protein-adsorbed file}} = (1 - \varphi_{\text{protein}}) \times \varphi_{\text{lipid in the lipid-only file}} \quad (20)$$

and the water fraction became:

$$\varphi_{\text{water}} = 1 - (\varphi_{\text{lipid}} + \varphi_{\text{protein}}) \quad (21)$$

If there was no penetration of the protein to the layer, the water-to-lipid ratio was changed and the water fraction was obtained as follows:

$$\phi_{\text{water}} = \frac{\text{SLD}_{\text{layer in D2O}} - \text{SLD}_{\text{layer in H2O}}}{\text{SLD}_{\text{D2O}} - \text{SLD}_{\text{H2O}}} \quad (22)$$

And the lipid fraction became then:

$$\phi_{\text{lipid}} = 1 - \phi_{\text{water}} \quad (23)$$

The formula (22) was derived by solving the system of 2 equations (see Eq. 7, Chapter 3) for D₂O and H₂O contrasts. These contrasts were chosen as they provide the biggest difference in the SLD values, enabling to interpret even the smallest change in the values.

For the protein layer with assigned hydration parameter, the protein fraction was determined as follows:

$$\phi_{\text{protein}} = 1 - \frac{\text{Protein hydration parameter}}{100} \quad (24)$$

The listed assumptions allowed to create a relatively simple algorithm for the fitted data analysis, which gave rise to the calculated values that made mathematical and physical sense.

6.5 Results

6.5.1 β -Pth vs. Net Charge-Varying Saturated Lipid Systems

The experiments were carried out using the instrument CRISP at ISIS Neutron Spallation Source (Harwell, UK).

Four bilayer systems were prepared for the experiment: d-DPPC:h-DPPS, d-DPPC:(h-DPPS:d-DPPC 1:1 mol:mol) and their two fully hydrogenated counterparts. The hydrogenated lipid bilayers were subjected to the 0.01 mg/mL solutions of β -Pth using the isotopic contrasts described above. The bilayers containing the deuterated DPPC in their inner leaflet had their lipid composition in both leaflets assessed.

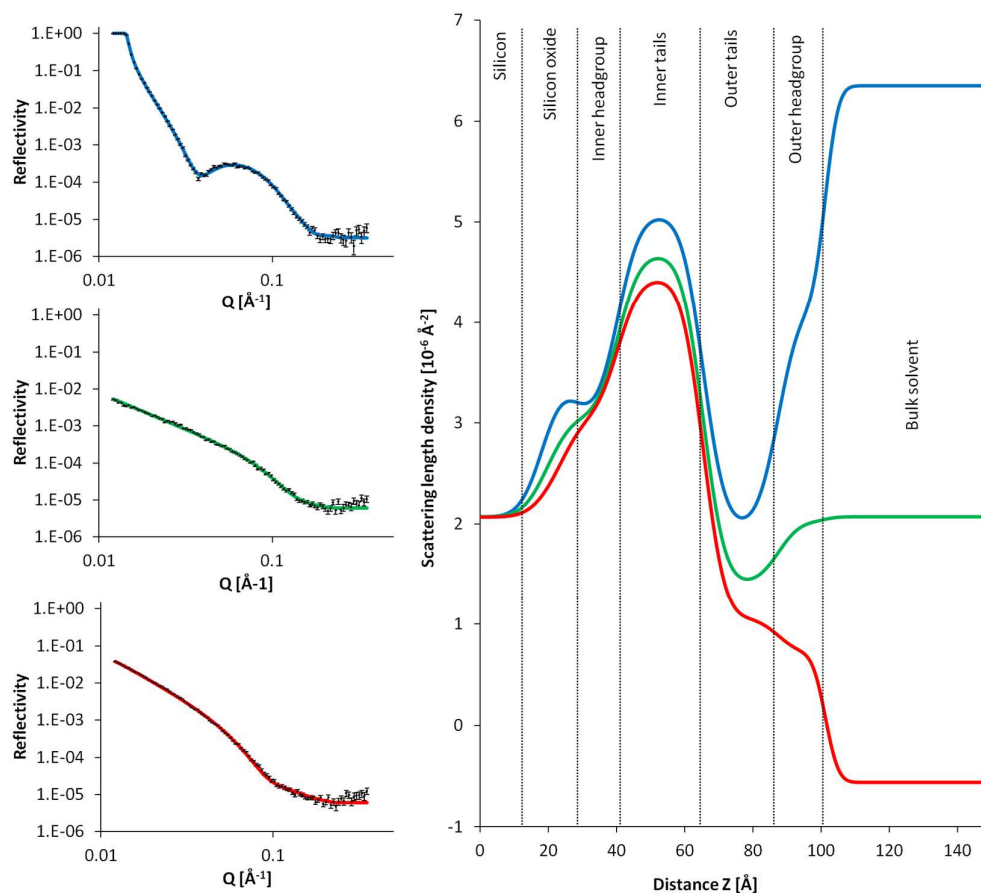


Figure 6.5 Neutron reflectivity profiles (left) and the fits describing these profiles (right) of the asymmetrically deposited d-DPPC: h-DPPS bilayer obtained in the three isotopic contrasts: 100% D₂O (blue line), silicon-SLD-matched water containing 38% D₂O (green line) and 100% H₂O (red line).

Table 6.1 Composition of the d-DPPC: h-DPPS bilayer showing the mixing of the lipids between the two leaflets. The water content values do not take into account the hydration levels of the phospholipid headgroups.

Layer	Thickness [Å]	$\varphi_{\text{d-DPPC}}$	$\varphi_{\text{h-DPPS}}$	φ_{water}	Roughness [Å]
Layer 1: silicon oxide	5.365 ± 0.693	N.A.	N.A.	0.218 ± 0.021	5.748 ± 0.438
Layer 2: inner headgroup	15.000 ± 1.356	0.617 ± 0.076	0.293 ± 0.073	0.090 ± 0.022	5.000 ± 0.510
Layer 3: inner tails	25.000 ± 1.012				
Layer 4: outer tails	22.114 ± 1.227	0.188 ± 0.052	0.678 ± 0.062	0.134 ± 0.034	
Layer 5: outer headgroup	13.750 ± 1.022				

The d-DPPC:h-DPPS bilayer was characterised by a fairly high asymmetry (see Figure 6.5 and Table 6.1). The lipid proportions in the outer and inner leaflet were well corresponding to the lipid distribution results for the similar lipid bilayer system in the study by Clifton *et al.*,⁸⁴ who also analysed the bilayer containing only the palmitoyl (C16:0) fatty acid chains.

Figure 6.6 shows the effect of β -Pth on the fully hydrogenated h-DPPC:h-DPPS bilayer. It can be seen from the reflectivity profiles obtained in the H₂O contrast that the introduction of β -Pth caused significant changes in the bilayer structure.

This has been confirmed by the appearance of the protein layer in the fit SLD profiles (see plot 8 in Figure 6.6) and in the calculated values of the protein fractions. A thick, fairly concentrated protein layer (see Table 6.2) enabled the protein molecules to take around a third of the volume of the outer headgroup layer.

This is in good agreement with both ATR-FTIR data (see Chapter 5, page 101) and with the surface pressure measurements results vs. the DPPS monolayer (see Chapter 4, page 63). The protein's presence also caused a slight increase in the water content of the outer tails region, which could be interpreted as loosening of the lipid structure to the small extent.

The thickness parameters for both deuterated and hydrogenated lipid bilayers correspond well to the ones obtained in the similar neutron reflectivity study carried out by Dabkowska *et al.*¹⁵⁵

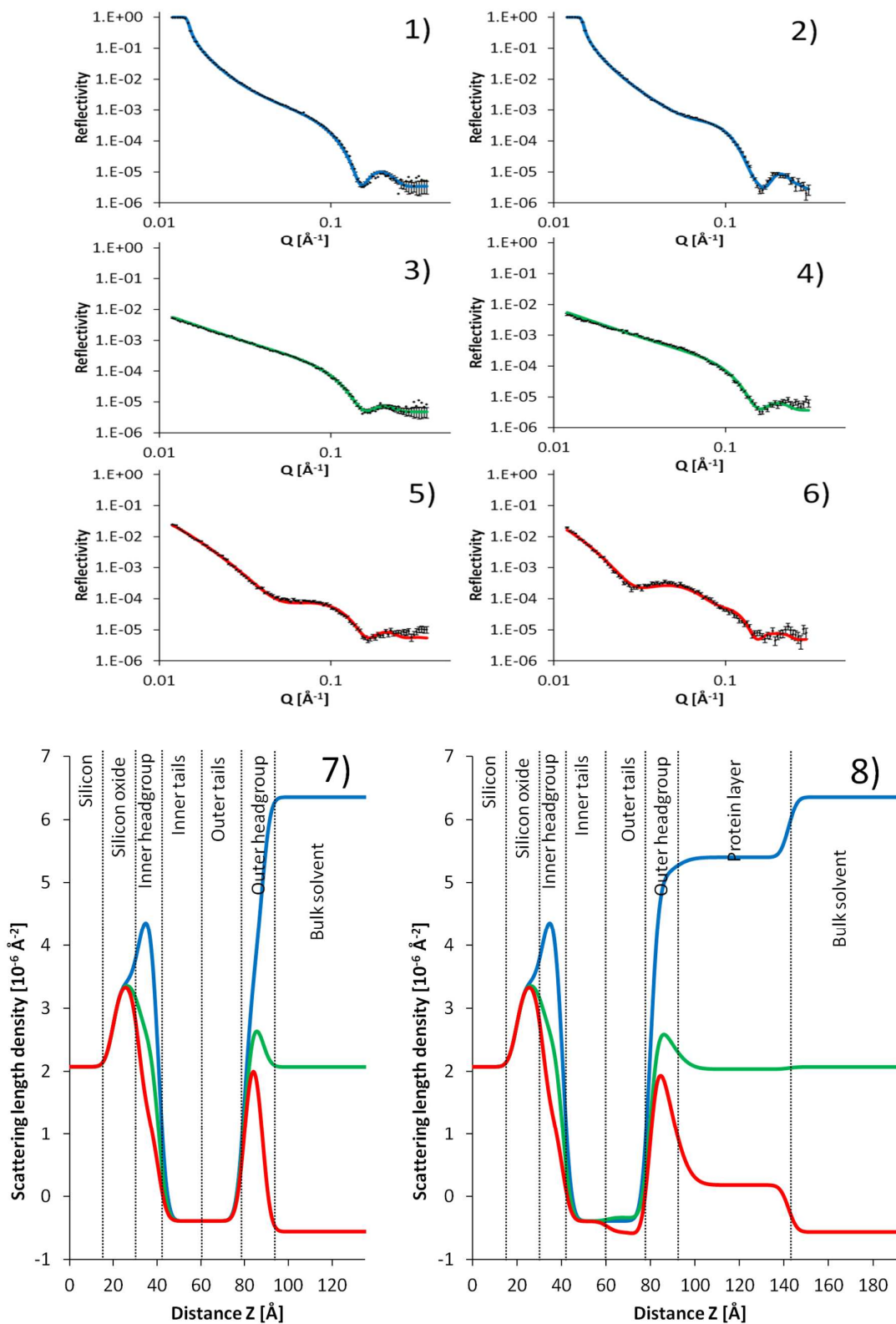


Figure 6.6 NR reflectivity profiles (1 – 6) and the fits describing these profiles (7 – 8) for the asymmetrically deposited h-DPPC:h-DPPS bilayer on its own (1,3,5,7) and interacting with 0.01 mg/mL β -Pth solution (2,4,6,8) obtained in the three isotopic contrasts: 100% D_2O (blue line), silicon-SLD-matched water containing 38% D_2O (green line) and 100% H_2O (red line).

Table 6.2 Results of the NR experiment on 0.01 mg/mL β -Pth interacting with the h-DPPC:h-DPPS lipid bilayer. The SLD values with no uncertainties were kept constant throughout the process of data fitting.

Layer	Contrast	Thickness [\AA]	SLD [10^{-6}\AA^{-2}]	ϕ_{lipid}	ϕ_{protein}	ϕ_{water}	$A_{\text{lipid}} [\text{\AA}^2]$	$\Gamma_{\text{lipid}} [\text{mg m}^{-2}]$	$A_{\text{protein}} [\text{\AA}^2]$	$\Gamma_{\text{protein}} [\text{mg m}^{-2}]$	Roughness [\AA]
Layer 1: silicon oxide	N.A.	11.835 ± 0.424	3.410	N.A.		0.000 ± 0.003	N.A.				3.000 ± 1.195
Layer 2: inner head-group	D ₂ O	8.733 ± 1.039	3.060 ± 0.056	0.500 \pm 0.030	0.000	0.500 \pm 0.030	78.412 ± 10.438	0.659 ± 0.088	0.000	0.000	3.000 ± 0.000
	SMW H ₂ O										
Layer 3: inner tails	D ₂ O	20.251 ± 0.183	-0.390	1.000 \pm 0.000	0.000	0.000 \pm 0.000	40.127 ± 0.362	1.751 ± 0.016	0.000	0.000	
	SMW H ₂ O										
Layer 4: outer tails	D ₂ O	19.187 ± 0.332	-0.390 ± 0.000	0.975 \pm 0.001	0.000 \pm 0.000	0.025 \pm 0.001	43.439 ± 0.753	1.618 ± 0.028	0.000 \pm 0.000	0.000 \pm 0.000	
	SMW		-0.332 ± 0.055								
	H ₂ O		-0.560 ± 0.021								
Layer 5: outer head-group	D ₂ O	8.000 ± 0.000	4.910 ± 0.327	0.599 \pm 0.058	0.301 \pm 0.002	0.100 \pm 0.058	57.471 ± 5.565	0.902 ± 0.087	2458.871 ± 16.339	0.337 ± 0.002	
	SMW		2.962 ± 0.096								
	H ₂ O		3.060 ± 0.054								
Layer 6: adsorbed protein	D ₂ O	54.132 ± 1.953	3.448	N.A.	0.327 \pm 0.017	0.673 \pm 0.017	N.A.	333.996 ± 21.293	2.481 ± 0.158	7.000 ± 0.000	
	SMW		1.964								
	H ₂ O		1.714								

Table 6.3 Summary of the NR experiment on 0.01 mg/mL β -Pth interacting with the h-DPPC:h-DPPS lipid bilayer.

Layer	ϕ_{lipid}	ϕ_{protein}	ϕ_{water}
Outer tails before protein	1.000 \pm 0.000	0.000	0.000 \pm 0.000
Outer tails with the protein	0.975 \pm 0.001	0.000 \pm 0.000	0.025 \pm 0.001
Outer headgroup before protein	0.857 \pm 0.034	0.000	0.143 \pm 0.034
Outer headgroup with the protein	0.599 \pm 0.058	0.301 \pm 0.002	0.100 \pm 0.058

The next analysed system of the fully saturated lipids was a bilayer consisting of an equimolar mixture of DPPC and DPPS deposited in its outer leaflet. This allowed to examine how the reduction in the net charge on the outer leaflet, caused by replacing half of the anionic DPPS molecules with the zwitterionic DPPC, influenced the action of β -Pth.

Figure 6.7 shows the smoother fringe in the reflectivity D_2O contrasts, characteristic of the relatively symmetric bilayers. The use of d-DPPC in both inner and outer leaflet allowed to better highlight the presence of the h-DPPS and led to the results presented in Table 6.4. Not surprisingly, the dominating lipid in both leaflets was d-DPPC, which is in agreement with the relatively high symmetry of the layer and can be expected to possess a significantly lower net charge in the outer headgroup region than the bilayer composed of h-DPPS only in the outer leaflet.

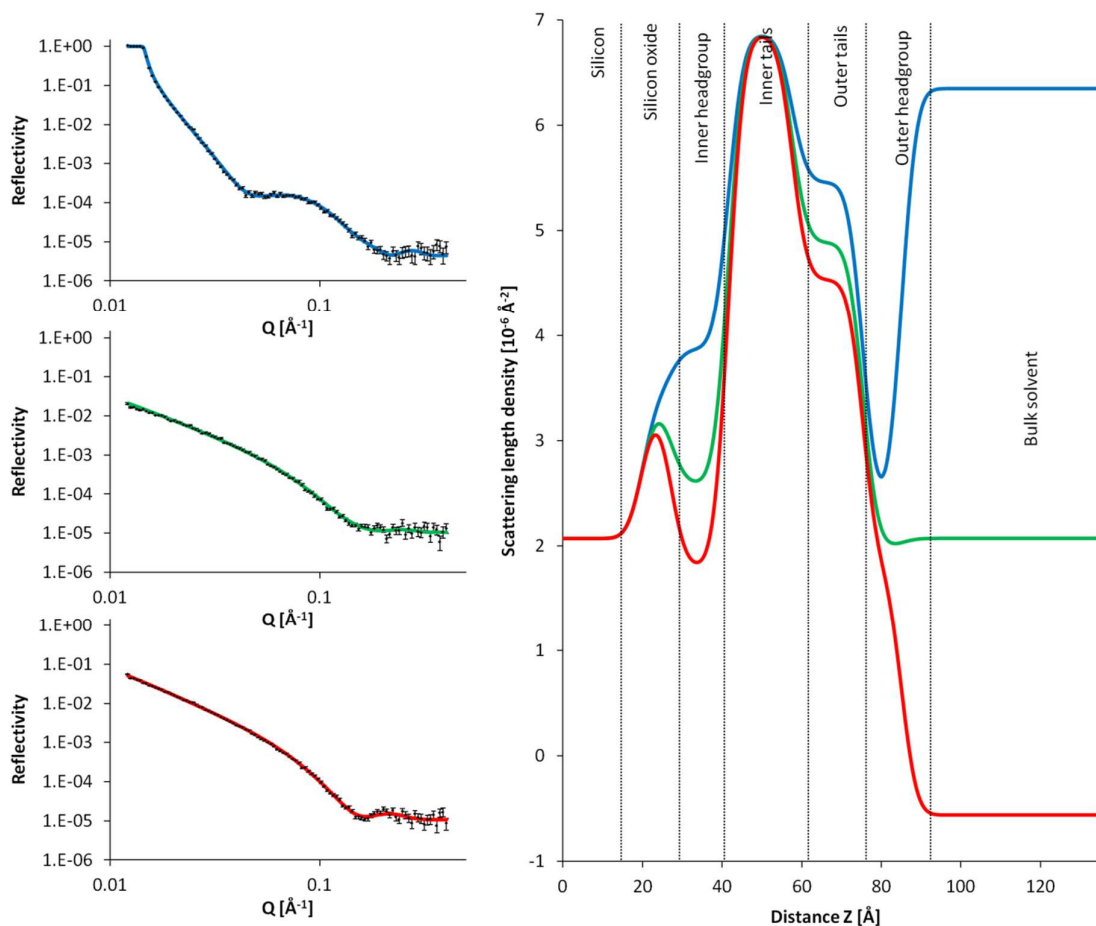


Figure 6.7 Neutron reflectivity profiles (left) and the fits describing these profiles (right) of the asymmetrically deposited d-DPPC:(h-DPPS:d-DPPC 1:1 mol/mol) bilayer obtained in the three isotopic contrasts: 100% D₂O (blue line), silicon-SLD-matched water containing 38% D₂O (green line) and 100% H₂O (red line).

Table 6.4 Composition of the d-DPPC:(h-DPPS:d-DPPC 1:1 mol/mol) bilayer showing the mixing of the lipids between the two leaflets. The water content values do not take into account the hydration levels of the phospholipid headgroups.

Layer	Thickness [Å]	$\varphi_{\text{d-DPPC}}$	$\varphi_{\text{h-DPPS}}$	φ_{water}	Roughness [Å]
Layer 1: silicon oxide	7.001 ± 0.535	N.A.	N.A.	0.000 ± 0.023	3.000 ± 0.708
Layer 2: inner headgroup	14.632 ± 1.278	0.925 ± 0.023	0.075 ± 0.003	0.000 ± 0.023	3.000 ± 0.239
Layer 3: inner tails	15.987 ± 1.346				
Layer 4: outer tails	17.724 ± 1.497	0.631 ± 0.172	0.235 ± 0.176	0.134 ± 0.035	
Layer 5: outer headgroup	9.752 ± 1.235				

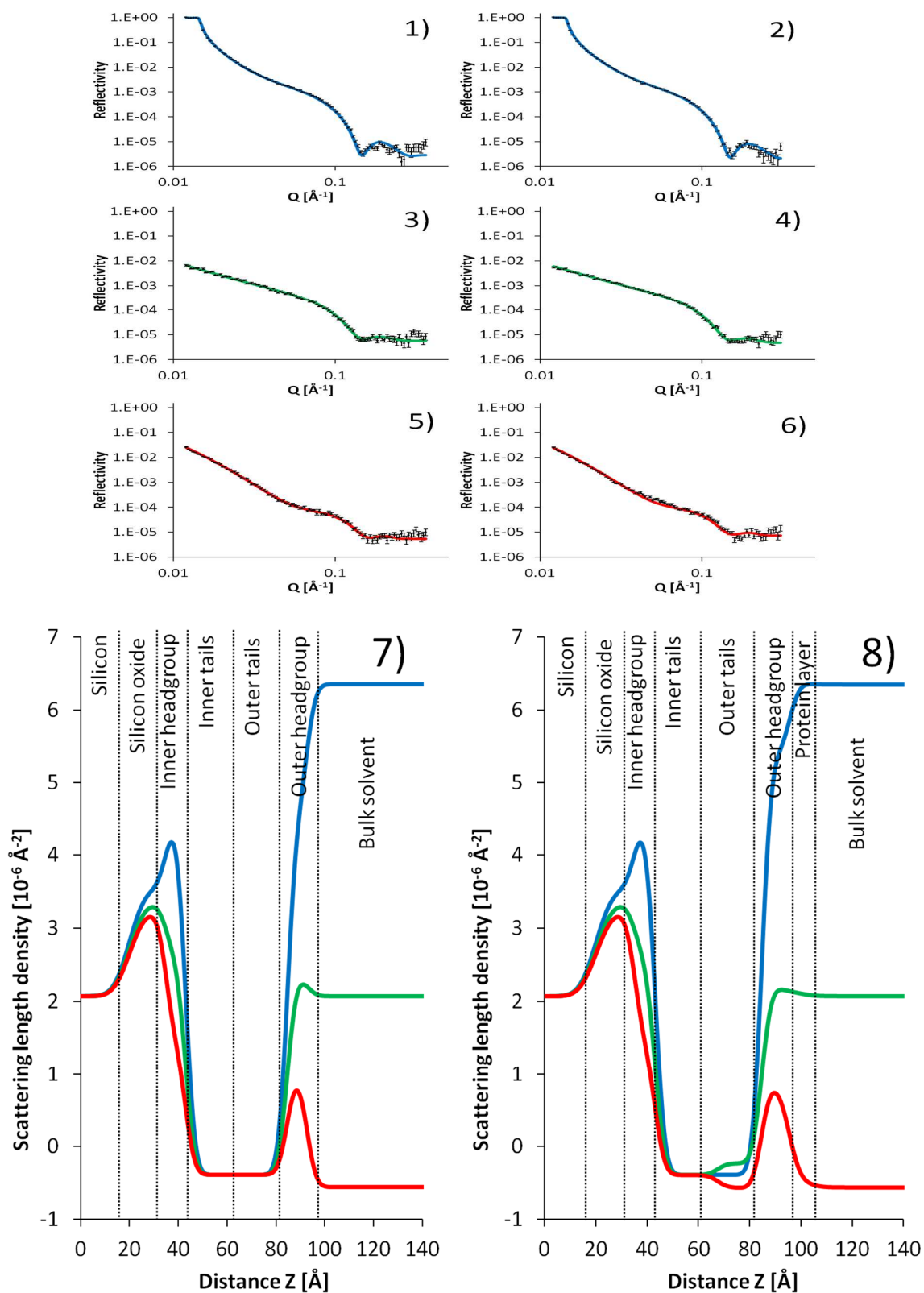


Figure 6.8 NR reflectivity profiles (1 – 6) and the fits describing these profiles (7 – 8) for the asymmetrically deposited h-DPPC:h-DPPS bilayer on its own (1,3,5,7) and interacting with 0.01 mg/mL β -Pth solution (2,4,6,8) obtained in the three isotopic contrasts: 100% D_2O (blue line), silicon-SLD-matched water containing 38% D_2O (green line) and 100% H_2O (red line).

As a consequence, the adsorbed protein layer turned out to be more dilute and thinner than the one described for the previous systems (see Figure 6.8 and Table 6.5). The experiment also revealed slight protein penetration to the outer headgroup region with the minimal increase in the water content of the outer tails layer (see Table 6.6).

Table 6.5 Results of the NR experiment on 0.01 mg/mL β -Pth interacting with the h-DPPC:(h-DPPS:h-DPPC 1:1 mol/mol) lipid bilayer. The SLD values with no uncertainties were kept constant throughout the process of data fitting.

Layer	Contrast	Thickness [Å]	SLD [10^{-6}Å^{-2}]	ϕ_{lipid}	ϕ_{protein}	ϕ_{water}	$A_{\text{lipid}} [\text{Å}^2]$	$\Gamma_{\text{lipid}} [\text{mg m}^{-2}]$	$A_{\text{protein}} [\text{Å}^2]$	$\Gamma_{\text{protein}} [\text{mg m}^{-2}]$	Roughness [Å]
Layer 1: silicon oxide	N.A.	15.080 \pm 2.083	3.410	N.A.		0.044 \pm 0.043	N.A.			5.096 \pm 0.255	
Layer 2: inner head- group	D ₂ O	8.000 \pm 2.010	3.060 \pm 0.406	0.552\pm0.093	0.000	0.448\pm0.093	77.553 \pm 23.459	0.666 \pm 0.201	0.000	0.000	3.000 \pm 0.005
	SMW										
	H ₂ O										
Layer 3: inner tails	D ₂ O	24.420 \pm 1.546	-0.390	1.000\pm0.000	0.000	0.000\pm0.000	33.275 \pm 2.106	2.112 \pm 0.134	0.000	0.000	
	SMW										
	H ₂ O										
Layer 4: outer tails	D ₂ O	17.187 \pm 1.598	-0.390 \pm 0.047	0.975\pm0.003	0.000\pm0.000	0.025\pm0.003	48.492 \pm 4.512	1.449 \pm 0.135	0.000 \pm 0.000	0.000 \pm 0.000	
	SMW		-0.231 \pm 0.046								
	H ₂ O		-0.560 \pm 0.001								
Layer 5: outer head- group	D ₂ O	8.000 \pm 0.008	5.471 \pm 0.995	0.475\pm0.001	0.049\pm0.000	0.475\pm0.001	78.878 \pm 0.183	0.656 \pm 0.002	15104.492 \pm 14.602	0.055 \pm 0.000	
	SMW		2.291 \pm 0.156								
	H ₂ O		1.129 \pm 0.689								
Layer 6: adsorbed protein	D ₂ O	2.950 \pm 8.605	3.448	N.A.	0.361\pm0.593	0.639\pm0.593	N.A.		5555.667 \pm 18594.227	0.149 \pm 0.499	7.000 \pm 0.600
	SMW		1.964								
	H ₂ O		1.714								

Table 6.6 Summary of the NR experiment on 0.01 mg/mL β -Pth interacting with the h-DPPC:(h-DPPS:h-DPPC 1:1 mol/mol) lipid bilayer.

Layer	ϕ_{lipid}	ϕ_{protein}	ϕ_{water}
Outer tails before protein	1.000 \pm 0.000	0.000	0.000 \pm 0.000
Outer tails with protein	0.975 \pm 0.003	0.000 \pm 0.000	0.025 \pm 0.003
Outer headgroup before protein	0.500 \pm 0.012	0.000	0.500 \pm 0.012
Outer headgroup with the protein	0.475 \pm 0.001	0.049 \pm 0.000	0.475 \pm 0.001

All results confirm the tendencies described in Chapter 4 (see page 63) that there is a strong relationship between the intensity of the protein's interaction with the lipid and the net charge the protein faces when adsorbing.

6.5.2 β -Pth vs. Fatty Acid Chain Saturation-Varying Lipid Systems

Similarly to the monolayer experiments, the bilayer study also covered the effect of the lipid unsaturation on the interaction with the wheat defence proteins.

The measurements were carried out using a reflectometer Inter at ISIS Neutron and Muon Spallation Source (Harwell, UK). Due to the relatively quick data collection on this instrument, it was possible to monitor the changes in the reflectivity profiles of the D₂O contrast directly after protein introduction (see Figures 6.10 and 6.12).

The analysed bilayers were composed of either d-DPPC or h-DPPC deposited on the inner leaflet of the bilayer and h-POPS or the equimolar mixture of h-DPPC and h-POPS providing the half-anionic and half-saturated properties of the lipid system in the outer leaflet.

The concentrations of the proteins were 0.01 mg/mL for the systems with h-POPS on the outer leaflet and 0.02 mg/mL for the systems with an equimolar mixture of DPPC and POPS in the outer leaflet (introduced due to no interaction observed for 0.01 mg/mL protein concentration).

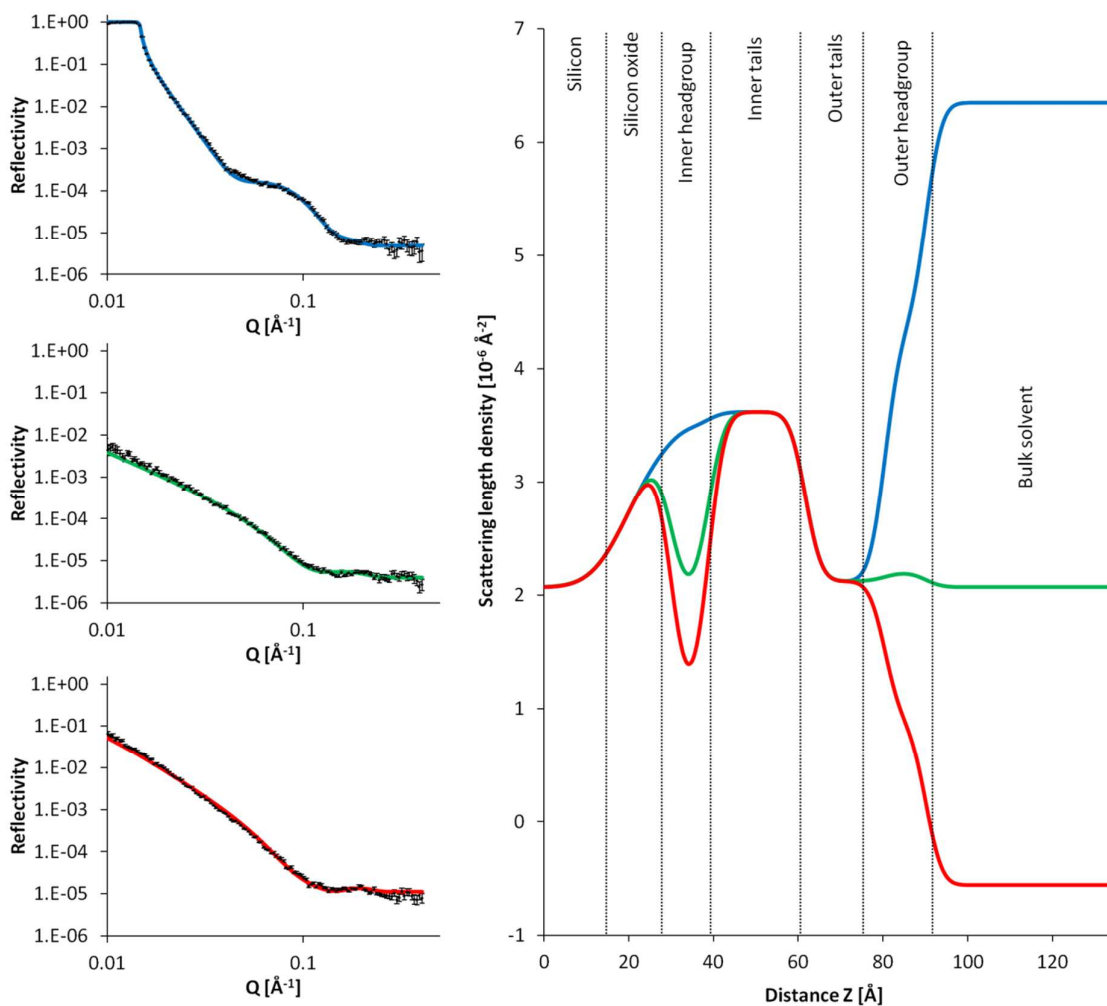


Figure 6.9 Neutron reflectivity profiles (left) and the fits describing these profiles (right) of the asymmetrically deposited d-DPPC:h-POPS bilayer obtained in the three isotopic contrasts: 100% D₂O (blue line), silicon-SLD-matched water containing 38% D₂O (green line) and 100% H₂O (red line).

Table 6.7 Composition of the d-DPPC:h-POPS bilayer showing the mixing of the lipids between the two leaflets. The water content values do not take into account the hydration levels of the phospholipid headgroups.

Layer	Thickness [Å]	$\varphi_{\text{d-DPPC}}$	$\varphi_{\text{h-POPS}}$	φ_{water}	Roughness [Å]
Layer 1: silicon oxide	9.872 ± 0.642	N.A.	N.A.	0.000 ± 0.000	7.000 ± 0.003
Layer 2: inner headgroup	8.978 ± 0.842	0.509 ± 0.006	0.491 ± 0.006	0.000 ± 0.000	3.000 ± 0.128
Layer 3: inner tails	22.822 ± 1.329				
Layer 4: outer tails	18.823 ± 1.507	0.316 ± 0.014	0.684 ± 0.014	0.000 ± 0.000	
Layer 5: outer headgroup	9.628 ± 1.441				

The d-DPPC: h-POPS bilayer turned out to be fairly symmetric, showing a smooth fringe in the D₂O contrast's reflectivity profile, as illustrated in Figure 6.9. Particularly high symmetry was noticed in the inner tails region and the water content was very low, which indicated the good coverage of the block with the lipids.

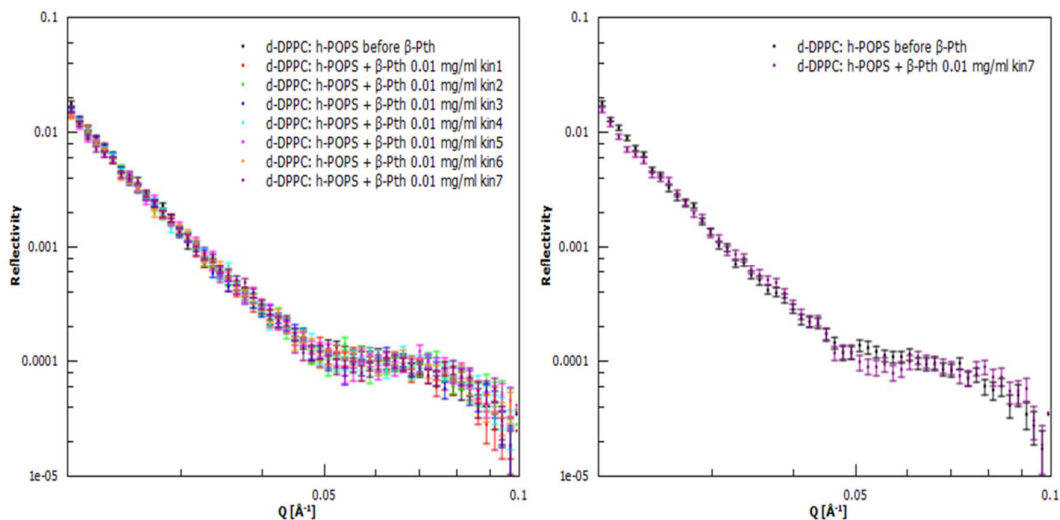


Figure 6.10 NR profiles of the d-DPPC:h-POPS bilayer recorded immediately after the protein injection (left) and the summary of the changes in the profile (right) showing the kinetics of the protein's interaction with the bilayer.

There was a noticeable change in the reflectivity profile upon the protein adsorption, yet it cannot be described as a particularly big one (see Figure 6.10).

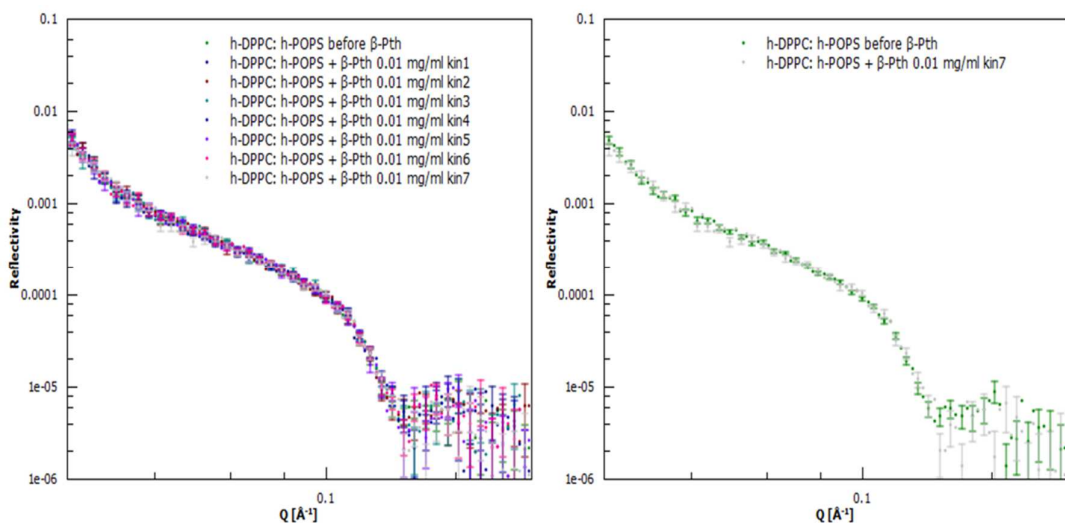


Figure 6.11 NR profiles of the h-DPPC:h-POPS bilayer recorded immediately after the protein injection (left) and the summary of the changes in the profile (right) showing the kinetics of the protein's interaction with the bilayer.

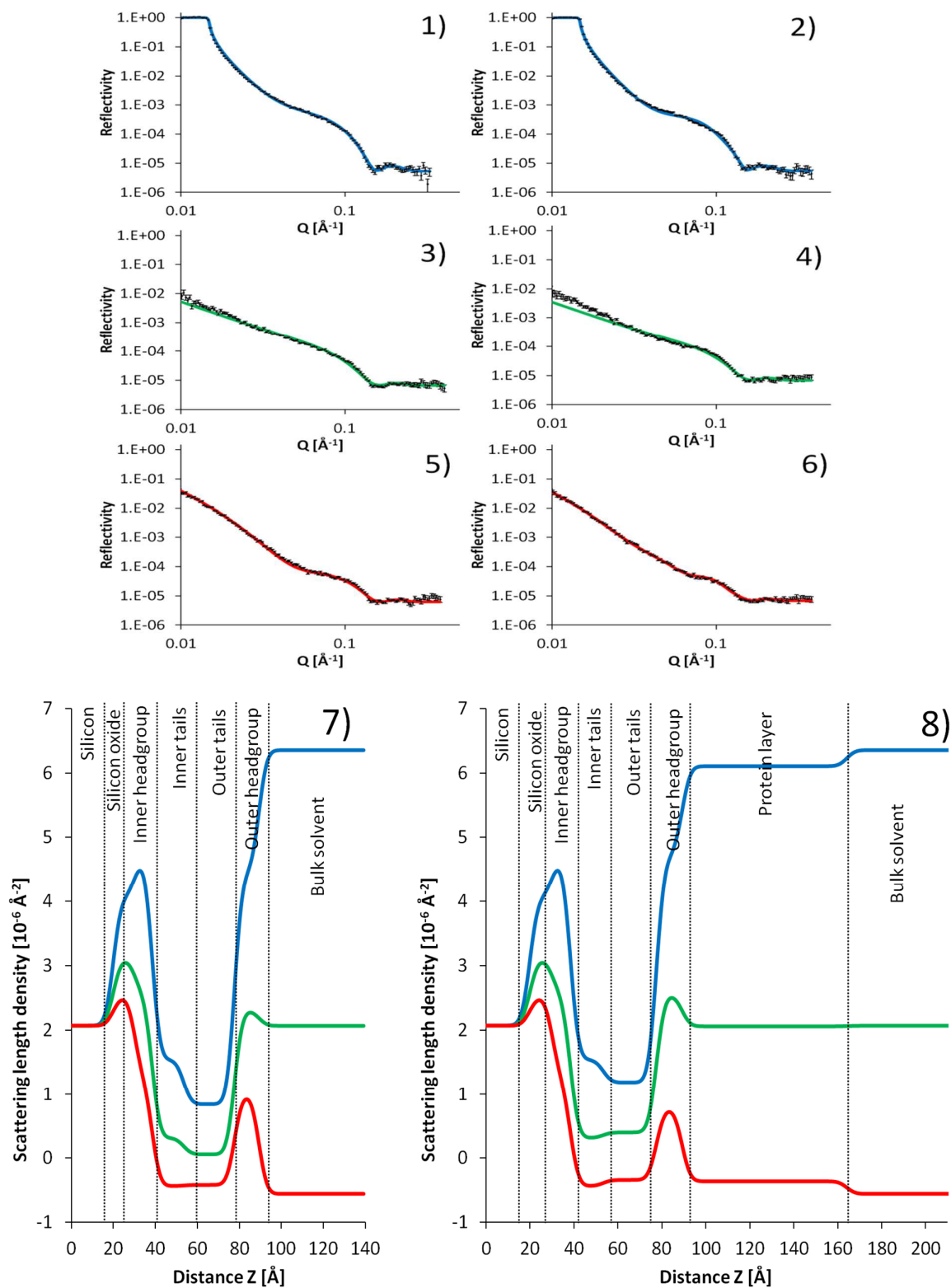


Figure 6.12 NR reflectivity profiles (1 – 6) and the fits describing these profiles (7 – 8) for the asymmetrically deposited h-DPPC:h-POPS bilayer on its own (1,3,5,7) and interacting with 0.01 mg/mL β -Pth solution (2,4,6,8) obtained in the three isotopic contrasts: 100% D_2O (blue line), silicon-SLD-matched water containing 38% D_2O (green line) and 100% H_2O (red line).

The hydrogenated lipid bilayer did not show any dramatic changes in the D₂O contrast in the kinetic studies (see Figure 6.11).

The reflectivity profile obtained for the protein-adsorbed bilayer in the silicon-scattering-length-density-matched contrast (SMW) showed slightly higher values at the low momentum transfer (see plot 4, Figure 6.12), which could possibly be due to the too fast data collection range without the full exchange of the D₂O buffer as this fragment of the profile was obtained as first. This imperfection has appeared occasionally in the other studies carried out on the lipid bilayers using Inter.

However, as the fitted SLDs obtained for the SMW contrast were not directly involved in the quantification of the bilayer's components, these fitting deviations did not affect the numerical results of the NR experiments.

The protein that adsorbed to the h-DPPC: h-POPS bilayer formed a thick, diluted layer (see Figure 6.12), yet no penetration was observed in both outer headgroup and outer tails regions (see Table 6.9). Outer headgroup's water content was slightly increased, suggesting the looser packing of the lipid molecules caused by the interaction.

Table 6.8 Results of the NR experiment on 0.01 mg/mL β -Pth interacting with the h-DPPC:h-POPS lipid bilayer. The SLD values with no uncertainties were kept constant throughout the process of data fitting.

Layer	Contrast	Thickness [\AA]	SLD [10^{-6}\AA^{-2}]	ϕ_{lipid}	ϕ_{protein}	ϕ_{water}	$A_{\text{lipid}} [\text{\AA}^2]$	$\Gamma_{\text{lipid}} [\text{mg m}^{-2}]$	$A_{\text{protein}} [\text{\AA}^2]$	$\Gamma_{\text{protein}} [\text{mg m}^{-2}]$	Roughness [\AA]
Layer 1: silicon oxide	N.A.	10.314 ± 1.487	3.410	N.A.		0.222 ± 0.050	N.A.			3.000 ± 0.031	
Layer 2: inner head- group	D ₂ O	8.127 ± 1.694	3.060 ± 0.030	0.500 ± 0.003	0.000	0.500 ± 0.003	84.265 ± 17.571	0.613 ± 0.128	0.000	0.000	
	SMW										
	H ₂ O										
Layer 3: inner tails	D ₂ O	15.000 ± 0.406	-0.390 ± 0.014	0.714 ± 0.039	0.000	0.286 ± 0.039	75.872 ± 4.635	0.926 ± 0.057	0.000	0.000	
	SMW										
	H ₂ O										
Layer 4: outer tails	D ₂ O	24.176 ± 0.970	1.184 ± 0.105	0.779 ± 0.033	0.000 ± 0.000	0.221 ± 0.033	41.055 ± 2.395	1.816 ± 0.106	0.000 ± 0.000	0.000 ± 0.000	
	SMW		-0.390 ± 0.045								
	H ₂ O		-0.343 ± 0.027								
Layer 5: outer head- group	D ₂ O	11.640 ± 0.767	4.710 ± 0.292	0.431 ± 0.046	0.000 ± 0.000	0.569 ± 0.046	54.896 ± 6.885	0.944 ± 0.118	0.000 ± 0.000	0.000 ± 0.000	
	SMW		2.916 ± 0.135								
	H ₂ O		0.776 ± 0.071								
Layer 6: adsorbed protein	D ₂ O	75.000 ± 3.158	3.448	N.A.	0.085 ± 0.012	0.915 ± 0.012	N.A.		926.707 ± 138.393	0.894 ± 0.134	3.000 ± 0.637
	SMW		1.964								
	H ₂ O		1.714								

Table 6.9 Summary of the NR experiment on 0.01 mg/mL β -Pth interacting with the h-DPPC:h-POPS lipid bilayer.

Layer	ϕ_{lipid}	ϕ_{protein}	ϕ_{water}
Outer tails before protein	0.818 \pm 0.011	0.000	0.182 \pm 0.011
Outer tails with protein	0.779 \pm 0.033	0.000 \pm 0.000	0.221 \pm 0.033
Outer headgroup before protein	0.500 \pm 0.028	0.000	0.500 \pm 0.028
Outer headgroup with the protein	0.431 \pm 0.046	0.000 \pm 0.000	0.569 \pm 0.046

Reducing the fluidity by half produced a much more symmetric bilayer (see Figure 6.13 and Table 6.10).

Reducing the net negative charge in the outer leaflet by half did not cause any significant changes in the direct interaction with the protein, *i.e.* there was no protein insertion observed in any part of the bilayer (see Tables 6.11 and 6.12), yet the adsorbed protein layers had their thicknesses reduced with the slight increase in the protein fraction in these layers (see Tables 5.20 and 5.22).

This could indicate the initial strong attraction of the protein that rapidly decreased leaving the very thin protein film on top of the bilayer, suggesting the overall weaker protein attraction as compared to the result obtained for the fully anionic outer leaflet system due to the fact that twice as much protein was used for the experiments on the half-saturated systems.

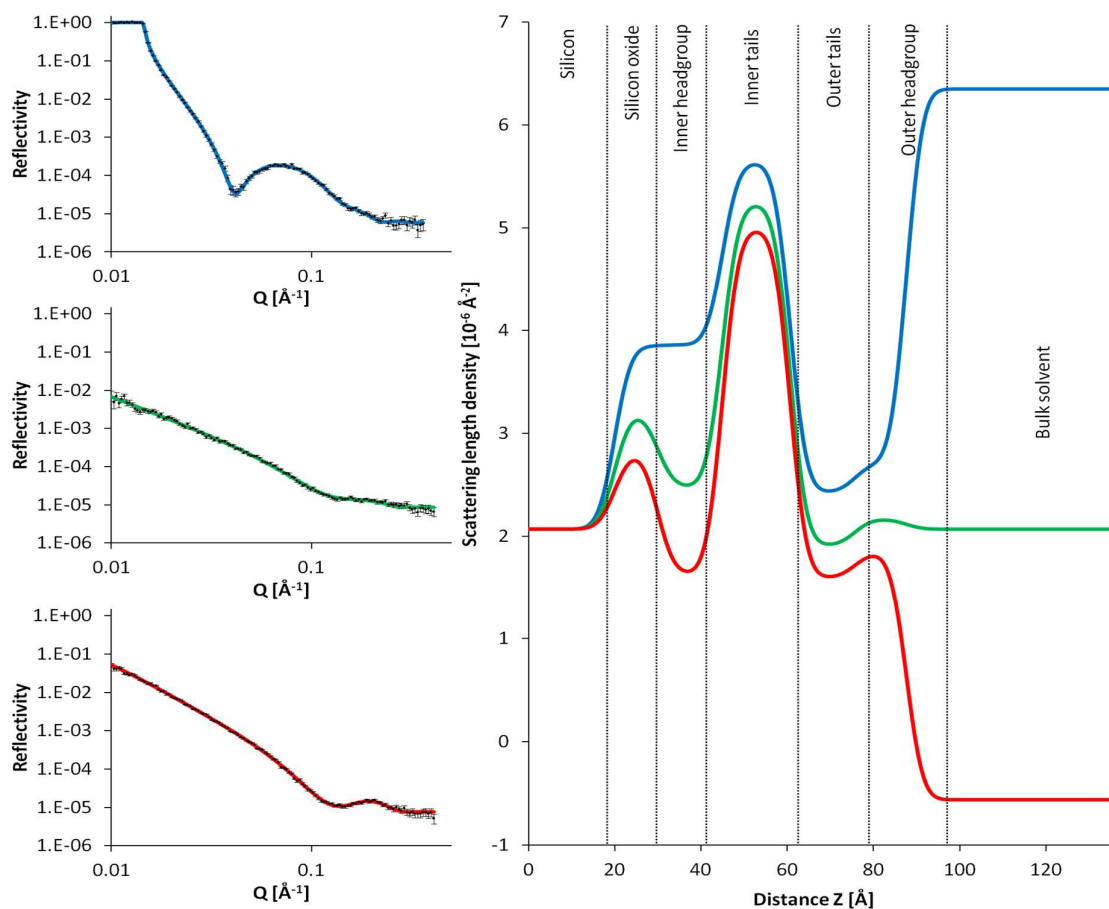


Figure 6.13 Neutron reflectivity profiles (left) and the fits describing these profiles (right) of the asymmetrically deposited d-DPPC:(h-DPPC:h-POPS 1:1 mol/mol) bilayer obtained in the three isotopic contrasts: 100% D₂O (blue line), silicon-SLD-matched water containing 38% D₂O (green line) and 100% H₂O (red line).

Table 6.10 Composition of the d-DPPC:(h-DPPC:h-POPS 1:1 mol/mol) bilayer showing the mixing of the lipids between the two leaflets. The water content values do not take into account the hydration levels of the phospholipid headgroups.

Layer	Thickness [Å]	$\varphi_{\text{d-DPPC}}$	$\varphi_{\text{h-DPPC:POPS 1:1}}$	φ_{water}	Roughness [Å]
Layer 1: silicon oxide	10.000 ± 0.176	N.A.	N.A.	0.148 ± 0.039	3.000 ± 1.255
Layer 2: inner headgroup	15.000 ± 0.248	0.687 ± 0.089	0.219 ± 0.082	0.094 ± 0.035	3.000 ± 0.415
Layer 3: inner tails	15.740 ± 0.829				
Layer 4: outer tails	15.000 ± 0.685	0.254 ± 0.135	0.626 ± 0.149	0.120 ± 0.062	
Layer 5: outer headgroup	11.953 ± 1.191				

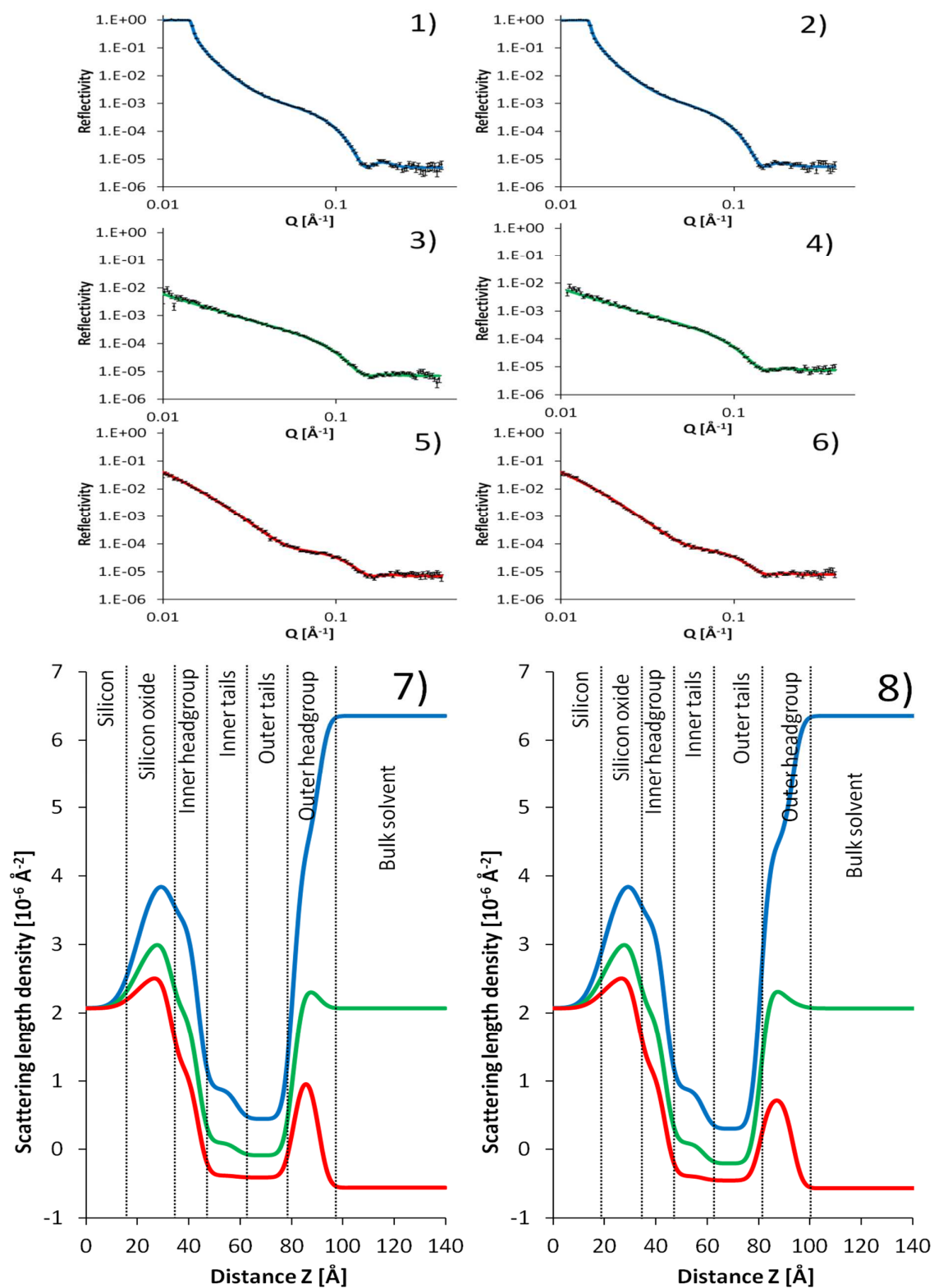


Figure 6.14 NR reflectivity profiles (1 – 6) and the fits describing these profiles (7 – 8) for the asymmetrically deposited h-DPPC:(h-DPPC:h-POPS 1:1 mol/mol) bilayer on its own (1,3,5,7) and interacting with 0.02 mg/mL β -Pth solution (2,4,6,8) obtained in the three isotopic contrasts: 100% D_2O (blue line), silicon-SLD-matched water containing 38% D_2O (green line) and 100% H_2O (red line).

The bilayer's fluidity seemed to have reduced the protein's insertion to the bilayer, which is in a fairly good agreement with the lower values of the overall surface pressure rise obtained for the monolayer experiments when compared with the DPPS system (see Chapter 4, page 66).

The reduction in charge and fluidity by half in the outer leaflet and increasing the protein concentration twice did not introduce noticeable changes in the protein penetrating capabilities but has slightly changed the pattern of the protein adsorption to the bilayer.

Table 6.11 Results of the NR experiment on 0.02 mg/mL β -Pth interacting with the h-DPPC:(h-DPPC:h-POPS 1:1 mol/mol) lipid bilayer. The SLD values with no uncertainties were kept constant throughout the process of data fitting.

Layer	Contrast	Thickness [\AA]	SLD [10^{-6}\AA^{-2}]	ϕ_{lipid}	ϕ_{protein}	ϕ_{water}	A_{lipid} [\AA^2]	Γ_{lipid} [mg m^{-2}]	A_{protein} [\AA^2]	Γ_{protein} [mg m^{-2}]	Roughness [\AA]
Layer 1: silicon oxide	N.A.	13.125 ± 1.186	3.410	N.A.		0.205 ± 0.037	N.A.				5.832 ± 1.361
Layer 2: inner head- group	D ₂ O	10.463 ± 1.797	1.980 ± 0.389	0.684 ± 0.093	0.000	0.316 ± 0.093	47.875 ± 10.500	1.079 ± 0.237	0.000	0.000	3.000 ± 0.793
	SMW										
	H ₂ O										
Layer 3: inner tails	D ₂ O	15.000 ± 1.358	-0.343 ± 0.027	0.818 ± 0.076	0.000	0.182 ± 0.076	66.251 ± 8.612	1.061 ± 0.138	0.000	0.000	
	SMW										
	H ₂ O										
Layer 4: outer tails	D ₂ O	22.233 ± 1.307	0.298 ± 0.049	0.892 ± 0.020	0.000 ± 0.000	0.108 ± 0.020	40.048 ± 2.520	1.808 ± 0.114	0.000 \pm 0.000	0.000 \pm 0.000	
	SMW		-0.200 ± 0.018								
	H ₂ O		-0.447 ± 0.037								
Layer 5: outer head- group	D ₂ O	9.864 ± 1.240	4.438 ± 0.521	0.466 ± 0.068	0.000 ± 0.000	0.534 ± 0.068	65.211 ± 12.558	0.793 ± 0.153	0.000 \pm 0.000	0.000 \pm 0.000	
	SMW		2.462 ± 0.078								
	H ₂ O		0.751 ± 0.343								
Layer 6: adsorbed protein	D ₂ O	2.620 ± 9.363	3.448	N.A.	0.607 ± 0.652	0.393 ± 0.652	N.A.	3725.126 \pm 13901.320	0.222 \pm 0.830	4.802 ± 2.388	
	SMW		1.964								
	H ₂ O		1.714								

Table 6.12 Summary of the NR experiment on 0.02 mg/mL β -Pth interacting with the h-DPPC:h-POPS lipid bilayer.

Layer	ϕ_{lipid}	ϕ_{protein}	ϕ_{water}
Outer tails before protein	0.877 \pm 0.034	0.000	0.123 \pm 0.034
Outer tails with protein	0.892 \pm 0.020	0.000 \pm 0.000	0.108 \pm 0.020
Outer headgroup before protein	0.517 \pm 0.050	0.000	0.483 \pm 0.050
Outer headgroup with the protein	0.466 \pm 0.068	0.000 \pm 0.000	0.534 \pm 0.068

6.5.3 β -Pth vs. Steroid-Containing Lipid Systems

Another tested parameter potentially affecting the interactions with the wheat defence proteins was the presence of the steroid in the membranes: the fungal steroid ergosterol formed half of the outer leaflet of the bilayer and the other half was h-DPPS. Therefore, the net charge of the outer leaflet's lipid mixture matched the half-anionic lipid systems used previously.

The experiments were carried out using instrument Inter at ISIS Neutron and Muon Spallation Source (Harwell, UK).

Table 6.13 Composition of the d-DPPC:(h-DPPS:ergosterol 1:1 mol/mol) bilayer showing the mixing of the lipids between the two leaflets. The water content values do not take into account the hydration levels of the phospholipid headgroups.

Layer	Thickness [\AA]	$\phi_{\text{d-DPPC}}$	$\phi_{\text{h-DPPS:ergosterol 1:1}}$	ϕ_{water}	Roughness [\AA]
Layer 1: silicon oxide	10.000 \pm 0.063	N.A.	N.A.	0.108 \pm 0.038	7.000 \pm 2.038
Layer 2: inner headgroup	10.824 \pm 0.725	0.602 \pm 0.343	0.369 \pm 0.342	0.028 \pm 0.026	3.000 \pm 0.113
Layer 3: inner tails	15.000 \pm 0.276				
Layer 4: outer tails	18.610 \pm 0.838	0.237 \pm 0.024	0.479 \pm 0.032	0.284 \pm 0.021	
Layer 5: outer headgroup	11.836 \pm 0.350				

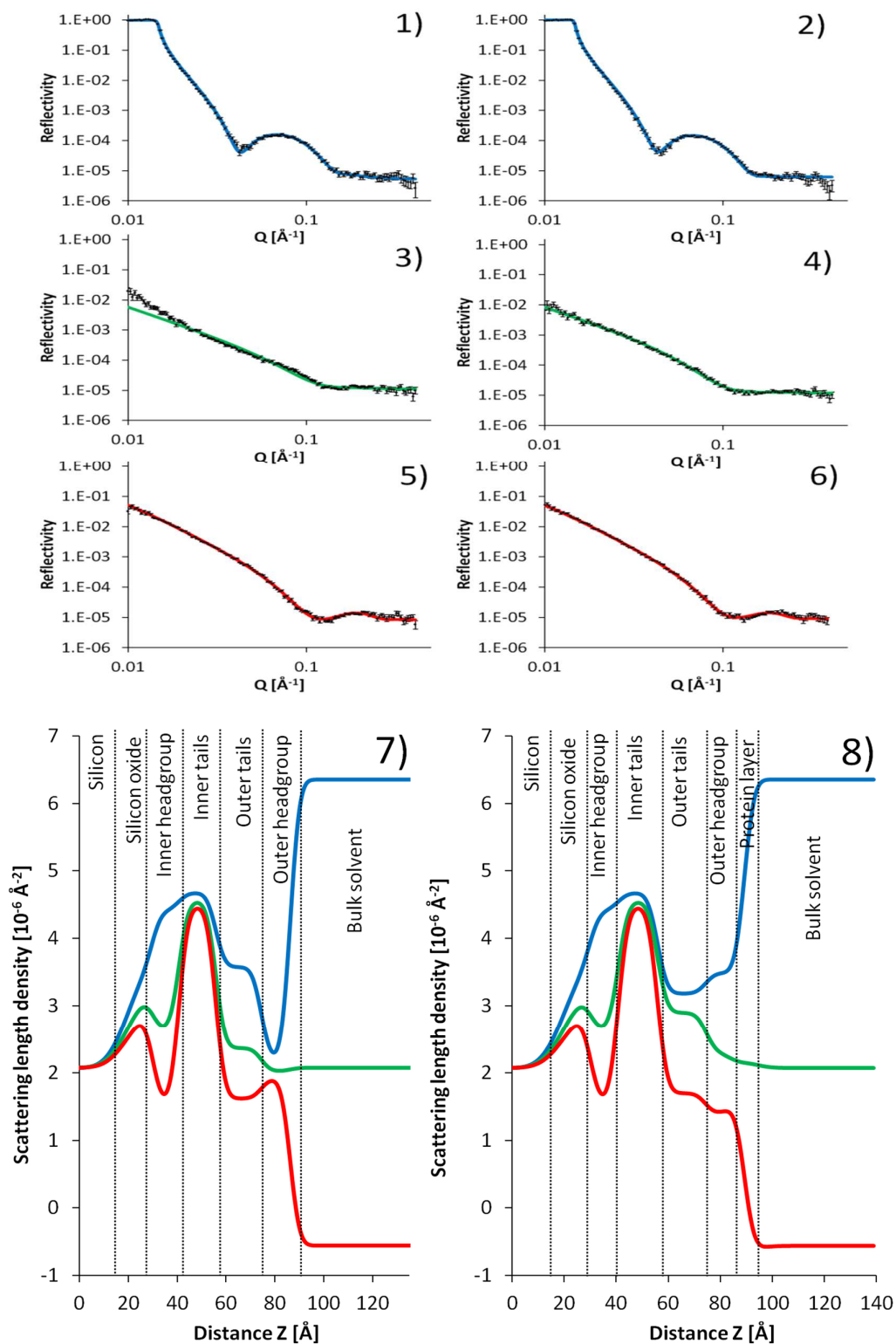


Figure 6.15 NR reflectivity profiles (1 – 6) and the fits describing these profiles (7 – 8) for the asymmetrically deposited d-DPPC:(h-DPPS:ergosterol 1:1 mol/mol) bilayer on its own (1,3,5,7) and interacting with 0.02 mg/mL β -Pth solution (2,4,6,8) obtained in the three isotopic contrasts: 100% D₂O (blue line), silicon-SLD-matched water containing 38% D₂O (green line) and 100% H₂O (red line).

The reflectivity studies on the obtained half-anionic, steroid containing lipid systems were carried out on the instrument Inter at ISIS Neutron and Muon Spallation Source. Due to the time restrictions, the data on the fully hydrogenated bilayer were not collected. The kinetics studies (analogous to the ones in Figures 6.10 and 6.11) did not reveal any noticeable changes in the reflectivity profile and were, therefore, not shown.

The obtained bilayer turned out to be fairly symmetric (see Table 6.13), as most bilayers that contained at least half of the outer leaflet occupied by the unsaturated lipid.

The changes in the reflectivity profiles were hardly noticeable when the protein's solution of the concentration 0.01 mg/mL was introduced (data not shown). Therefore, the concentration was doubled.

The adsorbed-protein layer was very thin and the protein did not reach any lipid layer (see: Tables 6.14 and 6.15). The presence of steroid did not show any impact on the interaction with the protein as the results resemble the ones obtained for the h-DPPC:(h-DPPC:h-POPS 1:1 mol/mol) bilayer.

Table 6.14 Summary of the NR experiment on 0.02 mg/mL β -Pth interacting with the d-DPPC:(h-DPPS:ergosterol 1:1 mol/mol) lipid bilayer.

Layer	ϕ_{lipid}	ϕ_{protein}	ϕ_{water}
Outer tails before protein	0.716 \pm 0.021	0.000	0.284 \pm 0.021
Outer tails with protein	0.785 \pm 0.011	0.000 \pm 0.000	0.215 \pm 0.011
Outer headgroup before protein	0.960 \pm 0.046	0.000	0.040 \pm 0.046
Outer headgroup with the protein	0.688 \pm 0.016	0.000 \pm 0.000	0.312 \pm 0.016

Table 6.15 Results of the NR experiment on 0.02 mg/mL β -Pth interacting with the d-DPPC:(h-DPPS: ergosterol 1:1 mol/mol) lipid bilayer. The SLD values with no uncertainties were kept constant throughout the process of data fitting.

Layer	Contrast	Thickness [Å]	SLD [10^{-6}Å^{-2}]	ϕ_{lipid}	ϕ_{protein}	ϕ_{water}	$A_{\text{lipid}} [\text{Å}^2]$	$\Gamma_{\text{lipid}} [\text{mg m}^{-2}]$	$A_{\text{protein}} [\text{Å}^2]$	$\Gamma_{\text{protein}} [\text{mg m}^{-2}]$	Roughness [Å]	
Layer 1: silicon oxide	N.A.	10.000±0.063	3.410	N.A.			0.108 ± 0.038			N.A.		7.000 ± 2.038
Layer 2: inner head- group	D ₂ O	10.824±0.725	3.060 ± 0.082	0.584 ± 0.051	0.000	0.416 ± 0.051	54.160 ± 5.948	0.954 ± 0.105	0.000	0.000	3.000 ± 0.113	
	SMW											
	H ₂ O											
Layer 3: inner tails	D ₂ O	15.000±0.276	4.625 ± 0.095	0.972 ± 0.026	0.000	0.028 ± 0.026	55.734 ± 1.823	1.446 ± 0.047	0.000	0.000		
	SMW											
	H ₂ O											
Layer 4: outer tails	D ₂ O	18.610±0.838	3.185 ± 0.090	0.785 ± 0.011	0.000 ± 0.000	0.215 ± 0.011	79.374 ± 3.742	1.015 ± 0.048	0.000 ± 0.000	0.000 ± 0.000		
	SMW		2.900 ± 0.043									
	H ₂ O		1.696 ± 0.068									
Layer 5: outer head- group	D ₂ O	11.836±0.350	3.500 ± 0.000	0.688 ± 0.016	0.000 ± 0.000	0.312 ± 0.016	33.819 ± 1.272	1.532 ± 0.058	0.000 ± 0.000	0.000 ± 0.000		
	SMW		2.355 ± 0.095									
	H ₂ O		1.345 ± 0.220									
Layer 6: adsorbed protein	D ₂ O	3.018 ± 0.907	3.448	N.A.	1.000 ± 0.001	0.000 ± 0.001	N.A.	1961.882 ± 589.543	0.422 ± 0.127	7.000 ± 1.375		
	SMW		1.964									
	H ₂ O		1.714									

6.5.4 Pin-a vs. Saturated Phospholipid Bilayers

The DPPC:DPPS lipid bilayers were shown to be strongly interacting with β -Pth (see: Section 6.5.1). Therefore, this system was used to assess the interactions of another wheat defence protein: Pin-a. The experiments were carried out using instrument Inter at ISIS Neutron and Muon Spallation Source (Harwell, UK).

The bilayer containing the deuterated lipid was highly asymmetric as illustrated in Figure 6.16 and Table 6.16. This is in good agreement with the results obtained for the identical bilayer in section 6.5.1.

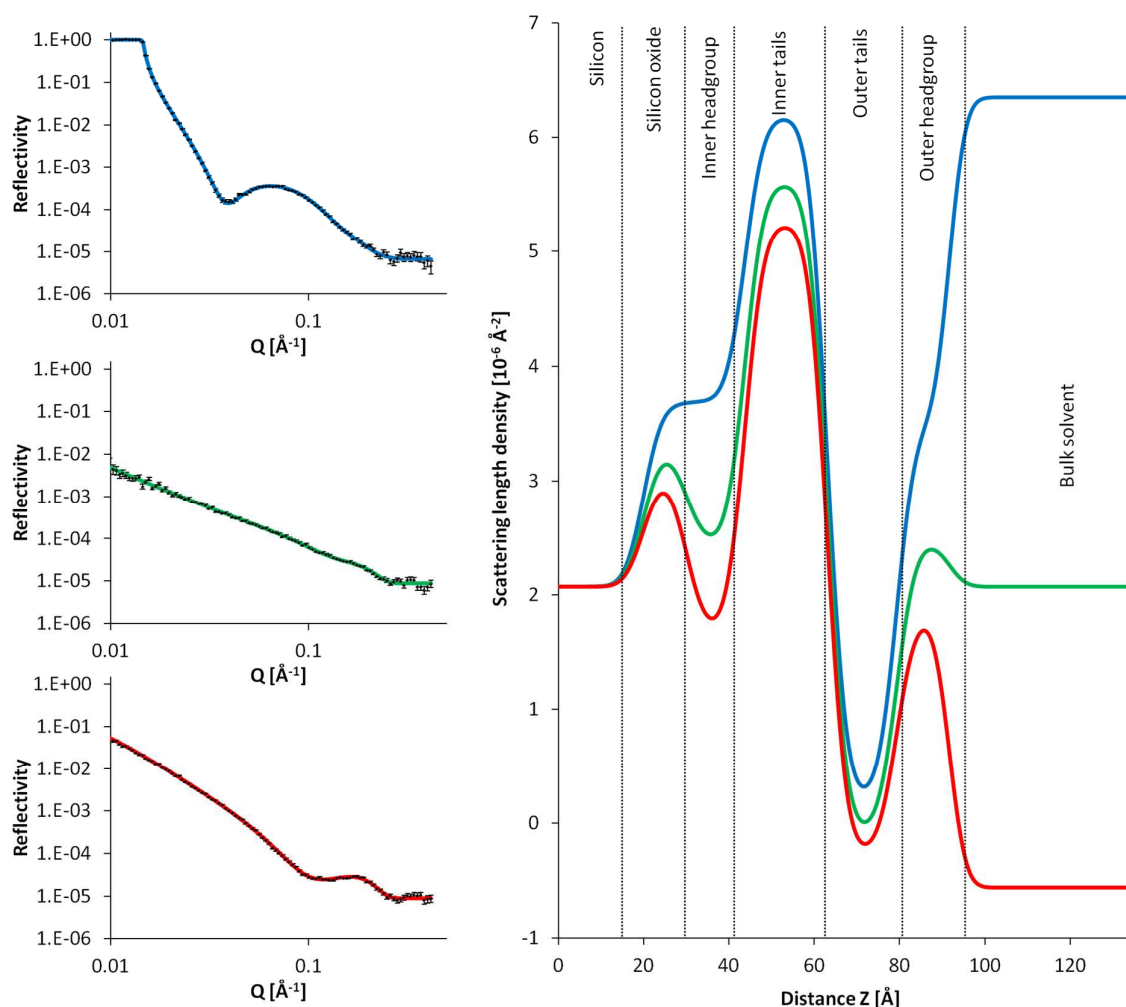


Figure 6.16 Neutron reflectivity profiles (left) and the fits describing these profiles (right) of the asymmetrically deposited d-DPPC:h-DPPS bilayer obtained in the three isotopic contrasts: 100% D_2O (blue line), silicon-SLD-matched water containing 38% D_2O (green line) and 100% H_2O (red line).

Table 6.16 Composition of the d-DPPC:h-DPPS bilayer showing the mixing of the lipids between the two leaflets. The water content values do not take into account the hydration levels of the phospholipid headgroups.

Layer	Thickness [Å]	ϕ_{d-DPPC}	ϕ_{h-DPPS}	ϕ_{water}	Roughness [Å]
Layer 1: silicon oxide	10.000 ± 0.529	N.A.	N.A.	0.087 ± 0.036	3.423 ± 0.841
Layer 2: inner headgroup	13.790 ± 0.923	0.720 ± 0.024	0.144 ± 0.018	0.136 ± 0.016	3.501 ± 0.390
Layer 3: inner tails	19.274 ± 1.226				
Layer 4: outer tails	16.263 ± 1.052	0.020 ± 0.018	0.912 ± 0.027	0.069 ± 0.020	
Layer 5: outer headgroup	12.359 ± 0.937				

No significant changes in the bilayer structure were detected upon the protein adsorption and the resulting protein layer, although thick, did not contain much protein (see Tables 5.28 and 5.30).

This conclusion is not in agreement with the corresponding monolayer studies, suggesting that β -Pth and Pin-a might have a different mode of the interaction with the anionic phospholipids.

One of the reasons behind the weak interaction of Pin-a is the tendency of the protein to adsorb to the solid interfaces, as observed by Clifton *et al.*⁹² and it can be speculated that the protein adhered to the walls and surface of the NR cell base.

Table 6.17 Summary of the NR experiment on 0.025 mg/mL Pin-a interacting with the h-DPPC:h-DPPS lipid bilayer.

Layer	ϕ_{lipid}	$\phi_{protein}$	ϕ_{water}
Outer tails before protein	0.955 ± 0.009	0.000	0.045 ± 0.009
Outer tails with protein	0.942 ± 0.015	0.000 ± 0.000	0.058 ± 0.015
Outer headgroup before protein	0.727 ± 0.045	0.000	0.273 ± 0.045
Outer headgroup with the protein	0.661 ± 0.015	0.000 ± 0.000	0.339 ± 0.015

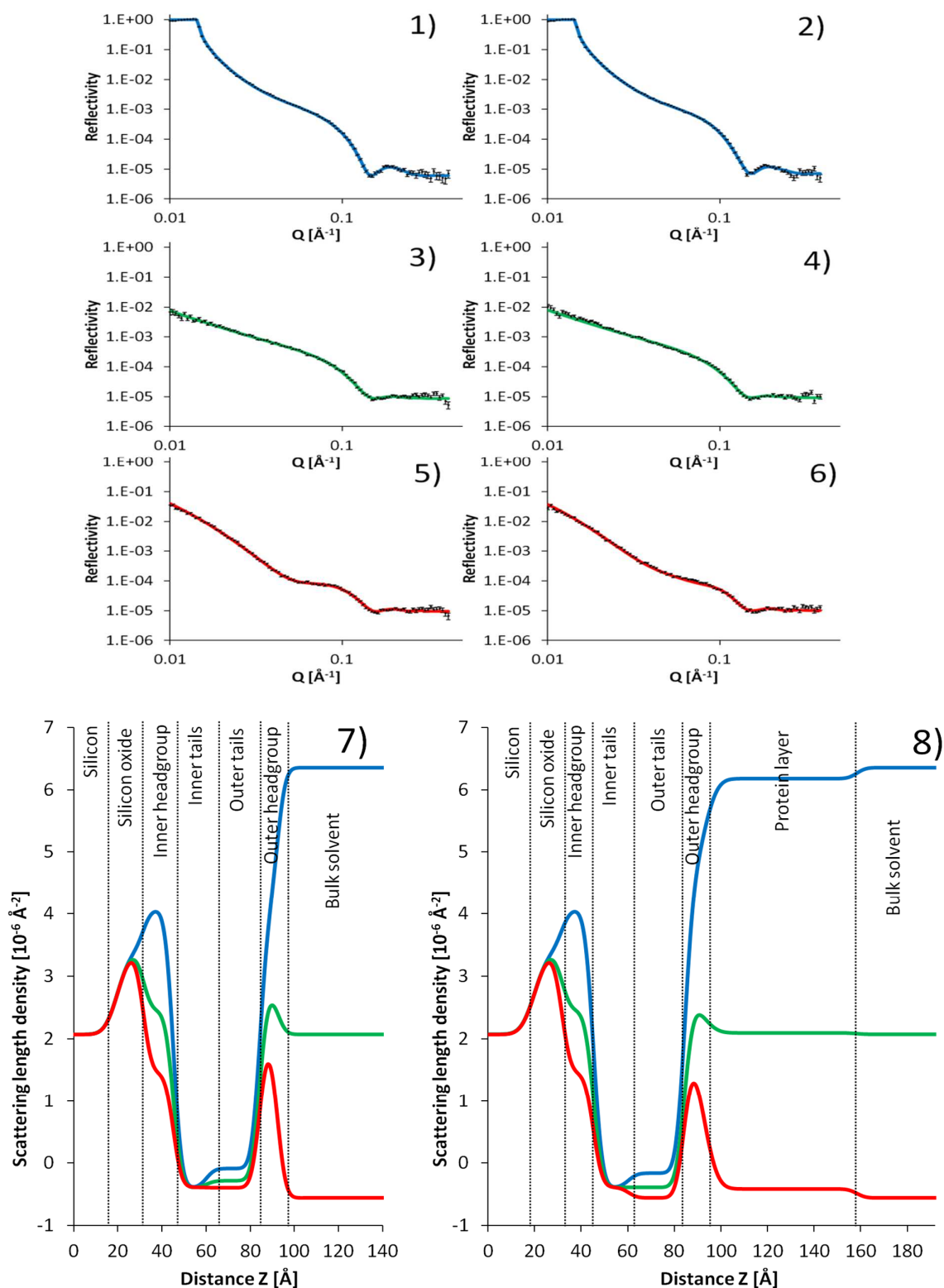


Figure 6.17 NR reflectivity profiles (1 – 6) and the fits describing these profiles (7 – 8) for the asymmetrically deposited h-DPPC:h-DPPS bilayer on its own (1,3,5,7) and interacting with 0.025 mg/mL Pin-a solution (2,4,6,8) obtained in the three isotopic contrasts: 100% D_2O (blue line), silicon-SLD-matched water containing 38% D_2O (green line) and 100% H_2O (red line).

Table 6.18 Results of the NR experiment on 0.025 mg/mL Pin-a interacting with the h-DPPC:h-DPPS lipid bilayer. The SLD values with no uncertainties were kept constant throughout the process of data fitting.

Layer	Contrast	Thickness [Å]	SLD [10^{-6}Å^{-2}]	ϕ_{lipid}	ϕ_{protein}	ϕ_{water}	$A_{\text{lipid}} [\text{Å}^2]$	$\Gamma_{\text{lipid}} [\text{mg m}^{-2}]$	$A_{\text{protein}} [\text{Å}^2]$	$\Gamma_{\text{protein}} [\text{mg m}^{-2}]$	Roughness [Å]
Layer 1: silicon oxide	N.A.	11.594 ± 0.217	3.410	N.A.		0.000±0.008	N.A.				4.655±0.769
Layer 2: inner head- group	D ₂ O	13.600 ± 0.870	2.676 ± 0.179	0.622±0.026	0.000	0.378±0.026	40.493±3.090	1.276±0.097	0.000	0.000	3.000±0.066
	SMW										
	H ₂ O										
Layer 3: inner tails	D ₂ O	15.082 ± 1.472	-0.390	1.000±0.020	0.000	0.000±0.020	53.879±5.363	1.304±0.130	0.000	0.000	3.000±0.066
	SMW										
	H ₂ O										
Layer 4: outer tails	D ₂ O	24.054 ± 1.402	-0.161 ± 0.041	0.942±0.015	0.000±0.000	0.058±0.015	35.863±2.166	1.959±0.118	0.000 ± 0.000	0.000± 0.000	3.000±0.066
	SMW		-0.390 ± 0.029								
	H ₂ O		-0.560 ± 0.001								
Layer 5: outer head- group	D ₂ O	8.000 ± 0.730	4.340 ± 0.193	0.661±0.015	0.000±0.000	0.339±0.015	52.080±4.895	0.995±0.094	0.000 ± 0.000	0.000± 0.000	3.000±0.066
	SMW		2.622 ± 0.147								
	H ₂ O		2.000 ± 0.119								
Layer 6: adsorbed protein	D ₂ O	66.010 ± 5.470	3.325	N.A.	0.058±0.009	0.942±0.009	N.A.	4065.165±734.294	0.534± 0.096	4.717±1.407	3.000±0.066
	SMW		2.447								
	H ₂ O		1.909								

6.5.5 β -Pth and Pin-a 1:1 mol/mol Mixture vs. Saturated Phospholipid Bilayers

The monolayer experiments on synergy between the wheat defence proteins revealed that there might be some cooperation in the antimicrobial mechanism of action between Pin-a and β -Pth (see Chapter 4, page 68).

This feature was examined by introducing an equimolar mixture of Pin-a and β -Pth (total final protein concentration 0.48 μ M) to the DPPC:DPPS bilayers. The experiments were carried out on Inter at ISIS Neutron and Muon Spallation Source (Harwell, UK).

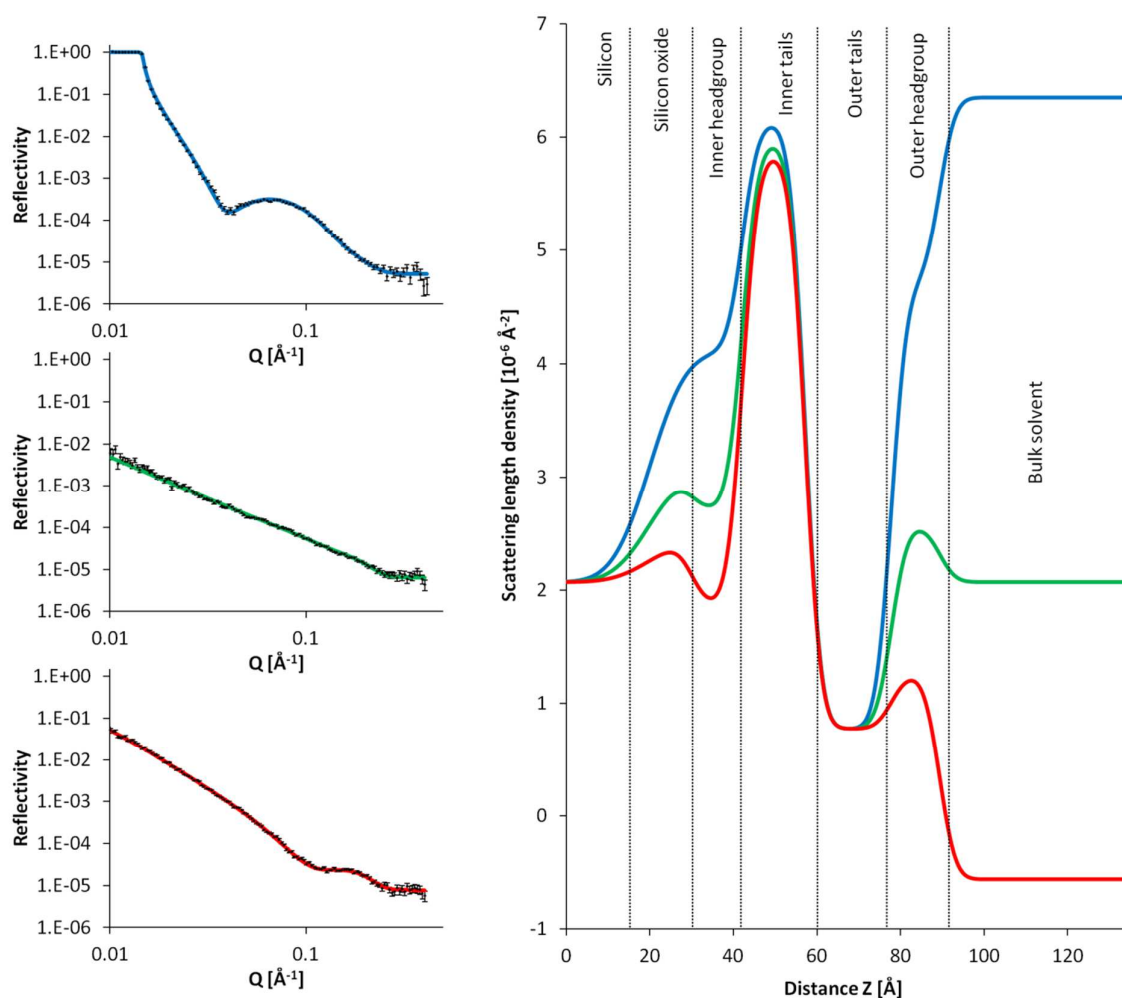


Figure 6.18 Neutron reflectivity profiles (left) and the fits describing these profiles (right) of the asymmetrically deposited d-DPPC:h-DPPS bilayer obtained in the three isotopic contrasts: 100% D_2O (blue line), silicon-SLD-matched water containing 38% D_2O (green line) and 100% H_2O (red line).

Table 6.19 Composition of the d-DPPC:h-DPPS bilayer showing the mixing of the lipids between the two leaflets. The water content values do not take into account the hydration levels of the phospholipid headgroups.

Layer	Thickness [Å]	ϕ_{d-DPPC}	ϕ_{h-DPPS}	ϕ_{water}	Roughness [Å]
Layer 1: silicon oxide	10.000 ± 0.434	N.A.	N.A.	0.242 ± 0.009	7.000 ± 0.367
Layer 2: inner headgroup	12.211 ± 0.516	0.795 ± 0.064	0.164 ± 0.062	0.041 ± 0.016	3.000 ± 0.035
Layer 3: inner tails	15.000 ± 0.167				
Layer 4: outer tails	20.644 ± 0.392	0.149 ± 0.011	0.851 ± 0.011	0.000 ± 0.002	
Layer 5: outer headgroup	11.503 ± 0.002				

The bilayer containing the deuterated lipid was highly asymmetric and did not contain much water, which indicates the high quality lipid bilayer with high level of coverage (see Table 5.32). This is well corresponding to the previous d-DPPC:h-DPPS bilayer structures (see Figures 6.5 and 6.16).

The fully hydrogenated bilayer revealed the proteins insertion to the outer headgroup to around a third of the layer's volume (see Tables 6.20 and 6.21). Moreover, a fairly thick protein layer was observed (see Table 6.21), indicating the relatively high adsorption to the bilayer. The result could not confirm the possible synergy between the Pin-a and β -Pth suggested in the monolayer studies (see Chapter 4, page 68). This could be due to the Pin-a's tendency to adhere to the surfaces of the NR cell and, therefore, not fully taking part in the adsorption to the lipid bilayer.

Table 6.20 Summary of the NR experiment on (Pin-a: β -Pth 1:1 mol:mol 0.0125:0.005 mg/mL) solution interacting with the h-DPPC:h-DPPS lipid bilayer.

Layer	ϕ_{lipid}	$\phi_{protein}$	ϕ_{water}
Outer tails before protein	0.981 ± 0.023	0.000	0.019 ± 0.023
Outer tails with protein	0.975 ± 0.000	0.000 ± 0.000	0.025 ± 0.000
Outer headgroup before protein	0.581 ± 0.043	0.000	0.419 ± 0.043
Outer headgroup with the protein	0.417 ± 0.010	0.284 ± 0.000	0.300 ± 0.010

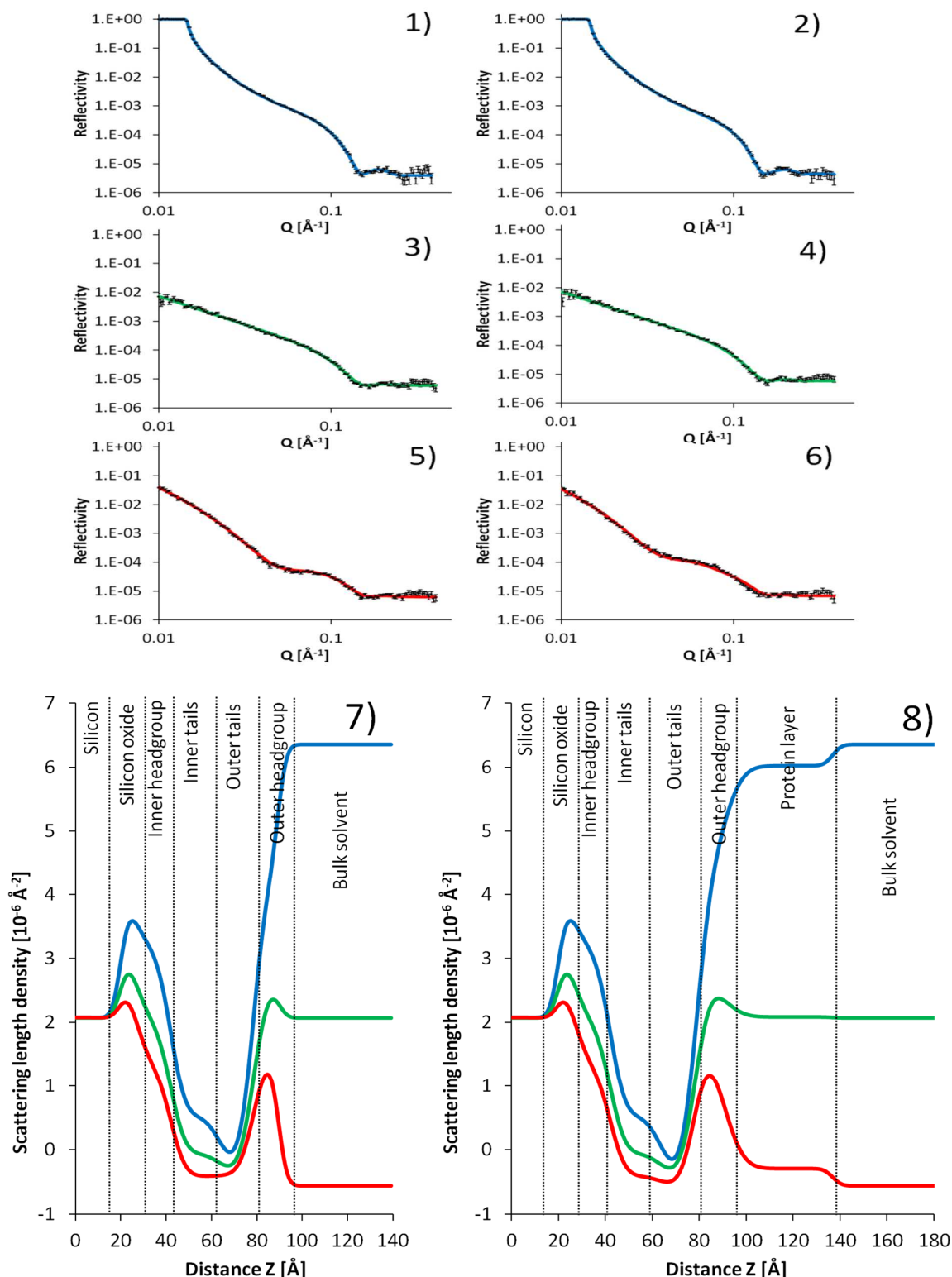


Figure 6.19 NR reflectivity profiles (1 – 6) and the fits describing these profiles (7 – 8) for the asymmetrically deposited h-DPPC:h-DPPS bilayer on its own (1,3,5,7) and interacting with (Pin-a: β -Pth 1:1 mol:mol 0.0125:0.005 mg/mL) solution (2,4,6,8) obtained in the three isotopic contrasts: 100% D_2O (blue line), silicon-SLD-matched water containing 38% D_2O (green line) and 100% H_2O (red line).

Table 6.21 Results of the NR experiment on (Pin-a:β-Pth 1:1 mol:mol 0.0125:0.005 mg/mL) solution interacting with the h-DPPC:h-DPPS lipid bilayer. The SLD values with no uncertainties were kept constant throughout the process of data fitting.

Layer	Contrast	Thickness [Å]	SLD [10^{-6}Å^{-2}]	ϕ_{lipid}	ϕ_{protein}	ϕ_{water}	$A_{\text{lipid}} [\text{Å}^2]$	$\Gamma_{\text{lipid}} [\text{mg m}^{-2}]$	$A_{\text{protein}} [\text{Å}^2]$	$\Gamma_{\text{protein}} [\text{mg m}^{-2}]$	Roughness [Å]
Layer 1: silicon oxide	N.A.	7.040 ± 0.491	3.410	N.A.		0.184±0.034	N.A.			3.000±0.204	
Layer 2: inner head- group	D ₂ O	15.000 ± 0.991	1.980 ± 0.012	0.733±0.015	0.000	0.267±0.015	31.124±2.149	1.660±0.115	0.000	0.000	3.000±0.056
	SMW										
	H ₂ O										
Layer 3: inner tails	D ₂ O	21.434 ± 0.532	-0.390	0.866±0.017	0.000	0.134±0.017	43.777±1.396	1.605±0.051	0.000	0.000	
	SMW										
	H ₂ O										
Layer 4: outer tails	D ₂ O	15.000 ± 0.399	-0.390 ± 0.000	0.975±0.000	0.000±0.000	0.025±0.000	55.562±1.476	1.265±0.034	0.000 ± 0.000	0.000±0.000	
	SMW		-0.390 ± 0.029								
	H ₂ O		-0.560 ± 0.000								
Layer 5: outer head- group	D ₂ O	10.892 ± 0.683	3.940 ± 0.188	0.417±0.010	0.284±0.000	0.300±0.010	60.635±4.069	0.855±0.057	3481.908±218.245	0.430±0.027	
	SMW		2.740 ± 0.084								
	H ₂ O		2.018 ± 0.121								
Layer 6: adsorbed protein	D ₂ O	47.496 ± 4.385	3.387	N.A.	0.112±0.012	0.888±0.012	N.A.	2021.503±279.890	0.741±0.103	7.000±0.000	
	SMW		2.206								
	H ₂ O		1.812								

6.6 Conclusions

Wheat defence protein adsorption to the model fungal bilayers and the structure of the lipid bilayers were studied by NR.

The lipid flipping between the bilayer leaflets in the deuterated lipid containing bilayers has been shown to be affected by the lipid composition, *i.e.* the higher bilayer asymmetry was observed for the fully saturated lipid systems, which could be due to the limited molecular movement arising from the tighter packing of the lipid molecules.

Assuming the similar lipid distribution for the fully hydrogenated lipid bilayers, it can be stated that the high asymmetry of the bilayer and, therefore, the high amount of negative charge in its outer leaflet, led to the stronger interaction with β -Pth. This result, together with the weaker protein adsorption to the lipid bilayers bearing more zwitterionic lipids, confirms the importance of the lipid charge in the protein-lipid interactions and is in good agreement with the findings from the monolayer studies (see Chapter 4, page 63).

The weaker adsorption of β -Pth to the POPS-containing bilayers could be explained by the presence of more zwitterionic lipids on the outer leaflet, following the assumption that the fully hydrogenated bilayers bear the similar lipid distribution to the bilayers containing the tail-deuterated analogues. The weakened attraction of the protein to the unsaturated phospholipid could be also caused by the fact that β -Pth showed slightly lower adsorptive properties towards the POPS in the monolayer studies (see Chapter 4, page 66).

The presence of the steroid in the bilayer did not result in strong interactions with the protein. However, as the experiment was carried out using the deuterated phospholipid system, the control experiments on the fully hydrogenated lipid bilayer would need to be carried out to increase the sensitivity of the lipid system to the changes in the SLD profile caused by the protein (see section 6.2, page 107).

To summarise, the study of the β -Pth adsorption to the lipid bilayers with varying lipid composition stressed the importance of the role of the lipid charge and lipid chain saturation in the protein-lipid interactions.

Table 6.22 contains all results of the NR experiments described in this chapter, pointing out the key features used to assess the strength of the protein interaction with the lipid bilayers, and thus the protein's potential level of antimicrobial action.

Table 6.22 Summary of the NR bilayer experiments showing the properties of the analysed lipid systems and the protein effect on their structure.

Lipid system	Properties of the lipids on the outer leaflet	Protein added and its concentration	Penetration to the outer headgroup (protein's volumetric fraction if applicable)	Penetration to the outer tails (protein's volumetric fraction if applicable)	Protein fraction in the protein layer and the protein layer's thickness [Å]
h-DPPC: h-DPPS	Anionic, saturated	β -Pth (0.01 mg/mL)	Yes (0.301 \pm 0.002)	No	0.327 \pm 0.017; 54.132 \pm 1.953
h-DPPC: (h-DPPS: h-DPPC 1:1 mol:mol)	Half anionic, saturated		Yes (0.049 \pm 0.000)	No	0.361 \pm 0.593; 2.950 \pm 8.605
h-DPPC: h-POPS	Anionic, unsaturated		No	No	0.085 \pm 0.012; 75.000 \pm 3.158
h-DPPC: (h-DPPC: POPS 1:1 mol:mol)	Half anionic, half saturated	β -Pth (0.02 mg/mL)	No	No	0.607 \pm 0.652; 2.620 \pm 9.363
d-DPPC: (h-DPPS: ergosterol 1:1 mol:mol)	Half anionic, steroid-containing		No	No	1.000 \pm 0.001; 3.018 \pm 0.907
h-DPPC: h-DPPS	Anionic, saturated	Pin-a (0.025 mg/mL)	No	No	0.058 \pm 0.009; 66.010 \pm 5.470
h-DPPC: h-DPPS	Anionic, saturated	Pin-a: β -Pth 1:1 mol:mol (0.0125:0.005 mg/mL)	Yes (0.284 \pm 0.000)	No	0.112 \pm 0.012; 47.496 \pm 4.385

The fully hydrogenated h-DPPC:h-DPPS bilayer has been also exposed to the other proteins to examine the role of the protein structure on the adsorption to the model fungal bilayer and, therefore, its antifungal mode of action.

There were some inconsistencies between the NR and ATR-FTIR results (see Chapter 5, page 101), *e.g.* the result for Pin-a, which could be explained by the high tendency of the protein to stick to many surfaces. However, in order to examine the cause of the disagreements between the results, the repeated experiments on the Pin-a interaction with the lipid bilayers are recommended in the future research (see Chapter 8, page 169).

Moreover, the results on the synergy between the Pin-a and β -Pth showed slightly weaker interaction than for the β -Pth on its own, which did not confirm the finding from the

monolayer studies (see Chapter 4, page 68). This could be due to the aforementioned adhesive properties of the Pin-a protein. Nevertheless, more repeats of the experiment would need to be carried out to test this hypothesis.

The good agreement between the NR and ATR-FTIR results was obtained for the β -Pth interaction with h-DPPC:h-DPPS bilayer. As mentioned before, the effect of the protein on the bilayer structure has been the most noticeable for this protein-lipid system.

It needs to be stressed, however, that nearly all protein-adsorbed bilayers produced very small changes in their reflectivity profiles. Therefore, the small changes in the calculated values *e.g.* volumetric fractions of water and lipid cannot be treated with high level of confidence.

The findings from the experiments described in this chapter allowed to confirm the strong dependence of the protein-lipid interactions on both model lipid composition and the type of protein / protein mixture. This is in good agreement with the conclusions from the monolayer experiments (see Chapter 4, page 81) and the results obtained by Sanders *et al.*⁵¹

To summarise, the use of bilayers as the tested systems requires the more complex preparation and analysis than the monolayer experiments, yet generates the more detailed, more informative results, better reflecting the real mechanisms of the antimicrobial action of the proteins.

Chapter 7

STUDIES ON LIPID VESICLES

7.1 Introduction

As shown in Chapters 5 and 6, lipid bilayers can serve as the models of natural lipid membranes. Flat bilayers deposited on the solid support are a better representations of the true membranes than the monolayer systems, yet they do not account for the natural membrane curvature. This feature can be examined in the studies involving lipid vesicles (liposomes). For more details on the types of vesicles and their structure, see Chapter 2, page 28.

Liposomes have been widely used to investigate the lipid interactions with various compounds by means of *e.g.* membrane leakage tests,¹⁶⁶ assessing the changes in the intrinsic protein fluorescence upon the interaction with vesicles,¹⁶⁷ isothermal titration calorimetry (ITC) experiments describing the thermodynamic parameters of the protein-lipid interaction,¹⁶⁸ and differential scanning calorimetry (DSC) indicating the changes in the thermal transitions of the lipid vesicles as a result of the protein interaction.¹⁶⁹

For example, Ravishankar *et al.*¹⁷⁰ studied the influence of the anticancer compounds on the DPPC Multilammellar Vesicles (MLVs) by DSC to reveal the membrane-penetrating properties of the synthetic flavonoid derivatives.

Moreover, Sanders¹³³ used DSC technique to examine the antibacterial properties of the Pin-b proteins by studying their influence on the Multilamellar Vesicles composed of DPPG, dipalmitoylphosphatidylethanolamine (DPPE) and DPPC. The findings stressed the influence of the phospholipid charge and the protein structure on the protein-lipid interactions.¹³³

This chapter aims to investigate the influence of the vesicles size and their composition on their interactions with wheat defence proteins. The experiments were carried out using Multilamellar Vesicles (MLVs) to reflect the microbial cell's size and Small Unilamellar Vesicles (SUVs) to provide more external charge on the membrane, a parameter shown to be crucial for the interactions (see Chapter 4, page 81).

7.2 Materials and Vesicles Preparation

Phospholipids and solvents used were the ones listed in Chapter 4, page 54. The vesicles solution were prepared following the protocol at the Avanti Polar Lipids website <https://avantilipids.com/tech-support/liposome-preparation/>. The choice of the lipids for the analysed liposome systems based on the membrane composition of the yeast *Saccharomyces cerevisiae* (see Chapter 1, page 11) and the findings from the monolayer studies (see Chapter 4, page 81).

The lipid solutions (1 g/L) were prepared as described in Chapter 4 (see page 55). The solvent was removed on the rotary evaporator Rotavapor R-215 obtained from BÜCHI (Flavil, Switzerland). The obtained lipid cake was hydrated with phosphate buffer pH 7 to the lipid concentration of 1 g/L. To create MLVs, the resulting lipid dispersion underwent five freeze-thawing cycles using dry ice and water bath. This ensured the good mixing of the lipids and creation of multiple layers. The SUVs were obtained by sonicating the hydrated lipid film for 2 h at the temperature above the melting point of the used lipid/lipid mixture.¹¹⁴

Protein solutions were prepared in phosphate buffer pH 7 as described previously (see Chapter 4, page 55).

7.3 Dynamic Light Scattering (DLS) Measurements

For quality control purposes, the vesicles solutions had their average sizes assessed by means of the Dynamic Light Scattering (DLS) technique. DLS is based on measuring the intensity of the scattered light from the moving particles in the analysed suspension. Knowing the analyte's viscosity and the refractive index, one can obtain the size distribution of the particles in the analysed sample.¹⁷¹ The DLS measurements enabled to determine the size distribution of the particles in the vesicles solution and were used for this purpose only.

The measurements were carried out using a ZetaSizer Nano (obtained from Malvern Instruments, Malvern, UK) equipped with a 5003 multi-digital autocorrelator. The linearly polarised light of the 633 nm wavelength, produced by a He-Ne laser, was scattered at the angle $\theta = 173^\circ$. For each measurement, 1 mL of the vesicles solution was pipetted into a

polystyrene cuvette and the sample was placed in the instrument's sample chamber for the light intensity readings at 25°C.

7.4 Differential Scanning Calorimetry (DSC) Experiments

Differential Scanning Calorimetry analyses the changes in the substance's thermal transitions, thereby informing about the compound's stability or its interaction with other compounds. More details on the principles of this technique can be found in Chapter 2, page 29.

The technique served as a tool to estimate the interaction between the compounds in various experiments: dendrimers,¹⁷² drugs such as tamixofen,¹⁷³ cyclic peptides such as gramicidin S¹⁷⁴ and cyclodextrins¹⁷⁵ interacting with membrane vesicles. It was also used for studying the wheat defence protein interactions with the bacterial cell membranes.¹³³ The most frequent two modes of the DSC experiments studying the protein-lipid interactions are: creating the vesicles with the proteins embedded in the membranes or mixing the pre-prepared vesicles solution with the protein solution. This study examines the protein antimicrobial action *in vitro*, therefore the second approach was chosen for carrying out the DSC experiments.

Each analysed sample contained 0.2 mg lipid and the appropriate amount of protein solution was added to reach the proper lipid-protein molar ratios (listed further in each section). The protein-lipid mixture was topped up with phosphate buffer to the final volume of 0.75 mL and shaken well to mix. The sample was then degassed under vacuum for 15 minutes, vortexed and inserted into the DSC calorimeter's sample cell.

The measurements were carried out using a Nano DSC calorimeter obtained from TA Instruments (Borehamwood, UK) in a heating mode between 20°C and 80°C at the rate 1°C/min using pure phosphate buffer pH 7 in the reference cell. Before each measurement, the purity of the cells was determined by scanning the blank sample containing phosphate buffer pH 7 and if there were no peaks detected (*i.e.* the sample cells were clean), the protein-lipid samples were analysed.

The peaks in all DSC thermograms point to the direction of the endothermic changes. The sample containing only the protein solution (0.2 mg of protein) was run as control experiment

and there was no peak present between 20°C and 120°C (data not shown). This result was expected due to the high thermal stability of the wheat defence proteins, resulting from the presence of the disulphide bridges in their structures (see Chapter 1, pages 5 and 18). Therefore, no peak in the DSC scans was assigned to the protein-only structure.

7.5 Results

7.5.1 Vesicles Size Determination by Dynamic Light Scattering (DLS)

Figure 7.1 shows the size distribution of the DPPC vesicles prepared by two different methods: the MLVs obtained after five freeze-thaw cycles (green peak) and the SUVs exposed to 2 h of sonication at 45°C (red peak). The MLVs diameters ranged from 2000 nm to 6000 nm, which is well corresponding to the average size of the baker's yeast *Saccharomyces cerevisiae* cell: 3-6 μm .¹⁷⁶ Therefore, the measurement justified the use of the DPPC MLVs as models of the fungal cell.

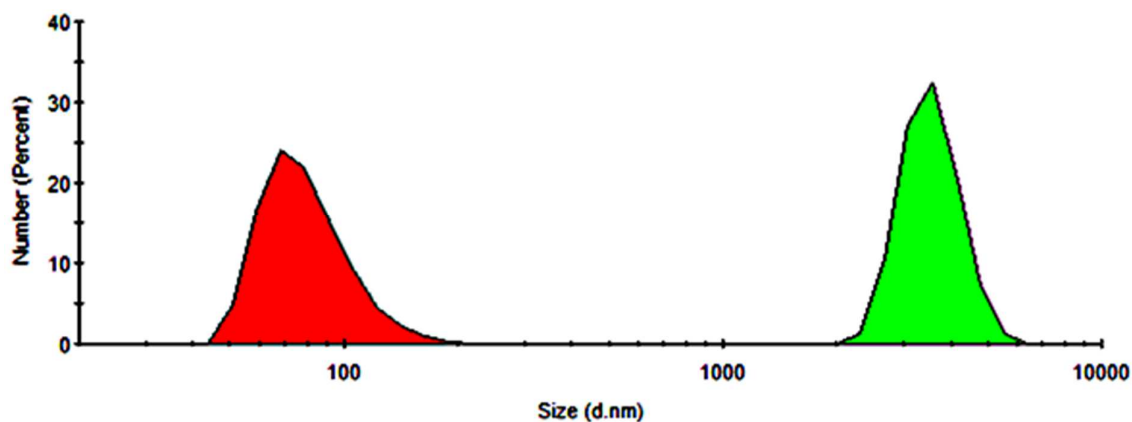


Figure 7.1 Size distribution by number of the DPPC vesicles: MLVs (green) obtained after five freeze-thawing cycles and SUVs (red) obtained after 2 hours of sonication at 45°C.

The vesicles became dramatically smaller, around ten-fold, after incubating them in the sonication bath above the lipid's melting point: $\sim 41^\circ\text{C}$.¹⁷⁷ The high mobility of the molecules and the external mechanical waves enabled the huge agglomerates of the lipids to significantly shrink in diameter (see red peak in Figure 7.1). The liposomes' sizes were then much closer to the diameter range typical of the Small Unilamellar Vesicles (SUVs): 25-100 nm (see Chapter 2, page 28). Therefore, more direct exposure of the protein to the charge is

expected in the Differential Scanning Calorimetry experiments involving SUVs than in the case of the MLVs studies.

7.5.2 Differential Scanning Calorimetry (DSC) Sample Preparation Development: Effect of the Sample Vortexing on the DSC Results

The effect of the sample homogenization technique on the produced DSC scans was assessed by comparing four samples:

1. shaken sample of the DPPS lipid
2. shaken sample DPPS lipid interacting with β -Pth at the lipid-molar ratio 10:1
3. vortexed sample of the DPPS lipid
4. vortexed sample DPPS lipid interacting with β -Pth at the lipid-molar ratio 10:1

The results are presented in Figure 7.2: the first three scans include the sharp peak at $\sim 54^\circ\text{C}$, which is the DPPS melting point.¹⁷⁷

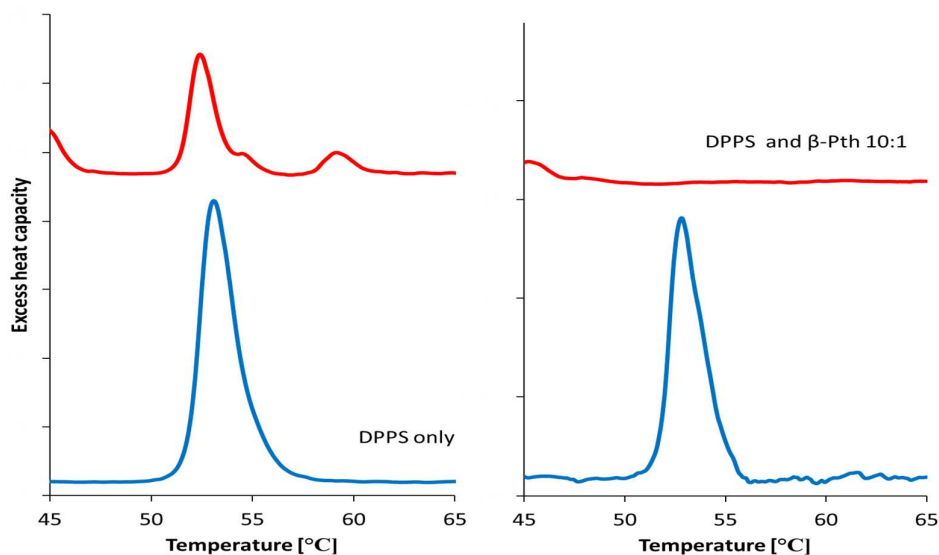


Figure 7.2 DSC measurements of β -Pth added to the DPPS MLVs in 1:10 protein:lipid molar ratio (red line) and of the DPPS MLVs on their own (blue line) without vortexing (left plot) and with vortexing (right plot).

The DPPS transitions remained unchanged for the lipid-only samples, suggesting that the vesicle structures did not undergo any solubilisation stage.

In contrast to the lipid-only samples, the peak disappeared in the vortexed lipid sample with β -Pth (Figure 7.2 red line, right plot). This indicates the complete destruction with possible solubilisation of the DPPS vesicles, *i.e.* there are not enough DPPS molecules present next to each other to produce the typical melting point signal.

The peak is still present in the analogous sample that underwent shaking only, indicating that some of the vesicles remained intact. However, the reduced size of the peak suggests that the significant portion of the vesicles was destroyed. The difference between the scans of the protein-including samples can be explained by the increased contact area between the protein and the vesicles, occurring as a consequence of the increased mechanical impact caused by vortexing. Therefore, to better depict the interaction of β -Pth with lipid vesicles, the next samples for the DSC experiments were prepared including the vortexing step.

7.5.3 Repeatability of the Measurements

To establish the reproducibility of the DSC experiments, the following measurements were carried out in triplicates. The lipid system consisting of the equimolar amounts of DPPC (zwitterionic lipid) and DPPS (anionic lipid) allowed to examine the effect of the lipid system's charge reduction by half on the interactions with β -Pth (also see the monolayer experiments, page 63).

The mixed lipid system displayed the intermediate phase change behaviour: there was one smooth transition at around 46.5°C (see Figure 7.3), which is nearly the middle value between the phase transition temperature values of the system components: DPPC (41°C)¹⁷⁷ and DPPS (54°C).¹⁷⁷ The smoothness of the transition, relative symmetry of the transition peak and the middle value of the melting point of the system's components indicate a high level of the lipids mixing in the vesicles and, therefore, the uniform charge distribution.

The splitting of the peak and rough transition, on the other hand, would be an indication of the lower degree of mixing and possible presence of the DPPC-only and DPPS-only islets / rafts in the liposomes' structure. Good mixing of the lipids allowed to better control the net charge value of the vesicles and, therefore, more reliable results of the experiments on the charge reduction effect on the interactions with β -Pth.

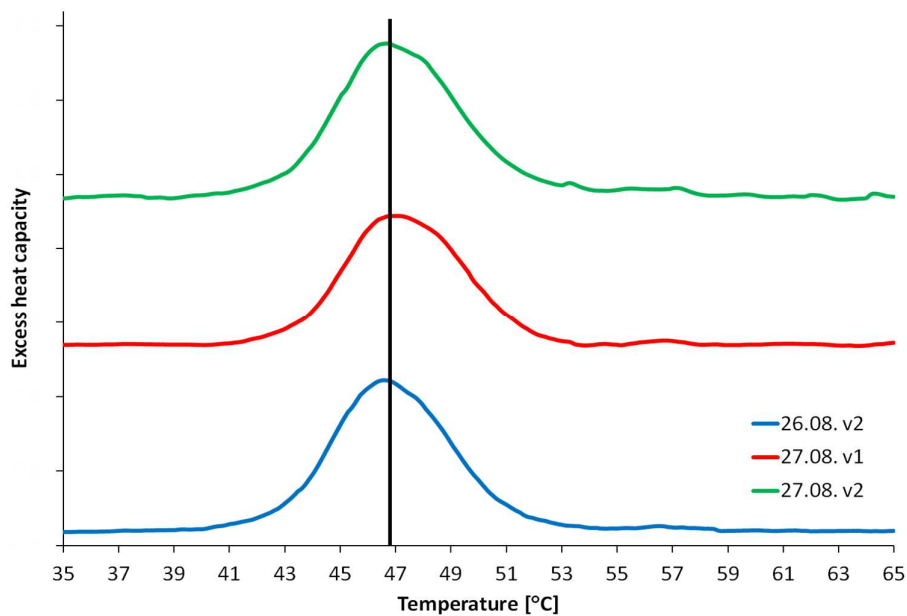


Figure 7.3 DSC measurements of the DPPC:DPPS 1:1 mol:mol MLVs. Dates and repeats of the experiments are shown in the legend.

Both lipid-only system (Figure 7.3) and the one interacting with the protein (Figure 7.4) showed the good repeatability of the readouts.

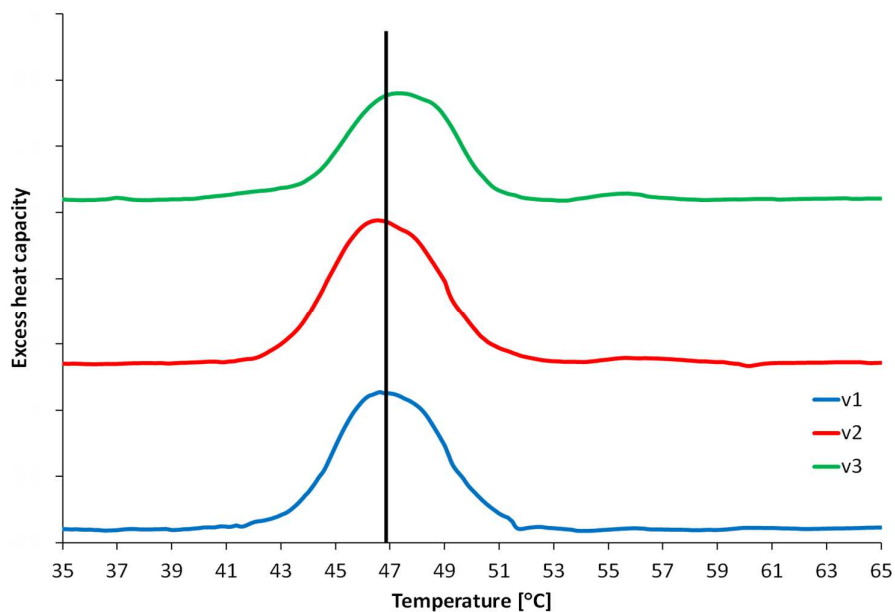


Figure 7.4 DSC measurements of β -Pth added to the DPPC:DPPS 1:1 mol:mol MLVs in 1:100 protein:lipid molar ratio. The numbers of repeats are shown in the legend.

The experiments with the protein were carried out on the same day whereas the lipid-only readouts were obtained for the freshly prepared vesicles (Figure 7.4 blue line) and after overnight incubation at -20°C (Figure 7.4 green and red line).

Short storage of the vesicles in the freezer did not affect the lipid transition, which suggests the relatively high stability of the liposome solutions. It can be also noted that adding β -Pth to the DPPC:DPPS 1:1 mol:mol lipid vesicles at the 1:100 protein:lipid molar ratio did not result in significant changes to the lipid system. The effect of this protein on the mixed lipid system at various protein:lipid proportions is described in detail in Section 7.5.5.

7.5.4 β -Pth vs. DPPC and the Effect of the Lipid Batch on the DSC Profile

The effect on the DPPC lipid batch on the DSC profile was examined by creating the DPPC MLVs from two different batches of the lipid. Batch nr 1 (showed in Figure 7.5 blue line) showed a smooth transition with no significant pre-transition peak.

Batch 2 of the DPPC vesicles, on the other hand, produced a much sharper transition with a pre-transition peak at around 36.5°C (see: Figure 7.6 blue line), similar to the one in the study by Ali *et al.*¹⁷⁸

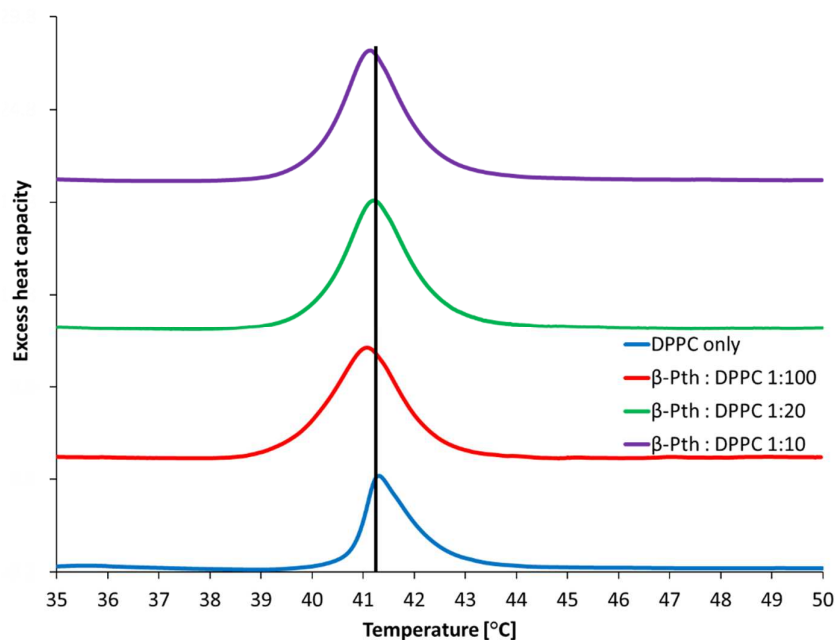


Figure 7.5 DSC measurements of β -Pth added to the DPPC MLVs (batch 1) in various molar ratios.

It also showed the main transition starting around 39°C. Despite the clear differences in the transition kinetics, both batches produced the main transition peak with the maximum around 41°C, characteristic of the DPPC lipid.¹⁷⁷

The DPPC liposomes produced from both batches did not interact strongly with β -Pth. Increase of the protein concentration did not result in any significant changes in the liposomes' structure, *i.e.* the peak's intensity stayed roughly the same and the peaks became more symmetric, suggesting the more ordered transition, possibly driven by the initial weak electrostatic interaction with the protein. This interaction, however, did not lead to the destruction of the vesicles' structure as seen in the case of the DPPS liposomes (see Figure 7.2).

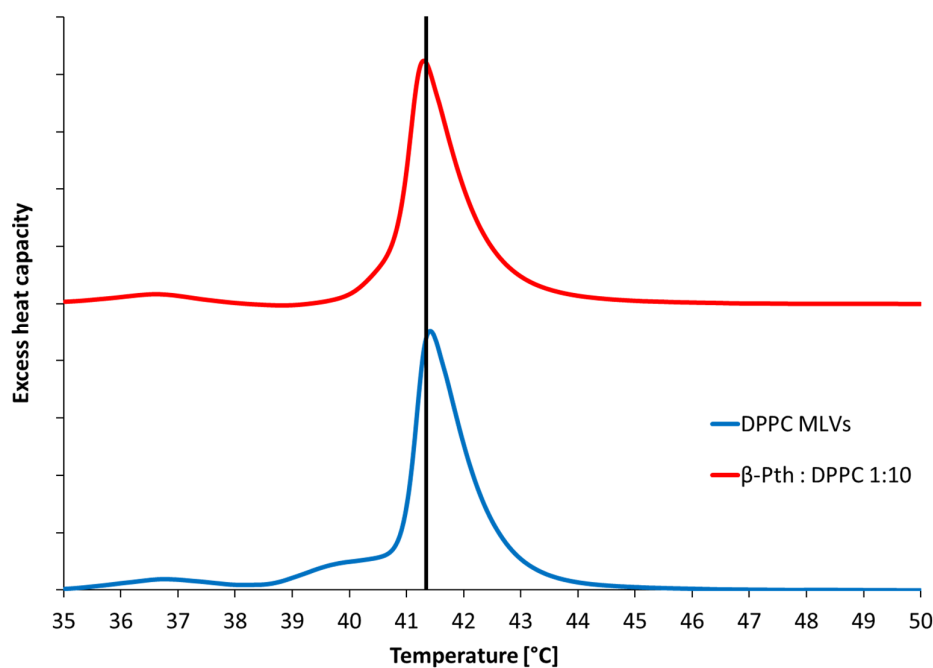


Figure 7.6 DSC measurements of β -Pth added to the DPPC MLVs (batch 2) in 1:10 protein:lipid molar ratio.

Repeatability of the DSC profiles between the batches was not as pronounced as in case of the repeats obtained from the same vesicles solution but the results of the protein interaction with both batches allow to draw the same conclusion: no significant shift or decrease in the peak area indicating very weak effect of the protein on the DPPC vesicles.

7.5.5 β -Pth vs. Vesicle Systems with Varying Net Charge

It has been shown in previous sections that β -Pth interacts stronger with the anionic DPPS system than with the DPPC one, which is in agreement with the findings from the monolayer experiments (see page 63).

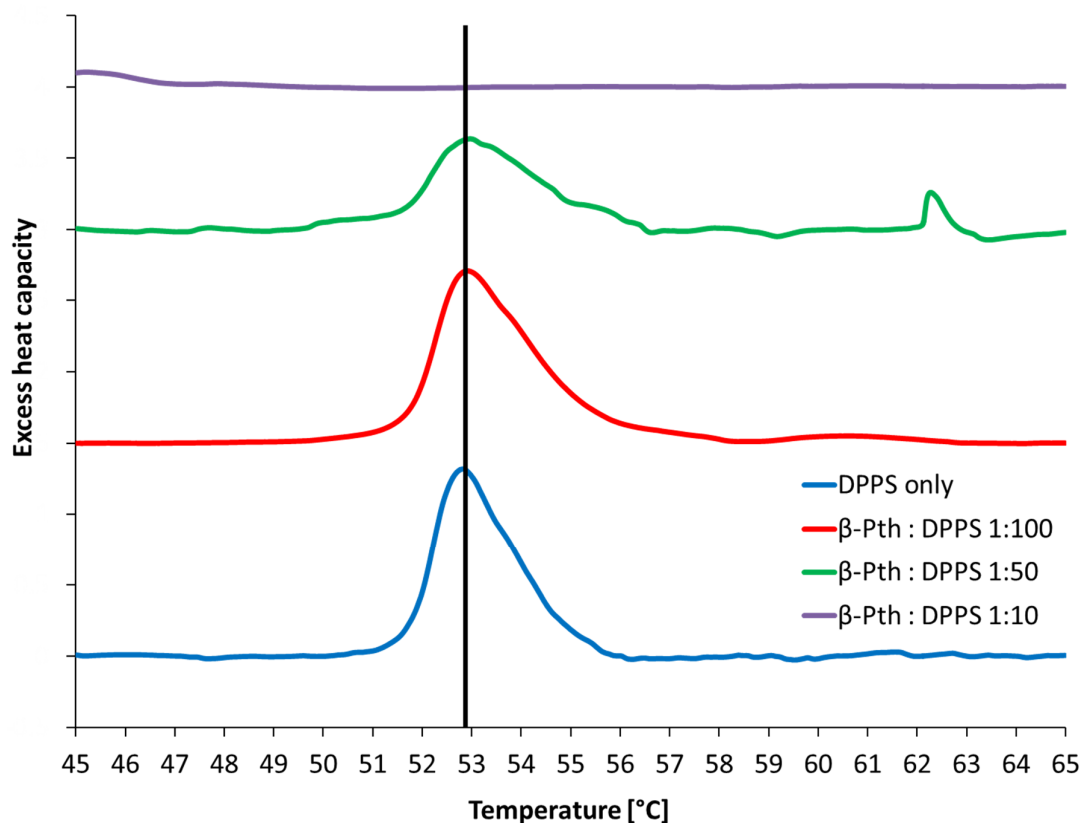


Figure 7.7 DSC measurements of β -Pth added to the DPPS MLVs in various protein:lipid molar ratios.

Figure 7.7 illustrates how the intensity of the interactions with DPPS vesicles varies with the amount of the protein added. The vesicles are not particularly affected by the protein in the protein:lipid 1:100 molar ratio experiment, only insignificant reduction in the peak's area can be observed. Doubling the protein amount, however, resulted in the noticeable decrease in the peak's size, suggesting that there was the destruction of some part of the vesicles. The ratio of protein:lipid 1:10 showed the strongest destructive properties of the protein and the solubilisation of the vesicles indicated by the absence of the transition peak at around 52.8°C.

Figure 7.8 shows the β -Pth effect on the mixed DPPC:DPPS 1:1 mol:mol lipid system, representing the intermediate system between DPPC and DPPS possessing half of the DPPS-

only lipid system's net charge. As seen in Section 7.5.4, introducing the protein at the 1:100 protein:lipid molar ratio did not produce significant changes to the system, which is in agreement with the previous analysed systems. At the 1:10 molar ratio, however, the main transition peak significantly shrank and a small peak around 43°C appeared. Because the appearance of the peak indicates the presence of the molecules sharing the same melting point and being adjacent to each other, it can be speculated that a small group of DPPC molecules was isolated, possibly forming the DPPC-rich lipid raft.¹⁷⁹ Furthermore, the reduced size of the main transition peak indicates partial solubilisation of the mixed lipid vesicles.

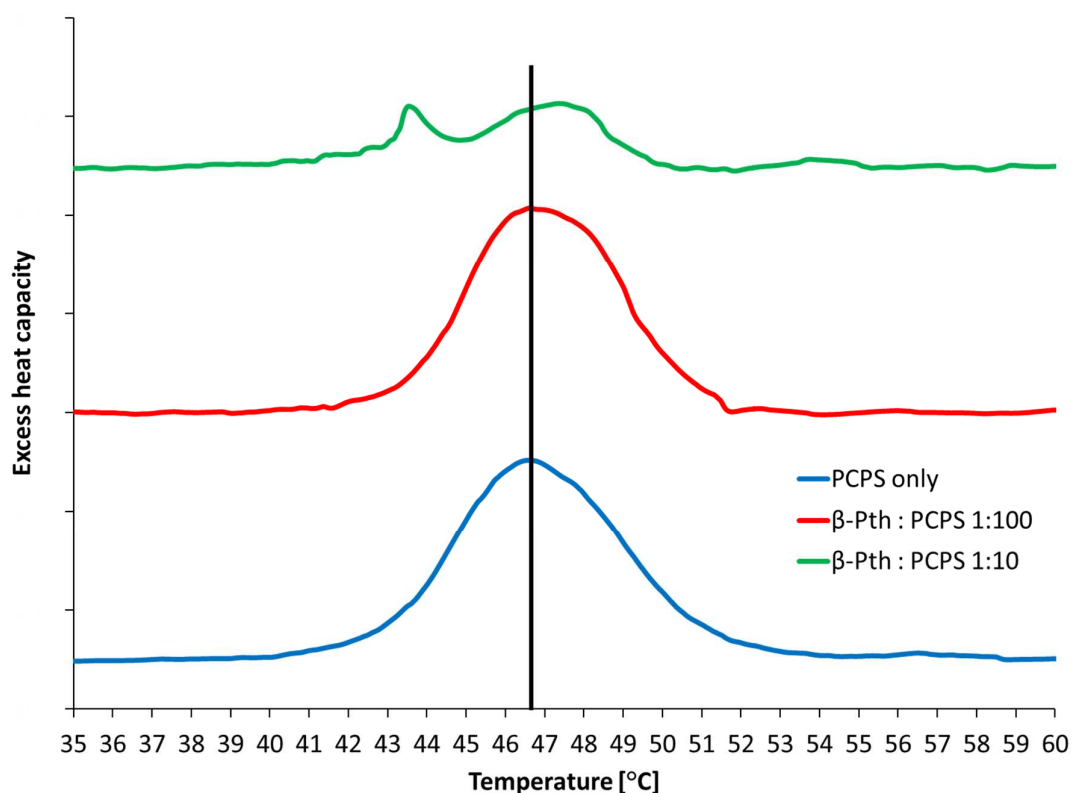


Figure 7.8 DSC measurements of β -Pth added to the DPPC:DPPS 1:1 mol:mol MLVs in various protein:lipid molar ratios.

The findings from this experiment are in good agreement with the ones from the monolayer studies (see Chapter 4, page 63) and the NR data (see Chapter 6, pages 120 and 125) and stress the strong dependence of the protein's action on the net charge of the phospholipids it faces.

7.5.6 Various Wheat Defence Proteins vs. DPPS MLVs

As shown in the previous section, the anionic DPPS lipid system displayed the strongest interactions with β -Pth when the protein is introduced at the 1:10 protein:lipid molar ratio (see Figure 7.7). Therefore, this lipid system and this protein:lipid ratio were chosen to test the antimicrobial action of other wheat defence proteins: Pin-a and α_2 -Pth.

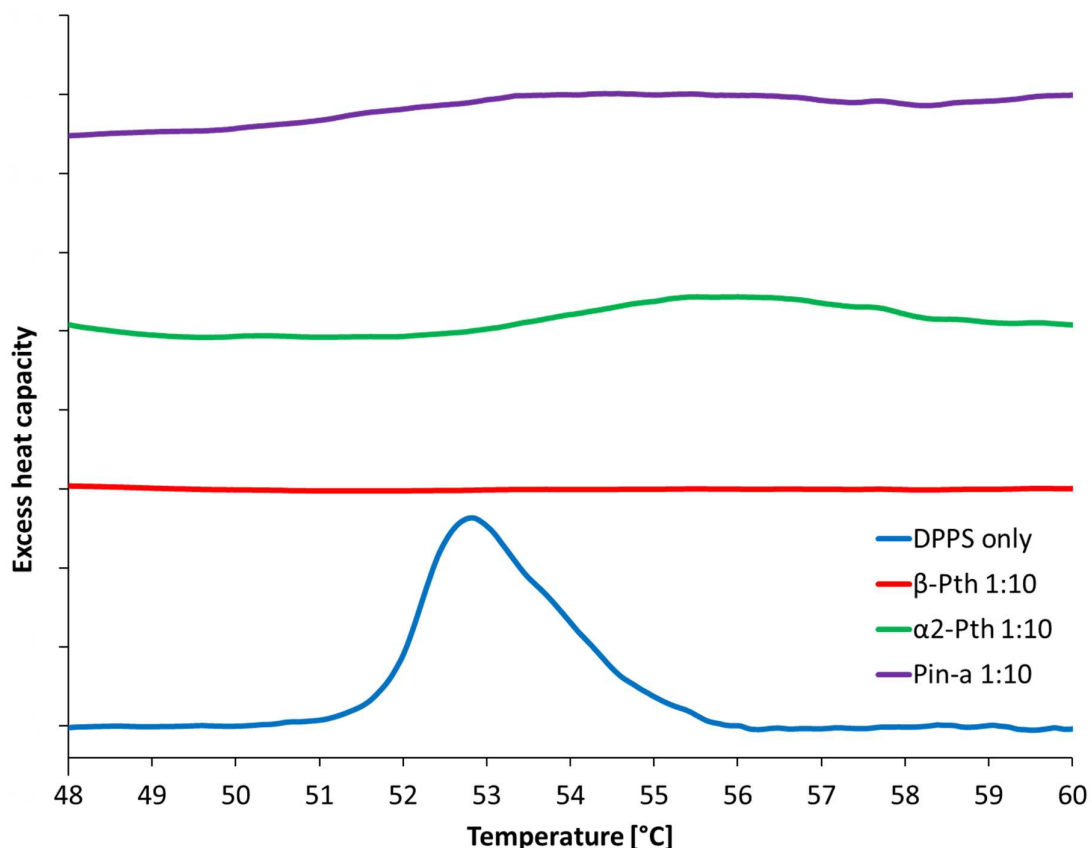


Figure 7.9 DSC measurements of various wheat defence proteins added to the DPPS MLVs in 1:10 protein:lipid molar ratios.

All proteins acted destructively on the DPPS lipid vesicles as none of the DSC scans showed any sign of the main transition peak (see Figure 7.9). The results are in good correlation with the findings from the studies on the lipid monolayer systems (see Chapter 4, page 81) and the lipid bilayer systems (see Chapter 5, page 103).

7.5.7 Experiments on Small Unilamellar Vesicles (SUVs)

The studies on the lipid SUVs allowed for better protein exposure towards the charge, *i.e.* the lipid headgroups were not hindered by the multilayers as in case of the MLVs (see vesicle structures in Chapter 2, page 28). The experiments were carried out by student Sylwia Meszko as part of the MPharm project ‘The interaction of the wheat defence protein β -Pth with models of fungal membranes’.¹⁸⁰

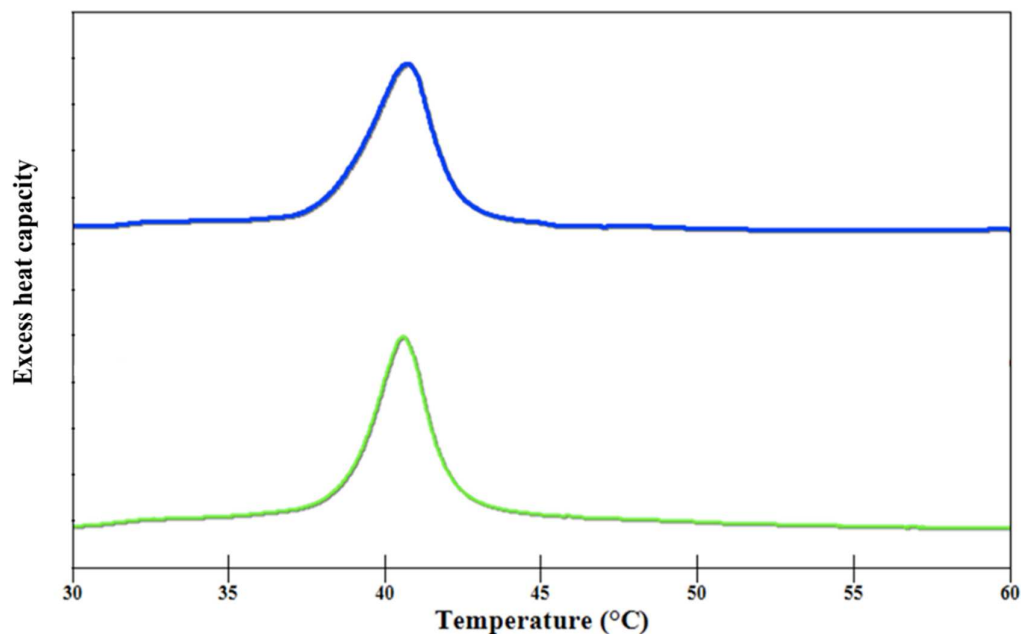


Figure 7.10 DSC thermograms of the DPPC SUVs (blue line) and DPPC SUVs interacting with β -Pth in 1:10 protein:lipid molar ratio.¹⁸⁰

All SUVs experiments show good agreement with the MLVs experiments when assessed by the melting point values. The DPPC SUVs, similarly to the DPPC MLVs, were hardly affected by the presence of the protein (compare Figures 7.5 and 7.10). Just like the DPPC MLVs lipid batch 1, the DPPC SUVs did not produce any pre-transition peak in their DSC scans and the thermograms with the protein resemble more the analogous ones obtained for the MLVs created from the lipid batch 1 (see Figure 7.5).

The DPPS SUVs, however, interacted strongly with the protein, yet no full solubilisation was observed (see Figure 7.11). There was a smaller peak in the main transition region and the new peak appeared around 43°C, suggesting partial solubilisation of the SUVs and the formation of structures possessing a different melting points, possibly protein-lipid islets or aggregates.¹⁸¹

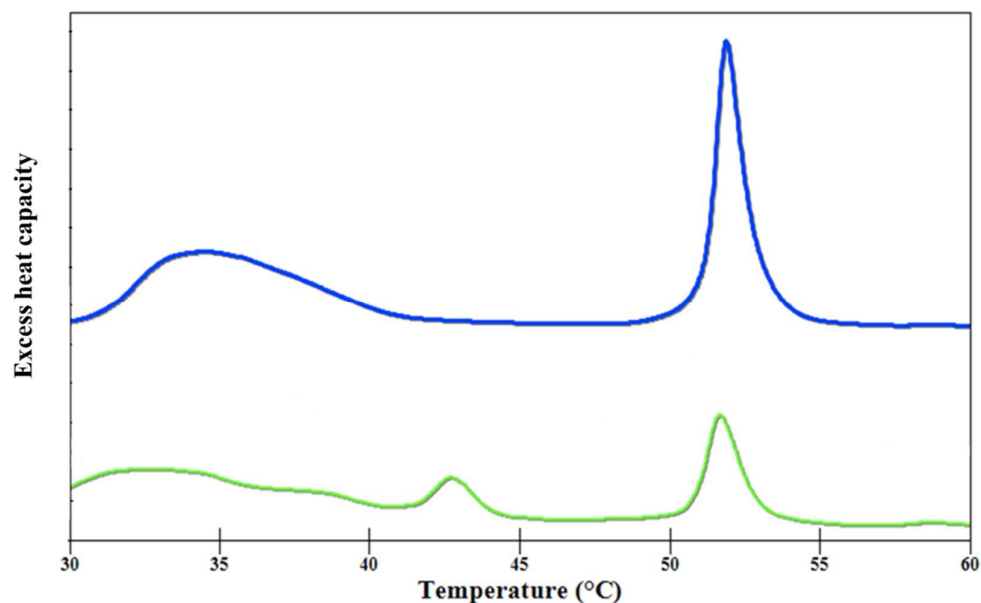


Figure 7.11 DSC thermograms of the DPPS SUVs (blue line) and DPPS SUVs interacting with β -Pth in 1:10 protein:lipid molar ratio.¹⁸⁰

The mixed lipid vesicles (see Figure 7.12) underwent the slight structure separation, which can be deduced from the peak splitting.¹⁷⁹ This splitting, however, was not very pronounced and, together with the overall decreased peak size, suggest the intermediate-strength interaction with the protein.¹⁸¹

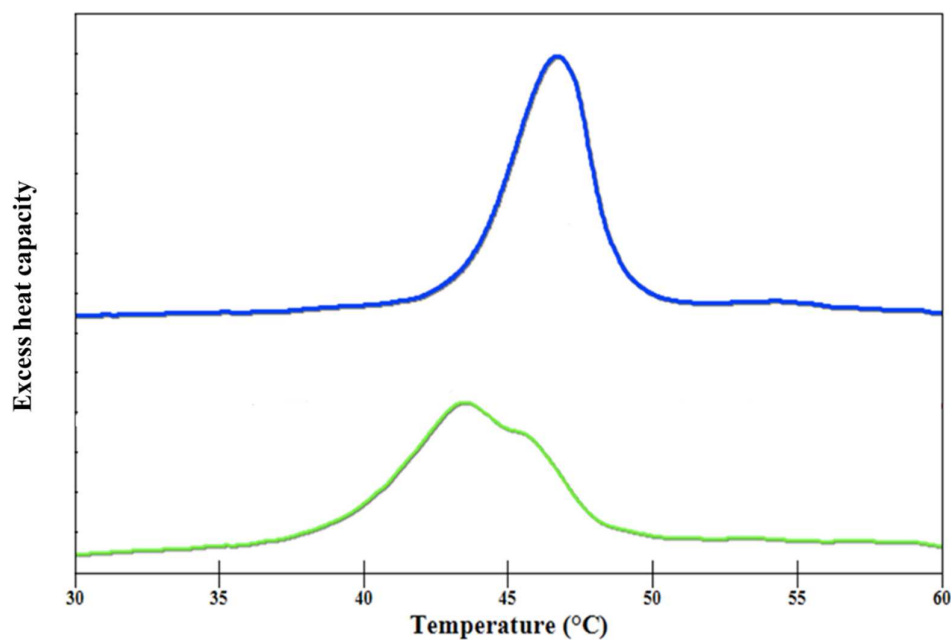


Figure 7.12 DSC thermograms of the DPPS:DPPC 1:1 mol:mol SUVs (blue line) and DPPS:DPPC 1:1 mol:mol SUVs interacting with β -Pth in 1:10 protein:lipid molar ratio (green line).¹⁸⁰

The findings from the SUV experiments are in good overall agreement with the ones obtained from the MLV ones: the direct dependence of the interactions on the lipid's net charge. In the project by Meszko¹⁸⁰ it was also shown that the SUVs had limited stability and that the storage conditions affected the quality of the lipid samples. This difficulty also occurred in the studies by Drazenovic *et al.*¹⁸² It is, therefore, recommended that the studies on the SUV lipid systems are carried out as soon as the lipid sample is produced.

The slightly milder action of the β -Pth on the DPPS and mixed lipid systems in the SUV experiments may suggest that the protein's presence is more destructive for the lipid structures of the size close to a microorganism's cell. This could indicate that the natural cell membrane curvature could potentially strengthen the antimicrobial action of the wheat defence proteins.

7.6 Conclusions

The study examined the wheat defence proteins interactions with lipid vesicles. The folded lipid bilayer systems enabled to investigate how the membrane's curvature affects the proteins' mode of action.

Wheat defence proteins showed the strong membrane-interacting properties when exposed in a high-enough concentration to the anionic lipid system. The dependence of the interactions on the lipid's net charge was confirmed by both MLVs experiments and SUVs experiments. The above-mentioned findings are in good agreement with the results from the monolayer experiments (see Chapter 4, page 81) and the flat bilayer experiments (see Chapter 5, page 103).

The membrane-solubilising properties of the wheat defence proteins described in this chapter were much more pronounced than the ones obtained in the research by Sanders¹³³ on Pin-b interaction with model bacterial membranes. This difference stresses the influence of both lipid and protein structures on the strength of the protein-lipid interactions.

The MLVs lipid systems showed good repeatability of the measurements if stored overnight in the freezer, whereas the stability of the SUV solutions in various storage conditions was not as high as the MLV lipids.¹⁸⁰ This fact, together with the generally stronger membrane-

solubilising properties observed for the MLVs experiment, allows to recommend the use of MLVs systems for the studies on the protein-lipid interactions.

Although it was impossible to determine the exact distribution of the lipid components in the mixed lipid systems (compare with the lipid mixing results in the flat bilayer leaflets – Chapter 6, page 116), the experiments using liposomes gave valuable insight into the study on the protein-lipid interactions: the impact of membrane curvature, which could play a role in enhancing the antimicrobial action of the wheat defence proteins.

Chapter 8

CONCLUDING REMARKS AND FUTURE WORK

The research aimed at describing the antifungal properties of the wheat defence proteins. The biocidal effect of the proteins was assessed by studying the protein-lipid interactions using the lipid systems mimicking the natural cell membrane of the yeast *S.cerevisiae*. Each analysed lipid system, therefore, consisted of the components found in the yeast's cell membrane and reflected different physical properties: membrane's negative charge created by the anionic phospholipids, membrane's fluidity coming from the presence of the unsaturated fatty acid chains in the phospholipid molecules or presence of steroid affecting the rigidity of the membrane.

Each analysed lipid system, in the form of monolayer, bilayer or a vesicle, provided valuable insight into the protein-lipid interactions. Various analytical techniques allowed to determine different details on the interaction's strength and kinetics. The main findings of this research are gathered in Table 8.1.

All wheat defence proteins showed strong adsorptive properties towards the anionic, saturated phospholipids, which has been confirmed by the studies on the monolayer, bilayer and vesicle lipid systems. There was hardly any interaction seen with the fully zwitterionic lipid systems and the medium-strength interactions was observed for the systems composed of the equimolar amounts of the anionic and zwitterionic lipids. These results confirm the direct dependence of the interaction's strength on the net charge the protein is facing.

Slightly milder interactions appeared for the unsaturated lipid systems and the protein adsorption displayed the different kinetics than the saturated system, which suggests that the presence of the more fluidic lipids in the membrane could play the supportive role in the lipid-binding by the protein and / or could lead to the further membrane destruction once the protein's action was initiated.

Table 8.1 Summary of the information gathered from all experiments in the study.

Protein	Lipid system	Results
β -Pth	DPPS	<ul style="list-style-type: none"> • Monolayer: high surface pressure rise due to the high level of the protein adsorption, gradual monolayer saturation reflected by the XRR measurements • Flat bilayer: significant penetration of the bilayer reflected by the ATR-FTIR and NR experiments • Vesicle: complete destruction of the MLVs and of the significant proportion of the SUVs
	DPPC	<ul style="list-style-type: none"> • Monolayer: no significant surface pressure rise indicating low protein adsorption • Flat bilayer: no bilayer penetration detected by ATR-FTIR • Vesicle: no changes in the MLVs and SUVs structure
	DPPC:DPPS 1:1 mol:mol	<ul style="list-style-type: none"> • Monolayer: medium surface pressure rise due to the mean level of the protein adsorption • Flat bilayer: no penetration of the bilayer reflected in the NR experiments • Vesicle: partial destruction of the MLVs and of the small proportion of the SUVs
	POPS	<ul style="list-style-type: none"> • Monolayer: medium surface pressure rise due to the mean level of the protein adsorption, different adsorption kinetics than the saturated, anionic DPPS system shown by XRR: adsorption rapid at the beginning and quickly stabilised. • Flat bilayer: no penetration of the bilayer shown in the NR experiments
	DPPC:POPS 1:1 mol:mol	<ul style="list-style-type: none"> • Flat bilayer: no penetration of the bilayer reflected in the NR experiments
	DPPS:ergosterol 1:1 mol:mol	<ul style="list-style-type: none"> • Flat bilayer: no penetration of the bilayer reflected in the NR experiments
Pin-a	DPPS	<ul style="list-style-type: none"> • Monolayer: high surface pressure rise due to the high level of the protein adsorption • Flat bilayer: significant penetration of the bilayer reflected by ATR-FTIR and no penetration reflected by the NR experiments • Vesicle: complete destruction of the MLVs
Pin-a: β -Pth 1:1 mol:mol	DPPS	<ul style="list-style-type: none"> • Monolayer: high surface pressure rise due to the high level of the protein adsorption: slightly synergistic behaviour between the proteins • Flat bilayer: slight penetration to the outer headgroup region reflected in one of the NR experiments
α_2 -Pth	DPPS	<ul style="list-style-type: none"> • Monolayer: high surface pressure rise due to the high level of the protein adsorption • Flat bilayer: significant penetration of the bilayer reflected by ATR-FTIR • Vesicle: complete destruction of the MLVs
α_2 -Pth: β -Pth 1:1 mol:mol	DPPS	<ul style="list-style-type: none"> • Monolayer: high surface pressure rise due to the high level of the protein adsorption: possibility of slightly competitive behaviour between the thionins.

The research also involved the successful design and introduction of the new piece of equipment: the dipping trough allowing to cover the solid support with the lipid bilayers of the controlled molecular thickness. The trough enabled the development of a new analytical method: ATR-FTIR applied to study the protein adsorption to the lipid bilayers deposited on the germanium crystal's surface by means of the Langmuir-Blodgett and Langmuir-Scafeffer dipping techniques. It provided the reproducible results that served as the preliminary studies used for the selection of the lipid bilayer systems to be further analysed by means of Neutron Reflectometry.

The collected data allow to speculate that the thionins could act as pore formers and could potentially display the synergistic antifungal behaviour with puroindolines. There were no significant indications of the competition or synergy between the members of the purothionin group: β -Pth and α_2 -Pth. It can be speculated that the mechanism of antimicrobial action of thionins based on the initial electrostatic attraction towards the anionic phospholipid-rich regions of the curved cell membrane and, with possible help of unsaturated lipids, on the further formation of small pores leading eventually to membrane solubilisation.

This process could be supported by a puroindoline, *e.g.* Pin-a, which, having been initially attracted to the membrane, could form the carpet-like layer thanks to its adhesive properties,⁹² preventing the exchange of the molecules in the cell. The two processes combined could lead to the faster destruction of the microbial cell than each of them individually, which could serve as an explanation of the cooperative biocidal mechanism of the puroindolines and the purothionins.

Future experiments aiming at characterising the antifungal activity of the wheat defence proteins could involve both analytical method development side and the analysed lipid / protein system development side. The method development part of the work could focus on advancing the dipping technique of the ATR-FTIR crystal, thus allowing the better coverage with the lipid bilayer.

The inconsistency between the ATR-FTIR and NR experiments on the Pin-a's antifungal action could be further examined by repeating the NR bilayer experiments using the simple DPPC: DPPS bilayer.

Moreover, the more elaborate lipid systems could be used for the bilayer and MLVs experiments. For example, as the NR studies on the lipid systems containing ergosterol were carried out only using the deuterated lipid systems, the future work could involve studying the fully hydrogenated lipid bilayer containing ergosterol and its structural changes upon the protein adsorption. This steroid could also be used as a partial component in the MLV studies – the SUV studies gave a very low intensity peak.¹⁸⁰ Furthermore, ergosterol could be incorporated into the more complex flat bilayers used for the ATR-FTIR techniques. However, the use of steroid in the monolayer experiments as a partial component led to the irreproducible results (data not shown).

More detailed studies on the unusual kinetics of the protein adsorption to the unsaturated lipid systems could be carried out by analysing the various saturated lipid: unsaturated lipid ratios in the lipid systems by *e.g.* an experiment on the protein adsorption to the partially unsaturated monolayers using the NR reflectometer Inter (ISIS Neutron and Muon Spallation Source, Harwell, UK).

Another suggestion for the future work would be the experiments using other wheat defence proteins, *e.g.* α_1 -Pth, Pin-b+, Pin-bS and their mixtures to test the destructive effect on the fungal membranes.

The development of the purification protocols of two wheat defensins γ_1 -Pth and γ_2 -Pth could lead to further tests on the antimicrobial action of the defence proteins, with possible experiments on the synergistic / competitive behaviour between the various wheat defence protein families.

To sum up, the work presented in this research gave an insight into the mechanism of the antimicrobial action of the wheat defence proteins and successfully developed the tools that could be used for the future analysis of the protein-lipid interactions.

ACKNOWLEDGEMENTS

I would like to thank my supervisors Prof. Richard Frazier, Dr Rebecca Green and Dr Luke Clifton for giving me a chance to work on this project. I received immense support and guidance throughout the work and could not be more grateful.

I would also like to thank the University of Reading and the Science and Technology Facilities Council for the funding of this project.

I would not have been able to start my work if it were not for the help and advice I received from Dr Michael Sanders.

I would also like to express my gratitude to Dr Tom Arnold for his support at the X-Ray Reflectometry experiments carried out at the Diamond Light Source.

No Neutron Reflectometry experiment would be successful without the help from Dr Maximilian Skoda, Dr Filip Ciesielski and Dr Arwel Hughes.

I would also like to thank Marleen Wilde and Marcia English for assisting at the Neutron Reflectometry experiments and going through the data analysis.

I am also grateful to Sylwia Meszko who contributed to the Differential Scanning Calorimetry experiments in the project.

I would also like to thank all colleagues from the laboratory for their support and creating the great working atmosphere.

Finally, special thanks to my family and friends for supporting me throughout the work.

APPENDIX

Table 1. Neutron scattering length values of the elements appearing in this study.¹²⁸

Element	Scattering length, b [10^{-5} Å]
C	6.65
H	-3.74
D	6.67
S	2.85
O	5.80
N	9.40
P	5.10

Table 2. Volumes of the bonds and functional groups used for calculating the scattering length densities of the molecules.⁸⁹

Bond type	Volume, V [Å ³]
>C=, big trigonal, unbranched and aromatics	9.7
>CH-, aliphatic CH branched	13.2
CH ₂	24.3
CH ₃	36.7
NH ₃ ⁺	21.4
O=	15.9
OH	18.0
PO ₄	89.0

Examples of the calculations on a DPPS molecule:

Molecular formula: C₃₈H₇₃NO₁₀P

Molecular volume calculation:

$$V = (3 \cdot 9.7 + 2 \cdot 13.2 + 31 \cdot 24.3 + 2 \cdot 36.7 + 21.4 + 6 \cdot 15.9 + 95.4 + 89) \text{ Å}^3 = 1088 \text{ Å}^3 \quad (25)$$

XRR SLD calculation:

$$\text{xrSLD} = \frac{2.818 \cdot 10^{-5} \text{ Å} \cdot (38 \cdot 6 + 73 \cdot 1 + 10 \cdot 8 + 1 \cdot 7 + 1 \cdot 15)}{1088 \text{ Å}^3} = 10.44 \cdot 10^{-6} \text{ Å}^{-2} \quad (26)$$

NR SLD calculation:

$$\text{SLD} = \frac{(38 \cdot 6.65 + 73 \cdot (-3.74) + 10 \cdot 5.8 + 9.4 + 5.1) \cdot 10^{-5} \text{ Å}}{1088 \text{ Å}^3} = 0.48 \cdot 10^{-6} \text{ Å}^{-2} \quad (27)$$

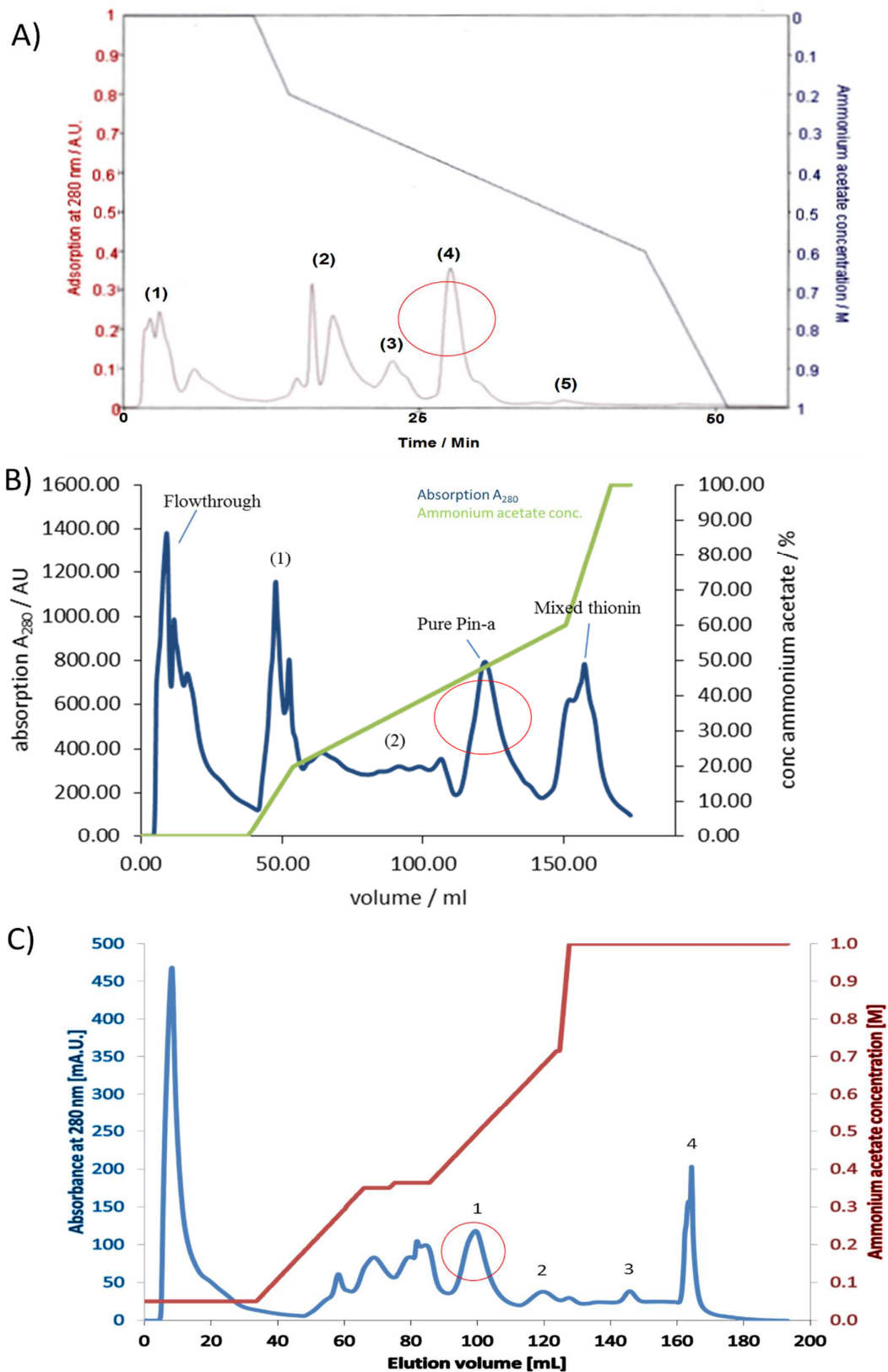


Figure 1. FPLC elution profiles showing the purification of Pin-a from the crude wheat flour extracts, carried out by Luke Clifton (A),⁸⁰ Michael Sanders (B)¹³³ and Olga Florek (C). Pin-a peaks marked with red circle.

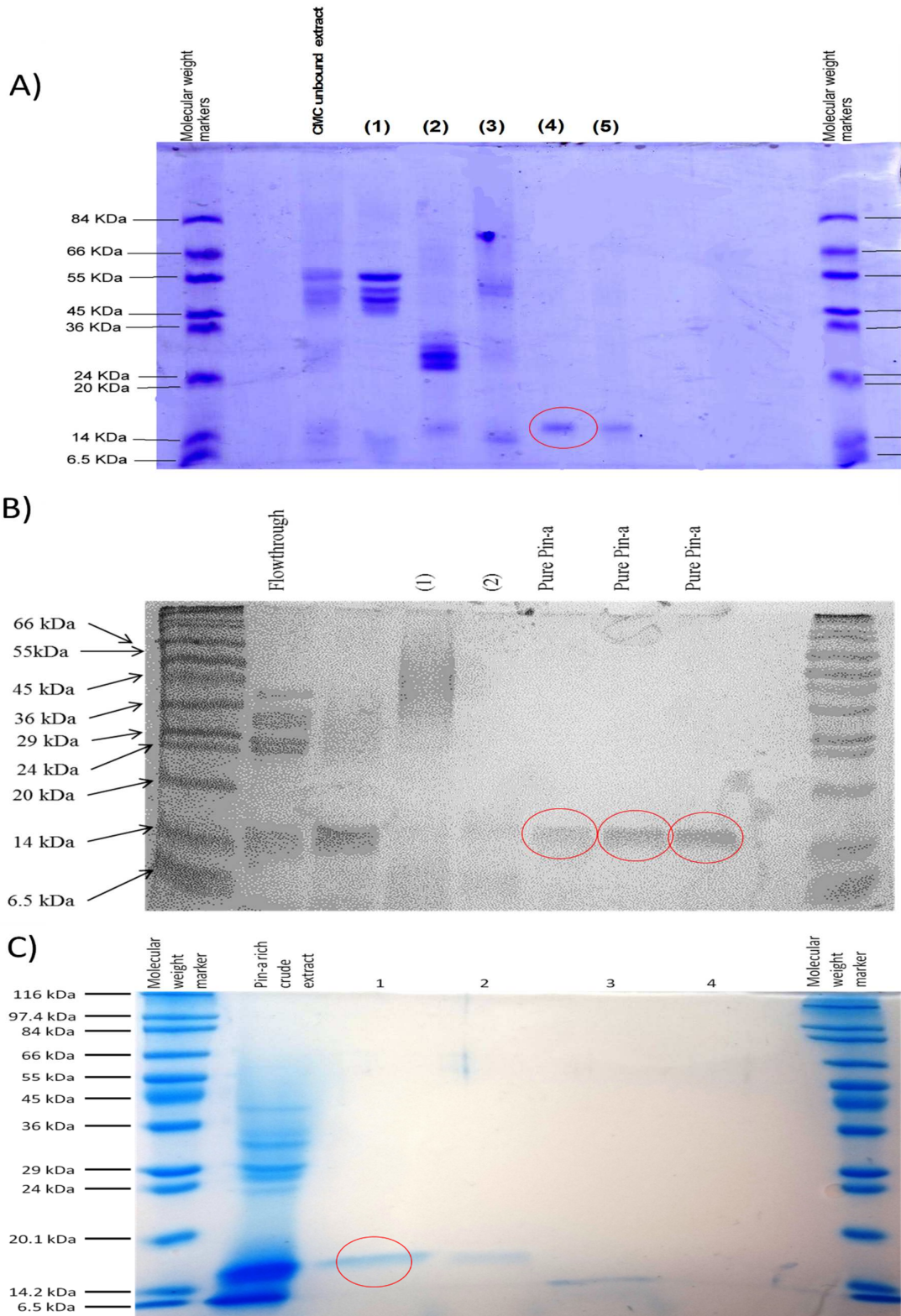


Figure 2. SDS-PAGE results of the Pin-a purification peaks corresponding to the chromatograms in Figure 1, obtained by Luke Clifton (A),⁸⁰ Michael Sanders (B)¹³³ and Olga Florek (C). Pin-a bands marked with red circle.

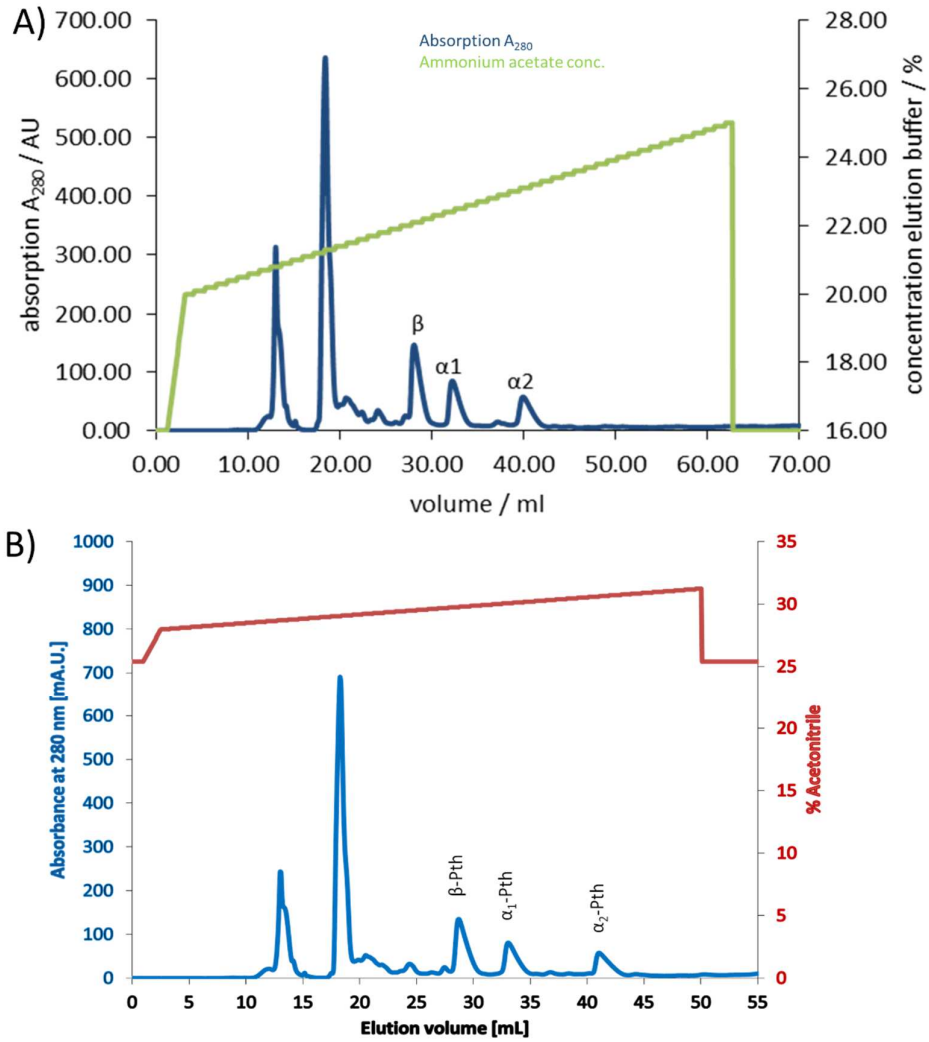


Figure 3. RP-HPLC chromatograms showing the purothionin purification by Michael Sanders (A)¹³³ and Olga Florek (B).

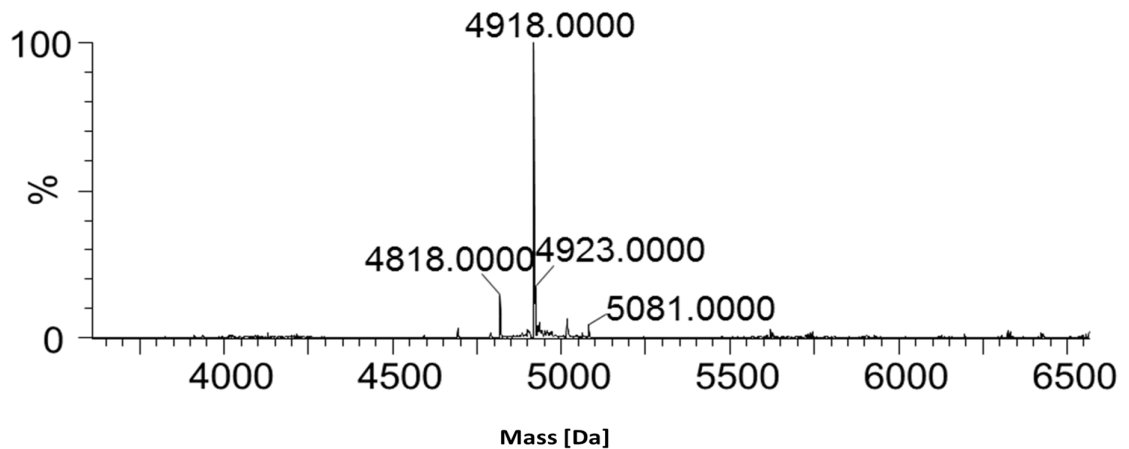


Figure 4. Deconvoluted mass spectrum from raw data for β -Pth indicating the purity of the mass fragments.¹³³ Difference between the measured molecular weight and the one reported for the protein in the literature⁵⁶ is caused by the minor changes in the post-translational modifications between the two batches.

Figure 5.

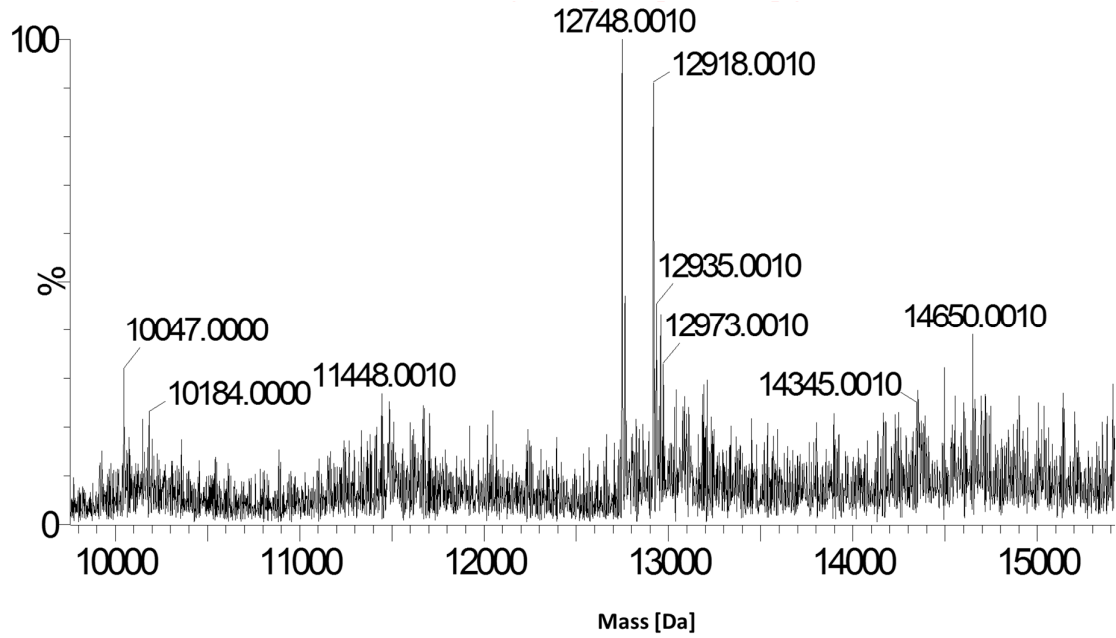


Figure 6. Deconvoluted mass spectrum of Pin-a corresponding to peak 1 in Figure 1 C and indicating the purity of the mass fragments. The presence of the two dominating peaks is caused by the variety in the post-translational modifications of the protein isolated from the wheat extract.

REFERENCES

1. Oliver, R. & Schweizer, M. (1999). *Molecular fungal biology*, Cambridge, Cambridge University Press.
2. García-Olmedo, F., Molina, A., Alamillo, J. M. & Rodríguez-Palenzuela, P. (1998). Plant defense peptides. *Peptide Science*, **47**, 479-491.
3. Maget-Dana, R. (1999). The monolayer technique: a potent tool for studying the interfacial properties of antimicrobial and membrane-lytic peptides and their interactions with lipid membranes. *Biochimica Et Biophysica Acta-Biomembranes*, **1462**, 109-140.
4. DeLuca, A. J., Bland, J. M., Jacks, T. J., Grimm, C., Cleveland, T. E. & Walsh, T. J. (1997). Fungicidal activity of cecropin A. *Antimicrob Agents Chemother*, **41**, 481-3.
5. Wu, T., Tang, D., Chen, W., Huang, H., Wang, R. & Chen, Y. (2013). Expression of antimicrobial peptides thanatin(S) in transgenic Arabidopsis enhanced resistance to phytopathogenic fungi and bacteria. *Gene*, **527**, 235-42.
6. Terras, F. R., Eggermont, K., Kovaleva, V., Raikhel, N. V., Osborn, R. W., Kester, A., Rees, S. B., Torrekens, S., Van Leuven, F., Vanderleyden, J. & et al. (1995). Small cysteine-rich antifungal proteins from radish: their role in host defense. *Plant Cell*, **7**, 573-88.
7. Broekaert, W. F., Terras, F. R., Cammue, B. P., & Osborn, R. W. (1995). Plant defensins: novel antimicrobial peptides as components of the host defense system. *Plant Physiology*, **108(4)**, 1353–1358.
8. Cauvain, S. P. & Young, L. S. (1997). *Technology of breadmaking*. London: Blackie.
9. Garcia-Olmedo, F., Rodriguez-Palenzuela, P., Hernandez-Lucas, C., Ponz, F., Marafia, C., Carmona, M.J., Lopez-Fando, J., Fernandez, J.A., Carbonero, P. (1989). The thionins: a protein family that includes purothionins, viscotoxins and crambins. *Oxford Surveys of Plant Molecularolme Cell Biology*, **6**, 31-60.
10. Decaleya, R. F., Carboner.P, Gonzalez.B & Garciaol.F (1972). Susceptibility of Phytopathogenic Bacteria to Wheat Purothionins in-Vitro. *Applied Microbiology*, **23**, 998-1000.
11. Decaleya, R. F., Hernandezlucas, C., Carbonero, P. & Garciaolmedo, F. (1976). Gene-Expression in Allopolyploids - Genetic-Control of Lipopurothionins in Wheat. *Genetics*, **83**, 687-699.

12. Egorov, T. A., Odintsova, T. I., Pukhalsky, V. A. & Grishin, E. V. (2005). Diversity of wheat anti-microbial peptides. *Peptides*, **26**, 2064-2073.
13. Rodriguezpalenzuela, P., Pintortoro, J. A., Carbonero, P. & Garciaolmedo, F. (1988). Nucleotide-Sequence and Endosperm-Specific Expression of the Structural Gene for the Toxin Alpha-Hordothionin in Barley (*Hordeum-Vulgare-L*). *Gene*, **70**, 271-281.
14. Samuelsson, G., Pettersson, B.M (1970). Separation of viscotoxins from the European mistletoe *Viscum album* L. (Loranthaceae) by chromatography on sulfoethyl Sephadex. *Acta Chemica Scandinavica*, **24**, 2751-2756.
15. Vanetten, C. H., Nielsen, H. C., Peters, J. E. (1965). A crystalline polypeptide from the seed of *Crambe abyssinica*. *Phytochemistry*, **4**, 467-473.
16. Castagnaro, A., Marana, C., Carbonero, P. & Garcia-Olmedo, F. (1992). Extreme divergence of a novel wheat thionin generated by a mutational burst specifically affecting the mature protein domain of the precursor. *J Mol Biol*, **224**, 1003-9.
17. Hernandez-Lucas, C., Fernandez de Caleyra, R. & Carbonero, P. (1974). Inhibition of brewer's yeasts by wheat purothionins. *Appl Microbiol*, **28**, 165-8.
18. Carrasco, L., Vazquez, D., Hernandez-Lucas, C., Carbonero, P., Gracia-Olmedo, F. (1981). Thionins: Plant peptides that modify membrane permeability in cultured mammalian cells. *Eur J Biochem* **116**, 185-189.
19. Kramer, K. J., Klassen, L. W., Jones, B. L., Speirs, R. D. & Kammer, A. E. (1979). Toxicity of purothionin and its homologues to the tobacco hornworm, *Manduca sexta* (L.) (*Lepidoptera:Sphingidae*). *Toxicol Appl Pharmacol*, **48**, 179-83.
20. Carmona, M. J., Molina, A., Fernández, J. A., López-Fando, J. J. and García-Olmedo, F. (1993). Expression of the α -thionin gene from barley in tobacco confers enhanced resistance to bacterial pathogens. *The Plant Journal*, **3**: 457-462.
21. Stec, B. (2006). Plant thionins-the structural perspective. *Cell Mol Life Sci*, **63**, 1370-85.
22. Wada, K., Ozaki, Y., Matsubara, H. & Yoshizumi, H. (1982). Studies on purothionin by chemical modifications. *J Biochem*, **91**, 257-63.
23. Hughes, P., Dennis, E., Whitecross, M., Llewellyn, D. & Gage, P. (2000). The cytotoxic plant protein, beta-purothionin, forms ion channels in lipid membranes. *Journal of Biological Chemistry*, **275**, 823-827.
24. Giudici, A. M., Regente, M. C., Villalain, J., Pfuller, K., Pfuller, U. & de la Canal, L. (2004). Mistletoe viscotoxins induce membrane permeabilization and spore death in phytopathogenic fungi. *Physiologia Plantarum*, **121**, 2-7.

25. Stec, B., Markman, O., Rao, U., Heffron, G., Henderson, S., Vernon, L. P., Brumfeld, V. & Teeter, M. M. (2004). Proposal for molecular mechanism of thionins deduced from physico-chemical studies of plant toxins. *J Pept Res*, **64**, 210-24.
26. Majewski, J. & Stec, B. (2010). X-ray scattering studies of model lipid membrane interacting with purothionin provide support for a previously proposed mechanism of membrane lysis. *European Biophysics Journal with Biophysics Letters*, **39**, 1155-1165.
27. Clifton, L. A., Sanders, M. R., Hughes, A. V., Neylon, C., Frazier, R. A. & Green, R. J. (2011). Lipid binding interactions of antimicrobial plant seed defence proteins: puroindoline-a and beta-purothionin. *Physical Chemistry Chemical Physics*, **13**, 17153-17162.
28. Richard, J.-A., Kelly, I., Marion, D., Pézolet, M. & Auger, M. (2002). Interaction between β -Purothionin and Dimyristoylphosphatidylglycerol: A ^{31}P -NMR and Infrared Spectroscopic Study. *Biophysical Journal*, **83**, 2074-2083.
29. Clifton, L. A., Sanders, M., Kinane, C., Arnold, T., Edler, K. J., Neylon, C., Green, R. J. & Frazier, R. A. (2012). The role of protein hydrophobicity in thionin-phospholipid interactions: a comparison of alpha 1 and alpha 2-purothionin adsorbed anionic phospholipid monolayers. *Physical Chemistry Chemical Physics*, **14**, 13569-13579.
30. Molina, A. & García-Olmedo, F. (1994). Expression of Genes Encoding Thionins and Lipid-Transfer Proteins. A Combinatorial Model for the Responses of Defense Genes to Pathogens. In: Coruzzi, G. & Puigdomènech, P. (eds.) *Plant Molecular Biology: Molecular Genetic Analysis of Plant Development and Metabolism*. Berlin, Heidelberg: Springer Berlin Heidelberg.
31. Gautier, M. F., Aleman, M. E., Guirao, A., Marion, D. & Joudrier, P. (1994). Triticum-Aestivum Puroindolines, 2 Basic Cystine-Rich Seed Proteins - Cdna Sequence-Analysis and Developmental Gene-Expression. *Plant Molecular Biology*, **25**, 43-57.
32. Yau, W. M., Wimley, W. C., Gawrisch, K. & White, S. H. (1998). The preference of tryptophan for membrane interfaces. *Biochemistry*, **37**, 14713-14718.
33. Bhave, M. & Morris, C. F. (2008). Molecular genetics of puroindolines and related genes: regulation of expression, membrane binding properties and applications. *Plant Molecular Biology*, **66**, 221-231.
34. Lillemo, M., Simeone, M. C., Morris, C. F. (2002). Analysis of puroindoline a and b sequences from *Triticum aestivum* cv. 'Penawawa' and related diploid taxa. *Euphytica*, **126**, 321-331.

35. Le Bihan, T., Blochet, J.-É., Désormeaux, A., Marion, D. & Pézolet, M. (1996). Determination of the Secondary Structure and Conformation of Puroindolines by Infrared and Raman Spectroscopy. *Biochemistry*, **35**, 12712-12722.
36. Pauly, A., Pareyt, B., Fierens, E. & Delcour, J. A. (2013). Wheat (*Triticum aestivum* L. and *T. turgidum* L. ssp. *durum*) Kernel Hardness: I. Current View on the Role of Puroindolines and Polar Lipids. *Comprehensive Reviews in Food Science and Food Safety*, **12**, 413-426.
37. Guo, H., Zhang, H., Li, Y., Ren, J., Wang, X., Niu, H. & Yin, J. (2011). Identification of Changes in Wheat (*Triticum aestivum* L.) Seeds Proteome in Response to Anti-*trx s* Gene. *PLoS ONE*, **6**, e22255.
38. Dubreil, L., Gaborit, T., Bouchet, B., Gallant, D. J., Broekaert, W. F., Quillien, L. & Marion, D. (1998). Spatial and temporal distribution of the major isoforms of puroindolines (puroindoline-a and puroindoline-b) and non specific lipid transfer protein (ns-LTPle(1)) of *Triticum aestivum* seeds. Relationships with their in vitro antifungal properties. *Plant Science*, **138**, 121-135.
39. Capparelli, R., Palumbo, D., Iannaccone, M., Ventimiglia, I., Di Salle, E., Capuano, F., Salvatore, P. & Amoroso, M. G. (2006). Cloning and expression of two plant proteins: similar antimicrobial activity of native and recombinant form. *Biotechnol Lett*, **28**, 943-9.
40. Jing, W., Demcoe, A. R. & Vogel, H. J. (2003). Conformation of a bactericidal domain of puroindoline a: structure and mechanism of action of a 13-residue antimicrobial peptide. *J Bacteriol*, **185**, 4938-47.
41. Dubreil, L., Compoin, J. P. & Marion, D. (1997). Interaction of puroindolines with wheat flour polar lipids determines their foaming properties. *Journal of Agricultural and Food Chemistry*, **45**, 108-116.
42. Martin, J. M., Meyer, F. D., Morris, C. F. & Giroux, M. J. (2007). Pilot scale milling characteristics of transgenic isolines of a hard wheat over-expressing puroindolines. *Crop Science*, **47**, 497-506.
43. Morris, C. F., Lillemo, M., Simeone, M. C., Giroux, M. J., Babb, S. L. & Kidwell, K. K. (2001). Prevalence of puroindoline grain hardness genotypes among historically significant North American spring and winter wheats. *Crop Science*, **41**, 218-228.
44. Morrison, W. R., Greenwell, P., Law, C. N. & Sulaiman, B. D. (1992). Occurrence of friabilin, a low molecular weight protein associated with grain softness, on starch

- granules isolated from some wheats and related species. *Journal of Cereal Science*, **15**, 143-149.
45. Giroux, M. J. & Morris, C. F. (1998). Wheat grain hardness results from highly conserved mutations in the friabilin components puroindoline a and b. *Proceedings of the National Academy of Sciences of the United States of America*, **95**, 6262-6266.
46. Giroux, M. J. & Morris, C. F. (1997). A glycine to serine change in puroindoline b is associated with wheat grain hardness and low levels of starch-surface friabilin. *Theoretical and Applied Genetics*, **95**, 857-864.
47. Giroux, M. J., Talbert, L., Habernicht, D. K., Lanning, S., Hemphill, A. & Martin, J. M. (2000). Association of puroindoline sequence type and grain hardness in hard red spring wheat. *Crop Science*, **40**, 370-374.
48. Martin, J. M., Froberg, R. C., Morris, C. F., Talbert, L. E. & Giroux, M. J. (2001). Milling and bread baking traits associated with puroindoline sequence type in hard red spring wheat. *Crop Science*, **41**, 228-234.
49. Clifton, L. A., Lad, M. D., Green, R. J. & Frazier, R. A. (2007). Single amino acid substitutions in puroindoline-b mutants influence lipid binding properties. *Biochemistry*, **46**, 2260-2266.
50. Clifton, L. A., Green, R. J., Hughes, A. V. & Frazier, R. A. (2008). Interfacial Structure of Wild-Type and Mutant Forms of Puroindoline-b Bound to DPPG Monolayers. *Journal of Physical Chemistry B*, **112**, 15907-15913.
51. Sanders, M. R., Clifton, L. A., Frazier, R. A. & Green, R. J. (2016). Role of Lipid Composition on the Interaction between a Tryptophan-Rich Protein and Model Bacterial Membranes. *Langmuir*, **32**, 2050-2057.
52. Clifton, L. A., Green, R. J. & Frazier, R. A. (2007a). Puroindoline-b mutations control the lipid binding interactions in mixed puroindoline-a : puroindoline-b systems. *Biochemistry*, **46**, 13929-13937.
53. Sanders, M. R., Clifton, L. A., Neylon, C., Frazier, R. A. & Green, R. J. (2013). Selected Wheat Seed Defense Proteins Exhibit Competitive Binding to Model Microbial Lipid Interfaces. *Journal of Agricultural and Food Chemistry*, **61**, 6890-6900.
54. Colilla, F. J., Rocher, A. & Mendez, E. (1990). Gamma-Purothionins - Amino-Acid-Sequence of 2 Polypeptides of a New Family of Thionins from Wheat Endosperm. *Febs Letters*, **270**, 191-194.

55. Jones, B. L. & Mak, A. S. (1977). Amino-Acid Sequences of 2 Alpha-Purothionins of Hexaploid Wheat. *Cereal Chemistry*, **54**, 511-523.
56. Mak, A. S. & Jones, B. L. (1976). Amino-Acid Sequence of Wheat Beta-Purothionin. *Canadian Journal of Biochemistry*, **54**, 835-842.
57. Terras, F. R. G., Schoofs, H. M. E., Debolle, M. F. C., Vanleuven, F., Rees, S. B., Vanderleyden, J., Cammue, B. P. A. & Broekaert, W. F. (1992). Analysis of 2 Novel Classes of Plant Antifungal Proteins from Radish (*Raphanus-Sativus* L) Seeds. *Journal of Biological Chemistry*, **267**, 15301-15309.
58. Thevissen, K., Terras, F. R. G. & Broekaert, W. F. (1999). Permeabilization of fungal membranes by plant defensins inhibits fungal growth. *Applied and Environmental Microbiology*, **65**, 5451-5458.
59. Pelegrini, P. B. & Franco, O. L. (2005). Plant gamma-thionins: Novel insights on the mechanism of action of a multi-functional class of defense proteins. *International Journal of Biochemistry & Cell Biology*, **37**, 2239-2253.
60. Yeaman, M. R. & Yount, N. Y. (2003). Mechanisms of antimicrobial peptide action and resistance. *Pharmacological Reviews*, **55**, 27-55.
61. Shai, Y. (1999). Mechanism of the binding, insertion and destabilization of phospholipid bilayer membranes by α -helical antimicrobial and cell non-selective membrane-lytic peptides. *Biochimica et Biophysica Acta (BBA) - Biomembranes*, **1462**, 55-70.
62. Ehrenstein, G. & Lecar, H. (2009). Electrically gated ionic channels in lipid bilayers. *Quarterly Reviews of Biophysics*, **10**, 1-34.
63. Silva, P. M., Gonçalves, S. & Santos, N. C. (2014). Defensins: antifungal lessons from eukaryotes. *Frontiers in Microbiology*, **5**, 97.
64. Matsuzaki, K., Murase, O., Fujii, N. & Miyajima, K. (1995). Translocation of a Channel-Forming Antimicrobial Peptide, Magainin 2, across Lipid Bilayers by Forming a Pore. *Biochemistry*, **34**, 6521-6526.
65. Mor, A. & Nicolas, P. (1994). The NH₂-terminal alpha-helical domain 1-18 of dermaseptin is responsible for antimicrobial activity. *Journal of Biological Chemistry*, **269**, 1934-1939.
66. Santos, A. X. S. & Riezman, H. (2012). Yeast as a model system for studying lipid homeostasis and function. *Febs Letters*, **586**, 2858-2867.
67. Schneiter, R., Brugger, B., Sandhoff, R., Zellnig, G., Leber, A., Lampl, M., Athenstaedt, K., Hrastnik, C., Eder, S., Daum, G., Paltauf, F., Wieland, F. T. &

- Kohlwein, S. D. (1999). Electrospray ionization tandem mass spectrometry (ESI-MS/MS) analysis of the lipid molecular species composition of yeast subcellular membranes reveals acyl chain-based sorting/remodeling of distinct molecular species en route to the plasma membrane. *Journal of Cell Biology*, **146**, 741-754.
68. Singer, S. J. & Nicolson, G. L. (1972). Fluid Mosaic Model of Structure of Cell-Membranes. *Science*, **175**, 720-731.
69. Tuller, G., Nemeč, T., Hraštnik, C. & Daum, G. (1999). Lipid composition of subcellular membranes of an FY1679-derived haploid yeast wild-type strain grown on different carbon sources. *Yeast*, **15**, 1555-1564.
70. Vanderrest, M. E., Kamminga, A. H., Nakano, A., Anraku, Y., Poolman, B. & Konings, W. N. (1995). The Plasma-Membrane of *Saccharomyces-Cerevisiae* - Structure, Function, and Biogenesis. *Microbiological Reviews*, **59**, 304-322.
71. Zinser, E., Sperka-Gottlieb, C. D., Fasch, E. V., Kohlwein, S. D., Paltauf, F. & Daum, G. (1991). Phospholipid synthesis and lipid composition of subcellular membranes in the unicellular eukaryote *Saccharomyces cerevisiae*. *J Bacteriol*, **173**, 2026-34.
72. Patton, J. L. & Lester, R. L. (1991). The phosphoinositol sphingolipids of *Saccharomyces cerevisiae* are highly localized in the plasma membrane. *J Bacteriol*, **173**, 3101-8.
73. Blagovic, B. *et al.* (2005). Characterization of lipid components in the whole cells and plasma membranes of baker's yeast. *CROATICA CHEMICA ACTA*, **78**, 479-484.
74. Van Meer, G., Voelker, D. R. & Feigenson, G. W. (2008). Membrane lipids: where they are and how they behave. *Nat Rev Mol Cell Biol*, **9**, 112-24.
75. Martin, C. E., Oh, C.-S. & Jiang, Y. (2007). Regulation of long chain unsaturated fatty acid synthesis in yeast. *Biochimica et Biophysica Acta (BBA) - Molecular and Cell Biology of Lipids*, **1771**, 271-285.
76. Miano, F., Zhao, X., Lu, J. R. & Penfold, J. (2007). Coadsorption of Human Milk Lactoferrin into the Dipalmitoylglycerolphosphatidylcholine Phospholipid Monolayer Spread at the Air/Water Interface. *Biophysical Journal*, **92**, 1254-1262.
77. Löffler, J., Einsele, H., Hebart, H., Schumacher, U., Hraštnik, C. & Daum, G. (2000). Phospholipid and sterol analysis of plasma membranes of azole-resistant *Candida albicans* strains. *FEMS Microbiology Letters*, **185**, 59-63.
78. Křen, V., Pažoutová, S., Řezanka, T., Viden, I., Amler, E. & Sajdl, P. (1990). Regulation of Lipid and Ergot Alkaloid Biosynthesis in *Claviceps purpurea* by Chlorophenoxy Acids. *Biochemie und Physiologie der Pflanzen*, **186**, 99-108.

79. Palma-Guerrero, J., Lopez-Jimenez, J. A., Pérez-Berná, A. J., Huang, I. C., Jansson, H. B., Salinas, J., Villalaín, J., Read, N. D. & Lopez-Llorca, L. V. (2010). Membrane fluidity determines sensitivity of filamentous fungi to chitosan. *Molecular Microbiology*, **75**, 1021-1032.
80. Clifton, L. A. & University of Reading. School of Chemistry Food Biosciences and Pharmacy. (2008). *The effect of mutations on the tryptophan rich loop of puroindoline-b on puroindoline binding to lipids*. Thesis (PhD) - University of Reading, School of Chemistry, Pharmacy and Food Biosciences.
81. Bhattacharya, S. & Haldar, S. (2000). Interactions between cholesterol and lipids in bilayer membranes. Role of lipid headgroup and hydrocarbon chain-backbone linkage. *Biochimica et Biophysica Acta (BBA) - Biomembranes*, **1467**, 39-53.
82. Epanand, R. F., Savage, P. B. & Epanand, R. M. (2007). Bacterial lipid composition and the antimicrobial efficacy of cationic steroid compounds (Ceragenins). *Biochimica et Biophysica Acta (BBA) - Biomembranes*, **1768**, 2500-2509.
83. Ikeda, M., Kihara, A. & Igarashi, Y. (2006). Lipid Asymmetry of the Eukaryotic Plasma Membrane: Functions and Related Enzymes. *Biological and Pharmaceutical Bulletin*, **29**, 1542-1546.
84. Clifton, L. A., Skoda, M. W. A., Daulton, E. L., Hughes, A. V., Le Brun, A. P., Lakey, J. H. & Holt, S. A. (2013). Asymmetric phospholipid: lipopolysaccharide bilayers; a Gram-negative bacterial outer membrane mimic. *Journal of The Royal Society Interface*, **10**.
85. Daleke, D. L. (2003). Regulation of transbilayer plasma membrane phospholipid asymmetry. *Journal of Lipid Research*, **44**, 233-242.
86. Holthuis, J. C. M. & Menon, A. K. (2014). Lipid landscapes and pipelines in membrane homeostasis. *Nature*, **510**, 48-57.
87. Scanlon, M. D., Jennings, E. & Arrigan, D. W. M. (2009). Electrochemical behaviour of hen-egg-white lysozyme at the polarised water/1, 2-dichloroethane interface. *Physical Chemistry Chemical Physics*, **11**, 2272-2280.
88. Branlard, G., Amiour, N., Igrejas, G., Gaborit, T., Herbette, S., Dardevet, M. & Marion, D. (2003). Diversity of puroindolines as revealed by two-dimensional electrophoresis. *PROTEOMICS*, **3**, 168-174.
89. Lad, M. D. & University of Reading. School of Chemistry Food Biosciences and Pharmacy. (2006). *An investigation of protein and antimicrobial peptide interactions*

- with model lipid membranes*. Thesis (PhD) - University of Reading, School of Chemistry, Food Biosciences and Pharmacy.
90. Canfield, R. E. (1963). The Amino Acid Sequence of Egg White Lysozyme. *Journal of Biological Chemistry*, **238**, 2698-2707.
 91. Blochet, J.-E., Chevalier, C., Forest, E., Pebay-Peyroula, E., Gautier, M.-F., Joudrier, P., Pézolet, M. & Marion, D. (1993). Complete amino acid sequence of puroindoline, a new basic and cystine-rich protein with a unique tryptophan-rich domain, isolated from wheat endosperm by Triton X-114 phase partitioning. *Febs Letters*, **329**, 336-340.
 92. Clifton, L. A., Sanders, M. R., Castelletto, V., Rogers, S. E., Heenan, R. K., Neylon, C., Frazier, R. A. & Green, R. J. (2011). Puroindoline-a, a lipid binding protein from common wheat, spontaneously forms prolate protein micelles in solution. *Physical Chemistry Chemical Physics*, **13**, 8881-8888.
 93. Jing, W., Demcoe, A. R. & Vogel, H. J. (2003). Conformation of a Bactericidal Domain of Puroindoline a: Structure and Mechanism of Action of a 13-Residue Antimicrobial Peptide. *Journal of Bacteriology*, **185**, 4938-4947.
 94. Molina, A., Goy, P. A., Fraile, A., Sánchez-Monge, R. & García-Olmedo, F. (1993). Inhibition of bacterial and fungal plant pathogens by thionins of types I and II. *Plant Science*, **92**, 169-177.
 95. Tam, P. J., Wang, S., Wong, H. K. & Tan, L. W. (2015). Antimicrobial Peptides from Plants. *Pharmaceuticals*, **8**.
 96. Clifton, L. A., Green, R. J. & Frazier, R. A. (2007). Puroindoline-b mutations control the lipid binding interactions in mixed puroindoline-a : puroindoline-b systems. *Biochemistry*, **46**, 13929-13937.
 97. Aisenbrey, C., Goormaghtigh, E., Ruyschaert, J. M. & Bechinger, B. (2006). Translocation of amino acyl residues from the membrane interface to the hydrophobic core: thermodynamic model and experimental analysis using ATR-FTIR spectroscopy. *Molecular Membrane Biology*, **23**, 363-374.
 98. Wu, F., Gericke, A., Flach, C. R., Seaton, B. A. & Mendelsohn, R. (1998). Domain structure and molecular conformation in aqueous monolayers of annexin V dimyristoylphosphatidic acid Ca²⁺ complexes investigated by Brewster angle microscopy and IR reflection absorption spectroscopy. *Biophysical Journal*, **74**, A306-A306.

99. Pirc, K. & Ulrih, N. P. (2015). α -Synuclein interactions with phospholipid model membranes: Key roles for electrostatic interactions and lipid-bilayer structure. *Biochimica et Biophysica Acta (BBA) - Biomembranes*, **1848**, 2002-2012.
100. Lad, M. D., Birembaut, F., Frazier, R. A. & Green, R. J. (2005). Protein-lipid interactions at the air/water interface. *Physical Chemistry Chemical Physics*, **7**, 3478-3485.
101. Ananthanarayanan, B., Stahelin, R. V., Digman, M. A. & Cho, W. H. (2003). Activation mechanisms of conventional protein kinase C isoforms are determined by the ligand affinity and conformational flexibility of their C1 domains. *Journal of Biological Chemistry*, **278**, 46886-46894.
102. Green, R. J., Su, T. J., Joy, H. & Lu, J. R. (2000). Interaction of lysozyme and sodium dodecyl sulfate at the air-liquid interface. *Langmuir*, **16**, 5797-5805.
103. Blondelle, S. E., Lohner, K. & Aguilar, M. I. (1999). Lipid-induced conformation and lipid-binding properties of cytolytic and antimicrobial peptides: determination and biological specificity. *Biochimica Et Biophysica Acta-Biomembranes*, **1462**, 89-108.
104. Tripp, B. C., Magda, J. J. & Andrade, J. D. (1995). Adsorption of Globular Proteins at the Air/Water Interface as Measured via Dynamic Surface Tension: Concentration Dependence, Mass-Transfer Considerations, and Adsorption Kinetics. *Journal of Colloid and Interface Science*, **173**, 16-27.
105. Fendler, J. H. (1982). *Membrane mimetic chemistry : characterizations and applications of micelles, microemulsions, monolayers, bilayers, vesicles, host-guest systems and polyions*, New York ; Chichester, Wiley
106. Shankland, K., Spillman, M. J., Kabova, E. A., Edgeley, D. S. & Shankland, N. (2013). The principles underlying the use of powder diffraction data in solving pharmaceutical crystal structures. *Acta Crystallographica Section C*, **69**, 1251-1259.
107. Le Brun, A. P., Clifton, L. A., Halbert, C. E., Lin, B., Meron, M., Holden, P. J., Lakey, J. H. & Holt, S. A. (2013). Structural Characterization of a Model Gram-Negative Bacterial Surface Using Lipopolysaccharides from Rough Strains of Escherichia coli. *Biomacromolecules*, **14**, 2014-2022.
108. Sivia, D. S. (2011). *Elementary scattering theory: for X-ray and neutron users*. Oxford: Oxford University Press.
109. Arnold, T., Nicklin, C., Rawle, J., Sutter, J., Bates, T., Nutter, B., McIntyre, G. & Burt, M. (2012). Implementation of a beam deflection system for studies of liquid interfaces on beamline I07 at Diamond. *Journal of Synchrotron Radiation*, **19**, 408-416.

110. Nguyen, S., Adamczak, M., Hiorth, M., Smistad, G. & Kopperud, H. M. (2015). Interactions of liposomes with dental restorative materials. *Colloids and Surfaces B: Biointerfaces*, **136**, 744-751.
111. Shibata, H., Yoshida, H., Izutsu, K.-I., Haishima, Y., Kawanishi, T., Okuda, H. & Goda, Y. (2015). Interaction kinetics of serum proteins with liposomes and their effect on phospholipase-induced liposomal drug release. *International Journal of Pharmaceutics*, **495**, 827-839.
112. Tan, C., Feng, B., Zhang, X., Xia, W. & Xia, S. (2016). Biopolymer-coated liposomes by electrostatic adsorption of chitosan (chitosomes) as novel delivery systems for carotenoids. *Food Hydrocolloids*, **52**, 774-784.
113. Torchilin, V. P. (2005). Recent advances with liposomes as pharmaceutical carriers. *Nat Rev Drug Discov*, **4**, 145-160.
114. New, R. R. C. (1990). *Liposomes : a practical approach*. Oxford: IRL.
115. Nath, S., Satpathy, G. R., Mantri, R., Deep, S. & Ahluwalia, J. C. (1997). Evaluation of enzyme thermostability by enzyme assay and differential scanning calorimetry A study of alcohol dehydrogenase. *Journal of the Chemical Society, Faraday Transactions*, **93**, 3351-3354.
116. Chiu, M. H. & Prenner, E. J. (2011). Differential scanning calorimetry: An invaluable tool for a detailed thermodynamic characterization of macromolecules and their interactions. *Journal of Pharmacy and Bioallied Sciences*, **3**, 39-59.
117. Kumar, S., Bhargava, P., Sreekanth, V. & Bajaj, A. (2015). Design, synthesis, and physico-chemical interactions of bile acid derived dimeric phospholipid amphiphiles with model membranes. *Journal of Colloid and Interface Science*, **448**, 398-406.
118. Tamm, L. K. & Tatulian, S. A. Infrared spectroscopy of proteins and peptides in lipid bilayers. *Quarterly Reviews of Biophysics*, **30**, 365-429.
119. Pawłowski, J., Juhaniewicz, J., Güzeloğlu, A. & Şek, S. (2015). Mechanism of Lipid Vesicles Spreading and Bilayer Formation on a Au(111) Surface. *Langmuir*, **31**, 11012-11019.
120. Brian, A. A. & McConnell, H. M. (1984). Allogeneic stimulation of cytotoxic T cells by supported planar membranes. *Proceedings of the National Academy of Sciences of the United States of America*, **81**, 6159-6163.
121. Anderson, T. H., Min, Y., Weirich, K. L., Zeng, H., Fygenson, D. & Israelachvili, J. N. (2009). Formation of Supported Bilayers on Silica Substrates. *Langmuir*, **25**, 6997-7005.

122. Hamai, C., Yang, T., Kataoka, S., Cremer, P. S. & Musser, S. M. (2006). Effect of Average Phospholipid Curvature on Supported Bilayer Formation on Glass by Vesicle Fusion. *Biophysical Journal*, **90**, 1241-1248.
123. Tamm, L. K. & McConnell, H. M. (1985). Supported phospholipid bilayers. *Biophysical Journal*, **47**, 105-113.
124. Girard-Egrot, A. P. & Blum, L. J. (2007). Langmuir-Blodgett Technique for Synthesis of Biomimetic Lipid Membranes. In: Martin, D. K. (ed.) *Nanobiotechnology of Biomimetic Membranes*. Boston, MA: Springer US.
125. Stuart, B., Ando, D. J. & ACOL (Project) (1997). *Biological applications of infrared spectroscopy*, Chichester, John Wiley.
126. Lu, J. R., Zhao, X. & Yaseen, M. (2007). Protein adsorption studied by neutron reflection. *Current Opinion in Colloid & Interface Science*, **12**, 9-16.
127. Zhao, X., Pan, F. & Lu, J. R. (2009). Interfacial assembly of proteins and peptides: recent examples studied by neutron reflection. *Journal of The Royal Society Interface*, **6**, S659-S670.
128. Sears, V. F. (1992). Neutron scattering lengths and cross sections. *Neutron News*, **3**, 26-37.
129. Kleinschmidt, J. H. (2013). *Lipid-protein interactions : methods and protocols*. New York: Humana Press ; Springer.
130. Day, L., Bhandari, D. G., Greenwell, P., Leonard, S. A. & Schofield, J. D. (2006). Characterization of wheat puroindoline proteins. *FEBS J*, **273**, 5358-73.
131. Bordier, C. (1981). Phase separation of integral membrane proteins in Triton X-114 solution. *J Biol Chem*, **256**, 1604-7.
132. Sambrook, J. & Russell, D. W. (2001). *Molecular cloning: a laboratory manual*. 3rd ed. Cold Spring Harbor, N.Y.: Cold Spring Harbor Laboratory Press.
133. Sanders, M. R. & University of Reading. School of Chemistry, Pharmacy and Food Biosciences. (2014). *The investigation of the protein-lipid interactions of plant defence proteins within complex membrane environments*. Thesis (PhD) - University of Reading, School of Chemistry, School of Chemistry, Food & Pharmacy.
134. Greenwell, P. & Schofield, J. D. (1986). A starch granule protein associated with endosperm softness in wheat. *Cereal Chem.*, **63**, 379-380.
135. Lad, M. D., Birembaut, F., Clifton, L. A., Frazier, R. A., Webster, J. R. P. & Green, R. J. Antimicrobial Peptide-Lipid Binding Interactions and Binding Selectivity. *Biophysical Journal*, **92**, 3575-3586.

136. Chen, C., Chen, Y., Yang, C., Zeng, P., Xu, H., Pan, F. & Lu, J. R. (2015). High Selective Performance of Designed Antibacterial and Anticancer Peptide Amphiphiles. *ACS Applied Materials & Interfaces*, **7**, 17346-17355.
137. Mansour, H. M. & Zografi, G. (2007). Relationships between Equilibrium Spreading Pressure and Phase Equilibria of Phospholipid Bilayers and Monolayers at the Air–Water Interface. *Langmuir*, **23**, 3809-3819.
138. Liu, W., Wang, Z., Fu, L., Leblanc, R. M. & Yan, E. C. Y. (2013). Lipid Compositions Modulate Fluidity and Stability of Bilayers: Characterization by Surface Pressure and Sum Frequency Generation Spectroscopy. *Langmuir*, **29**, 15022-15031.
139. Ronzon, F., Desbat, B., Chauvet, J.-P. & Roux, B. (2002). Behavior of a GPI-anchored protein in phospholipid monolayers at the air–water interface. *Biochimica et Biophysica Acta (BBA) - Biomembranes*, **1560**, 1-13.
140. Rosengarth, A., Wintergalen, A., Galla, H.-J., Hinz, H.-J. & Gerke, V. (1998). Ca²⁺-independent interaction of annexin I with phospholipid monolayers. *Febs Letters*, **438**, 279-284.
141. Yun, H. J., Choi, Y. W., Kim, N. J. & Sohn, D. W. (2003). Physicochemical properties of phosphatidylcholine (PC) monolayers with different alkyl chains, at the air/water interface. *Bulletin of the Korean Chemical Society*, **24**, 377-383.
142. Luna, C., Stroka, K. M., Bermudez, H. & Aranda-Espinoza, H. (2011). Thermodynamics of monolayers formed by mixtures of phosphatidylcholine/phosphatidylserine. *Colloids and surfaces. B, Biointerfaces*, **85**, 293-300.
143. Saleem, M., Meyer, M. C., Breitenstein, D. & Galla, H.-J. (2008). The Surfactant Peptide KL4 in Lipid Monolayers: PHASE BEHAVIOR, TOPOGRAPHY, AND CHEMICAL DISTRIBUTION. *Journal of Biological Chemistry*, **283**, 5195-5207.
144. Dietrich, U., Krüger, P. & Käs, J. A. (2011). Structural investigation on the adsorption of the MARCKS peptide on anionic lipid monolayers – effects beyond electrostatic. *Chemistry and Physics of Lipids*, **164**, 266-275.
145. Martin, P. & Szablewski, M. (2004). *NIMA TECHNOLOGY, LANGMUIR-BLODGETT TROUGHS, OPERATING MANUAL, 6TH EDITION*, Coventry, Nima Technology Ltd.
146. Orczyk, M. & Wojciechowski, K. (2015). Comparison of the effect of two Quillaja bark saponin extracts on DPPC and DPPC/cholesterol Langmuir monolayers. *Colloids and Surfaces B: Biointerfaces*, **136**, 291-299.

147. Nerdal, W., Nilsen, T. R. S. & Steinkopf, S. (2015). CoenzymeQ10 localizations in model membranes. A Langmuir monolayer study. *Biophysical Chemistry*, **207**, 74-81.
148. Steinkopf, S., Hanekam, L., Schaathun, M., Budnjo, A., Haug, B. E. & Nerdal, W. (2012). Interaction of local anaesthetic articaine enantiomers with brain lipids: A Langmuir monolayer study. *European Journal of Pharmaceutical Sciences*, **47**, 394-401.
149. Bougis, P., Rochat, H., Pieroni, G. & Verger, R. (1981). Penetration of phospholipid monolayers by cardiotoxins. *Biochemistry*, **20**, 4915-4920.
150. Kamp, J. A. F. O. d. (1979). Lipid Asymmetry in Membranes. *Annual Review of Biochemistry*, **48**, 47-71.
151. Gerelli, Y., Porcar, L. & Fragneto, G. (2012). Lipid Rearrangement in DSPC/DMPC Bilayers: A Neutron Reflectometry Study. *Langmuir*, **28**, 15922-15928.
152. Jia, D., Tao, K., Wang, J., Wang, C., Zhao, X., Yaseen, M., Xu, H., Que, G., Webster, J. R. P. & Lu, J. R. (2011). Dynamic Adsorption and Structure of Interfacial Bilayers Adsorbed from Lipopeptide Surfactants at the Hydrophilic Silicon/Water Interface: Effect of the Headgroup Length. *Langmuir*, **27**, 8798-8809.
153. Clifton, L. A., Holt, S. A., Hughes, A. V., Daulton, E. L., Arunmanee, W., Heinrich, F., Khalid, S., Jefferies, D., Charlton, T. R., Webster, J. R. P., Kinane, C. J. & Lakey, J. H. (2015). An Accurate In Vitro Model of the E. coli Envelope. *Angewandte Chemie (International Ed. in English)*, **54**, 11952-11955.
154. Foglia, F., Lawrence, M. J., Demè, B., Fragneto, G. & Barlow, D. (2012). Neutron diffraction studies of the interaction between amphotericin B and lipid-sterol model membranes. *Scientific Reports*, **2**, 778.
155. Dabkowska, A. P., Fragneto, G., Hughes, A. V., Quinn, P. J. & Lawrence, M. J. (2009). Specular Neutron Reflectivity Studies of the Interaction of Cytochrome c with Supported Phosphatidylcholine Bilayers Doped with Phosphatidylserine. *Langmuir*, **25**, 4203-4210.
156. Lu, J. R., Perumal, S., Powers, E. T., Kelly, J. W., Webster, J. R. P. & Penfold, J. (2003). Adsorption of β -Hairpin Peptides on the Surface of Water: A Neutron Reflection Study. *Journal of the American Chemical Society*, **125**, 3751-3757.
157. Clifton, L. A., Skoda, M. W. A., Le Brun, A. P., Ciesielski, F., Kuzmenko, I., Holt, S. A. & Lakey, J. H. (2015). Effect of Divalent Cation Removal on the Structure of Gram-Negative Bacterial Outer Membrane Models. *Langmuir*, **31**, 404-412.
158. Hughes, A. V. (2015). *RasCAL*. Retrieved from <http://sourceforge.net/projects/rscl/>.

159. Hübner, W. & Mantsch, H. H. (1991). Orientation of specifically $^{13}\text{C}=\text{O}$ labeled phosphatidylcholine multilayers from polarized attenuated total reflection FT-IR spectroscopy. *Biophysical Journal*, **59**, 1261-1272.
160. Bahng, M. K., Cho, N. J., Park, J. S. & Kim, K. (1998). Interaction of Indolicidin with Model Lipid Bilayers: FTIR-ATR Spectroscopic Study. *Langmuir*, **14**, 463-470.
161. Verity, J. E., Chhabra, N., Sinnathamby, K. & Yip, C. M. (2009). Tracking Molecular Interactions in Membranes by Simultaneous ATR-FTIR-AFM. *Biophysical Journal*, **97**, 1225-1231.
162. Dluhy, R. A. & Cornell, D. G. (1985). Insitu Measurement of the Infrared-Spectra of Insoluble Monolayers at the Air-Water-Interface. *Journal of Physical Chemistry*, **89**, 3195-3197.
163. Cowsill, B. J., Coffey, P. D., Yaseen, M., Waigh, T. A., Freeman, N. J. & Lu, J. R. (2011). Measurement of the thickness of ultra-thin adsorbed globular protein layers with dual-polarisation interferometry: a comparison with neutron reflectivity. *Soft Matter*, **7**, 7223-7230.
164. Fragneto, G., Charitat, T., Graner, F., Mecke, K., Perino-Gallice, L. & Bellet-Amalric, E. (2001). A fluid floating bilayer. *EPL (Europhysics Letters)*, **53**, 100.
165. Hughes, A. V., Howse, J. R., Dabkowska, A., Jones, R. A. L., Lawrence, M. J. & Roser, S. J. (2008). Floating Lipid Bilayers Deposited on Chemically Grafted Phosphatidylcholine Surfaces. *Langmuir*, **24**, 1989-1999.
166. Ladokhin, A. S., Wimley, W. C. & White, S. H. (1995). Leakage of membrane vesicle contents: determination of mechanism using fluorescence quenching. *Biophysical Journal*, **69**, 1964-1971.
167. Dufourcq, J., Faucon, J. F., Lussan, C. & Bernon, R. (1975). Study of lipid—protein interactions in membrane models: Intrinsic fluorescence of cytochrome b5—phospholipid complexes. *Febs Letters*, **57**, 112-116.
168. Andrushchenko, V. V., Aarabi, M. H., Nguyen, L. T., Prenner, E. J. & Vogel, H. J. (2008). Thermodynamics of the interactions of tryptophan-rich cathelicidin antimicrobial peptides with model and natural membranes. *Biochimica et Biophysica Acta (BBA) - Biomembranes*, **1778**, 1004-1014.
169. Andrushchenko, V. V., Vogel, H. J. & Prenner, E. J. (2007). Interactions of tryptophan-rich cathelicidin antimicrobial peptides with model membranes studied by differential scanning calorimetry. *Biochimica et Biophysica Acta (BBA) - Biomembranes*, **1768**, 2447-2458.

-
170. Ravishankar, D., Watson, K. A., Boateng, S. Y., Green, R. J., Greco, F. & Osborn, H. M. I. (2015). Exploring quercetin and luteolin derivatives as antiangiogenic agents. *European Journal of Medicinal Chemistry*, **97**, 259-274.
171. Brown, W. (1993). *Dynamic light scattering : the method and some applications*. Oxford: Clarendon Press.
172. Klajnert, B., Janiszewska, J., Urbanczyk-Lipkowska, Z., Bryszewska, M. & Eppard, R. M. (2006). DSC studies on interactions between low molecular mass peptide dendrimers and model lipid membranes. *International Journal of Pharmaceutics*, **327**, 145-152.
173. Bilge, D., Sahin, I., Kazanci, N. & Severcan, F. (2014). Interactions of tamoxifen with distearoyl phosphatidylcholine multilamellar vesicles: FTIR and DSC studies. *Spectrochimica Acta Part A: Molecular and Biomolecular Spectroscopy*, **130**, 250-256.
174. Prenner, E. J., Lewis, R. N. A. H. & McElhaney, R. N. (1999). The interaction of the antimicrobial peptide gramicidin S with lipid bilayer model and biological membranes. *Biochimica et Biophysica Acta (BBA) - Biomembranes*, **1462**, 201-221.
175. Nishijo, J. & Mizuno, H. (1998). Interactions of Cyclodextrins with DPPC Liposomes. Differential Scanning Calorimetry Studies. *CHEMICAL & PHARMACEUTICAL BULLETIN*, **46**, 120-124.
176. Ahmad, M. R., Nakajima, M., Kojima, S., Homma, M. & Fukuda, T. (2008). The Effects of Cell Sizes, Environmental Conditions, and Growth Phases on the Strength of Individual W303 Yeast Cells Inside ESEM. *IEEE Transactions on NanoBioscience*, **7**, 185-193.
177. Marsh, D. (1990). *CRC Handbook of lipid bilayers*. Boca Raton: CRC Press.
178. Ali, S., Minchey, S., Janoff, A. & Mayhew, E. (2000). A differential scanning calorimetry study of phosphocholines mixed with paclitaxel and its bromoacylated taxanes. *Biophysical Journal*, **78**, 246-256.
179. Wiener, J. R., Wagner, R. R. & Freire, E. (1983). Thermotropic behavior of mixed phosphatidylcholine-phosphatidylglycerol vesicles reconstituted with the matrix protein of vesicular stomatitis virus. *Biochemistry*, **22**, 6117-6123.
180. Meszko, S. J. & University of Reading. School of Chemistry, Pharmacy and Food Biosciences. (2015). *The interaction of the wheat defence protein β -purothionin with models of fungal membranes*. Thesis (MPharm) - University of Reading, School of Chemistry, School of Chemistry, Food & Pharmacy.

181. McElhaney, R. N. (1986). Differential scanning calorimetric studies of lipid-protein interactions in model membrane systems. *Biochimica et Biophysica Acta (BBA) - Reviews on Biomembranes*, **864**, 361-421.
182. Drazenovic, J., Wang, H., Roth, K., Zhang, J., Ahmed, S., Chen, Y., Bothun, G. & Wunder, S. L. (2015). Effect of lamellarity and size on calorimetric phase transitions in single component phosphatidylcholine vesicles. *Biochimica et Biophysica Acta (BBA) - Biomembranes*, **1848**, 532-543.